applications of modern metallographic techniques

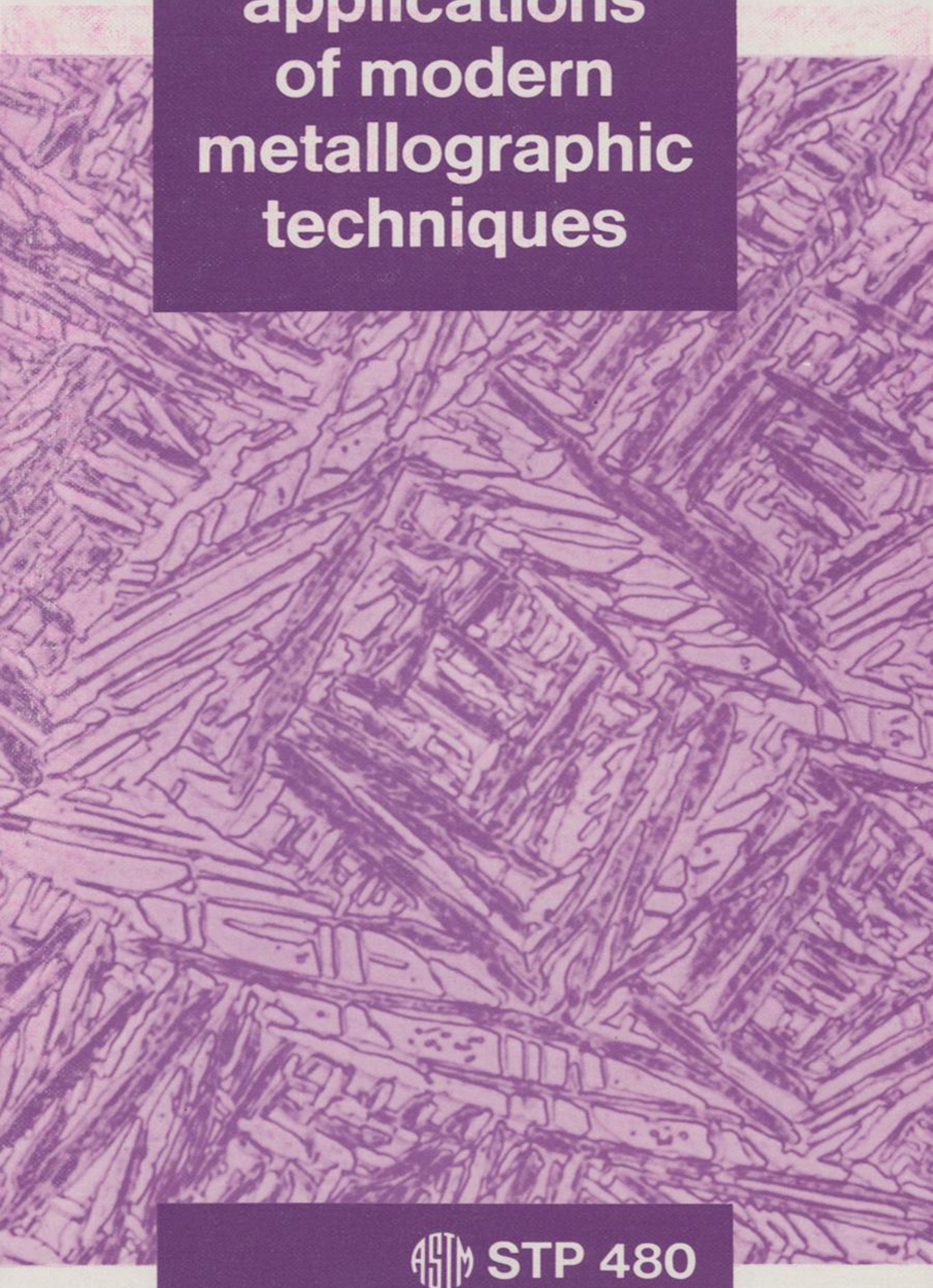

ASTM STP 480

AMERICAN SOCIETY FOR TESTING AND MATERIALS

APPLICATIONS OF MODERN METALLOGRAPHIC TECHNIQUES

A symposium
presented at the
Materials Engineering
Exposition and Congress
AMERICAN SOCIETY FOR METALS
Philadelphia, Pa., 13–16 Oct. 1969

ASTM SPECIAL TECHNICAL PUBLICATION 480

List price $17.00

AMERICAN SOCIETY FOR TESTING AND MATERIALS
1916 Race Street, Philadelphia, Pa. 19103

Library of Congress Catalog Card Number: 78-114749
ISBN 0-8031-0064-7

NOTE

Cover: Titanium-6Al-4V alloy (original magnification 2000, reduced two thirds for publication) heat-treated to above beta transformation temperature. The segmented light areas are partially spheroidized plates of alpha phase, which formed on cooling during the initial quench and then fragmented during heating at 1500 F. The dark-gray areas indicate beta phase that transformed to alpha plus beta on air cooling from this temperature.

Photograph courtesy of Theresea V. Brassard, Physical and Mechanical Metallurgy Lab, Watervliet Arsenal, Watervliet, N. Y. 12189.

Printed in Baltimore, Md.
September 1970

Foreword

ASTM Committee E-4 on Metallography and the American Society for Metals cosponsored the Symposium on Applications of Modern Metallographic Techniques given on 13 Oct. 1969. The session was presented at the ASM Annual Materials Engineering Exposition and Congress, held in Philadelphia, Pa., 13–16 Oct. 1969. The joint ASTM-ASM venture was arranged by the American Society for Metals, with W. D. Forgeng, Jr., United States Steel Corp., chairman of Committee E-4, presiding as symposium chairman.

Related ASTM Publications

Fifty Years of Progress in Metallographic Techniques, STP 430 (1968), $25.75

Electron Fractography, STP 436 (1968), $11.00

Electron Microfractography, STP 453 (1969), $16.00

Contents

Introduction

As a continuation of the excellent cooperation that has existed between the two societies, Committee E-4 on Metallography of the American Society for Testing and Materials was pleased to join with the American Society for Metals in the sponsorship of a one-day symposium on Applications of Modern Metallographic Techniques at the ASM Annual Materials Engineering Congress and Exposition on 13 Oct. 1969. Committee E-4 believed that this symposium afforded an ideal opportunity to introduce an overall view of its ASTM activities to the broad materials-oriented audience at the ASM annual meeting and, at the same time to present a useful collection of papers that show how modern metallography is being applied to both routine and special materials problems. The hopes of the Committee were fully realized, as the symposium was among the two or three best-attended sessions at the Materials Congress.

The terms "modern" and "applications" were the guiding criteria used by the Committee in selecting authors for the symposium and suggesting the topics for their presentations. In addition, the topics were to represent, as broadly as possible, the extensive activity of ASTM Committee E-4 and its subcommittees in the areas of research and standardization of metallographic methods.

The ten papers from the symposium that are published here describe new or improved applications of some of the most up-to-date methods in today's metallography: electron microscopy (thin foils, replicas, and scanning microscopy), electron microprobe analysis, X-ray microscopy and analysis, quantitative metallography (manual and electronic), high-speed dilatometry, special optical and etching techniques for improved color metallography, and the preparation and examination of irradiated materials.

Readers of this volume should find the papers a useful addition to their collections of practical information on metallography, and will also find the information a beneficial supplement to the more general discussions of metallography contained in the ASTM publication resulting from Committee E-4's Fiftieth Anniversary Symposium held in 1966, *Fifty Years of Progress in Metallographic Techniques, ASTM STP 430.*

The American Society for Testing and Materials and the program chairmen wish to thank the authors for their excellent contributions to this volume. They also particularly wish to acknowledge the cooperation of the American

Society for Metals in arranging the symposium and to thank the representative of ASM's Research Applications Program Committee, Dr. Klaus M. Zwilsky, who served as general chairman for the symposium sessions, for his assistance in the selection of topics and authors for the meeting.

W. D. Forgeng, Jr.
Applied Research Laboratory,
U. S. Steel Corp.,
Monroeville, Pa. 15146;
symposium chairman.

L. Toman, Jr.
Army Electronics Command,
Ft. Monmouth, N. J. 07703;
symposium cochairman.

G. A. Moore[1]

Is Quantitative Metallography Quantitative?

REFERENCE: Moore, G. A., "**Is Quantitative Metallography Quantitative?,**" *Applications of Modern Metallographic Techniques, ASTM STP 480,* American Society for Testing and Materials, 1970, pp. 3–48.

ABSTRACT: While the basic principles of quantitative metallography have been firmly established, the practice of such measurements yields highly variable results. Simple laws define the statistical limitation on any measuring method. Serious errors arise from improper selection and preparation of specimens. Anticipated gradients must be encompassed by a planned sampling scheme which guarantees unbiased representation and permits measurement of actual variation in the material studied. Specimen preparation must give a truthful image of the structure. Any free choices by the operator introduce bias. The precision of measurement of one micrograph is primarily controlled by a combination of statistical uncertainty and observational error at the edges of particles. The statistical uncertainty conforms to the ideal when the apparent particle size is small, but observation becomes inefficient as the average intercept width increases and the number of particles in the field decreases. Edge errors are maximum with small particles and vary with the observer or the instrument used. Maximum precision is obtained when these two errors are approximately equal. While quantitative metallography is a statistical, rather than exact, process and subject to serious or fatal errors when practiced crudely, carefully controlled measurements can yield several structural parameters with a precision adequate to satisfy any practical metallurgist.

KEY WORDS: measurement, metallography, metallurgical analysis, microscopy, photogrammetry, evaluation

Quantitative metallography is a specialized application of the more general art of quantitative microscopy, which is widely used in other material sciences such as ceramics and petrography and in biological research and medical practice. The more inclusive term "morphometry" is in use in many of these fields. This includes use of the same measuring methods on subjects visible without the aid of a microscope, as for example concrete and resource evaluation in photogrammetry. As a concession to the metallurgical interest of this symposium, the more limited title is used, permitting me to ignore such complications as nonplanar sections which occur in other fields.

---

[1] Physical metallurgist, Metallurgy Div., National Bureau of Standards, Washington, D. C. 20234. Personal member ASTM. Contribution of the National Bureau of Standards, not subject to copyright.

Quantitative metallography (or morphometry) is the art of estimating parameters such as percentage of phase and mean size, spacing, and number of particles of a dispersed phase in a heterogeneous material on the basis of microscopic observations of suitably prepared plane sections. The observations made, whether by visual-manual methods or by use of an optical-electronic scanning device, are generally counting processes or can be expressed as counting processes when they appear continuous. The reader will find it instructive to stop at this point and perform the experiment reproduced as Fig. 1.

In most cases the estimated parameter value is taken to represent a substantial "universe" of material, such as an entire heat of steel. The observations, however, are made on limited surface areas of a small number of specimens and at best represent a small statistical sample of this universe. The estimate thus is subject to statistical variations and errors at each level of sampling and also to experimental errors in both specimen preparation and measurement. Actual variability of the material is a pertinent parameter along with mean value and should be measured, while errors interfere with accurate estimates and may make the results meaningless. The question facing the experimenter or inspector is thus whether or not a feasible program of measurement can yield measurements of sufficient precision to be useful for a metallurgical purpose.

It will be demonstrated that careless application of morphometric methods, together with a limited number of observations, frequently leads to values of no quantitative significance. However, adequate experimental work with due attention to all potential sources of error can and will yield results whose precision is comparable to that of most property measurements generally made on metals. Thus, the answer to the title question should be: Quantitative Metallography is Quantitative if Done Correctly.

Definitions and Fundamental Principles

Until recently, no general text on morphometry existed in the English language. As this situation is now remedied [*1*, *2*],[2] it is legitimate in the present case to omit a general coverage of the history and theory as well as details of many operations useful in specialized applications. This discussion will be limited to a description of the practices which usually give reliable measurements of a few simple parameters which can generally be correlated with useful physical and mechanical properties of metals. Methods of estimating expected and actual precision are included.

It is important to note that all parameters determined by quantitative metallography are in dimensional terms—volumes, areas, and distances—

[2] Italic numbers in brackets refer to the list of references at the end of this paper.

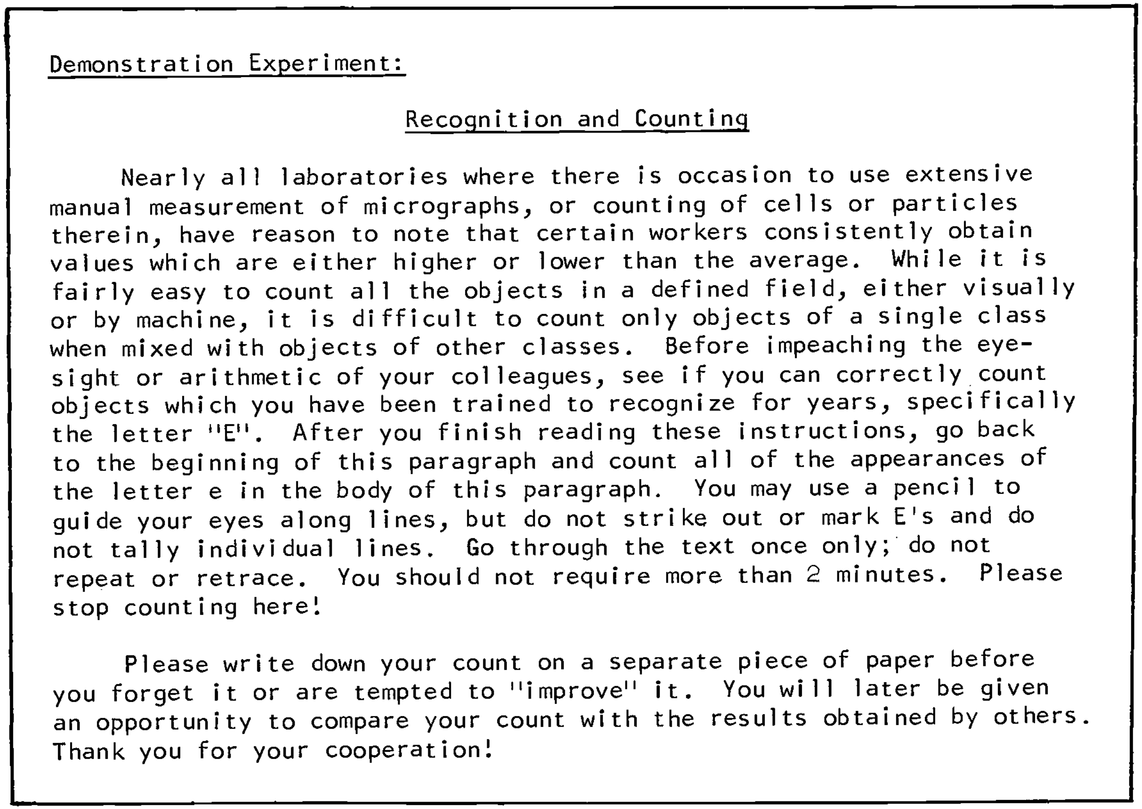

Demonstration Experiment:

Recognition and Counting

Nearly all laboratories where there is occasion to use extensive manual measurement of micrographs, or counting of cells or particles therein, have reason to note that certain workers consistently obtain values which are either higher or lower than the average. While it is fairly easy to count all the objects in a defined field, either visually or by machine, it is difficult to count only objects of a single class when mixed with objects of other classes. Before impeaching the eyesight or arithmetic of your colleagues, see if you can correctly count objects which you have been trained to recognize for years, specifically the letter "E". After you finish reading these instructions, go back to the beginning of this paragraph and count all of the appearances of the letter e in the body of this paragraph. You may use a pencil to guide your eyes along lines, but do not strike out or mark E's and do not tally individual lines. Go through the text once only; do not repeat or retrace. You should not require more than 2 minutes. Please stop counting here!

Please write down your count on a separate piece of paper before you forget it or are tempted to "improve" it. You will later be given an opportunity to compare your count with the results obtained by others. Thank you for your cooperation!

FIG. 1—*Please try this now:*

and refer to phases actually present. Separate calculations are required to compare these values with chemical percentages in weight or atomic terms.

Phase and Particle

The term "phase" is used in the limited context of quantitative metallography to designate all portions of a volume which have essentially the same composition and structure as revealed by the preparation method and magnification in use. Thus at low magnification a steel may be regarded as showing a ferrite and a pearlite phase, while higher magnification reveals the pearlite to consist of ferrite and carbide phases. Quantitative metallography may ignore the thermodynamic validity of phase identification.

A "particle" is a contiguous volume of the dispersed phase or, in common practice, a contiguous area of the dispersed phase seen on a plane section. Ideally, one particle = one grain, but complex particles ("stringers" or "clusters") are frequently encountered in which one particle may consist of several grains. Agreement on which is being counted will be required. Voids may be treated as particles of the 0 phase. Clearly delineated grains of a single phase metal may be treated as nondispersed particles.

Phase Percentage or Fraction

The fundamental principle underlying quantitative metallography, applicable also to plane or line sampling of any aggregate on any size scale, is the Delesse principle which, together with its correlaries, independently and repetitively discovered in many fields [*3–7*], states that phase fraction (or percentage) is a constant no matter how measured; namely,

$$V_V = A_A = L_L = P_P$$

within statistical limitations of sampling. Thus the fraction (or percentage) of points, P_P, in a point net which fall on phase particles or the fraction of line length, L_L, of a line array falling on phase are unbiased estimates of the phase area fraction, A_A, of the section and of the volume fraction, V_V, of the phase in the solid. Restrictions necessary to avoid bias are:

1. The sample section must be plane and flat and line samples must be straight lines. The bias introduced by curvature at a radius large compared to structural details is normally negligible, but curvature at a radius comparable to structural details may not permit unbiased measurement.

2. The equalities apply only to the plane surface of an opaque specimen. A thin section whose thickness is a significant fraction of the size of the structural details is biased toward overevaluating the opaque phase. Since such sections are rarely used for quantitative metallography, corrections will not be discussed here [*8*]. A rough section may be similarly biased to overevaluate the harder phase or phase least soluble in an etching agent.

3. A regular net or regular line array may not be used to sample a regular structure when the net or line spacing is comparable in size to the structural details. The use of a regular array in sampling a random structure does not introduce bias.

4. The sample section, microscopic field, and net or line placement must all be chosen to be unbiased and representative of the material sampled. While random selection is unbiased, care must be exercised that several random selections do not concentrate on a small area or volume which may not be representative of the whole. As it is nearly impossible to visually select a representative field, visual field selection and net placement should not be permitted. Blind selection at predefined locations is normally most representative.

5. The form of a point net or line array, the spacing, and the magnification have no biasing effects on volume fraction determinations, but they do affect precision of measurement and real and apparent variation between samples.

6. Direct measurement of A_A was commonly used by early morphometrists, but both the method of cutting out and weighing particle images (the "paper doll" method) and the planimeter method are laborious and difficult to perform accurately. Either lineal or point count methods give more precise results with less effort, hence direct area measurement should be reserved for special cases such as measurement of large or unique particles. Matching individual particles to sized masks involves errors similar to other direct area measurements.

Mean Free Path Between Particles

The mean free path $\bar{\ell}_\alpha$, or average distance in the matrix, α, between β phase particles, as measured by intercepts along any straight line array (including parallel lines) applied to a section, is an unbiased measure of the mean free path through the matrix in any or all directions in volume, provided the phase particles are isotropic in shape and statistically random in arrangement.

When the particles are anisotropic in shape or arrangement, the measured mean free path is correct only for the direction in which measured; thus the mean free path should be separately measured and stated for the three principle directions, as determined by the production process used for the metal being examined. An average mean free path may be calculated by summing the number of intercepts in all three directions and dividing into the total line length in the matrix phase. Alternatively, the test line may be applied repetitively to a series of micrographs made on nonparallel surfaces, with the line rotated through a small angle for each application, summing the intercepts and lengths in the matrix over the process. This method is laborious and tends to overweight the center area of each field. It has not been demonstrated to be superior to the simpler procedure above.

As the literature strongly indicates that the mean free path in the matrix is highly correlated with yield strength and ductility of aggregated structures and the performance of nuclear fuels, the determination of this quantity is frequently useful.

Particle Size—Mean Intercept Width

The only measurement of particle size in which the measured linear value is an unbiased estimate of the value in volume is the mean intercept width $\bar{\ell}_\beta$, which may be calculated from a lineal analysis by dividing the total line length in phase by the number of intercepts.[3] Use of a parallel line array is valid if the particle shape is isotropic or if particles are somewhat anisotropic but randomly oriented. Otherwise, separate determinations should be made in the principle directions and an average determined in the same manner as for mean free path.

For a structure treated as two phase, the mean intercept width and mean free path are derived from the same observational data. If one is known, the other may be computed by multiplying by the ratio of phase percentages:

$$\bar{\ell}_\beta/\bar{\ell}_\alpha = A_{\beta_A}/A_{\alpha_A}$$

Dimensions of specific particles in space cannot be determined from the dimensions of their sections. Such caliper quantities as height, width, and diameter of the observed section are almost invariably smaller than the corresponding values for the specific particle in space and, thus, are highly biased measurements. Direct measurement of such quantities is not generally useful except for the measurement of a few large particles, where it may be legitimately assumed that these exceptional particles have an important effect on useful properties or suitability for service.[4] Such measurements are highly sensitive to conformity to a specific procedure and should not be regarded as truly quantitative data.

When dispersed particles conform, or may reasonably be assumed to conform, to simple geometric shapes and may be assumed to represent a relatively narrow distribution of sizes in space, mean caliper dimensions of sections and solid particles can be computed by multiplying the mean intercept width by constants which can be calculated for each shape class. The constant for determining mean diameters of circles from mean intercept widths or for determining mean diameters of spheres from mean diameters of circles

---

[3] The intercept of a test line with a convex particle is one line segment. The intersection of a test line with a closed surface normally yields two points. In single-phase material, the second intersection is assigned to the next grain.

[4] ASTM Recommended Practice for Evaluating the Microstructure of Graphite in Iron Castings (A 247 - 67), Recommended Practice for Determining the Inclusion Content of Steel (E 45 - 63), and Standard Methods for Estimating Average Grain Size of Metals (E 112 - 63).

is $4/\pi$, about 1.273. For average equiaxed grains of one phase the constant is about 1.128. The constant is squared to compute mean volume diameter from mean intercept width.

Particle Shape

The shape and complexity of particles must at this time be considered primarily a matter for visual inspection and qualitative description. It must be emphasized that shapes seen on single sections limit, but do not unambiguously define, the shapes of particles in space. For example, rods cannot be distinguished from spheres on a transverse section, nor from plates on a normal section [*2*].

When anisotropic particles are oriented with their axes essentially parallel to the principle directions of the specimen, the ratios between mean intercept widths measured in principle directions are reliable measurements of the degree of anisotropy and may be expected to show at least as good correlation with useful properties as do caliper measurements obtainable only with significantly greater effort.

Number of Particles

Visual determination of the actual number of particles showing in a microscopic field is of low accuracy, particularly when the number is large or the field is confused by other structural details. The counting experiment which the reader was earlier asked to perform reasonably simulates such a confused micrograph. The reader may now compare his count with the results of 400 trials shown in Fig. 2. These trials were conducted by 13 members of ASTM Committee E-4 on Metallography in their own laboratories and by the writer at four locations, three of which were meetings related to morphometry. Most subgroups showed approximately the same distribution as in the summation.

It may be noted that both the modal and mean count values are substantially lower than the true value (112). Only 3.8 percent of the subjects counted correctly, and only 4.3 percent counted high. A vast majority (92 percent) submitted low counts—many very low. For no reason which could be anticipated, the standard deviation of counts, 12.28, is close to the Poisson standard deviation for the actual number of *e*'s ($\sqrt{112} = 10.58$) and the mean negative bias (-8.25) is almost exactly one formal probable error ($0.6745\ \sigma$).

In particle counting a clean binary field is obviously important, as is advance agreement on identification of particles of unusual appearance such as the two capital *E*'s included in the experiment. Social and mental sources of confusion may, however, be as important as structural confusion in the field. In general, valid counts can only be obtained by alternately marking particles on a print and tallying in a regular array on a score sheet. Use of

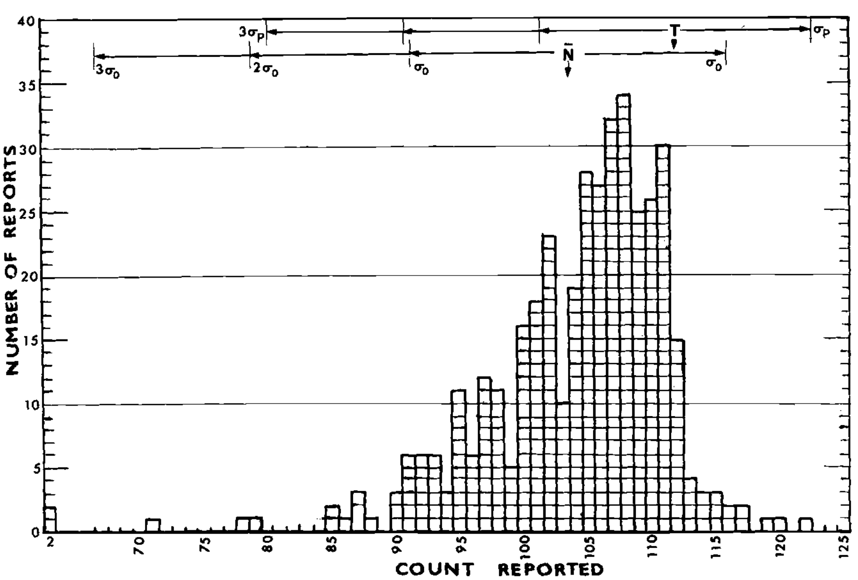

FIG. 2—*Results of experiment in counting* e*'s.*

five or more colored pencils in rotation to mark and tally coherent groups of ten particles will usually prevent false tallies.

On the whole, visual particle counting is difficult and usually inaccurate and subject to persistent negative bias. Thus this operation should be avoided wherever possible.

Relatively simple machine processes of counting particles on sections are available, subject to the restrictions that all particles are essentially circular and that there is no clustering. A large and complex computer operation is required to correctly count particles of complex shape. Both visual and automatic methods tend to ignore very small particles actually revealed by the microscope, and it must in most cases be anticipated that there are in fact some particles so small that they are not revealed.

Even a true count of particles encountered on a section is a highly biased measure of the actual number of particles in unit volume. No estimate of the true number in volume can be made unless a distribution of apparent size on the section has been obtained. As the particles become smaller, the probability that a particle will in fact be encountered by one section plane decreases, hence the observed number in each size class must, as a minimum, be weighted by multiplying by the number of section planes which would be required to encounter all particles of this size class. An additional correction allowing for small sections of large particles is required for a valid estimate of number in volume (Ref *1*, chapters 5 and 6).

There is no known evidence at this time that number of particles is itself significantly related to any useful metallic property or that this number is more useful than the directly measurable phase percentage, size, and spacing parameters.

The number of particles in a microscopic field is of interest in determining uniformity of a material, since the standard deviation of N among samples may confidently be expected to be directly related to the Poisson value ($\sigma_N = \sqrt{N}$). The departure of the observational estimate of σ_N from this value is a useful measure of actual uniformity. The actual variation of N among fields or specimens may be either greater or less than the Poisson value, which applies specifically to a random distribution of particles. A properly blended powder mixture should yield compacts in which this variation conforms closely to the Poisson value. Particles formed by precipitation from a uniform solid solution should show a uniform distribution which may be either regular or random in arrangement. Fields substantially larger than the local patterns of arrangement should show substantially less variation in particle number (and thus also in phase percentage) than that predicted by the Poisson rule. Many real metals are, however, segregated in chemical composition and can be expected to show substantially greater variation than that predicted. It is necessary, however, to compare the variation of observed values with the Poisson prediction before it can be said with certainty that the observations show segregation or a gradient rather than normal statistical uncertainty.

Because of the numerous difficulties in determining true particle counts, it will frequently be found desirable to limit counting processes to admittedly unreal but nevertheless reliably measured quantities:

1. The number of particles per field, or per unit area of section, which are larger than a stated smaller size limit.

2. The equivalent number of average particles—this number may be computed in the manner which follows. The height (or diameter) of an average particle is computed by multiplying the measured mean intercept width by the constant appropriate to the average shape. The number of times that a particle of this height should be intercepted by scan lines in the line array or raster in use is determined (to several decimal places). The observed intercept count is then divided by this expected number of intercepts per particle to give the equivalent number of average particles. While it is usually appreciably smaller than a true particle count, this number has several useful properties:

a. It has the same relationship to phase volume and mean free path or mean intercept width as it would if the particles were in fact uniform.

b. It will yield the correct phase interface area.

c. It overcounts clusters and stringers approximately in proportion to the number of particles which would result if such complex shapes were broken naturally into individual particles.

d. It undercounts particles smaller than average approximately in proportion to the decrease in size and is thus quite insensitive to the success of observing particles of minimum size.

Since very small particles make a negligible contribution to phase percentage even when present in quite large numbers, it is doubtful that small particles should be given much weight in evaluating variability of fields. Thus the effective number appears to be a better, or at least more conservative, base for statistical comparison than a true count.

Since technological opinion regarding possible adverse effects of second-phase particles generally regards the few largest particles as most important and the probable effect of small particles as negligible, this effective number has the generally desired weighting characteristics for a reproducible predictor of adverse effects.

Laminated or Fibrous Structures (Rating Index)

In rolled or drawn materials it is frequently desirable to obtain a quantitative index which indicates the severity of the laminated or fibrous nature of the structure. The parameter needed is one which indicates the variability between normal matrix metal and lines of lamination. Measurement of single particles or stringers fails to evaluate the structure as a whole.

A useful and reliable index of fibering or lamination may be obtained in the form of the standard deviation of the observations of a "slice analysis." For this analysis the field is sliced parallel to the longitudinal axis of the material to yield a substantial number of ribbon segments within which the percentage of the dispersed phase is separately estimated. To obtain a reproducible index it is necessary that the absolute length of the slices be pre-established at a value comparable to the longest individual particles, or disconnected but related strings of particles, encountered in the worst case and that the width of slices should be comparable to the mean thickness of the particles in the transverse direction.

In practice, it is sufficient that the percentage of second phase in each slice be estimated by either the percentage of points on phase along one line of a regular point raster or by the percentage of line length on phase for each line of a parallel line array, that is, by the total length of particles in each slice. The percentage obtained for each line, or line of points, is to be separately recorded, and the standard deviation of these percentages computed.

The relation of the slice index to the usual concepts of heavily weighting worst cases may be seen from the diagram, Fig. 3, which shows the index for various percentages of dispersed phase arranged in fully laminated structures

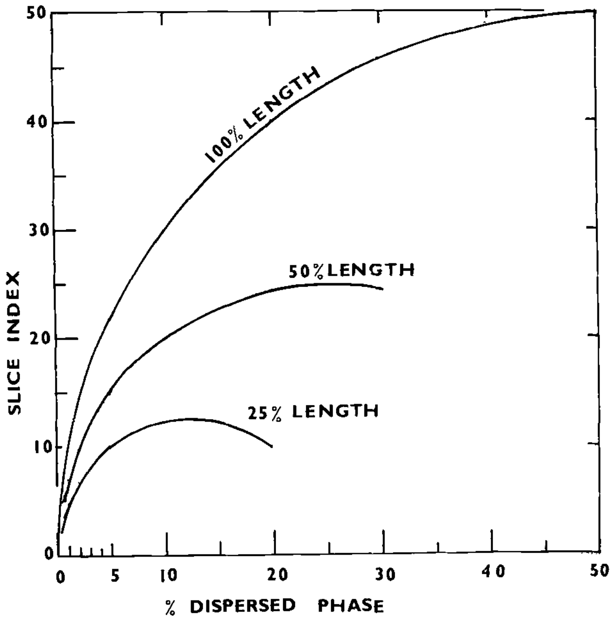

FIG. 3—*Slice index is sensitive to small percentage of dispersed phase.*

such that each individual slice yields a percentage of 100 (or 50 or 25) or is otherwise zero. This index will approach zero for a uniform distribution of circular sections at any concentration or if elongated particles are uniformly distributed into all slices or for a random distribution as the particles become smaller with respect to the length of the slices. The slice index appears to be the only appropriate quantitative measure of lamination which can be obtained by relatively simple calculation from either manual or machine observations and may be easily related to existing visual classifications, such as the number series of the JK inclusion charts of ASTM E 45, as in Fig. 4.

Laboratory Procedures

It is important that all procedures used in obtaining quantitative metallographic data be critically examined to ensure that (1) the metal to be rated is adequately and objectively sampled, (2) valid microscope images or photographs are obtained and that these are suitable for measurement, (3) the measuring method is accurate and unbiased, and (4) measurements are made in sufficient quantity that the data will be statistically reliable within the limits required for the purposes of the measurement. Failure to observe the necessary precautions at any step will in most cases cause the measurements to be without quantitative value.

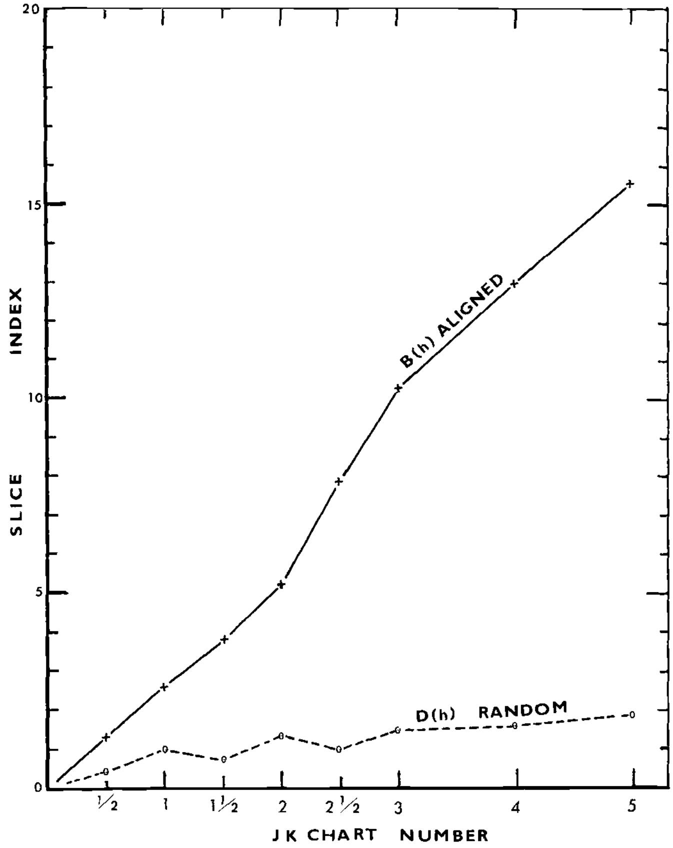

FIG. 4—*Relation of slice index to JK inclusion chart number.* (*Measurements on center 5 by 5-cm square of charts.*)

Selection of Specimens

Whenever a substantial volume of metal, such as a heat, is to be quantitatively evaluated, variations of structure and phase percentage may be confidently expected. Normally the presence of a gradient may be suspected. To distinguish a gradient in the presence of random variation at least five specimens should be taken. Typically, these specimens should be taken from the ends and midpoint of the supply and from two intermediate positions. If the stock is known or expected to be highly variable, additional specimens may be required. Supplementary information or close agreement may reduce the number of specimens required.

If the metal to be measured is expected to have an anisotropic structure, specimens showing two or three perpendicular planes should be taken at each location. Principle planes of the flow pattern are preferable to nominally random orientations.

Each specimen should have a usable section area of not less than 1 cm^2 unless this is prevented by the actual size of the metal sampled. Unusually coarse structures may require larger section areas to ensure that the full range of structure is represented. Macrographs or magnetic powder transfers can in general be treated in the same manner as micrographs.

Selection of Fields

In general, not less than five fields on each microsection should be examined and evaluated. For a valid statistical analysis, these fields must be objectively and blindly selected and should be taken at positions preselected to give representative coverage of the section. A suitable pattern consists of four fields at the corners of a square plus one at the center. This pattern is most representative if the four corner fields are about two thirds to three fourths of the radius out from the center. It is convenient to first center the stage and the specimen on the stage and subsequently offset the stage motion controls ± one-half radius to obtain the other four positions.

Where a best and worst field are felt to be necessary to adequately represent the range of structure in a section, such nonobjective selections should be accompanied by at least three fields blindly selected. A worse case inspection requirement means that all possible nonoverlapping fields of the section be examined and evaluated. A quantitative average of the section in this case requires inclusion of the data from all fields.

A visually selected representative field will in practically all cases be found to yield values which do not agree with the average of several blindly selected fields and, thus, may not legitimately to taken as a substitute for a representative group of blindly selected fields. The blindly selected fields should never be improved by small displacements before photographing or measuring.

It is not allowable to discard observations of a field because they appear to be out of line with expectation. More fields may be added, but not substituted, when evidence of unexpected variability is found.

Metallographic Methods

Specimen Preparation—Methods of specimen preparation must be such that the section plane is flat on both the gross and microscopic scale and that the size and shape of particles or other structural details are truthfully shown. In general, etching methods which outline the particles will not give valid measurements, since the position of the outline with respect to the actual boundary of the particle will shift with the extent of etching and will not be known. Such preparations are also unsuitable for machine measurement, since machines are usually unable to distinguish the inside and outside of outlines. Satisfactory preparation will result in showing the phase to be measured as a distinctly lighter or darker tone than the matrix or as a distinctly different color which may, by color filtering, be shown as a black-white contrast.

Several micrographs of the same Type 52100 steel prepared by different methods are shown in Figs. 5 and 6. Estimates of carbide concentration obtained from these microstructures vary from less than one half to more than three times the probable true values. It is evident that unsuitable preparation methods yield values of no quantitative significance. Electron micrographs of carbide particles in Type 52100 steel after several types of etching are shown in Fig. 7. Remembering that quantitative measurements must be made on a plane section, it can be seen that we require a preparation which reveals only the flat (slightly scratched) tops of the mesa structure shown in Fig. 7*a*. The sloping sides, which appear as dark rings in light micrographs are outside the true particle area in this example but intrude on the true area in some of the other etching methods.

The following basic procedure (for carbides in steel) may be adapted to other metals by suitable choice of laps, polishing agents, and reagents, following the methods found in ASTM E 3.

1. Grind the mounted specimen flat on an appropriate series of wet papers or on coarse laps.

2. Polish with diamond paste on thin cloth or on a wax wheel in accordance with ASTM Recommended Practice for Evaluating the Microstructure of Graphite in Iron Castings (A 247 - 67). Inspect the surface for scratches, hard

---

FIGURE 5

(*A*) Etched 0.4 percent picral 2.5 min (×2200). Circular polarized light shows mesa tops dark, slopes white. Estimated black tops about 3 percent, all tops up to 6 percent.

(*B*) Anodized; contrast enhanced by reversed negative on lithographic film (×865). Small particles and all in corners lost. A_{50} = 1.4 percent; $A_{\max}$ = 1.6 percent (estimated 2 percent with allowance for corners lost); mean intercept width (MIW) = 0.63 μm.

(*C*) Double polish, 0.08 percent picral 2.75 min, and Beraha stain (×1730). Light 4200 Å; A_x = 4.7 percent; MIW = 0.82 μm. (This photograph considered to be nearest to true value.)

(*D*) Same preparation as *C*, but with inadequate optical resolution (×2950). Fine carbides and edges lost. A_x = 2.4 percent; MIW = 0.63 μm.

(*E*) Same as *C*, but low-contrast print (×1730). A_x = 18.3 percent; MIW = 0.78 μm. (High area reading is result of counting light details in matrix as carbides.)

(*F*) Same as *C*, but with dark-field illumination (×1730). A_x = 27.1 percent; MIW = 1.68 μm. (High area reading is result of showing carbides too large.)

NOTE—Area and width values were determined for full-size (19 by 24-cm) prints, of which only a portion is shown. All measurements are from SADIE-III scanner except print *A*, which is not suitable for scanning.

FIGURE 6

(*A*) Double polish, 0.8 percent picral 3 min, and Beraha stain (×2200). Light 4200 Å; A_x = 12.1 percent; MIW = 0.624 μm. (Taken to be valid determination.)
(*B*) Etched 2 percent nital and Beraha stain (×4700). A_x = 23.6 percent; MIW = 0.704 μm. (Both overetching and inadequate resolution appear to contribute to high value.)
(*C*) Etched, concentrated Murakami reagent (×2200). Manual (L/L) black = 20.38, centers = 0.35, and total = 20.73 percent. Scanner (black only) A_{50} = 22.17 and A_x = 32.11 percent; MIW = 0.850 μm.
(*D*) Electrolytic etch, sodium picrate (×2200). Manual (L/L) black = 28.15, centers = 0.89, and total = 29.04 percent. Scanner (black only) A_{50} = 31.16 and A_x = 32.11 percent; MIW = 0.831 μm.
(*E*) Etched 45 s in super picral (×2200). Manual (L/L) black = 28.47, centers = 8.14, and total = 36.61 percent; manual (A/A) black = 29.64, centers = 9.29, and total = 38.93 percent. Scanner (black only) A_{50} = 33.56 and A_x = 32.81 percent.

NOTE—Prints *B–E* were contributed by members of ASTM Committee E-4, Subcommittee XIV. As the scanner could not determine the white centers of carbides *C–E*, these prints were manually measured at 1-mm resolution. For L/L, 36-line slices of 240-mm length were tallied with two real and two doubtful edge classes. Observed standard deviations of the total (from slice subsamples), in percent, are (*C*) S_o = 0.52 (K = 1.07), (*D*) S_o = 0.52 (K = 0.90), and (*E*) S_o = 0.66 (K = 1.01); but the nominal edge uncertainty is (*C*) 5.26, (*D*) 7.33, and (*E*) 6.79. The A/A value of *D* was determined from a 10 by 17-cm area counted in 170 blocks of 100 units each. The subsample standard deviation was S_o = 0.56 (K = 1.16) and the edge uncertainty was 7.16 percent. Nominal edge uncertainties for scanner blacks are (*C*) 0.31, (*D*) 0.39, and (*E*) 0.58 percent. The theoretical volume of carbide at 1 percent carbon by weight is approximately 15.9 percent, but some carbon remains unprecipitated after spheroidizing.

FIGURE 7

(*A*) Light superpicral etch shows true mesa shape. Residual scratches show flat polished sections of carbide unattacked (×19,500).
(*B*) Heavier superpicral etch excavates ditch around carbide (×19,500).
(*C*) Double etch (electrolytic chromic acid and 15 percent nital) attacks carbide and may remove some (×19,500).
(*D*) Electropolish (acetic-perchloric acid) and 1 percent nital etch rounds carbides, obliterating edge of polished section (×8650).

particles pulled from the matrix, smearing of voids, or embedding of polishing powder and repeat or change practice if necessary.

3. Etch this surface by immersion in a reagent normally suitable for this metal, developing the structure to a normal extent and removing all metal disrupted by polishing. Again inspect for evidences of unsatisfactory polish and repeat from intermediate grinding if necessary.

4. Repolish on the finest usable diamond lap until the etched structure is totally eliminated. Inspection should now show a featureless plane surface. If it is suspected that relief polishing may have occurred, recourse may be had to use of an optically flat, glass test plate or to an interference microscope,

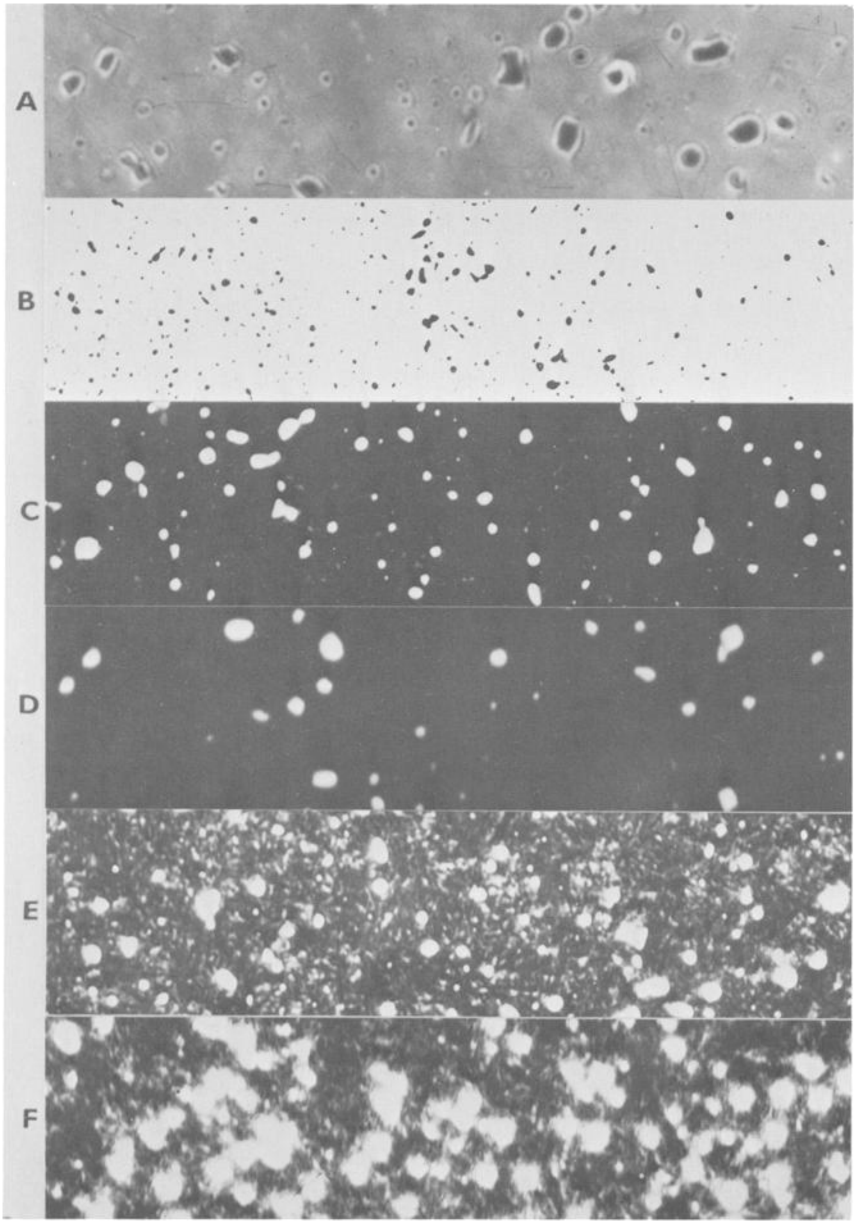

FIG. 5—*Effect of metallographic variables on apparent carbide content of 52100 gage block (T-556, hardened).*

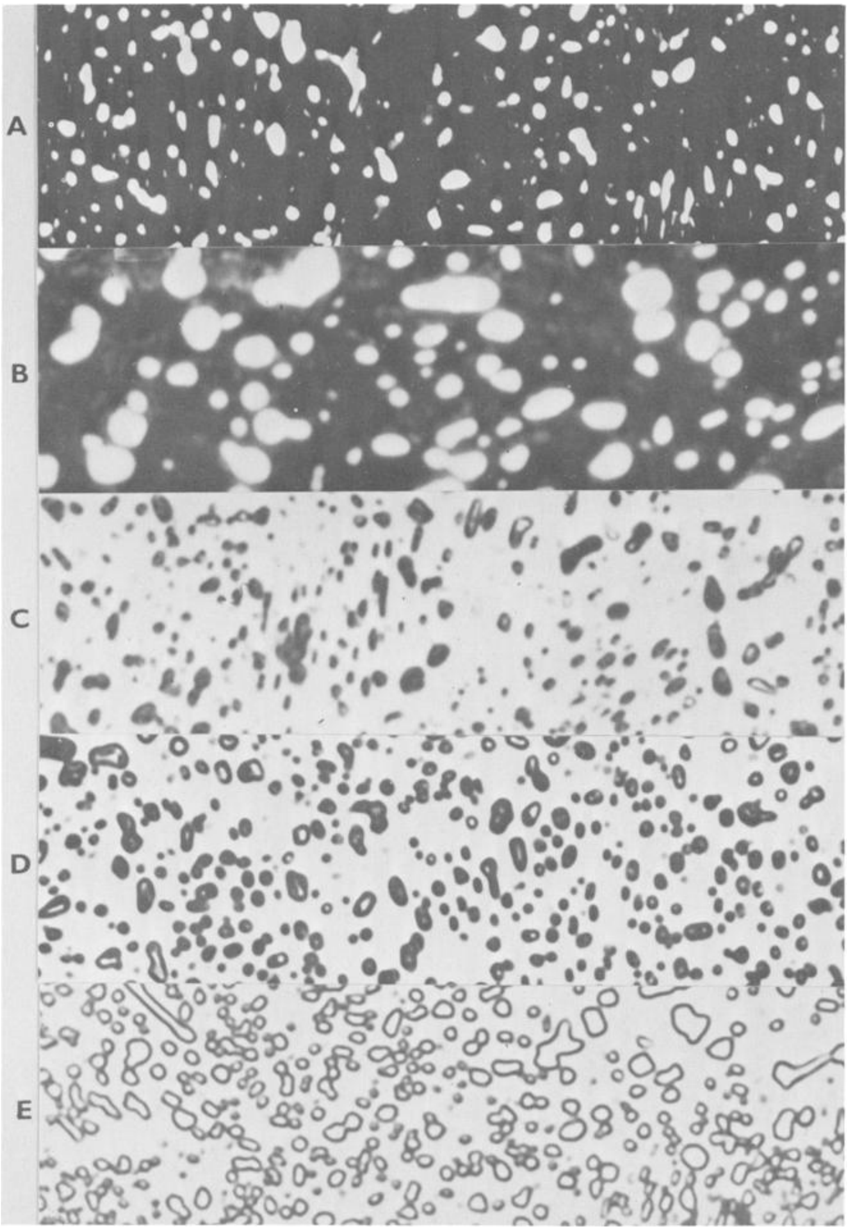

FIG. 6—*Effect of metallographic variables on apparent carbide content of 52100 round robin specimens.*

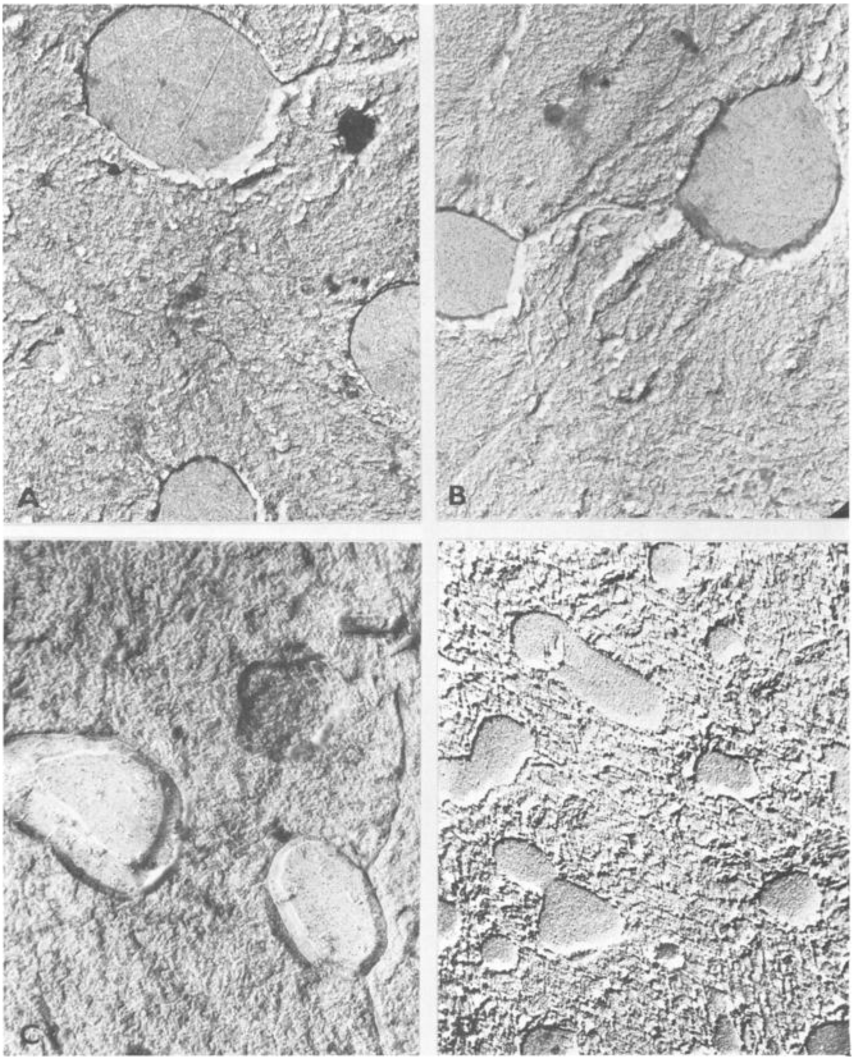

FIG. 7—*Falsification of carbide representation by etching—5211 gage block steel (electron micrographs by D. B. Ballard, NBS).*

inspecting to see that the diffraction fringes do not indicate details on the scale of the microstructure.[5]

[5] Electrolytic polishing has not been recommended since it commonly produces a nonflat surface. Where electrolytic polishing is the only applicable method, the interference test should be considered compulsory before this polishing method can be considered acceptable for quantitative purposes.

5. Prepare a very dilute solution of an etching agent appropriate to the metal and in this, by immersion, slowly remove the very thin polishing film resulting from step 4. (Example: for steel dilute 4 percent picral with 50 volumes of alcohol and etch for 2½ to 3 min.)

Microscopic inspection at this stage in ordinary light should show only a faint suggestion of the structure unless one phase is colored or consists of nonmetallic material or voids. Inspection by plane or circularly polarized light will frequently reveal the phase structure and permit determination of the minimum etching required to remove the polishing film. A structure clearly showing outlines in ordinary light must be considered overetched.

6. Either the phase to be measured or the matrix should now be darkened or colored by one of the following methods or by an equivalent procedure which does not generate a relief structure.

For steel:

a. A staining reagent (such as Beraha's reagent [9]).

b. Heat tinting.

For other metals:

c. Anodizing to develop a surface layer giving an interference color (Picklesimer method [*10*]).

d. Anodizing with dye absorption in the active anodized film.

e. Direct dye or strain absorption (generally applicable only to nonmetallic phases).

f. Vapor etching as with iodine vapor or dilute hydrogen sulfide (applicable to copper, silver, etc., where colored or dark tarnish films are easily formed).

g. Where no satisfactory staining method can be found, recourse may be made to circularly polarized light, although exposures will tend to be excessive at high magnification. Where this is not applicable, recourse may be taken to the scanning electron microprobe or scanning electron microscope.

Microscope Practice—The field to be measured may be evaluated directly on the microscope by use of eyepiece reticules or of point nets or line arrays ruled or etched on the ground glass or by electronic equipment in which the sensing head is attached to the microscope. Alternately, the field may be photographed and measurements made on the photographic negative or print by either manual or machine methods.

Magnification of field—Most precise results for any system and material will be obtained by use of magnification such that the actual errors of measurement and the statistical error in sampling with respect to the mean of the material are approximately equal. The best magnification thus varies with the measuring system as well as the material and should in the end be determined by separate analysis of the two types of uncertainty. The best magnification will in general be neither the highest nor lowest obtainable. As a point of departure, a magnification such that the mean intercept width of dispersed particles falls within the range of 1 to 5 percent of the field width will in general be found acceptable. Lower magnifications, giving better statistical sampling, are indicated as the precision of the measuring process improves, at lower percentages of dispersed phase, and where the field is taken to represent larger volumes of metal.

Resolution and microscope settings—It is the nature of any optical system to represent a point of light as a diffuse area or zone of confusion, which zone is ideally circular for a single point source. The distribution of light intensity over this zone is approximately Gaussian; hence its diameter depends on agreement on the fraction of the total light to be included in the zone. It will be apparent that the width of the zones of confusion around images places a limit on the accuracy with which any quantitative measurement can be made. For visual measurements it is allowable to permit one-half stop error in tone, thus, to consider a zone which contains 70 percent of the light originating at the point, with about 5 percent spill into each nieghboring zone. The radius of such a zone is approximately one standard deviation of the light distribution curve, and the diameter roughly the separation distance of a distinguishable line pair. Precision machine scanning may require or justify greater accuracy in light evaluation, in which case the zone of confusion must be considered to be larger.

It is customary to define the resolution limit of a lens as equal to $\lambda/2$N.A., this being the spacing, on the original object, of two distinguishable black or white lines. The radius of confusion of an ideal lens in representing the edge of a particle is thus nominally $\lambda/4$N.A. Objective lenses of the highest quality will in some cases come close to yielding this resolution, but the confusion distance will generally be larger than for an ideal lens.

For accurate quantitative measurement, the confusion distance on the final image to be measured should not be greater than 0.25 mm for visual processes or greater than the raster unit of an automatic scanning device if this unit is smaller. Magnifications giving a larger confusion distance are referred to as "empty magnifications" and contribute no additional precision of measurement but sacrifice statistical representation.

Since the resolution of the best microscope objectives is generally greater than that of available ocular or projection lenses, it is generally desirable to use the highest power objective capable of yielding the desired final magnification, coupling this with the lowest possible ocular power and the maximum feasible projection distance. If objectives corrected for infinite tube length are available, the ocular or projection lens may sometimes be omitted from the system. These classes of optical systems additionally favor flatness in the final image and production of a maximum usable field area.

To allow full resolution, the optical system must not be stopped down. Inadequate depth of focus should be corrected by better specimen preparation.

Monochromatic or narrow band blue light should be used whenever possible. Objectives are most completely corrected at a specific wavelength, which should be used if known.

The approximate magnification having been chosen to give a satisfactory apparent particle size, an exact magnification should be established which is convenient for obtaining true object sizes from measurements on the image. For visual measurements using a millimeter scale, ×100 and its simple multiples are most convenient. For machine measurements using a raster unit of 0.25 mm, a magnification of 250 gives measurements directly in micrometers (μm) on the specimen. An engraved stage micrometer (adequately calibrated or certified) should be used to establish the exact magnification. Micrographs of such a micrometer should be processed with each batch of photographs to be accurately measured.

Photographic Practice

Measurement of photographs avoids tying up a microscope for long periods for manual measurements, permits rechecking when desired, and permits some improvement of tone values or the distinction of phases. While bias can be introduced by poor practice, data from photographs are not necessarily less accurate than data taken directly from the microscope image, Negatives and prints on film base are somewhat more stable dimensionally than paper prints. Negatives are normally more accurate and have somewhat better resolution than even the best prints.

While it is feasible to measure several phases in the same micrograph, the accuracy of such measurements is substantially lower than when only black-and-white areas are shown. It is therefore usually desirable to increase the contrast of the image to fully utilize the tone scale of available photographic materials. To this end, practice will differ from that customary for showing detailed variation in structure in the direction that

1. A harder or slower film or plate will be used, usually a process or lithographic type.
2. Exposure will be shorter than normally recommended.
3. Development will be longer than usual or a harder (or clean working) developer will be used or both.
4. The negative so produced will be clear or very thin in the shadow areas, and some features may be deliberately below the exposure threshold. The highlights should be dense (density $\sim$2) but must not be overexposed. Halation resulting from overexposure, along with the zone of confusion from inadequate resolution or improper focus, will, under high-contrast processing, result in enlarging those areas which are white in the subject, thus biasing measurements of this phase upward. Such halation should not be tolerated.

Contact Printing—It has been found that when negatives are printed by contact using printers having a diffuse or multiple-lamp light source, the black areas of the print are significantly larger than the clear areas of the negative. Such printers are not suitable for use in quantitative microscopy. If a contact print is required, it should be obtained from a printing box having a single source of light located approximately 1 m from the working surface. Alternatively, the print may be made in a frame exposed by the light from an enlarger.

Enlargement—Manual measurements are most conveniently made on prints or negatives approximately 8 by 10 in. in size (19 by 24-cm image area). Enlargements in the range of ×2 to ×5 can be made on high-quality equipment without loss or falsification of information in the negative. To preserve adequate resolution in enlarged prints, however, the microscope objective must have originally been selected to have a numerical aperture adequate for the final print magnification. The entire negative should be printed without masking, or, at a minimum, it must be certain that the portion printed is not visually selected.

Print Processing—To utilize the full tone scale of the printing medium it will frequently be necessary to use sensitive paper harder than normal (No. 4 or No. 5). Exposure must be established to avoid any halation at edges and may be reduced to suppress unwanted detail in the matrix when the matrix is to be printed white. (The reverse tone situation is more hazardous.) Print development should be full and uniform—generally from 1.5 to 2 times the minimum time indicated by instruction sheets. All prints in a series should be processed in as nearly an identical manner as possible, paying particular attention to identical treatment in the print drying process.

If particle size or spacing is to be determined, at least one micrograph of the engraved stage micrometer should have been processed with each batch of negatives, which negative should be printed at the same time as the micrographs in the batch, and used to determine the final magnification of these prints. The magnification along the transverse and longitudinal direction of the final prints will normally be different; hence, if size measurements are to be made in both directions, two micrometer negatives are normally required. It will be apparent that the calibration obtained from a micrometer negative will not be valid if either the microscope settings or the enlarger settings have been changed within the batch.

Measuring Methods

Area

Manual and machine measuring methods are the same in principle and should in general yield comparable parameters expressed in dimensions on the actual specimen (normally μm). Machine methods are less laborious, generally faster, and usually more economical and give a statistically more reliable value. A machine is not necessarily more accurate than visual methods with respect to possible bias. Present machine methods of identifying and measuring individual particles are generally cumbersome and are not superior to manual methods when the number of particles is small.

Nature of a "Point"—A major portion of quantitative micrographic methods are in theory based on observing and counting points. It must be noted that neither a human nor electronic observer can actually observe a point; thus, that observation is in all cases one of a finite circle or square which can never be smaller than the circle of confusion of the microscope system or the effective resolution unit of the observing system. Ignoring this limit will generally introduce observational errors which more than balance the statistical advantage to be gained. The practical area of a point observation will be referred to as a "raster unit" and the distance between the centers of observed units as the "raster spacing."

Point Nets—Phase percentages are commonly determined by point counting over a point net superimposed on the micrograph or image. To avoid bias the net must be located without reference to visual observation of the field to be measured. No particular form of net pattern has any demonstrable superiority with respect to statistical precision or possible bias. Rectangular or square nets are generally more convenient for both visual and machine methods, but other patterns are acceptable when convenient, provided they sample all parts of the field equally.

Open nets—An open (or coarse) net is one in which the raster spacing is large compared with the raster unit. Open nets are commonly used for visual point counting at the microscope and have the advantage of statistical efficiency, since a large area of the specimen must be observed to obtain a useful number of point observations. Phase identity is tallied at the intersections of grid lines.

Nets used in the eyepiece are usually counted inaccurately if more than about 25 points appear in one field. Since many applications of such a small net are necessary, available devices to automatically shift the field are helpful. It is difficult to locate a small net objectively without use of a device immune to the whims of the operator. It may be noted that, if a habit is developed of always placing a certain point on phase, the apparent percentage of this phase will be biased upward by amounts as great as 4 percent for a 25-point net.

Open nets used on the ground glass may reasonably contain from 500 to 2000 points. The 500-point net formed by 20 and 25 lines at 1-cm spacing can be completely contained within a nominal 8 by 10-in. image area. A 5-mm net is appropriate to the 4 by 5-in format or for more precise measurements on 8 by 10-in. images. Finer nets are prone to miscounting in manual use and require more labor than a line array of equal precision. Objective placement is reasonably assured if the net is not visible when the field is centered and focused. The net should be applied to the predetermined field by mechanical means, as by substitution of the ruled ground glass after focusing.

Multiple application of an open net to the same field is not efficient, as repetition of previously used positions will normally occur after a few trials. As in all redundant measurements a false appearance of reliability will be obtained. The open net should always be applied to a continuing series of new fields until a statistically satisfactory number of points have been observed.

Fine Nets or Rasters—A fine net is normally one in which the width of the raster unit and the raster spacing are the same. Fine nets are normally used in machine methods. A regular fine net is commonly called a "raster." A raster collects all of the usable information in an image and thus delivers the highest possible statistical precision. Very small particles, which might be ignored when using a coarse net, will be included in the analysis. If each particle is hit by 1 to 12 raster points, the raster can be regarded as a fully efficient sampling device, but when the particles are significantly larger observations become redundant and the statistical efficiency decreases. Some loss of efficiency is acceptable in machine methods as a necessary cost of maximum accuracy.

Scanning machines normally average the light intensity over the raster unit and either compare this average with a binary threshold preset by the operator or assign one of several predefined tone values, permitting the point to be subsequently assigned to one of two or more phases or to an edge position. Fine nets may be used manually, usually by overlaying translucent graph paper on the print or negative on a light box. Such nets are frequently counted by evaluating squares rather than the crossing points of lines. Squares to be counted are usually marked on the graph paper. There is no theoretical difference between square counting and practical point counting, but slightly different values will usually be obtained. The squares used should be the smallest which can be rapidly and efficiently evaluated by the operator. Most operators find 2 or 1.5-mm squares satisfactory, while some can effectively use 1-mm squares. It is not efficient to try to visually evaluate any square closer than on phase, off phase, or doubtful (edge). If the fractional occupancy of squares is being rated, equivalent accuracy can be attained with less effort by using a finer net.

Fine nets used manually involve an effort which is seldom justified by obtaining phase percentage alone. Such nets should be tallied by subareas of 25 to 100 squares or by line slices, to permit calculation of variability within the field, or tallied as a lineal analysis.

Counting Methods for Area—All points (or squares) indicated by the applied net are counted and are tallied in three classes:

1. Points certainly within the dispersed phase particles (black points, P_1).
2. Points certainly within the matrix phase (white points, P_2). This count may be obtained by difference when the total of the net is known.
3. Uncertain or doubtful points (P_3).

One half of the count in Class 3 is then added to the actual count in Class 1, which when divided by the total of all points gives the phase fraction of this sample:

$$P_{\phi_P} = \frac{P_1 + 0.5\ P_3}{P_1 + P_2 + P_3}$$

Phase percentage = $100 \times P_{\phi_P}$.

Points in Class 3 arise from two causes. The most common doubtful points are those which fall within one resolution unit (raster unit) of the edge of a particle or which fall in the indistinct zone if the image is not completely sharp. The arithmetic may be simplified by counting such doubtful points as certain when they are at the top or left edge of a particle and ignoring them when at the bottom or right edge. Other doubtful points occur when the structure is not distinct and the tone at the net point cannot be observed with certainty or if some particles are smaller than the raster unit. The half-weight rule here does not completely guarantee an unbiased result, and a more suitable image should be used if possible.

An electronic system frequently uses a third method of disposing of doubtful points, counting or rejecting these as they yield more or less than 50 percent of the maximum signal intensity. This method is not practical in manual operation.

Bias Errors in Observation—The term "bias error" is used here in specific contrast to statistical variation, as in the examples of relief polishing, over-etching, etc., already noted. It is most important to note that, while increasing the number of observations will gradually reduce the statistical error of the final determination, such increased effort has no effect in reducing the error due to bias in either specimen preparation or observation.

It has been frequently found that two human observers using the same method will not only report different measurements but that one observer will also consistently report higher values than the other. Thus two humans do not necessarily see the same thing. One may see and count only areas which are in fact black, while the other may see and count areas which are not white. These are not the same. Other than by use of external standards it cannot be said which, if either, observer is actually correct. More distinct images and rigorous treatment of doubtful points will, however, reduce the disagreement.

Machine classification of doubtful points, primarily raster units at the edges of particles, is subject to the same kind of error as visual observation.

Basically, all signals whose levels are not clearly black or white (between 10 and 90 percent) are doubtful. Where the decision to count or not count can be set anywhere in this range, the count can include all or none of the edge units or any portion between. An objective method of adjustment to count one half of the doubtful units, or the equivalent, is clearly necessary if the accuracy is expected to be better than that of visual judgment.

Two methods of objectively controlling a machine decision are

1. A_{50}—*50 percent signal method*—If the machine is provided with a decision level or signal level scale divided from 0 to 100 and with supplementary contrast (gain) and brightness (base line) controls, the latter should be adjusted for each subject to give a signal of 100 on the brightest portions of the image and of zero on the darkest portions. Setting the decision control at 50 should now result in a correct count if the image is sharp and of uniform tone range and the control calibration linear.

Where only a single control is provided, this setting method can be approximated, but with reduced accuracy. In the commonly available vidicon scanners, nonlinearity near the ends of the light response scale prevents finding 0 and 100 percent settings, but scale readings can be determined, for example, for 98 percent light and for 2 percent of the estimated fraction of dark phase. The midpoint between these end settings is reasonably reproducible, provided other circuit parameters do not change, but is not necessarily the true 50 percent position, as the vidicon response is not linear.

2. A_X *differential cross method*—The input resistance to an amplifier stage in the machine video circuit may be shunted by an optional capacitor connected through a switch. With this connected the time derivative of the signal will be added to the actual tone level, in effect anticipating the tone of the next following raster unit and basing the count decision in part on the left side only rule. The decision level at which the same count is obtained with and without the differential circuit is a valid objective level which will correspond with the A_{50} decision, provided the image is sharp and truly black and white. When the image is less than perfect, the A_X decision level will shift away from A_{50} in the correct direction to compensate for image imperfection [*11*].

Limiting values—A_{max} *and* A_{min}—If a structure contains a portion of the dispersed phase as very small particles which are not fully resolved in the image (or, if resolved, are smaller than one raster unit), these particles will not appear to be either black or white but will be seen as a gray tone. Visual observation on the black or white criterion will ignore such particles, while observation on the not white or not black basis will include them but overvalue their area. The latter is similar to machine counting with the decision level far from the center of the tone scale (say at 10 or 90 percent signal). Under these conditions all doubtful points, both at the edges of large particles and on the diffuse areas of the small particles, will be counted, and the raw count will be high by one half the number of doubtful points. With a machine the number of doubtful points (or the number of intercepts, which is equal to half the doubtful points) must be separately determined, and the proper subtraction from the raw count made. In visual observation if all edge and gray points are tallied in Class 3, nearly correct evaluation of the maximum area including the small particles should be obtained.

Similarly, in machine operation, the decision level may be set close to the opposite end of the light intensity range so that only those points certainly within the particles (P_1 class) are counted. The number of intercept points is then separately determined and added to the low P_1 count to yield a minimum area $A_{\min}$. Knowledge of the limiting values $A_{\min}$ and $A_{\max}$ and of the position of the presumed true value between them is helpful in judging the magnitude of the bias error which may exist in the presumed true value. A true value close to the center of the possible range is expected if unresolved fine particles are absent.

Lineal Analysis

Lineal analysis is the generally applicable method for determining both phase percentage and the dimensions of particle sections on the plane of examination. No test line is in practice infinitely divisible; hence a line must properly be regarded as a finite row of equal resolvable units or of points representing areas no smaller than the raster unit discussed under point counting. For visual observation it is generally not profitable to consider increments shorter than 1 mm, but units as short as the radius of the zone of confusion of the microscope (~0.25 mm at the image plane) can be observed photoelectrically. Line lengths of 100, 200, or 250 mm are generally useful for visual observation. Metric units should be used in all cases.

Line Arrays—Data for the analysis are obtained by measurements along lines of a line array.

Curved lines—These cannot be recommended except for rough measurements where the discrepancy between the length of an arc and its chord can be ignored. Use of a circular pattern for number of intercepts only, in combination with a point count for phase percentage, is highly inefficient. A target pattern consisting of several concentric circles having a known total circumference has found considerable favor in estimating grain size in single-phase materials. This device should be calibrated against standard charts (ASTM E 112) to correct for the fact that the intercept count will be low by amounts which vary with the actual grain size.

Array patterns—Since a single line randomly and repetitively applied to an image overweights the central area, a fixed array of lines which sample all parts of the image equally is definitely to be preferred. Generally a parallel array of equally spaced lines of equal length is most representative. The line spacing may conveniently be 0.5 to 1 cm at the ground glass. The same precautions as described for objective placement of point nets must be observed. For anisotropic structures the parallel array should be applied to the image twice, once in each principle direction, and the data separately recorded.

For negatives or prints the use of a translucent overlay, as suggested for square counting, is effective. If the occupied squares are already marked, each row may be rescored as a line. Where statistical requirements permit, it is preferable to observe every second or even every fifth line of a 1-mm net rather than using a coarse net.

Linear analysis via the eyepiece—This cannot be effectively accomplished by use of a graticule or by a micrometer eyepiece, although these devices are effective for measuring individual (and exceptional) particles. A single point defined by two cross hairs in the eyepiece can be transversed over the image by use of a device which moves the stage in a slow and controlled manner. Such devices usually include tally registers in which the intercepts and line length in various phases may be automatically counted. Automated versions in which the test point is photoelectrically observed are also made.

Counting Methods—For a complete lineal analysis, the length of each line intercept through each particle of the phase to be measured should be separately tallied (thus automatically tallying the number of intercepts) and the tallies for each test line separated. From these tallies both the distribution of intercept widths and a slice analysis can be computed. The ratio of the total of intercept widths to the total length of the test line, L_L, yields the phase percentage. For determining average intercept width and phase percentage only, it is sufficient to record only total length in phase and number of intercepts. Such summation line by line—necessary in the visual method—still permits the slice analysis.

In the opposite extreme, the elementary Heyn measurement of grain size requires only counting intersections of grain boundaries with the line array, for which the 1-cm square ruling is entirely satisfactory.

Decision rules—It is not profitable to attempt to determine the length of any single line segment closer than one unit on the chosen scale of observation. Thus the line should be examined millimeter by millimeter, and each unit either counted or not counted according to the same considerations that apply to the point net, but without doubtful scoring. The decision may be determined either by (1) counting all fractional units at the beginning of the intercept and ignoring all fractional units at the end or (2) counting all fractional units over one-half unit. No significant discrepancy should be found between the two rules.

End of line rule—If the first point on the first test line falls on phase, it is scored as an intercept and the (shortened) line segment tallied as a normal segment. If the first point on any subsequent test line falls on phase, this point is counted as an intercept only if the last point of the previous line fell off phase. If this last point fell on phase, the length count is continued on the next line and added to the segment from the previous line for purposes of tallying an intercept width (but not for a slice analysis). No intercept is counted. This rule compensates for a bias toward low intercept width which otherwise occurs when one test line does not cover a large number of particles. The effect is to treat all test lines as segments of one continuous line.

Combination of Methods

A dense raster may with equal validity be regarded either as a fine point net or as a closely spaced line array. The distinction in this case becomes arbitrary, being based only on the logic and arithmetic used to analyze the point observations. It is most desirable that automatic systems be instrumented to yield numerical results in the characteristic forms for both the point and lineal methods.

Accuracy and Precision of Measurement

Since quantitative metallographic values are based on statistically small samples representing a large volume of frequently variable material, they may in no case be regarded as exact values. Usefulness of the values determined depends on reliable estimation of their accuracy and precision with reference to the actual mean values for the material sampled. Actual variability of the material is itself an important factor in quality control; hence the reliability in the determinations for individual fields and specimens should be sufficient to permit separation of actual variability of the material from uncertainties of measurement.

For any proposed application, it is necessary first to make an *a priori* estimate of the anticipated precision and, if inadequate, to increase the planned measurement program. When sufficient data have been obtained, the observed precision values should be substituted for the *a priori* estimates and the measurement program revised if necessary.

The principle errors and uncertainties which may be separated are:

1. Error or bias in representation of the local volume or the section by the optical image or photograph.
2. Error or bias in observation of doubtful points on the image or photograph.
3. Statistical uncertainty in sampling the image by the net or line array.
4. Statistical uncertainty in sampling of the specimen by the selected image field, or real variation between fields.
5. Variation between specimens taken at different locations in the mass of metal.

Error Factors (Accuracy)

The accuracy of the image or photograph is primarily dependent on use of an appropriate and reliable metallographic technique. The probability of error can usually be detected by critical examination of the image at high magnification, and the sign of probable bias can usually be predicted. The amount of possible bias is not exactly predictable but may be estimated as four times the ratio of the width of a doubtful zone to the particle width, and thus may be very large when the particles are small. The actual accuracy of the image can be firmly established only by comparing the mean of a substantial number of determinations with an analysis by an independent method or by identical preparation and measurements applied to an established material standard of similar nature.

Bias Errors—Bias errors in observation of a field are primarily due to the doubtful points on the observing net and are proportional to the fraction of such points in the total of net points and to the uncertainty of the decision process. In visual counting of a net the Class 3 tallies of points judged doubtful will vary substantially between observers and hence are of little value in predicting possible bias. However, in the lineal analysis of an image which is sharp as compared to the raster unit, the number of doubtful points is by definition twice the counted number of intercepts.

It is convenient to estimate the possible observational bias error in terms of the number of intercepts rather than the number of doubtful points. In the form of an estimated standard deviation,

$$S_B = (K_M \times P_i)/P$$

in phase fraction (absolute) or ×100 for phase percent. P_i is the number of intercepts and P the total of points on the net or of resolution units in the line array. The factor K_M is a fractional number characteristic of the observing method, basically the fraction of the light intensity or tone range over which the observations must be considered doubtful. For an average human observer, K_M is of the order of 0.5. Where electronic equipment is standardized by visual observation of a regenerated image, K_M cannot be expected to be smaller than in direct visual observation. With an electronic observing unit whose signal level has a standard deviation less than 1 percent, a K_M value of 0.05 is attainable for a sharp and uniform image.

It must be emphasized that the effect of a biasing error cannot be reduced simply by increasing the number of observations or by multiple determinations with the same decision threshold. The magnitude of the real observational error may be estimated by repeated measurements using the same net placement on the same field, each time allowing the decision threshold to vary within the reasonable limits of the system.

As the observation error is proportional to the fraction of points which are intercepts, it can be reduced by refining the raster unit to the limit set by microscope resolution or by using a higher magnification, thus obtaining a larger fraction of certain observations. This however runs contrary to statistical efficiency, hence a compromise relation between raster spacing and apparent particle size (intercept width) is always required.

Statistical Uncertainty

Sampling of One Image—Given an ideally perfect image and observing system, the anticipated standard deviation in the count of net points on phase (P_ϕ) would be given by the Poisson standard error of counting

$$\sigma_{P_\phi} = \sqrt{P_\phi} = \sqrt{pP} \qquad \text{(ideal)}^6$$

Use of the alternate binominal rule would give a slightly lower value near 50 percent of phase, which may be valid for a true binary system.

Since the image and the observer are never perfect, the ideal σ_{P_ϕ} is never attained, and the real standard deviation is greater:

$$\sigma_{P_\phi} = K_S\sqrt{P_\phi} = K_S\sqrt{pP} \qquad \text{(real)}$$

where K_S, the system constant, is always greater than 1 and frequently of the order of 3 to 5. The standard deviation of determinations of phase percentage thus becomes

$$\sigma_{\phi\%} = 100\, K_S(\sqrt{P_\phi}/P) = 100\, K_S(\sqrt{p}/\sqrt{P})$$

For a line array or a fine raster, information theory indicates that the contribution to K_S due to redundancy of observation (statistical inefficiency) may be estimated by allowing that each intercept contributes no more than four independent observations (the position of two edges and identification of each as entry or exit). This reduces the effective value P_ϕ^* of P_ϕ to

$$P_\phi^* = 4\, P_i$$

from which

$$\sigma_{P_\phi} = 2\, K_S\sqrt{P_i}$$

Since the effective total of all points is reduced in the same proportion, the smaller value of σ_{P_ϕ} is not a benefit but must be interpreted in the relationships:

$$\sigma_P = (0.5\, K_S/\sqrt{P_i})p$$

or

$$\sigma_{\phi\%} = (0.5\, K_S/\sqrt{P_i})\phi\%$$

---

[6] $p = P_p = P_\phi/P$.

The residual value of K_S will however be nearer unity than it was before the redundancy factor was treated separately.

Combined Uncertainty of One Image—Taking the statistical uncertainty just described and the observational edge error σ_{P_ϕ} as the principle causes of uncertainty in measuring one image, it is apparent that these have opposite trends with apparent particle size at the image plane and, thus, with magnification. Figure 8 shows a construction diagram useful for determining the best apparent particle size and an *a priori* estimate of the probable uncertainty (as σ) of the determination. Values were computed for 50 percent of each phase; the binominal equation was used.

The statistical ideal and redundancy effect in large particles is shown for two dense raster arrays, (*A*) 1000 by 1000 lines, appropriate to a precision mechanical scanner [*11*, *12*], and (*B*) 200 by 200 lines, appropriate either to the use of 1-mm graph paper manually or to a vidicon television microscope. The edge error, hopefully without persistent bias, is shown as 3 lines, *1*, *2*, and *3*, as fixed fractions of the intercept count at various particle sizes. Line *3* is appropriate to visual judgment and a visually standardized television image. Line *2* is regularly attained by the writer with sharp paper prints, using objective standardization of the mechanical scanner, and slightly bettered with negatives. Line *1* is a theoretical, and unobtained, ideal limit.

The combined effect of error lines *1* or *2* with statistical limits *A* or *B* is shown by the saddle-shaped curves. Both the predicted standard deviations and the best particle size decrease at lower concentrations of the measured phase. Figure 9 shows the *2A* curves at various concentrations for a 19 by 24-cm raster at 0.25-mm resolution. Many points on this chart have been realized in practice, and uncertainties only about three times as great have been realized by a skilled visual observer using a 1-mm net on the same images.

Estimation of Actual Variability

As has been previously noted, we are attempting to determine values for parameters such as phase percentage and particle size characteristic of a substantial universe of metal, such as a heat, from limited measurements on a limited number of sample surfaces. This universe has real variability of composition and structure on both macroscopic and microscopic scales, and we normally wish to estimate these variabilities. The problem is further compounded by statistical variations in the measurements and by real errors in observation or in specimen preparation.

Such a system may be statistically classified as a problem of "nested" universes from which we have obtained nested samples, a problem treated by Wernimont [*13*]. Full analysis of the several components of variance and proper estimation of confidence limits on the material mean are beyond the scope of this paper. It should, however, be noted that customary corrections

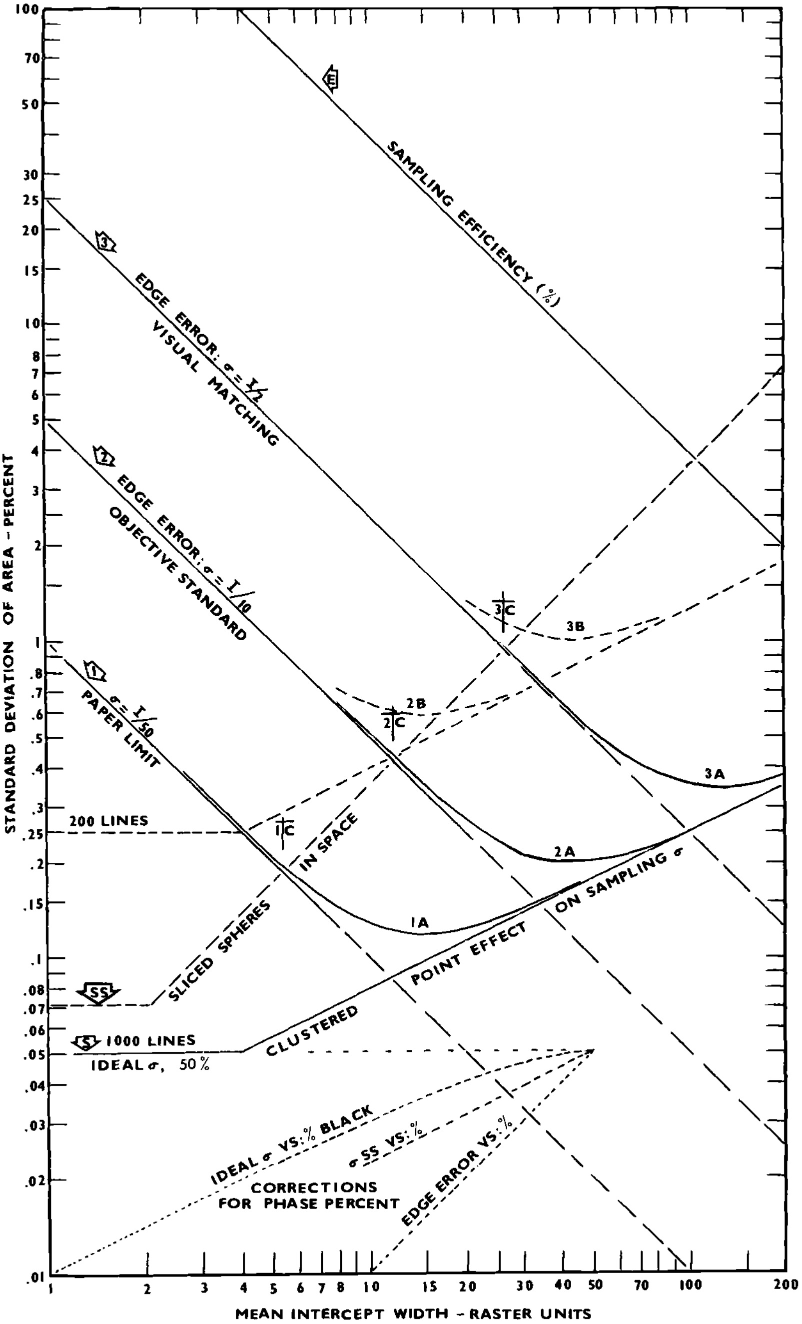

FIG. 8—*Curves for estimating expected precision of area measurement for various micrographs and scanning conditions.*

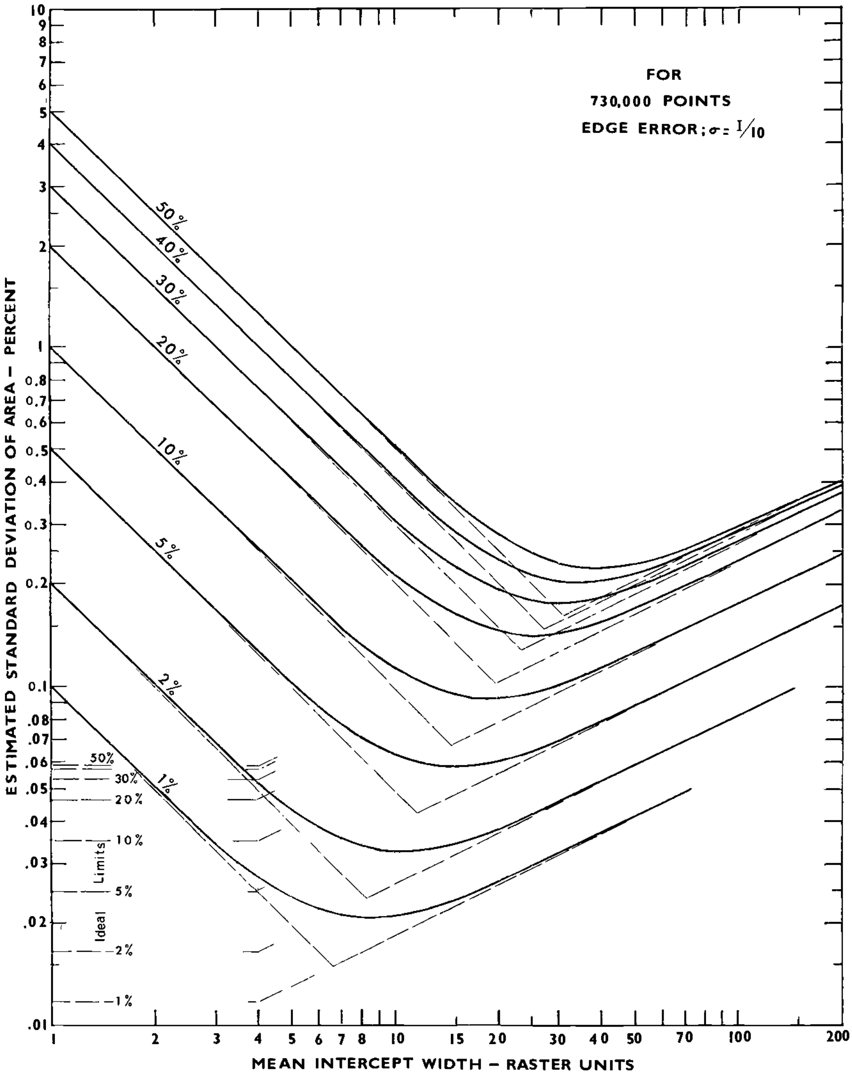

FIG. 9—*Curves for estimating expected precision of area measurement for 760-line (8 by 10-in.) micrographs having various actual phase areas.*

for small sample size do not correct for multiple sources of variability. Thus, if two or more of the components of variance are of significant size, a standard deviation and resulting confidence limit computed in the usual single universe manner will normally be too small, and often far too small.

The present discussion will therefore be confined to approximate estimation of the factors of variability in cases where one factor is large compared to all others. Typically this applies to the common case where there is a substantial composition gradient in the material to be rated, sufficient measurements are made on each field, and sufficient fields are measured that the uncertainties at these lower levels are relatively small. In the opposite case of very limited observations, the characteristically high uncertainty will be disclosed but the actual material variability will not.

For the purpose of providing working numbers it has been found convenient to calculate, at each level, the simple uncorrected variance of the nest of observations about their own means:

$$V_o = \overline{x^2} - (\bar{x})^2$$

the x values being individual measurements at the lowest level and the averages of balanced sets of measurements for the larger nests. The square root of this estimate, $S_o = V_o^{1/2}$, is in the form of a standard deviation and may be compared with *a priori* predictions at the same level. These estimates are used primarily to determine whether sufficient data have been accumulated to permit observation of variability at the next higher level.

The V_o and S_o values are biased downward with reference to true variance and standard deviation by the fact that no sample size adjustment[7] is yet included, and by a greater amount if redundant determinations are included in the x values. They are, however, raised with reference to the variance assignable to the cause surveyed by the set to the extent that variances due to lower level causes are included in these data. In general there appears to be no completely valid method of determining the true variance or standard deviation of the set of observations except by substituting the true parameter value in place of the mean of observations in the variance calculation. This value normally will be available only for a standardized reference material, but use of the final material mean will give an indication of the magnitude of the discrepancy between the apparent variance of observations and the true variance. I feel that the statement of a value corrected for only one cause of variability incurs serious danger that it will be mistakenly used as a true value.

Apparent Variance in Measurement of a Field

This estimate can be based either on repeated measurements of the same field, particularly with a coarse net, or on subsampling of the field when

---

[7] Normally $V = V_o[n/(n - 1)]$.

fine nets or lineal analysis are used. It is important to note that remeasurement with the same net in the same position using the same observer or the same machine setting determines only the ability of the observer to count, normally an insignificant fraction of the total variance. When a coarse net is displaced to obtain additional samplings, the displacement should be performed mechanically in such a way that the same or an equivalent placement is not inadvertently repeated.

Subsamples of a fine net or raster may be obtained either by counting the field in square blocks or in the slices of the slice analysis. The apparent variance of intercept lengths in lineal analysis can also be used. The three subsample types respond to somewhat different variations in the structure, hence any one alone will tend to give a somewhat low estimate of the total variability within the field.

The bias assignable to specimen preparation, to photography, and to differences in visual judgment or inaccuracy of edge discrimination in a machine should be separately estimated periodically, at least once for each material class and whenever any change of practice may have occurred. Estimates of these factors should preferably be made using the identical field and measuring array. Practices should be selected which yield reasonably stable values in spite of inherent small variations. Where the A_{50} and A_X standardizations are available from a machine, their difference serves as an indication of the overall magnitude of bias due to metallographic factors. With standarized practice the metallographic bias is constant at all levels of the nested system, hence its inclusion may sometimes be deferred until the final parameter values of the material are obtained.

The apparent statistical confidence in the mean parameter value obtained for one field should be estimated for the sole purpose of estimating whether enough observations have been made to permit subsequent detection of variability between fields. The subsampling process is not necessarily repeated for every field. If a V_o value was computed for the subsamples, this is divided by $\sqrt{n-1}$, n being the number of samplings, to give the apparent 67 percent confidence limit in the mean field value against sampling statistics alone. If a V value corrected for number of samplings was computed, V is divided by $\sqrt{n}$ to obtain the same numerical value. It is desirable that this apparent confidence limit should be on the order of 10 percent of the apparent variance between fields subsequently determined, but the labor of adequate observation frequently will force acceptance of a larger limit.

Variation Between Fields

A Priori *Estimate*—Significant variation must always be anticipated between the phase percentage determinations made on several fields of the same specimen. This may arise both from local variations of composition and structure and from a composition gradient such as ingot segregation preserved in the cross section of a bar. In the latter case the gradient may be surveyed by measuring a line of fields along a radius, but it must be remembered that the average of such an array of fields is not a valid measurement of the specimen mean, since there are many fields like the outer field and only one center field. The anticipated gradient may be known from chemical analysis.

Statistical variation between fields can be expected to be closely related to a Poisson prediction based on the average number of particles of the minor phase appearing in each field. The actual variation may however range from substantially less than the Poisson value to several times as great. Some specific cases will be noted.

1. If the material is essentially uniform in composition, as, for example, uniform particles precipitated from a homogeneous solid solution, and if the field dimensions are 10 or more times the interparticle spacing, the actual variation in number of particles per field may be insignificant. The dominant factor will then be the variance of particle sections in measuring the volume of a particle. The standard deviation of a series of parallel plane sections of a sphere is 44 percent of their mean area. Hence, if the raster measures each such section much closer than 44 percent, the anticipated standard deviation between fields will be that of N individual particles each uncertain by 44 percent, thus

$$\sigma_{\phi\%} = 0.44\,(\phi\%/\sqrt{N-1})$$

If, however, such a uniform material is measured by a coarse net which provides only about one observation point per particle, the uniformity will be concealed and the observed variation between fields may be expected to fall in the range of 1.1 to 1.4 times the Poisson value.

2. In ideally mixed powders the structure could be truly random, in which case the number of particles per field would show Poisson variation and the standard deviation of phase percentage between fields will be

$$\sigma_{\phi\%} = k(\phi\%\sqrt{N})$$

where k is ideally 1, but 1.09 with allowance for section variation, and about 1.5 with an open raster giving 1 point per particle.

3. Most real powder mixtures and many metals having local segregation are far from ideally random. In such cases the field to field variation will be considerably greater than anticipated from the number of particles. The standard deviation may easily be 2 to 3 times, and the variance 4 to 10 times, that predicted by the Poisson rule. In such cases the increase of the observed variance due to coarse sampling may be negligible.

The apparent variation between the mean parameter values determined for each of several fields should be determined and compared with the Poisson prediction to indicate which of the above classes of material is at hand. Only the sample size correction based on N equal to the number of fields, not measurement sets, should be included in estimating an apparent confidence limit in the mean of the specimen. This value remains uncorrected for metallographic or edge observation bias.

Special care must be exercised when the principle uncertainty in measuring one field is the observation error, or uncertainty in setting the threshold or discrimination level. This situation is characteristic of current vidicon instruments. The bias remaining in any fixed setting is not reduced by measuring many fields. Two separate sets of measurements may be made:

1. With the threshold setting fixed, multiple fields may be measured to give an acceptable measure of variability, but little confidence can be placed in the mean specimen composition.

2. If the threshold setting is redetermined for each field, reasonable confidence can be placed in the validity of the sample mean and its calculated confidence limit, but the apparent variation among fields will be unrealistically large.

As the real variability among fields is highly sensitive to the number of particles in each field, it is totally uninstructive to report the observed standard deviation among fields directly. For meaningful results the mean number of particles per field should be determined. When an actual particle count is not feasible the equivalent number of average particles estimated from lineal analysis may be used. The meaningful measure of field variability is the ratio of the observed standard deviation among fields to the nominal Poisson standard deviation:

$$\text{Variability index} = \frac{\sigma_{\phi\%}\ (\text{obs})}{\phi\%\sqrt{N}}$$

Values of this index not exceeding unity indicate high uniformity, while values appreciably greater than unity indicate real variation greater than random.

Variation Between Specimens

The variation between sections of a large body of metal (or a heat) is primarily a function of the production process and cannot be predicted *a priori*. The anticipated magnitude may, however, be indicated by other available data, such as chemical analyses. This variation should in all cases be regarded as a quantity to be determined by the analysis. In the absence of a composition gradient or other large-scale segregation, the variation between fields from different specimens may hopefully be no greater than the variation between fields of the same specimen. Attainment of such ideal uniformity can, however, rarely be expected in practice.

Identification and estimation of a real variation between specimens require essentially the same procedure as used for variations between fields. To identify an apparent variation as real, it is ncessary that the standard error of the mean determined for each specimen should be no more than one half to one third of the apparent variation between specimens. As previously noted, distinction of a gradient from a random variation requires a minimum of five specimens.

Confidence in Final Mean Values

In customary sets of measurements in which n independent observations are made within a single universe with a single significant source of variance, the $\pm 1\sigma$ (or 67 percent) confidence limit is computed by dividing the corrected standard deviation of all observations, S, by $\sqrt{n}$ or, alternatively, their apparent standard deviation, S_o, by $\sqrt{n-1}$. A quantitative metallographic program represents nests of universes which contain metallographic imperfection and edge observation uncertainty together with point sampling uncertainty and redundancy at the lowest level, as well as real variation of structure and composition between fields and specimens. This situation violates the assumptions of the sample case, thus the various determinations cannot be combined in the customary manner.

The confidence which can be placed in a final mean can be based only on the observed variation in the highest level surveyed. Thus, for the material mean, the standard deviation between the averages of each of several specimens is determined and the confidence limit calculated on the basis of n equal to the number of specimens. The statistical variations at the lower levels will have been incorporated in the determined values for the specimens, but will have a minor effect in decreasing the final precision if the uncertainty at each level is small relative to the actual variability at the higher level.

Special attention must be given to the permanent bias which may result from metallographic factors, observer bias, or permanent error in machine adjustment. Such biases will not have been averaged out at the lowest levels and, hence, will not be incorporated in the statistical variation at low levels. In these circumstances the variance assignable to the permanent factors should be separately estimated and added to the variance determined statistically before a confidence limit is assigned. In most cases where specimens are separately prepared and measured the permanent factors can be expected to be averaged out at the final level.

Example—If we now imagine a set of observations in which a relatively coarse net is applied five times to each field (with small displacements) and five fields are measured on each of five specimens, a total of 125 measurements will have been made. The mean of these 125 measurements is in fact the best available estimate of the mean of the material sampled. If, however, confidence in this mean is taken to be the standard deviation of the 125 measurements divided by $\sqrt{125}$, an unrealistically small confidence limit is obtained. Where the variation between specimens is significant, the standard deviation of the 5 specimen averages may be as large as that of the measurements. This standard deviation divided by $\sqrt{5}$ may thus be as much as five times as great as the unrealistic value.

Adequacy of Observation Programs

Many futile efforts have been undertaken in the past in quantitative microscopy without proper consideration of the inherent limitations of these methods. The resulting unreliable and even false results are responsible for considerable doubt that the methods are in fact quantitative. Before undertaking any program of quantitative metallographic measurements it is therefore necessary to determine what accuracy is in fact required and whether the proposed system of measurements can be expected to yield values of usable accuracy or, alternatively, whether values of usable accuracy can be obtained within a measurement program requiring a feasible level of effort. Work undertaken without this precaution will, at best, be wasted and, at worst, lead to a false conclusion.

Other than using specimen preparation methods which do not yield a valid representation of the material, the commonest error in designing an observational program is grossly underestimating the number of observations which will be required. It will be apparent, by solving the statistical equations previously given for number of observations, that very large numbers of net points or line increments are required to obtain only moderate precision in determining the phase percentage of a field.

Example 1—Suppose that the percentage of dispersed phase in a specimen is required to be measured with an absolute precision of 1 percent, that the specimen actually contains 20 percent of this phase, and that measurements are made by counting on a 500-point open net. At each application roughly 100 net points fall on the dispersed phase. A naive observer may assume that a count is probably correct to 1 point and that it is very unlikely that one count is in error by more than 5 points. Such an observer may believe that one net application met the requirement. Even an observer who has absorbed the statistical necessity that knowledge increases only in proportion to the square root of the effort expended may still assume ideal observations and apply Poisson's rule without qualification. Thus he will take the standard deviation of the 100 points on phase to be 10 points and believe the result to be 20 ± 2 percent. For 1 percent precision he now displaces the net to three or four additional positions and believes the average of these few nets to meet the required precision. Although this coarse net is relatively efficient, the real standard deviation will rarely be less than three times the Poisson ideal. To return to a real standard deviation of 1 percent, the ideal number of points must again be increased by a factor of about ten, leading to a final requirement of around 20,000 to 25,000 points for 1 percent precision. This will require about 50 applications of the 500-point net, always avoiding redundant placement. Even this level of effort makes no allowance for actual field to field variation in the specimen. If this variation is to be determined observations of at least 5 fields at the 25,000-point level will be required, in which case a finer net applied at lower magnification will be convenient. Additional fields may be required if the material variation is large to obtain a specimen mean with a precision of 1 percent. However, if it were known that the field to field variation did not exceed 1 percent, the combined variance would only be doubled and a total of 40,000 to 50,000 points might prove sufficient. This could most efficiently be accomplished by applying the 500-point net to 80 to 100 different fields.

The desirability of using machine methods is obvious when precision on the order of 1 percent or better is required. However, if a somewhat lower precision can be tolerated, this can be obtained by properly designed manual methods without excessive effort.

Example 2—If an overall standard deviation of 3 percent is acceptable, each of the three major errors may be allowed a standard deviation up to 1.7 percent. If we are confident that the nominal 20 percent composition does not vary by more than 1.7 percent on a large scale and that the particle arrangement is not worse than random, we can quite easily check the phase percentage of the specimen with an open point net. To keep the edge error within 1.7 percent, the magnification should be sufficient to make the average particle width about 30 times the actual resolution size of a point—say 30 mm at the ground glass. Poisson's rule calls for observing a minimum of 134 points on phase and 134 particles. While 667 total points will not simultaneously satisfy both requirements, 1000 points may be sufficient. The required observations may be obtained either by applying an 80-point ground-glass net at 25-mm spacing to 12 to 15 fields or by about 40 applications of a 25-point eyepiece net. Information as to actual variability will not be obtained and occasional errors of 6 to 9 percent should be expected, but this low effort procedure may nevertheless be sufficient for some purposes.

Design of Measurement Programs

Advance estimation of the variation to be expected at each of the three levels will permit design of an efficient sampling strategy. Clearly, a highly variable material calls for a relatively large number of specimens but demands only moderate precision in measuring each field. This allows operation at a lower magnification than required for highest precision on a single field. In theory, ultimate statistical efficiency would be obtained when the particle size is reduced to about one raster unit; but under such conditions all observations are doubtful points, and there is no way in which a valid area determination could be made by either machine or visual methods. A minimum particle width of several raster units must be tolerated to permit even reasonably valid observation. Tolerance of extremely imprecise measurements of each field is never justified, even for a variable material, since the final precision will be substantially reduced by combination of measurement errors with the field variability and the actual quality of the metal will not be determinable.

More uniform material demands fewer specimens but higher measurement precision so that the actual variation between specimens may be properly demonstrated or the uniformity be disclosed.

Use of Material Standards

The accuracy of a system of quantitative metallographic methods cannot be established except by reference to reliable analysis by an independent method or to some adequately calibrated or certified material standard. The National Bureau of Standards has for some time been engaged in research toward providing such material standards, but very serious difficulties have been encountered in obtaining materials of sufficient uniformity to permit certification at a useful level of accuracy. Thus no date can yet be projected at which such standards might be available. In the interim, any laboratory extensively using quantitative metallography should find it highly useful to calibrate some single specimen by the most precise measurements feasible, in combination with other classes of analysis when possible, and to employ this specimen as a temporary working standard, which, if not actually accurate, can at least ensure that all measurements are made on the same basis.

Assuming such a material standard to be available, it must be recognized that the standard itself is of necessity somewhat variable on the microscopic scale. The degree of this variability will presumably be known. Because of this variability it is not proper to measure the standard by an arbitrary procedure and then try to apply a mathematical correction factor to bring results of this procedure in line with true values.

Proper use of an external standard requires that errors or inaccuracies in the quantitative metallographic system be corrected to the point that measurements of the standard will agree with the established value, within the combined variance of the method and of the standard or within the required precision limit defined by the purpose of the measurements. The average of all such measurements over a period of time should approach the established value.

Figure 10 is presented to show that under favorable conditions highly consistent measurements can be obtained. In a first experiment, five fields of

FIGURE 10

SADIE-III scanner results for 729,600-point raster (×*2485*):	Field 6	Field 7
A_{min} (lower limit)	8.090 %	...
A_{max} (upper limit)	13.229 %	...
A_{50} standardization	11.082 %	11.108 %
A_x standardization	12.169 %	12.093 %
Mean intercept width (MIW)	0.624 μm	0.624 μm
Equivalent number of particles	1767/field	1759/field
A priori *deviation estimates for these fields:*		
Ideal S.D. of raster	0.041 %	
Raster S.D., redundant	0.051 %	
Edge Error, 0.1 × intercepts	0.194 %	
Poisson S.D. for 1763 particles	0.289 %	

the 52100 steel round robin specimen were photographed at ×1250 and measured at ×2912 with the SADIE-III scanner. The standard deviation among fields averaged 1.05 percent. Subsequently the two randomly chosen fields shown, which appear quite different, were photographed at ×1000 and measured at ×2485, with more rigorous control of all steps. The agreement is consistent with *a priori* raster statistics and within about one third of the anticipated edge error and less than one quarter of the Poisson error for number of particles. These results indicate that the carbide concentration is probably uniform rather than random. The A_{50} percentage of the last two micrographs is within 0.06 percent of the mean A_{max} value of the first five; hence, the major uncertainty remains the relation of the various objective standardizations to the unknown true value.

Summary and Applications

It has been shown that the practice of quantitative metallography is subject to numerous pitfalls, any one of which can, if undetected, lead to results of little or no quantitative significance. Known pitfalls have been noted and typical precautions for their avoidance outlined. Straightforward measurement methods for obtaining percentage of a phase and a few generally useful size and distribution parameters have been described.

It has been emphasized that the number of observations actually required to obtain a specified level of precision is substantially greater than frequently presumed. A precision of 1 percent or better can, however, be obtained by entirely feasible manual methods, while 0.2 percent or better is obtainable with high-precision automatic scanning equipment. The admittedly high labor requirement for precise manual measurement creates a strong demand for automatic equipment. Such equipment, unfortunately, is not free of characteristic errors and pitfalls of its own.

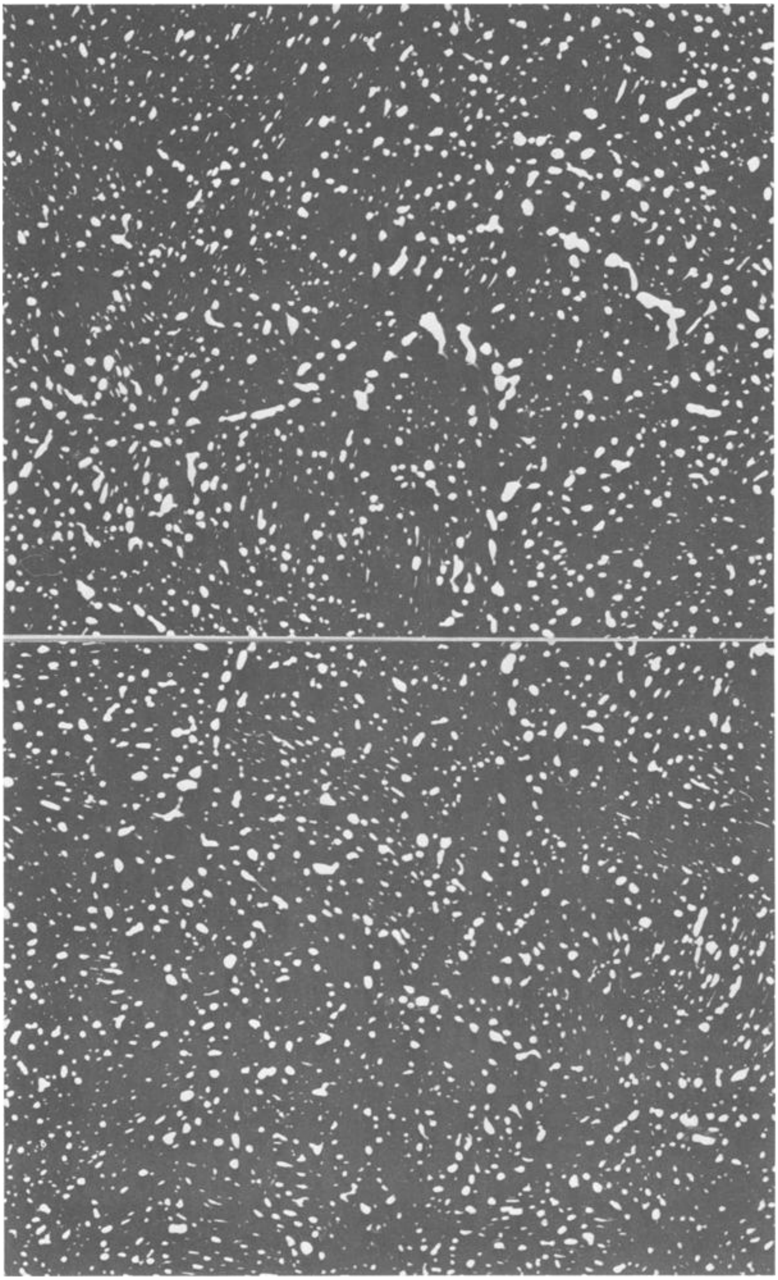

FIG. 10—*Duplication of results is possible! 52100 steel, round robin specimen, double polish, 0.08 percent picral 3 min, and Beraha stain. Light 4200 Å. Two randomly selected fields,* *# 6* (top), *# 7* (bottom) (×*1000*).

In metallurgical research there are many cases where qualitative relations are known or presumed between measurable parameters of the microstructure and useful properties of the metal. There is substantial need for work to make these relationships quantitative by adequate measurements under well-defined conditions. In may cases measurement of all of the simple metallographic parameters is necessary to determine which parameter should be regarded as causing the property change.

In quality control and inspection, several semiquantitative metallographic standards are in general use. These rely, in part, on visual judgment by the inspector and are thus less than objective. Improved control will require application of truly quantitative methods to yield objective ratings. Introduction of machines in this application contributes special problems in that unthinking machines are generally incapable of making the logical discriminations which are inherent in these standards as presently written. The appropriate standards committees must therefore consider whether they should officially accept machine ratings in terms appropriate to the abilities of simple machines or should require more elegant machine methods, generally including large computer processes, necessary to incorporate characteristically human decisions in the present standards.

Acknowledgments

I wish to acknowledge the contributions of several members of ASTM Committee E-4 on Metallography, Subcommittee XIV on Quantitative Metallography, who cooperated in the counting experiment and who supplied micrographs or measurements of round robin specimens or prints. These members, often inadvertently, have supplied several illustrations of the nature and magnitude of departures from ideal results. Under the terms of the round robin tests, their names are held confidential.

Acknowledgment is also made of very valuable assistance rendered by National Bureau of Standards staff members H. Yakowitz, D. B. Ballard, T. R. Shives, P. M. Giles, L. C. Smith, and P. A. Boyer in preparation of micrographs and manual measurements.

References

[1] *Quantitative Microscopy*, R. T. DeHoff and F. N. Rhines, Eds., McGraw-Hill, New York, 1968.
[2] *Stereology*, H. Elias, Ed., Springer-Verlag, New York, 1967.
[3] Delesse, A., *Annales des Mines*, ANMSA, Vol. 4, No. 13, 1848, p. 379; also *Memoires de la Societe Geologique de France*, MSCFA, Vol. 4, 1852, p. 67.
[4] Rosiwal, A., *Verhandlungen K. K. Geologischen Reich Wein*, Vol. 5–6, 1898, p. 143.
[5] Shand, S. J., *Journal of Geology*, JGEOA, Vol. 24, 1916, p. 394.
[6] Thompson, E., *Journal of Geology*, JGEOA, Vol. 38, 1938, p. 193.
[7] Glagolev, A. A., *Engineering Mining Journal*, EGMJA, Vol. 135, 1934, p. 399.
[8] Hilliard, J. E. in *Quantitative Microscopy*, Chapter 3, DeHoff and Rhines, Eds., McGraw-Hill, New York, 1968 (Refs *1*, *20*, *22*, *23*).

[*9*] Beraha, E., *Journal of the Iron and Steel Institute*, JISIA, Vol. 203, May 1965, p. 454.
[*10*] Picklesimer, M. L., "Anodizing as a Metallographic Technique for Zirconium-Base Alloys," AEC-ORNL Report 2296, Atomic Energy Commission, 1957.
[*11*] Moore, G. A., *Journal of Pattern Recognition*, Vol. 2, 1970.
[*12*] Moore, G. A. in *Pictorial Pattern Recognition*, Cheng, Ledley, Pollock, and Rosenfeld, Eds., Thompson, Washington, 1968, pp. 275–326.
[*13*] Wernimont, G., *Analytical Chemistry*, ANCHA, Vol. 23, Nov. 1951, pp. 1572–1576.

Harvey Yakowitz[1]

Some Uses of Color in Metallography

REFERENCE: Yakowitz, Harvey, "**Some Uses of Color in Metallography,**" *Applications of Modern Metallographic Techniques, ASTM STP 480,* American Society for Testing and Materials, 1970, pp. 49–66.

ABSTRACT: The application of various methods for using color in metallography is outlined. The methods include plane and circularly polarized light, color etching, and color separation photography. Instruments used to obtain subjects for the color metallography examples shown in this paper include the optical microscope, the electron probe microanalyzer, the scanning electron microscope, and the transmission electron microscope. A brief discussion of color films is given. The technique used to obtain color photographs is given in detail for each aspect of color metallography discussed.

KEY WORDS: color photography, electron microscopy, electron probes, metallography, microscopy, polarized electromagnetic radiation, evaluation

The use of color in metallography can often aid materially in the examination and interpretation of a microsection. Improvements in the production and processing of color films have been made steadily over the last 35 years. Costs of color reproduction, with the exception of printing for publication, are no longer prohibitive in money or time. Color transparencies and prints can often be obtained commercially from sheet film within 24 h. The Polaroid process, when it can be used for metallography, reduces the time factor to a few minutes. Furthermore, it is not always necessary to photograph in color to use the advantages provided by color methods.

There are two general categories into which the use of color in metallography falls: (1) contrast enhancement, in which a particular color usually does not have any intrinsic relation to the material (color is useful here because the eye can distinguish thousands of color shadings but relatively few gray ones, including white and black), and (2) color as an indicator of composition, in which specific colors indicate elements or phases. The latter category includes the use of certain color etchants and also encompasses color separation photography of X-ray area scans from an electron probe microanalyzer.

---

[1] Lattice Defects and Microstructures Section, Metallurgy Division, Institute for Materials Research, National Bureau of Standards, Washington, D. C. 20234.

The approach taken in this paper will be to outline methods for using color, to give examples, and to describe in some detail the technique used to obtain the example. The methods discussed include polarized light examination, color etching, and color separation photography.

General Comments on Color Metallography

A wide range of colors can be obtained by mixing the three primary colors, red, green, and blue, in varying proportions in additive mixing. None of the primaries can be obtained by mixing the other two. Red, green, and blue add to make white. The intermediate colors are:

$$\begin{aligned}\text{cyan} &= \text{blue} + \text{green} = \text{white} - \text{red}\\ \text{yellow} &= \text{green} + \text{red} = \text{white} - \text{blue}\\ \text{magenta} &= \text{red} + \text{blue} = \text{white} - \text{green}\end{aligned}$$

The color resulting from subtracting a single primary from white is the complement of that primary.

Cyan, yellow, and magenta are called the subtractive primaries. They absorb only one third of the visible spectrum. Thus, any pair of subtractive primaries may be combined to yield the additive primary complementary to the third subtractive primary. For example, cyan and magenta combine to make blue. Any color can be produced by the subtractive method—using only one white light source— by mixing cyan, yellow, and magenta. The three subtractive primaries combine to give black.

Color film, whether reversal type yielding a positive transparency or negative type, depends upon the subtractive method to produce the final colored image. Color films have three sensitized layers which when exposed to light form dyes in an amount proportional to the amount of light energy absorbed. Development makes these layers cyan, magenta, and yellow. The layers act as filters so that only the light not absorbed by them reaches the eye. Thus, an area seen as red on a positive transparency projected using a white light source actually consists of the yellow and magenta dyes superimposed on one another. This superposition permits only red components of light to pass through.

In color negative films such as Agfacolor, Kodacolor, or Ektacolor the layers are cyan, magenta, and yellow. Paper or film upon which the color print is made has a set of three emulsion layers consisting of the subtractive primaries. Again subtractive color mixing provides the colors seen in the final finished positive print. Usually, an orange mask is also included [*1*].[2] The orange mask serves two purposes: (1) it permits a black-and-white print to be made from the color negative and (2) it brings the transmission charac-

---

[2] Italic numbers in brackets refer to the list of references at the end of this paper.

teristics of the three dyes in the transparency more into balance. The orange mask retards blue buildup in the print and preserves the red and yellow components [*1*].

Now that color films have been discussed in a general way, more specific arrangements for metallography must be considered. In the past ten years I have encountered only tungsten filament lamps and zirconium and xenon arc lamps on metallographs. After experimenting with several types of positive and negative color films, the following procedure has been adopted: (1) the original subject is photographed on a reversal film to provide a positive transparency, (2) if prints are required a color negative (internegative) is made from the positive, and (3) the prints are prepared from the internegative using the original positive transparency as a color guide.

Tungsten lamps should be balanced to a color temperature of 3200 K. Then readily available films can be used without filters to provide the color micrograph. The zirconium arc lamps encountered in our laboratory have a yellowish cast. The effect is to retard the blue and to provide a micrograph (on a film balanced for tungsten light) which has very good color balance. No filters are used. Xenon arc lamps have a color temperature approaching 6000 K. They have a bluish cast. Thus, films balanced for daylight used in conjunction with Wratten 4 or 6 filters yield useful micrographs.

The direct preparation of micrographs on color negative film is not used in our laboratory. Often prints are desired from only a few color subjects. In many cases the positive transparency is sufficient to provide the necessary information. If prints are needed the cost of the internegative in time and money is negligible.

Polaroid rapid-access-type photography has become increasingly popular because of the ease and speed of the method. However, while Polacolor film follows the same general color mixing principles as other color films, the color balance is different. Using the xenon arc source, we have had good success with most subjects using a CCO5R (color correcting) filter.

Exposure times vary with subject and photographic setup. Experience is the best teacher—usually only a few trial shots at the beginning will train the metallographer in the use of a particular arrangement. Successful pictures on some films have been obtained at exposure times up to 20 min, so a very wide latitude of conditions is possible.

In summary, the requirements for using color for metallography are suitable color films, a set of color correcting (CC) filters, a set of Wratten filters including numbers 4, 6, 12, 25, 29, 33, 45, 47, 49, 58, 61, 92, 93, and 94, access to a color processing laboratory, a high-quality metallograph, some patience, and, at times, a sense of humor. (Metal microsections in color may win a prize in an abstract art show.) Now some specific uses of color can be considered.

Polarized Light Techniques

The amount of reflected plane polarized light can be a function of specimen topography, anisotropy, grain orientation, and, indirectly, composition. These factors are interrelated because an etchant produces topographical effects on the surface by attacking structural components at different rates. The attack rates, in turn, depend on specimen composition and grain orientation.

In the past the metallograph has been used as a polarizing microscope to use colors to identify phases—especially those associated with inclusions [*2*]. Today, except for certain cases [*3*], access to electron probe microanalyzers has made this practice obsolete. Hence, present use of polarized light in metallography is often concerned with using the colors produced to increase contrast and possibly to give some qualitative idea of relative orientation of microconstituents. For these two purposes color itself need not have any intrinsic meaning in terms of composition, topography, or orientation. Color differences produced by these effects are sought.

Such color differences can often be found in a very simple way. Almost all modern metallographs are equipped with polarized light capabilities. Converting from ordinary bright-field examination to polarized light requires no more than 15 or 20 s. Usually there is also provision for inserting an optical plate between the polarizer and analyzer. This plate can be a wedge causing quarter-, half-, or full-wave retardation. Alternatively, a Babinet compensator (a double wedge) [*4*] can be used; the compensator causes a variable retardation. The polarizer-analyzer system is placed very near the crossed position. The wave plate causes light in a narrow wavelength band to be the predominant reflection component; in other words, the matrix of the specimen will reflect light of a given color. With the full-wave plate or Babinet compensator this color can be made to range from red to blue.

Any topographic difference in the specimen surface will cause a difference in phase, causing topographic features to appear differently colored from the matrix. The color seen in the specimen can be varied by rotating the polarizer, the analyzer, the specimen, and the wave plate. Thus the metallographer has great latitude in providing the color combination yielding the most contrast or other desired characteristic.

The method even works well for metals of cubic lattice symmetry since topographic and orientation differences are revealed. Figure 1, Plate 1 shows an NBS standard-cast brass (C-1102) at a region about ¾ in. above the chill-cast face [*5*]. Orientation differences between the main grains are clearly shown by color differences. The subdendritic structure is easily distinguished from the main grain configuration. This brass is homogeneous to electron probe microanalysis in zinc and copper at micrometer levels of spatial resolution [*5, 6*]. However, for the dendritic region to exist some gradient of

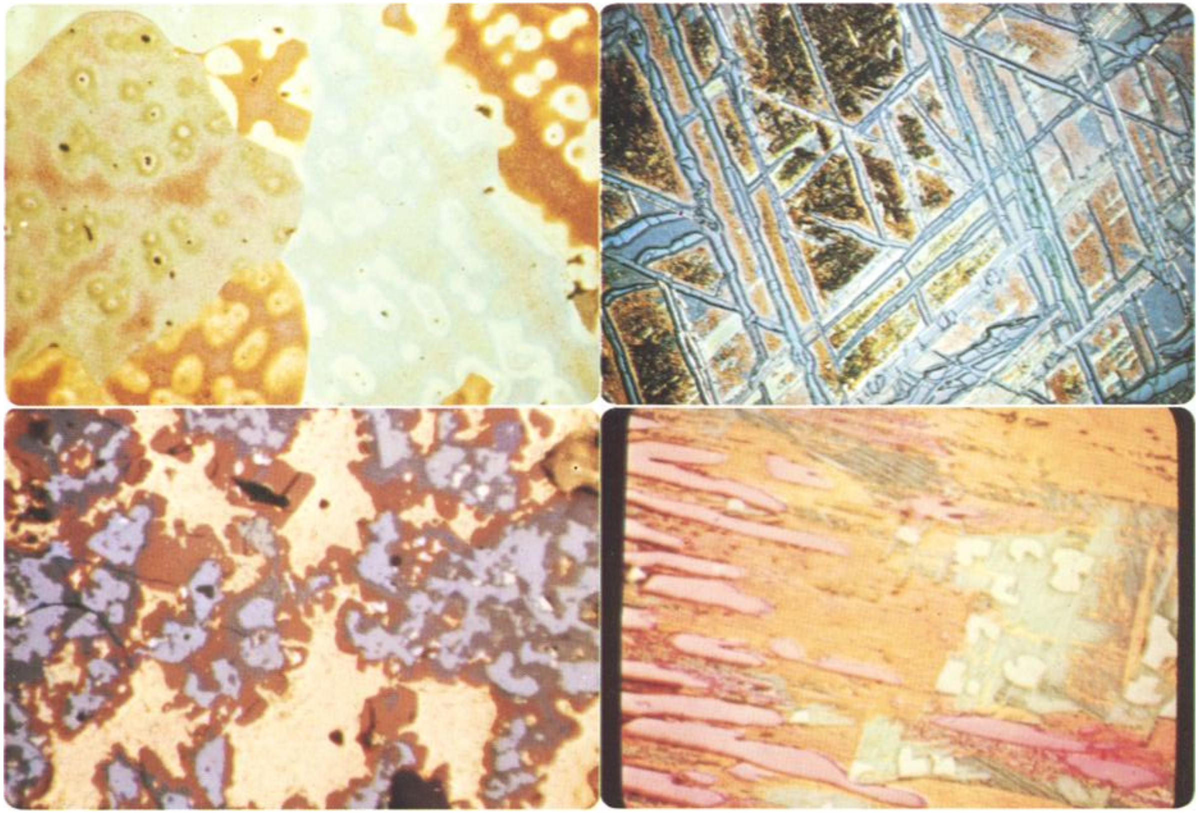

FIG. 1—*Plate 1, top left; 2, top right; 3, bottom left; 4, bottom right.*

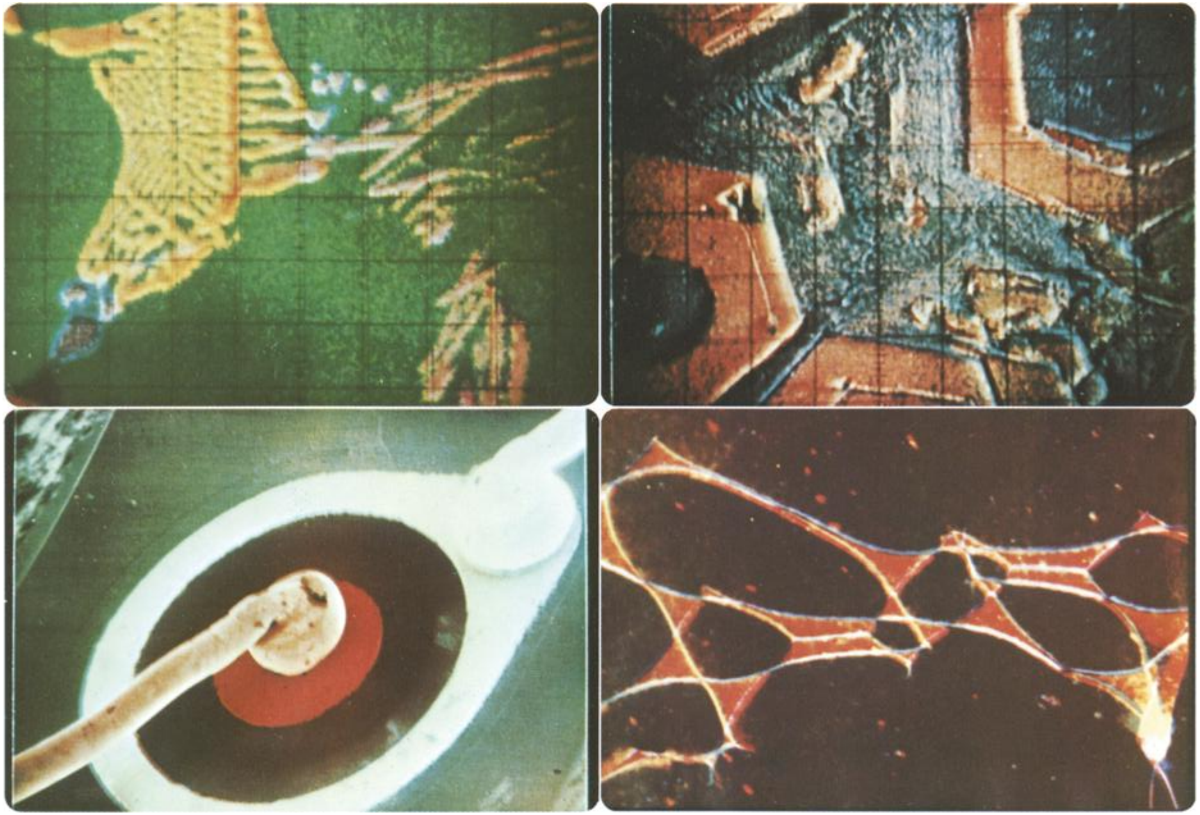

FIG. 1 (Continued)—*Plate 5, top left; 6, top right; 7, bottom left; 8, bottom right.*

Figure 1

Plate 1—National Bureau of Standards cartridge brass (C-1102) about ¾ in. above chill-cast face. Etched in 10 percent $(NH_4)_2SO_4$-90 percent H_2O and photographed in polarized light with full-wave plate between polarizer and analyzer (×75).

Plate 2—Tazewell, Tenn., meteorite—Fe-16.7 percent Ni. Etched in 1 percent nital and photographed in polarized light with full-wave plate between polarizer and analyzer (×100).

Plate 3—Columbium-tin hot-pressed powders heated to 1050 C at 30 C/min and cooled at 3 C/min. Anodized in Picklesimer's solution [*10*] at 30 V for 25 s. Photographed in bright-field illumination using a Zr arc source and no filters for Type B chrome film. Colors indicate composition differences (×500).

Plate 4—Ti-6Al-4V alloy nitrided in purified nitrogen for 48 h at 955 C (1800 F). Anodized in Picklesimer's solution at 85 V for 90 s. Photographed in bright-field illumination using a Zr arc source and no filters for Type B chrome film. Colors show that block-like grains and elongated grains have different composition (×75).

Plate 5—Tool steel—Type M2. Color composite using the photographs in Fig. 3 as color separation positives. Iron is green, tungsten is red, and vanadium is blue. The photograph shows the structure in terms of the composition. The eutetic at the left is Fe-W alloy with some V, and the stringers at the right are basically W-V alloy.

Plate 6—Titanium iron borides grown from the melt. Scanning electron image is superimposed on Ti (red) and Fe (blue) X-ray images. The result shows topography, microstructure, and composition on a single photograph. Photograph courtesy of K. F. J. Heinrich (×400).

Plate 7—Solid state device diode. Voltage contrast photographs from commercial scanning electron microscope (courtesy of H. B. Merrill, Scientific Instruments and Sales Co., Atlanta, Ga.) were combined with 0-V condition red and +3-V bias as cyan. Outer ring is active in both cases (red plus cyan equals white); inner ring inactive in the +3-V condition. Insulator ring (red-black) does not cause a short which would be seen as white.

Plate 8—Dislocation network in a low stacking fault energy, hcp silver-tin alloy. Partial dislocations having the same Burgers vector are the same color; faulted areas are red.

composition is required. This gradient cannot be found by means of electron probe microanalysis and is therefore less than one percent of the amount of Cu (72.85 percent) and Zn (27.10 percent) present [*5*]. Nevertheless, the polarized light method easily reveals the dendritic structure. In bright field there is not enough contrast to satisfactorily photograph the subdendritic region within the main grains.

A case where the etchant-polarized light combination can be used to indicate composition or phase differences is found in the study of iron meteorites [*7*]. As a molten iron meteorite cools below 730 C, the FCC γ phase, called taenite, decomposes into a mixture of body centered cubic (bcc) α phases, called kamacite and taenite. In meteorites having more than 6 percent nickel the kamacite develops into plates which are often seen as the familiar Widmanstatten pattern in a polished section. These plates are in turn surrounded by taenite.

If two meteorites have the same nickel content, the meteorite with the lower cooling rate will have the larger kamacite plates [*7*]. Similarly, the iron-nickel constitution diagram [*8*] predicts that, if two meteorites have the same cooling rate, the one with the lower Ni content will exhibit the larger kamacite plates. It is not particularly difficult to determine the bulk Ni content in the meteorite. Furthermore, the electron probe microanalyzer can determine the point-to-point Fe-Ni concentrations across a taenite-kamacite band. By combining this information with the Fe-Ni constitution diagram, Goldstein and Short [9] were able to predict the cooling rate and parent body size of meteorites. An accurate measurement of the kamacite bandwidth is essential for obtaining correct cooling rates.

In such a case deep etching to differentiate between taenite and kamacite can be dangerous, because some of the kamacite plate width may be lost. But light etching and color polarized light examination often remove the problem. It is possible to get color differentiation between taenite and kamacite in this way. Plate 2 shows kamacite plates, blue, surrounded by white taenite bands in the Tazewell, Tenn., meteorite. The orange and orange-black areas are plessite which is $\alpha + \gamma$. In addition to the taenite-kamacite differentiation, preferred orientation in the plessite regions is revealed. The cooling rate of the Tazewell meteorite is 2.2 C per million years [9].

Measurements of plate widths are carried out on the microscope so that very little color photography is necessary. There are many cases where color methods can be used without the need of color photography; however, the photographic technique when using the color polarized light method is not complicated. The only difficulty is that exposure times may be long because of the extra components in the optical train. Therefore, the xenon arc is recommended as a source if it is available. Good results can be obtained with other light sources as well; Plate 2 was made using the Zr arc lamp. Exposure times of up to 20 min have not greatly affected the color balance of the reversal films used in conjunction with the color polarized light method.

Color Etching

Color etching implies that a particular phase or composition is to be given a definite color. Direct identification of phases by means of color differentiation then becomes possible. Contrast improvement caused by coloring the specimen is often a welcome dividend but rarely is it the primary reason for using color etching. Color etchants have been used for a long time [2]. It is not the purpose of this paper to document a list of color etchants and their characteristics but rather to try to give an overall view of the way in which these etchants can be used to obtain information about metal specimens. Accordingly, two broad types of coloring agents will be considered: surface films, anodic or otherwise, on the etched or unetched specimen and chemical coloring agents.

In the surface film category, the film thickness produces interference colors. Variations in the thickness produce different colors. The oldest of these techniques is heat tinting, in which a specimen is heated in an oxidizing atmosphere. Thin oxide layers, having a thickness governed by the difference in oxidation rates of the various phases, form on the surface; hence, the interference colors produced by the oxide can be used to delineate phases. Heat tinting does not work for all materials nor is it as easy to control as one would like.

A step forward was made by Picklesimer [*10*], who described anodic etching of metallographic specimens. Colors are produced by anodic oxide films whose thickness, which controls the color, depends on the anodizing voltage, the anodizing solution, and the composition or structure of the phase or both.

Anodizing can be carried out using a standard electropolishing source. The cathode is stainless steel and the anode is the specimen. Electrical connection must be made from the source to the specimen—not to another conductor in contact with the specimen. The voltage must be very stable; any ripple causes uneveness in the colors produced. The voltage seems to depend on the specimen; for T-6Al-4V the voltage was nearly three times that for columbium-tin alloys (85 to 30 V). There appears to a mass effect of the specimen on the time required. The process seems to be additive, but if one overetches a few seconds of polishing on a Linde B wheel removes the film without harming the specimen.

The baths devised by Picklesimer work with columbium-, tantalum-, titantium-, zirconium-, and uranium-base alloys. Picklesimer believes that, if the oxide film is adherent and nonporous and its thickness characteristic of the applied voltage, then anodizing can be used for any alloy system [*10*].

The obvious appeal of the method is that by initial experimentation one can find conditions so that one designated phase in the specimen can be assigned a definite color within the range of colors produced by anodizing for the system. All other colors are then fixed so that phase identification by means of color can be carried out. In fact, it has been shown that an anodized specimen can be analyzed directly in the microprobe with no loss of accuracy due to the presence of the anodic film [*11*, *12*].

Once the anodizing conditions have been established, the method provides entirely reproducible color results for the alloy system under study [*12*]. With the basic conditions established the time to prepare the bath and anodize a single metallographically polished specimen is about 15 min. Thereafter, about one minute per specimen is all that is needed.

Plate 3 shows the interior of a specimen of hot pressed powders of Cb and Sn after heating to 1050 C at 3 C/min followed by cooling to room temperature at 3 C/min. The phase which is lightest blue is unreacted Cb. In the study of the Cb-Sn the anodizing procedure was standardized so that Cb always assumed this light beryl blue coloration. Then all other phases appeared with fixed colors which could be used for phase identification purposes. Each phase composition was originally determined by means of microprobe analysis in both the anodized and unetched conditions. Microprobe analysis was unaffected by the anodized layer.

The red-purple colored phase is $CbSn_2$, the darkest blue colored phase is probably Cb_3Sn, the intermediate blue colored area has a range of composition centering near Cb_4Sn, and the yellow phase is unreacted tin. Black areas are voids. The phases in dozens of Cb-Sn alloy specimens were read directly with the help of the anodizing technique. Only a few specimens had to be checked on the electron probe microanalyzer once the anodizing procedure was standardized.

A case in which the anodizing technique revealed previously unsuspected composition differences is shown in Plate 4. The specimen is Ti-6Al-4V alloy nitrided 48 h in purified nitrogen at 955 C (1800 F) [*13*]. The elongated grains are pinkish and the block-like grains are pale green. The matrix tends to appear green in the vicinity of the block grains and yellow in the vicinity of the elongated grains. Thus the anodizing method indicates that the block and elongated grains are different in composition and that there are composition variations in the matrix as well. Ordinary bright-filed examination revealed only the possibility of differences within the matrix. Figure 2 is a micrograph,

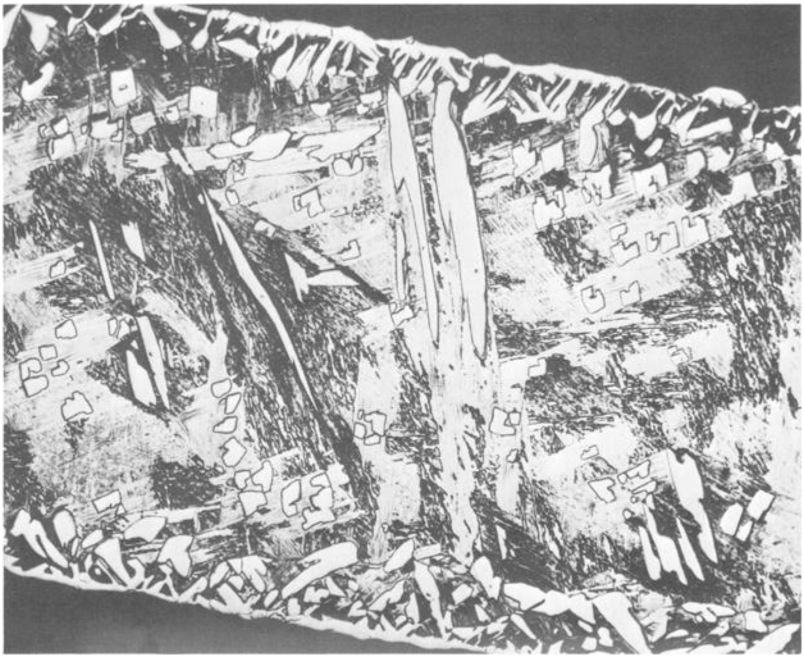

FIG. 2—*Ti-6A-4V alloy nitrided in purified nitrogen for 48 h at 955 C (1800 F). Etched in 5 percent HF-95 percent H_2O. Elongated and block-like grains appear very similar (×75).*

taken in bright field, of the nitrided Ti-6Al-4V etched in 5 percent HF-95 percent H_2O. Until the anodizing method was used the block grains were thought to be merely an end-on view of the elongated grains, but the electron probe microanalyzer proved the anodizing method to be a valid indicator of the true situation.

The elongated grains contain 83.3 percent titanium, 3.3 percent vanadium and 8.9 percent aluminum by weight, as determined by microprobe analysis. The balance is assumed to be nitrogen. The block grains contain 51.7 percent Ti, 4.3 percent V and 29 percent Al by weight. Thus the block grains have far more Al and, presumably, nitrogen than do the elongated grains. The matrix is variable in composition, but the Al is depleted from its original 6 weight percent. These and other studies indicate that Al stabilizes the two varieties of very large grains. No such large grains appeared when pure titanium was given the same nitriding treatment as the Ti-6Al-4V alloy [*13*]. Plates 3 and 4 were photographed in bright field with unfiltered light from the Zr arc.

Again, color photography of the specimens in the two studies just illustrated was necessary for only a few specimens. However, the color anodizing method greatly increased the efficiency of the investigation. The anodizing method, when it can be applied, gives a reproducible and sensitive color differentiation based on composition differences.

Some agent which could be applied to all materials as an interference color film producing agent would be invaluable. Gray [*14*] has mentioned vacuum-deposited TiO_2 as such a possibility. According to Gray, it is very useful in revealing phases having a reflectance like that of the matrix. In addition, Gray indicates that orientation differences cause some color effects when the method is used.

Chemical Coloring Agents

Strictly speaking any color etch produces a film which in turn produces the observed color. For purposes of discussion let a chemical coloring agent be considered as a substance formed on the specimen surface as an ordinary etching agent would be applied; in other words, the coloring agent is applied by dipping or swabbing the specimen. The coloring agent is usually at room temperature but need not be necessarily. No electric current, high-temperature oxidation, or vacuum evaporator is used in producing the coloration of the specimen. In recent years, the most active person in producing and using chemical coloring agents has almost certainly been Emanuel Beraha of the Israeli Air Force Laboratories. The Hebrew name Beraha means "a blessing" and to many metallographers that indeed is what Beraha's reagents have been.

Beraha has developed coloring agents to identify such constituents as cementite, phosphides, and nitrides in cast iron, steel, stainless steel, and superalloys [*15–21*]. The reagents can be divided into two groups. Quoting Beraha[3] these are "anodic reagents, in which a sulfide film is precipitated on the anodic areas (ferritic and austenitic matrix), and cathodic reagents in which a complex of molybdate oxide or elementary selenium films are precipitated on the microcathodes (carbides, nitrides, etc.) by the process of reduction at the microcathodes. The color effect in the anodic films is due to the interference phenomenon and is connected with the thickness of the film. The thickness of this film varies from grain to grain and also on twins as a function of the crystallographic orientation (difference in the surface energy). The various reagents cause the coloration of different phases, so that it is possible, by the correct choice of the reagent to color distinctly from one another any phase at will." Very complete details concerning the composition and handling of the reagents are given in Refs *15–21*. About a dozen color photographs illustrating the application of Beraha's reagents can be found in Refs *20* and *21*. Several irons, steels, and superalloys are represented in this group.

Other coloring agents, there use, and some examples are described in Ref *2*. The basis for their application is the creation of interference films whose thickness is a function of composition. In using any color etch a fair amount of initial experimentation is necessary to establish conditions giving optimum reproducible color results. Then the composition of the etchant and the etching conditions must be maintained constant for reproducibility.

Photography of color-etched specimens is almost always done directly in bright field with or without color balance correcting filters. Occasionally polarized light is used in conjunction with the color etch to enhance contrast. In this case, circularly polarized light—obtained by placing a quarter-wave plate before the polarizer and a second quarter-wave plate before the analyzer —is recommended. Orientation effects seen by rotating the specimen are removed when using circularly polarized light. Thus a possibly confusing extra source of color differentiation can be deleted when color-etched specimens are examined in polarized light. Parenthetically, circularly polarized light is often useful for polarized light examination of metals containing constituents yielding polarization figures, such as the crosses produced by spherical carbides. Circularly polarized light removes the figures and leaves the color contrast.

Color Separation Metallography

As the name implies, color separation metallography usually means that colors will arbitrarily be assigned to features by the metallographer; in other words, color is created where no color exists in nature. Furthermore, the

---

[3] Private communication with E. Beraha, Israeli Air Force Laboratories, Bat-Yam, Israel.

familiar metallograph is almost never used in this context. For the most part we now concern ourselves with instruments such as the scanning electron microscope or microprobe and transmission electron microscope. Each of these instruments provides metallographic information which could not be obtained otherwise. Color separation methods often greatly enhance the value of this information.

The metallographer is usually called upon to correlate structure with composition and with material properties. The electron probe microanalyzer has revolutionized metallography; elemental distributions within a specimen surface can be ascertained quickly and accurately. Hence, a technique assigning a color to each phase, combined with electron probe microanalysis, enables the metallographer to read the composition in the specimen directly. The next step is to provide micrographs in which color represents composition.

The scanning electron probe microanalyzer [*22*, *23*] can produce images of microscopic areas by the emission of X-rays or of electrons. The various electron images provide mainly topographic information, while the X-ray images show the spatial distribution of the elements present in the specimen. Thus the scanning electron probe is a microscope as well as an X-ray spectrometer.

In the scanning electron probe microanalyzer, an electron beam about 0.5 μm in diameter is scanned over a square area on the specimen surface up to 0.5 mm on an edge. The electron beam is of energy sufficient to excite characteristic X-rays from the elements present in the scanned area. The usual range of voltages is 3 to 30 kV. The X-rays emitted from each point in the area are collected by a proportional counter-crystal spectrometer system. The amplified signal from the counter-spectrometer system is made to modulate the brightness of a cathode-ray tube (CRT) scanned in synchronism with the probe. Thus a picture (on the CRT) is obtained by the variation of X-ray emission of the surface. A bright dot on the screen corresponds to the recording of a sufficient X-ray intensity produced by an element in the scanned area. An X-ray area scan shows tones ranging from black to white: in places of high concentration of the element in the scanned area, the picture will be nearly photographically white; it will be gray where the element's concentration is lower and black where the element is absent.

Black-and-white photographs of the CRT, taken with standard commercial cameras made for this purpose, showing the distribution of a single signal with the scanned area are widely used [*24*]. Figure 3 shows three X-ray area scans taken of solidification structures in an M2-type tool steel. Correlation of compositional and structural details is difficult. It is hard to say whether or not there is iron present in the eutectic-like region at the left or if the eutectic-like region is complex in composition but fairly uniform in appearance.

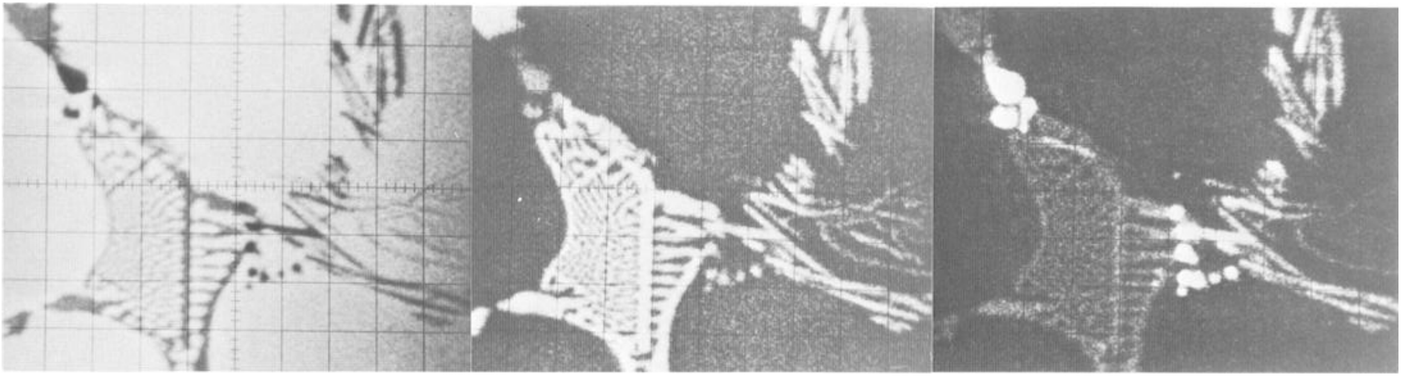

FIG. 3—*Tool steel—Type M2. X-ray area scans taken on the electron probe micraonalyzer. Photographs courtesy of J. I. Goldstein, R. W. Kraft, and R. H. Barkalow, Lehigh University, Bethlehem, Pa.* (left) *Area scan for iron,* (center) *area scan for tungsten, and* (right) *area scan for vanadium* (×*500*).

Furthermore, it is difficult to state the compositional nature of the stringer-like material to the right of the eutectic-like region from Fig. 3. We shall see that color separation photography using the three pictures of Fig. 3 as color separation positives [*24*] provides answers to all the above questions at a glance.

The color separation technique consists of preparing black-and-white scanning pictures and using them as color separation positives, with appropriate filters, to make color prints and can be easily used on a routine basis by semiskilled personnel with little training. Another important advantage is the possibility of selecting the best color combination after the individual black-and-white pictures have been taken. The yield can be 15 to 20 color composites of uniform quality per hour.

The color photograph is prepared as follows:

1. The appropriate X-ray or electron signal scans are prepared as positive black-and-white prints by photographing the cathode-ray tube of the microprobe using an oscillographic standard camera loaded with Polaroid pack film; the film is developed according to manufacturers specifications.

2. The registered separation positives are sequentially photographed by the copying camera (which is loaded with Polaroid color film). For each partial exposure a different color filter is placed between the camera lens and the separation positive.

The success of this technique depends upon (1) the quality of the black-and-white images, (2) the characteristics of the light source, film, and color filters, (3) the exposure times, (4) the proper choice of color for each partial image, and (5) registration—avoiding the relative displacement of the black-and-white images during the color exposure.

Color mixing, if any, will be additive because each successive exposure is stored on the film. Only three primaries can be used if any color mixing on the color composite is to be interpreted in terms of the primaries. For example, let three separation positives represent iron, chromium, and nickel such that the red filter is used for Fe, the green for Cr, and the blue for Ni in preparing the composite. Then, Fe-Cr-Ni combinations are white, Fe-Cr yellow, Fe-Ni magenta, and Cr-Ni cyan on the finished composite.

To standardize our procedures, we balance the reproduction. The proper balance of color on the film for a given set of filters is achieved when the addition of equal lightnesses on the black-and-white pictures yields a neutral gray on the color picture. This criterion can be satisfied by obtaining a color picture of a standard paper gray scale, adjusting the exposure time for each filter until the photograph shows neutral gray steps. Changing the exposure time for a given filter changes the color balance.

There are at least three sets of filters which can be properly balanced and which yield good color quality when using the Polaroid color film presently available [*24*]: standard Wratten series numbers 25, 58, 47, numbers 92, 93, 94, and numbers 33, 93, 45 for red, green, and blue, respectively. The first set is that used to match the dye peaks of sheet color films, such as Ektachrome or Anscochrome, the second was recommended by the film manufacturer, and the third was found after some experimentation. The exposure times for each filter set are shown in Table 1. With a variety of input subjects the 33, 93, 45 set gave the most satisfactory results. The mixed colors could easily be interpreted and color quality was good [*24*]. This set was used to prepare the illustrations of the technique shown in this paper.

TABLE 1—*Exposure times for color composites.*

Wratten Filter Set Number	Color	Time, s
Light source: four reflector flood lamps spaced 2 ft apart, 3 ft from subject. Camera 20 1/4 in. from subject. Lens setting *f*5.6.		
92	Red	1/4
93	Green	12
94	Blue	60 (add 1/30 white)
25	Red	1/8
58	Green	5/8
47	Blue	5
33	Red	1/5
93	Green	10
45	Blue	3 (add 1/60 white)
Light source: two cold white fluorescent tubes 15 in. long placed 18 in. from subject. Camera 3 1/2 in. from subject. Lens setting *f*5.6.		
33		1.5
93		40
45		7.5 (add 1/60 white)

Using the 33, 93, 45 set of filters, blue is occasionally difficult to distinguish from black. The lightness of blue can be increased by adding a small amount of white light to the blue subject. One exposes a subject using the blue filter and then reexposes the same subject for a much shorter time with no filter.

The color composite obtained using the three pictures of Fig. 3 as separation positives is shown in Plate 5. The color filters used were green-iron, red-tungsten and blue-vanadium. The eutectoid material is complex, being an

Fe-W alloy, shown as yellow (red plus green), containing some regions rich in W-V alloy, as shown by the magenta (red plus blue) regions at the periphery of the eutectoid region. The stringers are basically W-V alloy without Fe. There appears to be a region very high in V and one very high in W at the upper left of the eutectoid region. The yellow salt and pepper effect in the iron-rich matrix is due to the tungsten in the alloy. The composite not only clearly shows the compositional relations but also provides a micrograph of the structure comparable to that obtainable from the optical microscope.

Several other advantages of the method are that the viewer's attention may be directed to preselected areas of the structure by using bright colors such as red or yellow for those regions. No microprobe time is consumed in preparing the color composites by this method. Results are available in about 2 min and so can be quickly adjusted if desired, that is, changing the color of a given feature, etc. If transparencies are desired copies can be made on reversal films with very little color degradation. Fifty good-quality copies of a single color composite can be obtained for about $20.00. Thus the cost of including such pictures in reports is not prohibitive. The main advantage is that a single color picture can provide both compositional and structural details directly.

A variation of the three-color X-ray method has been made by Heinrich.[4] In his scheme X-ray information is combined with the topographic information obtained by using the scanning microprobe as a scanning electron microscope. Then, backscattered electron or target current signals [*23*] showing topographic detail, with about 2000-Å resolution, are obtained. This resolution is far superior to that of the X-ray signals. The resolution of the X-ray signals is degraded because X-rays may be produced all along the electron diffusion path in the specimen. Thus, combining X-ray and electron signals not only gives additional topographic information but also sharpens the resulting composite considerably.

An example is shown in Plate 6. The specimen is titanium iron boride grown from the melt. Titanium is red, iron is blue, and the electron micrograph is superimposed without any filter. Combinations of Ti and Fe are shown as magenta, but the main feature is the greatly increased topographical detail. The hexagonal titanium boride (red) rises out of the surface, and structural details in the matrix are very clearly delineated. Superimposing the structural information has caused little color degradation. Topographic detail can be superimposed on three-color composites as well. This method shows great promise for giving compositional and topographic details on a single picture.

[4] Private communication with K. F. J. Heinrich, National Bureau of Standards, Washington, D. C. 20234.

The scanning electron microscope provides electron images with about 200-Å resolution [*25*, *26*]. Color separation methods for direct photography of the CRT of the scanning electron microscope have been outlined elsewhere [*27*].

An area of scanning electron microscopy amenable to the filter-copying camera methods just described is the so-called voltage contrast mode. In this mode a solid state electronics device is biased electrically and scanned. The secondary electron emission coefficient is a function of the electrical properties and thus provides a visual brightness measure of the electrical events taking place in the device. An example is shown in Plate 7. The specimen is a diode. The red filter was used for the 0-V condition and cyan (blue filter plus green filter exposed sequentially) was used for a positive bias of 3 V. Clearly, the outer ring has the same electrical properties in the 0 and +3-V cases (red plus cyan equals white) while the inner ring is inactive in the +3-V bias case —it is red.

The voltage contrast method is becoming an accepted quality control indicator for solid state electronics [*26*]. The color separation method shows promise in determining electrical defects by using color mixing to pinpoint the fault. In other words, if the diode of Plate 7 were defective, some region on the inner band may have shown up as white or a region of the outer band shown up as red or a short between the two may have been revealed as a white path between the red and white rings. The red-black central ring in Plate 7 is there to prevent such a short, but its failure could be clearly documented by the color method.

In certain cases the color separation techniques just described can be advantageously applied to transmission electron micrographs. Plate 8 is a case where color aids in seeing and studying lattice defects in a silver-tin alloy. The color composite displays a dislocation network of extended nodes and double ribbons observed in a low stacking fault energy, hexagonal close packed (hcp) silver-11.9 atom percent tin alloy. Partial dislocations having the same Burgers vector are in most cases the same color. Stacking fault areas are red. Adjacent nodes in the network are extended and contain the same type of intrinsic stacking fault. The double ribbon configuration consists of a pair of intrinsic faults bounded by partial dislocations all having the same Burgers vectors. By making measurements on isolated examples of nodes and double ribbons the stacking fault energy in this alloy was found to be 5.5 erg/cm^2 [*28*].

The color composite was prepared from prints having reversed contrast to the three black-and-white positive prints shown. The slight misregistry and incorrect color, especially noticeable in the lower partial dislocation of the double ribbon on the right, are a consequence of parallax and different dislocation image shifts and contrast profiles among the original bright-field micrographs. A more faithful composite representation would be obtained by using a careful dark-field technique.

Conclusions

It is almost always worthwhile to take a look at any metallographic specimen by means of the color polarized light method. At worst, about 1 min is wasted; at best, the increased contrast may offer an avenue to increased information from the specimen.

Color etching is a valuable tool provided the etchant is controllable, gives reproducible results, and gives colors which can be cross-checked by means of microprobe analysis for validity in phase identification. Unfortunately, not all metals are amenable to color etching.

Color separation photography can provide composition and structural information on a single color composite, or, composition and topographic information can be obtained simultaneously. Even basic lattice defects such as dislocations or stacking faults can be highlighted. Color separation metallography is inexpensive in time, money, and capital equipment. About fifteen composites per hour can be obtained using a standard copying camera setup. This arrangement means that expensive instruments need not be tied up to obtain color photographs.

References

[1] Waddell, J. H. and Waddell, J. W., *Research-Development*, REDEA, Vol. 20, No. 5, 1969, p. 64.

[2] *Symposium on Metallography in Color, ASTM STP 86*, American Society for Testing and Materials, 1949.

[3] Snow, R. B., *Journal of Metals*, JOMTA, Vol. 20, No. 10, 1968, p. 55.

[4] Martin, L. C., *The Theory of the Microscope*, American Elsevier, New York, 1966.

[5] Yakowitz, H., Vieth, D. L. and Michaelis, R. R., *Advances in X-ray Analysis*, AXRAA, Vol. 9, 1966, p. 289.

[6] Birks, L. S., Gilfrich, J. V. and Yakowitz, H. in *Fifty Years of Progress in Metallographic Techniques, ASTM STP 430,* American Society for Testing and Materials, 1968, p. 343.

[7] Goldstein, J. I. and Yakowitz, H., "The Iron Meteorites: Their Microstructures and Thermal History," *Scientific American*, in press.

[8] Goldstein, J. I. and Ogilvie, R. E., *Transactions of the Metallurgical Society*, AIME, TMSAA, Vol. 233, 1965, p. 2083.

[9] Goldstein, J. I. and Short, J. M., *Geochimica et Cosmochimica Acta*, GCACA, Vol. 31, 1967, pp. 1001–1023.

[10] Picklesimer, M. L., "Anodizing as a Metallographic Technique for Zirconium-Base Alloys," Report ORNL-2296, Clearinghouse for Federal Scientific and Technical Information, 1957.

[11] Hallerman, G. and Picklesimer, M. L. in *Electron Probe Microanalysis*, Advances in Electronics and Electron Physics, Suppl. 6, A. J. Tousimis and L. Martin, Eds., Academic Press, New York, 1969, pp. 197–226.

[12] Wyman, L. L., Cuthill, J. R., Moore, G. A., Park, J. J. and Yakowitz, H., *Journal of Research of the National Bureau of Standards*, JNBAA, Vol. 66A, 1962, p. 351.

[13] Cuthill, J. R., Hayes, W. D. and Seebold, R. E., *Journal of Research of the National Bureau of Standards*, JNBAA, Vol. 66A, 1960, p. 119.

[*14*] Gray, R. J. in *Fifty Years of Progress in Metallographic Techniques, ASTM STP 430,* American Society for Testing and Materials, 1968, p. 17.
[*15*] Beraha, E., *Journal of the Iron and Steel Institute,* JISIA, Vol. 202, 1964, p. 696.
[*16*] Beraha, E., *Journal of the Iron and Steel Institute,* JISIA, Vol. 203, 1965, p. 454.
[*17*] Beraha, E., *Journal of the Iron and Steel Institute,* JISIA, Vol. 204, 1966, p. 248.
[*18*] Beraha, E., *Metal Progress,* MEPOA, Vol. 90, No. 3, 1966, p. 135.
[*19*] Beraha, E., *Journal of the Iron and Steel Institute,* JISIA, Vol. 205, 1967, p. 866.
[*20*] Beraha, E., *Praktische Metallographie,* PMTLA, Vol. 4, No. 8, 1967, p. 416.
[*21*] Beraha, E., *Praktische Metallographie,* PMTLA, Vol. 5, No. 9, 1968, p. 501.
[*22*] Heinrich, K. F. J., *Applied Spectroscopy,* APSPA, Vol. 22, No. 5, 1968, p. 395.
[*23*] Heinrich, K. F. J. in *Fifty Years of Progress in Metallographic Techniques, ASTM STP 430,* American Society for Testing and Materials, 1968, p. 315.
[*24*] Yakowitz, H. and Heinrich, K. F. L., *Journal of Research of the National Bureau of Standards,* JNBAA, Vol. 73A, 1969, p. 113.
[*25*] *Scanning Electron Microscopy-1968,* proceedings of a symposium on the Scanning Electron Microscope: the Instrument and Its Applications, Illinois Instutute of Technology Research Institute, Chicago, Ill., 30 April–1 May, 1968.
[*26*] *Scanning Electron Microscopy-1969,* proceedings of a symposium on the Scanning Electron Microscope: the Instrument and Its Applications, Illinois Institute of Technology Research Institute, Chicago, Ill., 29 April–1 May, 1969.
[*27*] Pawley, J. and Hayes, T. L., "Color Modulation for Use in Scanning Electron Microscope," presented at SEM Symposium, Illinois Institute of Technology Research Institute, Chicago, Ill., 1969.
[*28*] Ruff, A. W. and Ives, L. K., *Acta Metallurgica,* AMETA, Vol. 17, 1969, p. 1045.

R. J. Gray,[1] *E. L. Long, Jr.,*[1] *and A. E. Richt*[1]

Metallography of Radioactive Materials at Oak Ridge National Laboratory*

REFERENCE: Gray, R. J., Long, E. L., Jr., and Richt, A. E., "**Metallography of Radioactive Materials at Oak Ridge National Laboratory,**" *Applications of Modern Metallographic Techniques, ASTM STP 480,* American Society for Testing and Materials, 1970, pp. 67–96.

ABSTRACT: The preparation and examination of radioactive and toxic materials has required metallographers to discard the close "touch" which at one time was considered so important. Basically, the same preparation and examination steps are carried out with the specimen, but when working with radioactive and toxic materials the simplest operation may be highly involved and require the metallographer to use sensitive manipulators and remotely operated equipment while he is protected by biological shielding. Shielding demands are determined by the materials under study and can vary from a cell with 3-ft-thick, high-density concrete to ¼-in.-thick glass. Metallographs, microhardness testers, X-ray diffraction equipment, and microprobe analyzers have been fabricated with biological shielding as an integral part of the instruments. The in-cell equipment, in particular, may have to approach a "Rube Goldberg" design to be operable, repairable, or replaceable, all by remote methods, and still not downgrade its function by these basic requirements. An important variable—radiation—must be considered along with mechanical and physical effects in the interpretation of the often complex microstructures of metals, alloys, cermets, and ceramics. Some of the materials, as well as information concerning them, are extremely rare and some elements are a product of the nuclear reactor. Examples of equipment requirements and the microstructures of some nuclear fuels and structural materials after exposure in a nuclear reactor are presented.

KEY WORDS: autoradiography, ceramics, construction materials, electron microscopy, electron probes, heat treatment, irradiation, metallography, microscopy, microstructure, nuclear fuel elements, nuclear reactor, photomicrography, radioactive materials, radiation shielding, replicas

Considerable progress has been made in the metallography of radioactive materials when we consider that this particular era began only about 25 years

---

[1] Supervisor, group leader, Radiation Metallography, and metallurgist, respectively, Metallography Group, Metals and Ceramics Div., Oak Ridge National Laboratory, Oak Ridge, Tenn. 37830.

* Research sponsored by the U. S. Atomic Energy Commission under contract with the Union Carbide Corp.

ago. Because of the biological hazards involved, the artistic touch which previously was considered so essential to the metallographer must often be completely discarded. The direct use of our senses of sound, touch, sight, and their interrelationships in metallography are not so apparent until they must be replaced by a mechanical, electrical, or optical go-between. The simplest operation in this unique type of metallography may require very detailed maneuvers with intricate equipment and ten times more time and patience of the metallographer in the preparation and examination of radioactive materials.

Generally, the preparation and examination steps parallel the standard approach in metallography. The performance of these steps, however, requires much gadgetry, so there is a need for a design engineer who can understand the complications in working with highly radioactive materials. The equipment must be sturdy but, if possible, not too heavy to restrict portability. It must be compact because working space is at a premium. It should be repairable—*in situ* if possible—by remote control, because downtime for decontamination and transportation to another area is time consuming and expensive. Surprisingly, the results from the preparation and examination are expected to be of, and often exceed, the quality of work performed on nonradioactive materials.

The intent of this presentation is to show some of the equipment and techniques used in the metallography of radioactive materials at Oak Ridge National Laboratory, Oak Ridge, Tenn., and also demonstrate how the metallographer is an indispensable member of the materials team in the nuclear field. He is constantly faced with diagnostic decisions on materials which carry little or no previous technology. Just as in general metallography, many different techniques are successfully applied by other metallographers in the examination of radioactive materials. This presentation is not intended to be considered the only method of making investigations of this type.

Equipment for Radiation Metallography

There is a definite need for a preirradiation metallographic facility for microstructural comparisons in the before-and-after examinations. Except for some limitations, because of the toxicity of some materials and the low level radiation of some fuel materials, the preparation of unirridiated specimens is relatively similar to that in a conventional metallography laboratory.

Basically, the radioactive materials that must be examined can be classified as alpha (α),[2] beta (β),[2] gamma (γ),[2] and neutron[2] emitters [*1*].[3] Single emission

---

[2] An alpha particle is a positively charged unit of two neutrons and two protons. A beta particle is a high-speed electron emitted from a disintegrating nucleus. Gamma rays, similar to X-rays but of shorter wavelength, are emitted during some nuclear transformations.

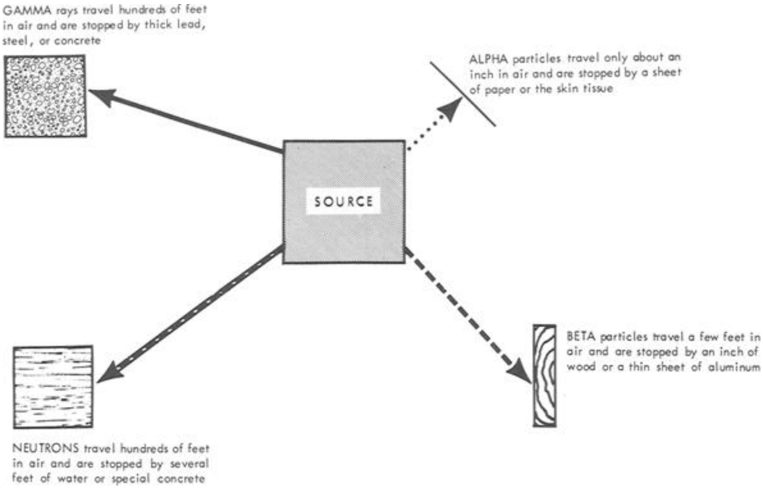

FIG. 1—*Four kinds of radiation and the required shieldings.*

or combinations of any of the four may exist. Representative shieldings required for these radiations are shown in Fig. 1. On this basis, the preparation of radioactive materials for metallographic study can be separated into three types of shielded facilities: (1) glove boxes, (2) shielded hoods, and (3) heavily shielded hot cells.

Glove Box Metallography

Alpha-emitting materials can be prepared in a well-contained box designed with glove ports for the operator's hands and arms. In Fig. 2 a metallography laboratory is enclosed in a continuous glove box line [*2*]. The U-shaped configuration was required because of space limitations. This particular facility was designed primarily for plutonium and plutonium-bearing compounds. Plutonium is a highly toxic alpha-emitting material [*3*], so a policy of complete containment is necessary. Steel glove boxes with glass or plexiglas windows securely gasketed in place can meet the containment and shielding requirements. The toxicity of plutonium is considered to be about 1000 times that of arsenic; thus extensive care must be exercised so that the material does not unintentionally gain entry into the human body.

The entry of specimens, abrasives, etchants, or anything needed in the box or the removal of waste, equipment, or anything not needed in the box must follow a careful transfer procedure by being sealed in plastic sleeves. This is

---

Neutrons are emitted in the disintegration of some artificially produced elements and in fission (the breakup of certain heavy elements under neutron bombardment).

[3] Italic numbers in brackets refer to the list of references at the end of this paper.

FIG. 2—*Alpha metallography facility. Specimens which are high alpha radiation emitters must be prepared here.*

commonly referred to as a "bag-in" or "bag-out" operation. All boxes operate at a negative pressure of −0.5 to 1.0-in. water with either air or argon atmosphere as dictated by the specimen requirements. All the preparatory steps of (1) cutting, grinding, and mounting, (2) mechanical polishing, (3) microscopic inspection, (4) chemical and electrolytic etching, (5) autoradiography, equipment repair, and replication for optical and electron microscopy, and (6) microscopy and photomicrography are performed in the six boxes. Two separate boxes are used for macrohardness measurements and photomacrography.

Fortunately, it is possible to confine the various operations in the designated glove boxes in much the same manner as separating the operations in individual rooms or areas of a room in a conventional metallography laboratory. When possible, commercial equipment is utilized; however, varying amounts of modifications usually are required for adaptation to the glove box operation. Sometimes a complete design and fabrication is necessary. The first glove box is for cutting, grinding, and mounting. A modified commercial lapping machine and a specifically designed and fabricated cut off machine were installed in this box. The next three boxes are for specimen polishing, microscopic inspection, and chemical and electrolytic etching. Vibratory polishing [*4–6*] is the principal method of specimen preparation.

The microscopy and photomicrography box [*7*] is shown in Fig. 3. A standard Bausch & Lomb Research metallograph was cut into three sections. The microscope is positioned inside the box, and the camera and light source

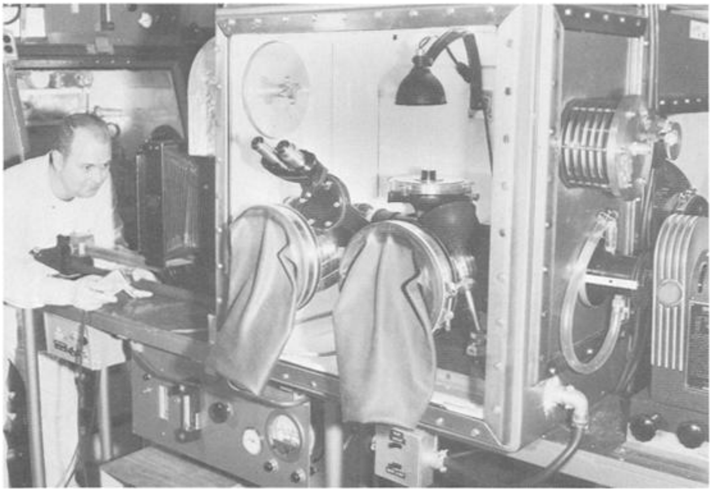

FIG. 3—*Glove box for microscopy and photomicrography.*

are outside the box on the left and right ends, respectively. The light source, microscope, and camera are connected by optical relays.[4] An optical relay also is positioned between the microscope and the binocular viewer. The integrity of the box is maintained by sealing the lenses in the optical relays. After the field is selected and the operator is ready to take the photomicrograph, the focusing is accomplished with a step motor (remote controlled) which is connected to the microfocusing knob of the metallograph. A panel below the box monitors its negative pressure.

Shielded Hood

The success of this type of operation requires good judgment of the operator. Often the economics related to a program necessitates a hood, which is properly ventilated, with portable shielding such as lead bricks. If glove boxes that have been shielded with lead are available, they are ideal for this work. However, the particular studies may be of short duration, so a safe, temporary, less expensive facility is arranged in a hood. Close cooperation and the guidance of Health Physics Division personnel are mandatory in any study of radioactive materials, but additional contact is required in a temporary arrangement because of unestablished operating procedures. Approval of such facilities by a survey committee is required.

---

[4] An optical relay is a system of lenses which transports an image from one location in an optical system (microscopy) to another location with a minimum change in magnification, resolution, or abberation. The optical relay may be several inches or several feet long as required.

Shielded Hot Cells

Hot cells vary somewhat in size and design, but basically they are enclosures constructed of high-density concrete with high-density glass (liquid filled or lead glass) viewing windows providing a shielding equivalent to the walls. One of the more modern cells for performing metallographic studies is located in the High Radiation Level Examination Laboratory (HRLEL) at Oak Ridge National Laboratory. The plan of the cells and adjacent working area is shown in Fig. 4. For functional purposes these cells are arranged in the form of a "U" with the metallography cell comprising one leg. The exterior of the cell, shown in Fig. 5, has 3-ft-thick, high-density concrete walls. A pair of master-slave mechanical manipulators can be seen at each window. These manipulators are designed for light-duty service and are capable of lifting only about 14 lb each. Heavier objects are managed with electromechanical manipulators and a companion 3-ton crane that share the same bridge. The interior, Fig. 6, is completely lined with stainless steel, and all penetrations

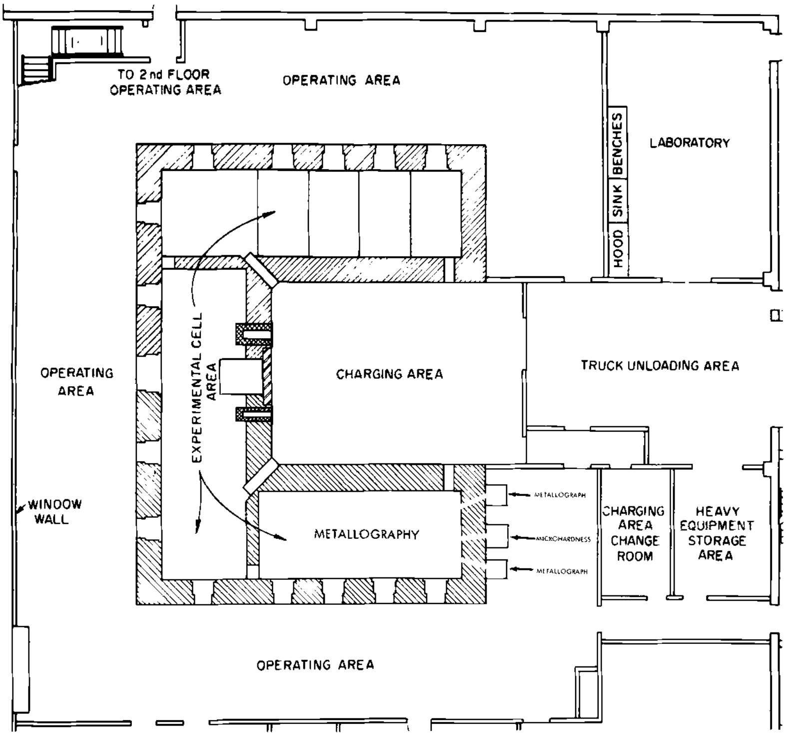

FIG. 4—*First floor, hot cells, and adjoining operating areas, high radiation level examination laboratory (HRLEL).*

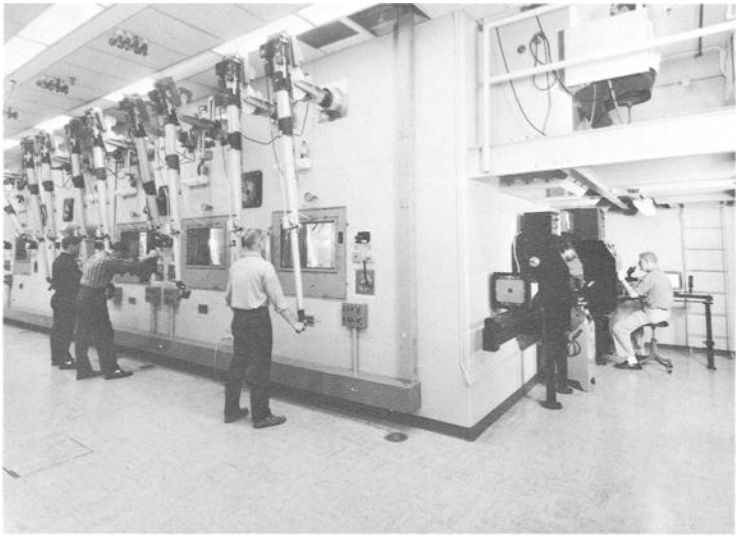

FIG. 5—*Metallography cell in the HRLEL. Cutting, mounting, grinding, polishing, and etching are in process on the left; two shielded metallographs are on the right; and a shielded microhardness tester is on the mezzazine.*

into the cell are sealed to maintain the required integrity and shielding for α, β, and γ radiation. The shielding can attenuate gamma radiation up to 500,000 Ci[5] of mixed fission products. The metallography cell is 10 ft deep by 24 ft long by 14 ft high.

Various levels of negative pressure are maintained in the facility, decreasing from the office areas to the cell interior. There is a minimum number of penetrations through the front of the cell (see Fig. 4). Controls for the services are extended underneath the cell to the operating area. All equipment in the cell is operated by remote control and can be transported out of the cell for repair, modification, etc. A cutoff machine and mounting press, not visible in Fig. 6, are operated from control panels located in the operating area. Most specimen mounting, however, is done with epoxy resin. Equipment not shown in the photograph includes cutting, grinding, and lapping machines.

Specimen polishing is done with vibratory polishing units [*8*]. A standard Rockwell hardness tester and a General Mills manipulator can be seen at the end of the cell (Fig. 6). In this same photograph the in-cell portion of specimen transfer lines can be seen. The mounted specimen is placed in a motor-driven carrier and transported through the wall to the various instruments which will be described later.

[5] Curie, Ci, is a quantity of a radioactive nuclide in which there are 3.7×10^{10} disintegrations per second.

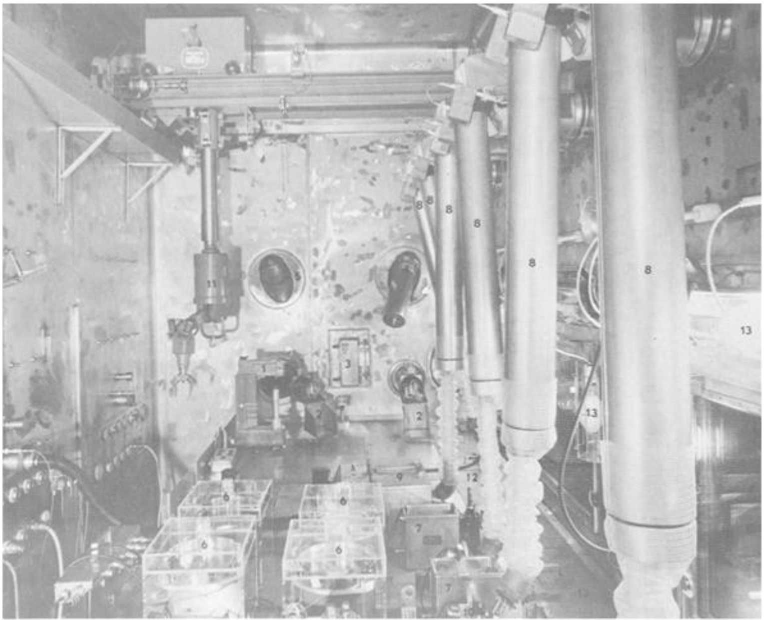

(1) Hardness tester; (2) specimen transfer to metallograph; (3) specimen transfer to shielded X-ray diffraction unit or shielded microprobe analyzer on second floor; (4) specimen transfer to microhardness tester; (5) spare transfer opening; (6) vibratory polisher; (7) ultrasonic cleaner; (8) hand manipulator; (9) chemical etching sink and hood; (10) specimen dryer; (11) heavy duty manipulator; (12) air filters; and (13) cell lights. Services are available from the back (left of photo) of the cell.

FIG. 6—*South view of interior of HRLEL metallography cell.*

An example of the equipment complexities is shown in Fig. 7. A conventional stereomicroscope is shown on the bench and compared with the shielded remote stereomicroscope. The sketch of the shielded stereomicroscope with the complicated optical relays is shown in Fig. 7*b*. Heavy lead shielding is required at each end of the horizontal, through-the-wall mounting sleeve. This unit is removable for repair or transfer to another cell location. A periscope, not shown in Fig. 7*a*, with camera attachment can be used to survey the entire cell. This periscope also can be removed through a sleeve in the cell wall.

Some easily recognized tools which are readily available in a conventional laboratory have been adapted—to fit the fingers of the manipulator hand—for in-cell use, Fig. 8. Chemical etching is well known to everyone who has ever been involved in metallography. The chemical etching of a radioactive specimen by remote operation in a hot cell is shown in Fig. 9. The specimen is placed on a small stand above a sink and is shown receiving a swab etch. The cotton saturated with the etchant is held in the manipulator fingers (see

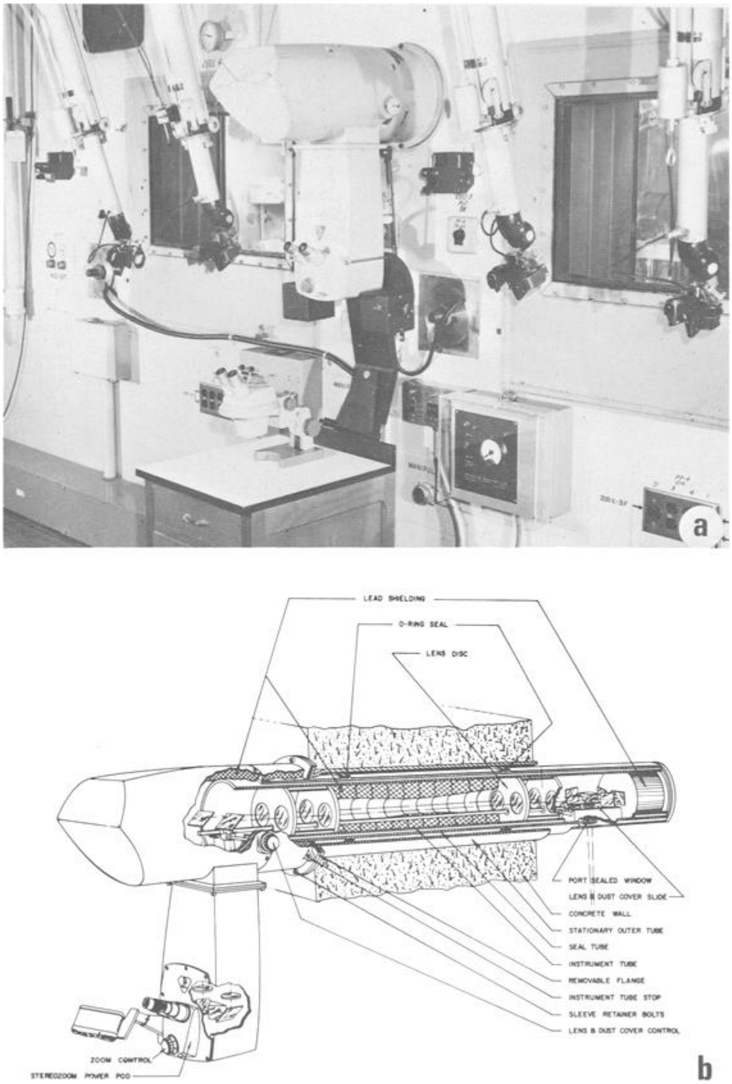

FIG. 7—*Shielded and unshielded stereomicroscopes in HRLEL:* (a) *conventional bench microscope and shielded microscope;* (b) *drawing of shielded microscope.*

Fig. 8) and applied to the specimen. The metallograph and the microhardness tester (Fig. 5) have 8-in. and 6-in.-thick steel shielding, respectively, and are designed to be used as a "blister" appendage to the cell wall. Modifications to a metallograph for the examination of α-, β-, and γ-emitting specimens go far beyond the alterations described for the alpha metallograph (Fig. 3). The

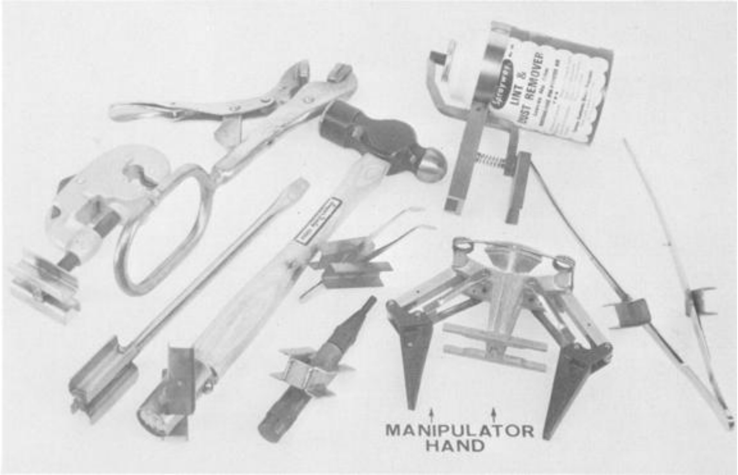

FIG. 8—*Conventional tools adapted for remote operation.*

heavily shielded metallograph requires optical relays and a viewing window of nonbrowning glass. All controls for focusing, movement of filters and diaphragm, etc., must have a rotary movement to facilitate sealing. The shafts for these controls penetrate the 8-in, shielding, allowing the metallographer to operate the instrument in all normal functions. Individual specimens are transferred through the cell wall to the stage of the metallograph or hardness tester. With this design, the shielding demands are primarily for the specimen being examined; however, this too can be almost unbelievable. Fuel specimens less than 500 μm in diameter may have a radiation level of 2000 R/h.[6] Specimens with a radiation level of 40,000 R/h have been prepared, examined, and photographed. The cells are designed so all in-cell equipment must be repaired *in situ* or removed through the cell roof to decontamination and repair cells on the second floor. Personnel have not entered this cell complex since the first radioactive specimens were introduced over five years ago.

One of the newest developments in equipment for metallography in this laboratory is the shielded electron microprobe analyzer.[7] Specimens are transferred from inside the metallography cell (Fig. 6) to the second floor into an 8-in.-thick steel wall cubicle juxtaposed to the hot cell wall. A second transfer is made to the shielded X-ray diffraction unit or the shielded microprobe

---

[6] Roentgen, R, is an exposure dose of X or gamma radiation such that the associated corpuscular emission per 0.001293 g of air produces, in air, ions carrying 1 electrostatic unit of charge of either sign. A lethal dose may be expected if the body receives at least 500 R over a short period of time.

[7] Materials Analysis Company Model 450, Palo Alto, Calif.

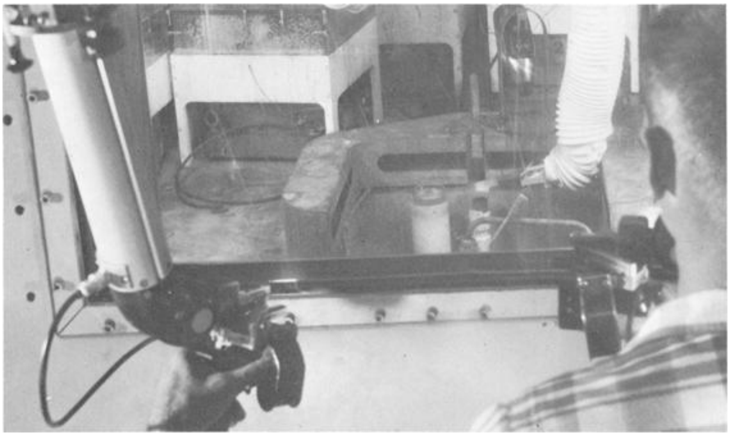

FIG. 9—*Radioactive specimen receiving a chemical swab etch by remote operation.*

analyzer. The steel cubicle with its high-density glass door and manipulators and the shielded microprobe analyzer are shown in Fig. 10. An elevation drawing showing the two floors with the shielded metallographs, hardness tester, and microprobe analyzer is given in Fig. 11.

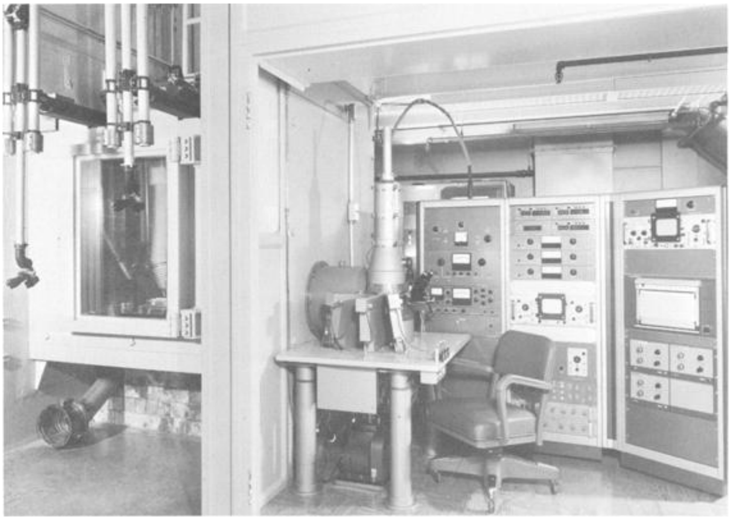

FIG. 10—*Shielded electron microprobe analyzer: specimen can be transferred from the steel cubicle* (left) *to shielded microprobe.*

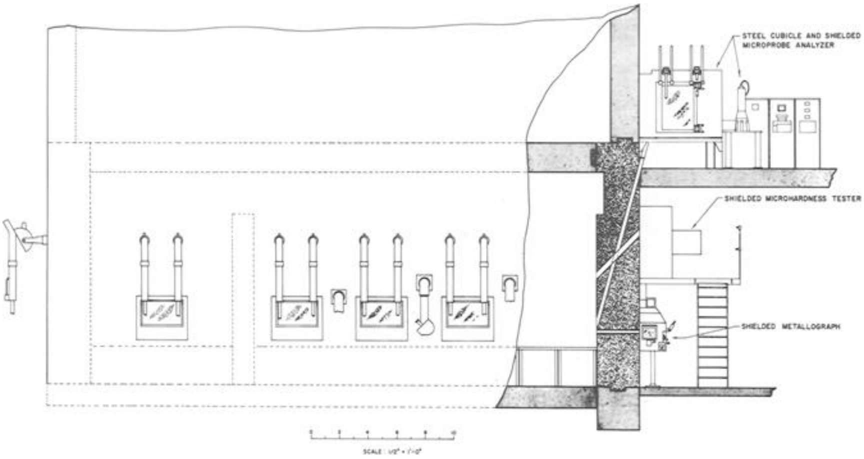

FIG. 11—*Elevation view: metallography cell and related equipment in the HRLEL.*

Microstructures of Radioactive Materials

The great scope of materials and radiation effects cannot be covered in this review, so generalization is necessary. Only a few selected examples of fuel and structural materials are presented to show the effects of radiation. Radiation levels are presented but, for brevity, direct reference to designs of fuel, material, and their relationship to specific reactors may not be made.

It must be emphasized that metallographers involved in the examination of radioactive materials usually analyze specimens that have received extensive and unusual radiation exposures—even to the extent of failure. It must not be construed that these microstructures are always representative of specimens receiving minimum or even normal operating radiation exposures.

Fuel Materials

Reactors vary greatly in design size and power [9]. The Oak Ridge National Laboratory (X-10) Graphite Reactor, now a National Historical Monument, was placed in operation in 1943. This reactor, which is a 24-foot cube, used 35 tons of aluminum-clad natural uranium fuel slugs and 620 tons of graphite to produce a power level of about 3800 kW and a thermal neutron flux of about 10^{12} neutrons/cm^2-s. This design can be contrasted with today's High Flux Isotope Reactor [*10*]. This new reactor is a plate-type, cylindrically shaped reactor with highly enriched U_3O_8 fuel dispersed in aluminum powder in the core of aluminum-clad plates. The reactor core, Fig. 12, is about the size of a 20-gal garbage can and operates at a power level of 100,000 kW and

FIG. 12—*High Flux Isotopic Reactor fuel element.*

a flux of 5 × 10^{15} neutrons/cm^2-s. It is cooled and moderated[8] by light water and reflected with beryllium. For comparison, the well-known hydroelectric power generators at Norris Dam have a generating capacity of 100,800 kW. Although the above information is not directly connected to the assigned title of this paper, there is an indirect relationship to the advancement in reactor technology and the service position of metallography in making these achievements possible.

In some types of heterogeneous solid fuel reactors, the fuel is a compound (oxide, carbide, metallic, etc.) of uranium or some other fissionable material

---

[8] A moderator slows down the fast fission neutrons to thermal energies. Beryllium, graphite (carbon), and heavy water, which all have low atomic weights, are most effective in slowing down the fission neutrons to thermal velocities.

distributed in a metallic matrix [*11*]. In a hermetically sealed sandwich construction, this dispersion fuel and matrix constitute the meat and the two cladding layers are the two layers of bread of the fuel plate. This very simplified description represents many years of development of dispersion fuel reactors.

The cross section of two types of U_3O_8 fuel dispersions in aluminum and the subsequent changes after irradiation can be seen in Fig. 13. Reaction between the fuel and the matrix is obvious. Some unreacted fuel remains, however, and the fission gas has collected and formed spherical voids. Progressive changes in a UAl_3 fuel dispersed in aluminum with 6061 aluminum cladding can be seen in Fig. 14. An example of a dispersion fuel of UO_2 in a stainless steel matrix is shown in Fig. 15. The etched microstructure of the fuel and stainless steel matrix and cladding can be seen. The fragmentation of the UO_2

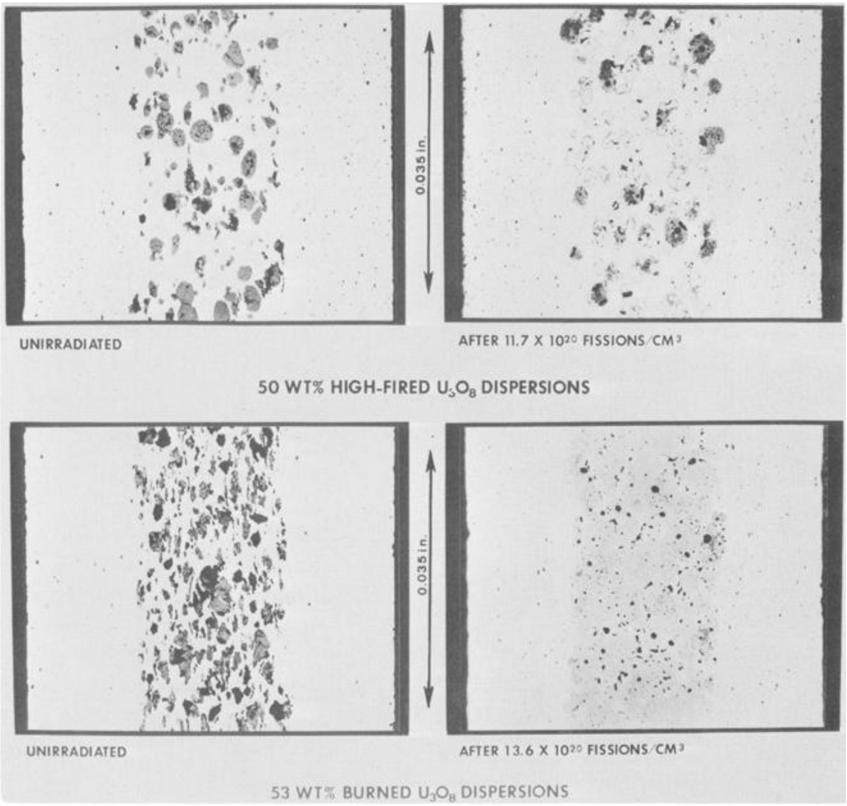

FIG. 13—*Typical microstructures of aluminum-based U_3O_8 dispersion fuel plates before and after irradiation.*

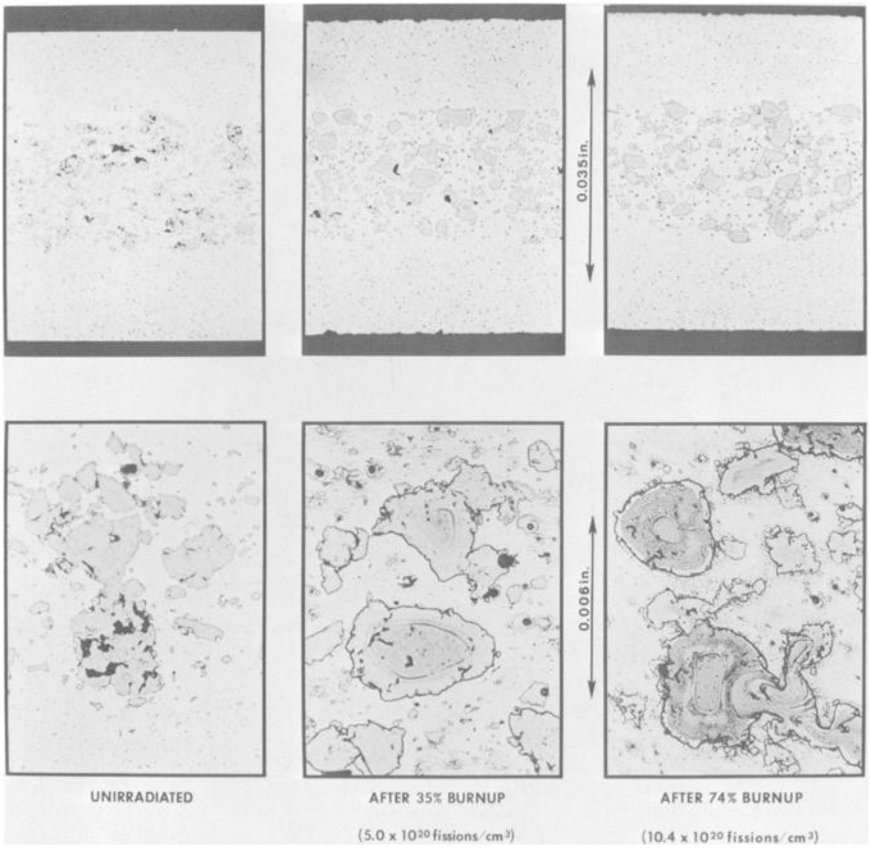

UNIRRADIATED

AFTER 35% BURNUP (5.0 x 10^{20} fissions/cm^3)

AFTER 74% BURNUP (10.4 x 10^{20} fissions/cm^3)

FIG. 14—*Typical microstructures of aluminum-clad, aluminum-*UAl_3 *dispersion fuel plate:* (top) *core cross section;* (bottom) *core microstructure.*

due to the rolling operation can be seen in the photomicrographs of the as-fabricated plate. After irradiation the fuel particles near the clad or the plate surface show greater neutron damage and capture than those nearer the center of the plate, where some shielding took place. Each fuel particle produced a halo in the metallic matrix due to fission recoil. Undoubtedly, a high dislocation density is present in this halo area, and the area is harder and less resistant to the etching action.

Another concept of fuel and reactor design requires the dispersion of fine spherical particles of the fuel in graphite [*12–14*]. The small spheres, 100 to 500 μm in diameter, are fabricated with individual or collective coatings of silicon carbide, alumina, or pyrolytic carbon to retain the fission products,

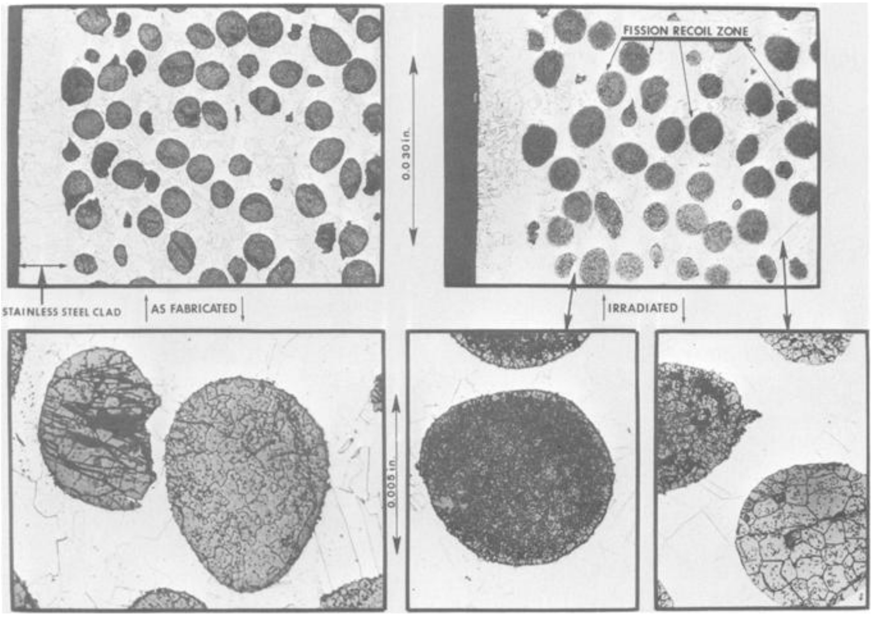

FIG. 15—*Irradiation-induced microstructural changes, stainless-steel-clad, stainless steel-UO_2 dispersion fuel plate.*

simplify handling and fabrication, and prevent reaction of some fuel compounds with the graphite matrix.

Microstructures of irradiated UO_2 fuel particles which have received an inner buffer coating of low-density porous carbon, a middle layer of silicon carbide, and an outer layer of high-density isotropic pyrolytic carbon are shown in Fig. 16. The protective responsibility of these three layers to maintain the integrity of the coated fuel is illustrated well in this metallographic study. Uranium dicarbide fuel particles protected by the same coatings (silicon carbide and pyrolytic carbon) are shown in Fig. 17. Fuel characteristics may change considerably after exposure to radiation, and, under severe experimental conditions, interaction and diffusion of the fuel and coatings can be seen in the microstructure. Interesting changes often occur in the microstructures in relation to temperature differentials. Note in Fig. 17 that reaction (if such developed) between the fuel and coatings has occurred on one quadrant of the sphere, seen in the polished median plane. The driving force of the reaction is directly related to the location of the coated fuel particle with respect to the higher temperature and flux regions of the reactor.

Another type of reactor fuel is a pressed and sintered right cylinder pellet [*15*], which can be stacked longitudinally in a stainless steel tube to make a fuel element. Marked microstructural changes are seen in UO_2 fuel when it

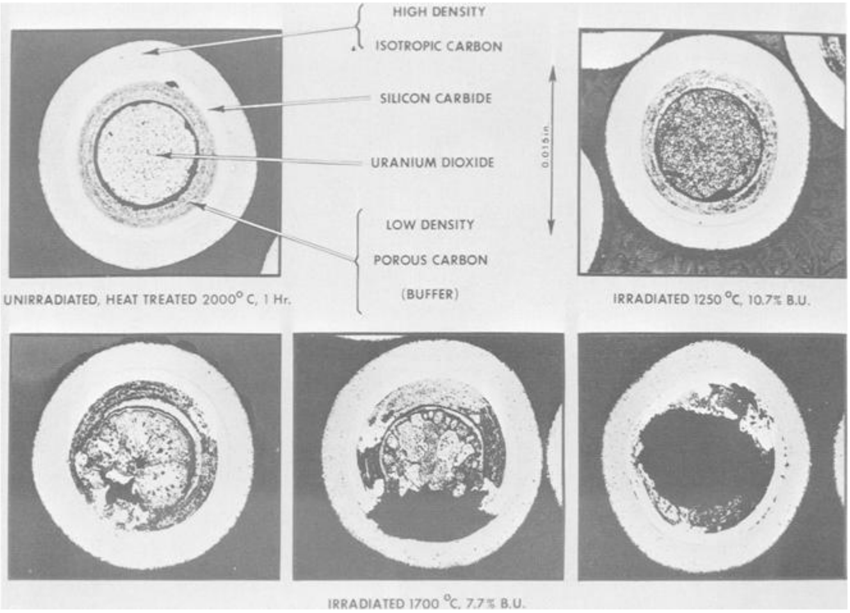

FIG. 16—*Irradiation behavior of buffer, SiC, and isotropic carbon-coated* UO_2.

is irradiated above 1800 C. A longitudinal view of the microstructure at the end contact of two pellets is shown in Fig. 18. The outer third of the radii of the two pellets shows little or no change from the original microstructure. The heat-affected zone shows a dramatic change in the development of columnar grains. It was first thought that these columnar grains could be attributed to a previous molten stage and the subsequent slow cool. This condition was discounted, however, by nuclear physicists, so other explanations were explored. It was concluded that columnar grains were developed by the migration of coalesced fabrication pores up the temperature gradient (toward the center of the pellet). Typical migrating lenticular voids are shown in Fig. 18. This void movement has erased the gap between the two pellets over about two thirds of the radii. This lenticular void movement occurs when uranium dioxide sublimes from the hot side within the void and condenses on the cold side [*16*, *17*]. As the void migrates toward the higher temperature (the hotter ($>$1800 C) center of the pellet), a columnar grain of a single orientation is formed. Fission gases in the path of the lenticular void are trapped within the void and carried to the center of the fuel pellet.

One approach under investigation in the fabrication of a reactor fuel rod or element is the packing of various sized fuel particles or microspheres of the desired materials, such as thoria, urania, plutonia, or any combinations,

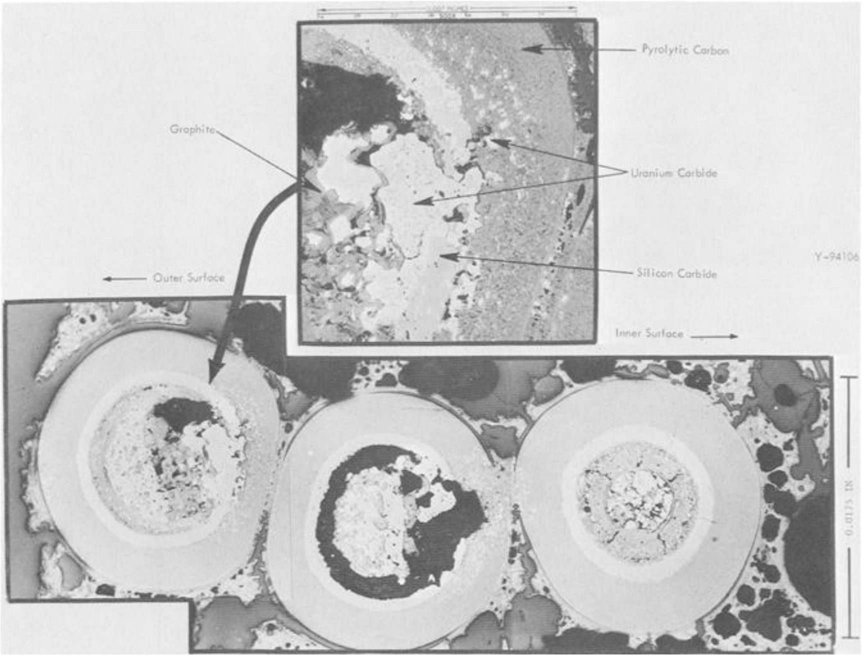

FIG. 17—*Uranium carbide microspheres (~200 μm) coated with alternate layers of pyrolytic carbon and silicon carbide. Maximum irradiation test temperature, 1700 C.*

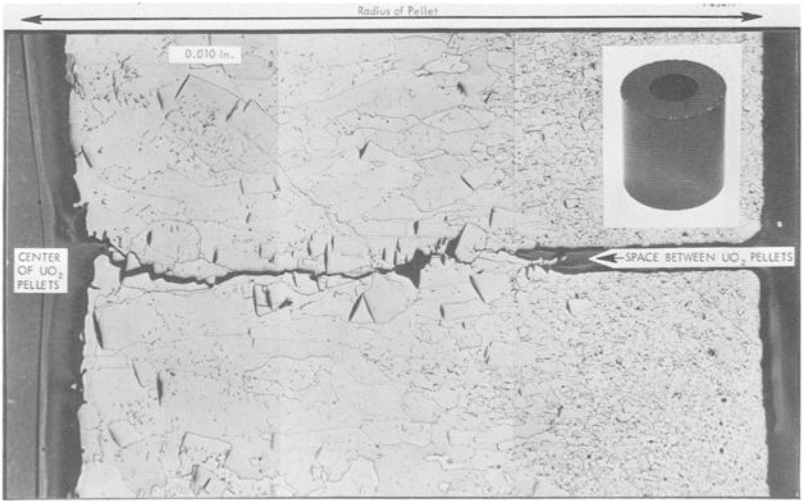

FIG. 18—*Longitudinal view of two UO_2 pellets after irradiation. Inset shows typical UO_2 fuel pellet prior to irradiation.*

in a tube or some other container configuration [*18*]. For example, a cylindrical tube container of Type 304 stainless steel of the required diameter is filled with coarse-sized microspheres of a $-35 + 40$ mesh (500 to 450 μm in diameter). A second addition of microspheres follows with -325 mesh (<44 μm in diameter). With the aid of low-energy vibratory compaction, 88 percent theoretical density is achieved by filling the interstices of the larger spheres. The spheres can be fabricated by the sol-gel process and are economically attractive. Metallography is highly important in the entire program of any such developments, from the fabrication of the spheres to the final analysis after irradiation in a reactor. Metallographic examination of the microspheres during fuel development is necessary to evaluate the microstructure for homogeneity, voids, and general morphology. The general appearance of a median plane view of these spheres is shown in Fig. 19. In this same figure the results of irradiation at various neutron flux levels on the microstructure of fuel pins loaded by means of the Sphere-Pac process can

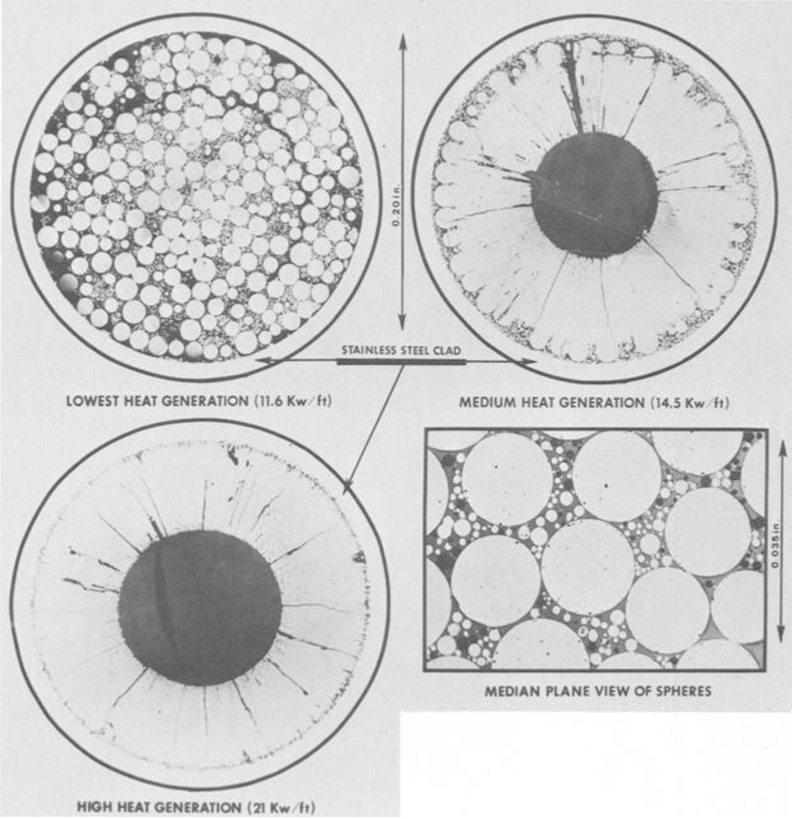

LOWEST HEAT GENERATION (11.6 Kw/ft)

MEDIUM HEAT GENERATION (14.5 Kw/ft)

HIGH HEAT GENERATION (21 Kw/ft)

MEDIAN PLANE VIEW OF SPHERES

FIG. 19—*Sphere-Pac fuels.*

be seen. The position of metallography is to determine the amount of sintering of the fuel particles and the general appearance of the microstructure. The previously described phenomenon of densification of the fuel by sublimation and lenticular void movement is evident in cross-sectional examinations of these Type 304 stainless steel containing Sphere-Pac oxide fuels. Lowest heat generation (11.6 kW/ft) shows sintering of the small spheres; medium heat generation (14.5 kW/ft) shows advanced sintering of the large and small spheres; high heat generation (21 kW/ft) shows almost complete sintering. Near theoretical density is achieved in the solid areas, and the previous interstitial voids have migrated to the center.

Electron Microscopy

The need for electron microscopy in addition to optical metallography of radioactive materials became apparent and has resulted in great progress within the past five years. The development of replication [*19–23*] and thinning techniques [*24–26*] has allowed investigators to shed new light on what is occurring in fuels and structural materials. Since electron microscopy is skillfully covered by other authors in this symposium, we shall only touch on the relation of this important method of investigation to our assigned topic. One example of the usefulness of electron microscopy is shown in Fig. 20. The presence of the fission gas bubbles in the uranium nitride fuel is apparent in the light optics photomicrographs, but the morphological characteristics of the bubbles are revealed when a replica of a fracture is examined with an electron microscope, aptly defining the limitations of resolution and magnification of the former. Replication of highly radioactive specimens is accomplished in the hot cell with the manipulator fingers performing the steps normally done in the laboratory by hand. The cellulose acetate (5 to 6 mils thick) is softened on one side with acetone and pressed onto the specimen

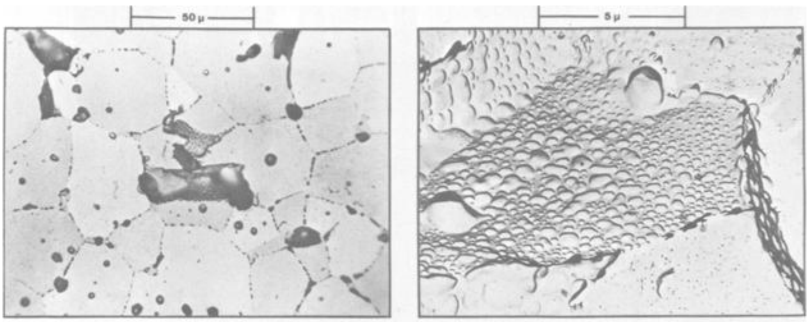

METALLOGRAPHIC SECTION (LIGHT OPTICS)

FRACTOGRAPHIC SECTION (ELECTRON OPTICS)

FIG. 20—*Fission gas bubbles in a nuclear fuel as revealed by standard metallography and electron microscopy.*

FIG. 21—*In-cell replication techniques:* (left) *replication of polished and etched specimen;* (right) *replication of a fractured specimen.*

(also wet with acetone) with a rubber stopper and allowed to dry (Fig. 21). The first three replicas are discarded to remove loose particulates, then three replicas are made, placed in clean plastic bags, and removed from the cell. Specimens with activity levels of 30,000 R/h have been replicated with the replicas having an activity level of 50 mR/h to 10 R/h. After a preliminary examination, the accepted replicas are shadowed with chromium and re-replicated with carbon or chromium metal. The cellulose acetate is dissolved in acetone after placing the secondary replica next to the electron microscope specimen screen. The specimen with the secondary replica is washed in a reflux condenser with acetone. The activity level of the replica that is placed in the electron microscope is normally 0 to 20 mR/h [*23*].

By working with shielded hoods and glove boxes, the electron microscopist is able to thin radioactive materials for transmission electron microscopy. The philosophy for the preparation and examination of relatively low radiaction levels varies with each laboratory and microscopist. Electron microscopists at Oak Ridge National Laboratory [*24*] have used conventional transmission electron microscopy on very clean electropolished specimens reading up to 10 R/h. It was necessary to deviate from conventional techniques to develop procedures that require a minimum of handling of the specimens. Fairly high radiation levels can be tolerated because the exposure time is short. Some recent investigations [*27*] have been reported on the transmission electron microscopy of irradiated ceramics. Since irradiation damage is often difficult to detect in the postirradiation examinations of structural materials, transmission electron microscopy is particularly helpful. Selected examples of the use of this technique will be presented in the following subsection.

Structural Materials

The mechanical properties of reactor structural materials usually are influenced by radiation. The extent of this effect is dependent on the flux, time, and temperature. Structural materials such as aluminum, stainless steel, and many others receive the attention for metallographic examination. An example of some tensile fracture characteristics of 8001 aluminum (0.17 percent Si, 0.45–0.7 percent Fe, 0.15 percent maximum Cu, 0.9–1.3 percent Ni, and the balance Al) in the unirradiated and irradiated conditions are shown in Fig. 22. The reduction in ductility after irradiation at this fluence is quite obvious. The microstructures of the same aluminum in the as-irradiated condition and after heat treatment of the irradiated aluminum are shown in Fig. 23. Precipitates tend to become coarse and large gas bubbles grow at these particles after high-temperature heat treatments.

A recent report by Stiegler et al [*28*] describes the effect of irradiation damage on aluminum. A general review of radiation damage to aluminum has been compiled by Cunningham [*29*]. An example of the effects of irradiation on 1100 aluminum is shown in some comparison electron micrographs, Fig. 24. The unirradiated microstructure shows relatively clear grains with some globular silicon containing inclusions. The irradiated material received

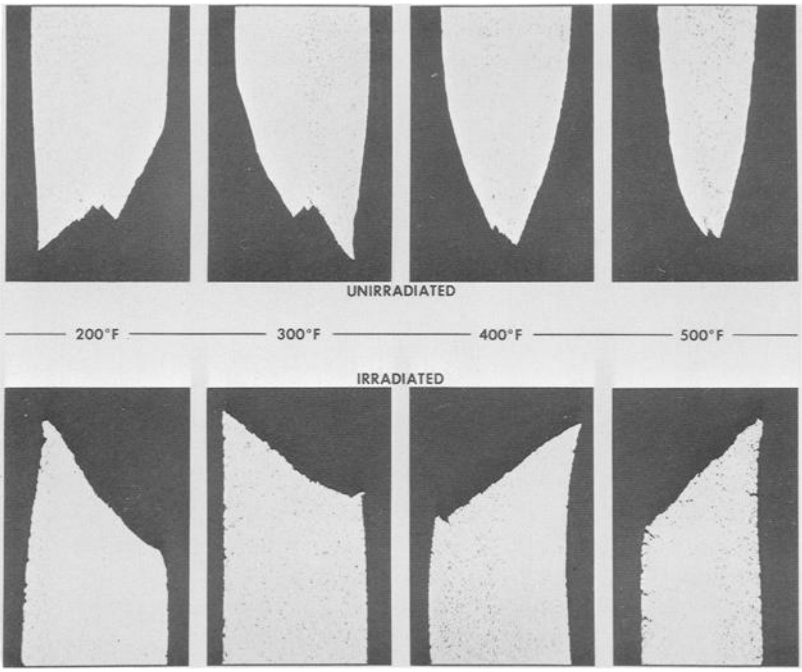

FIG. 22—*Profiles of aluminum tensile fractures in the unirradiated and irradiated conditions.*

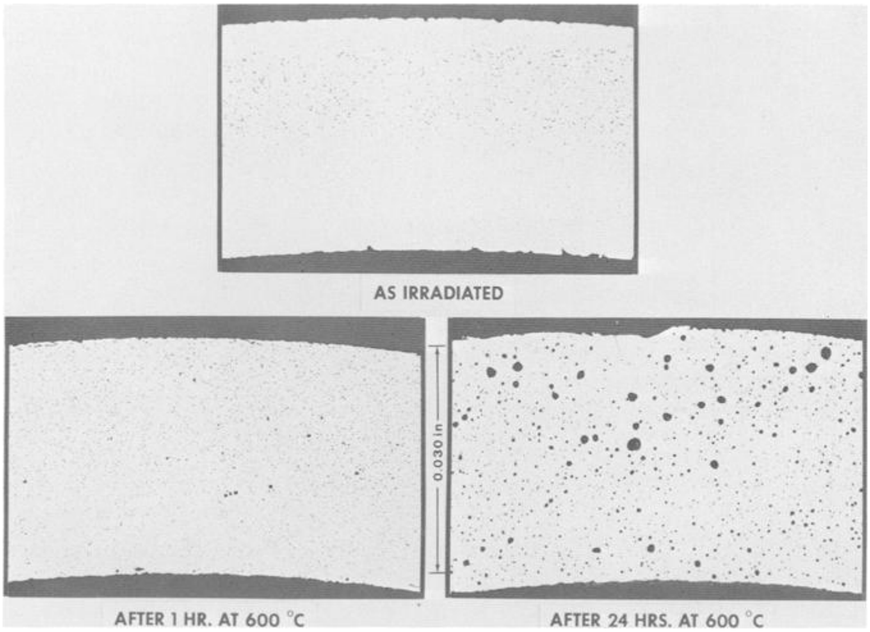

FIG. 23—*Voids and precipitates in irradiated 8001 aluminum.*

an exposure of 1.5 × 10^{22} neutrons/cm^2 at 45 C and was annealed 20 h at 90 C. Cubical voids, which are crystallographically oriented, have formed probably as a result of precipitation of vacancies produced during irradiation. It is interesting to note a lineup of these cubical voids adjacent to the grain boundaries, which certainly does not enhance the mechanical properties of 1100 aluminum.

Transmission electron micrographs of graphite are shown in Fig. 25. The characteristic "ribbons" seen in the unirradiated specimen (Fig. 25*a*) have been erased in the irradiated specimen. The interpretation and significance of these observed changes are under investigation by Yust et al [*30*] at Oak Ridge National Laboratory. The study of the irradiation effects on graphite is of prime importance, because in the Molten Salt Reactor Experiment [*31*] the nuclear fuel is a molten fluoride salt (75 LiF, 20.1 BeF_2, 5 ZrF_4, 0.9 UF_4 mole percent) moderated by unclad graphite. With the graphite in direct contact with the environment of the molten salt, there is concern over what changes take place in this moderator material. Within the limitations of optical metallography there is little or no evidence of change. Changes are evident, however, as shown previously (Fig. 25), when the investigation is extended to electron microscopy.

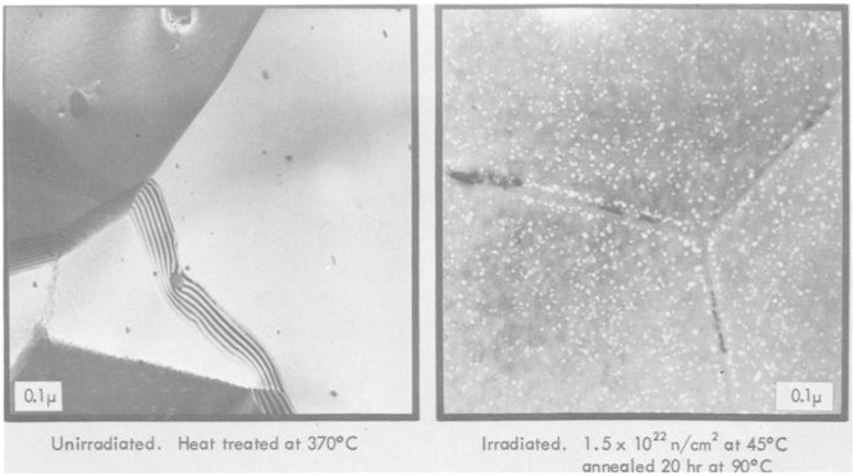

Unirradiated. Heat treated at 370°C

Irradiated. 1.5×10^{22} n/cm^2 at 45°C annealed 20 hr at 90°C

FIG. 24—*Transmission electron micrographs of unirradiated and irradiated aluminum.*

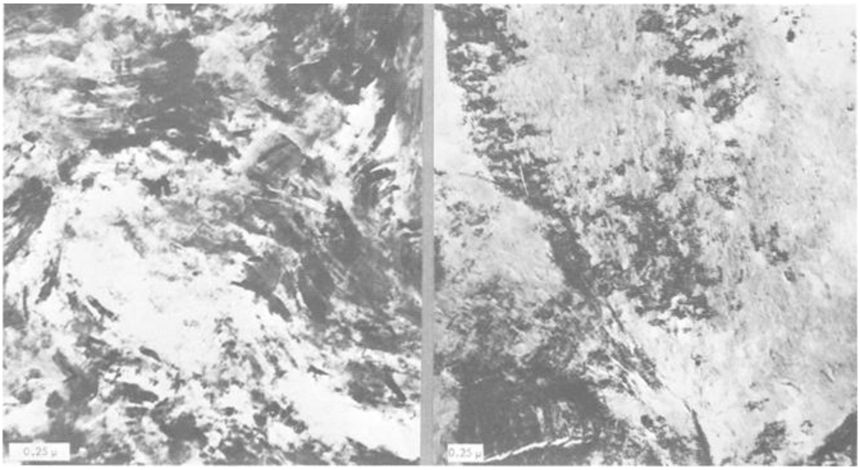

FIG. 25—*Transmission electron micrographs of graphite (AXF):* (left) *unirradiated;* (right) *irradiated.*

In this same reactor (Molten Salt Reactor Experiment) Hastelloy N,[9] a structural material, must also be exposed to and be compatible with an environment of 1.3×10^{20} neutrons/cm^2 thermal and the fast dose of 10^{19} neutrons/cm^2 at 645 ± 10 C. Comparative tensile properties of irradiated and unirradiated Hastelloy N are under investigation by McCoy [*32–35*]. Changes in the microstructure of Hastelloy N determined by light optics in the irradiated and unirradiated conditions are shown in Fig. 26. These

[9] 16Mo-6Cr-3.3Fe-0.055C-balance Ni.

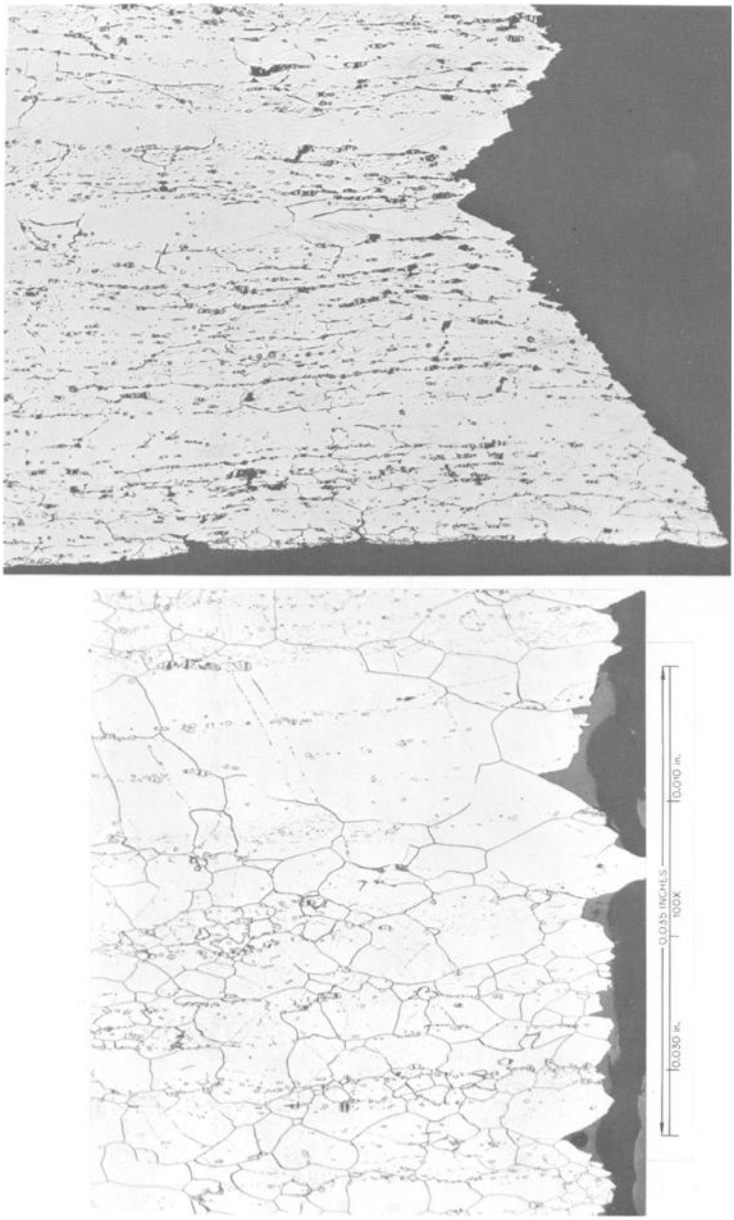

FIG. 26—*Microstructures at tensile fracture of unirradiated and irradiated Hastelloy N:* (top) *unirradiated;* (bottom) *irradiated.*

microstructures at the fracture areas show the extensive deformation and transgranular shear-type failure of the unirradiated specimen and the contrasting intergranular failure of the irradiated specimen. Additional explanation of the fracture characteristics and the tensile data can be seen with a transmission electron micrograph, Fig. 27. Helium bubbles are shown along a grain boundary in the Hastelloy N. Helium is produced from neutron radiation of ^{10}B. The generation of helium bubbles in the grain boundaries results in a reduction of the fracture strain. This research makes it apparent that heat treatment or changing the composition of the alloy or both are necessary to compensate for this irradiation damage.

Autoradiography

Only a few of the many techniques utilized in the examination of radioactive materials have been described. One technique, autoradiography, must not be excluded. Since both natural and induced radioactivities are present

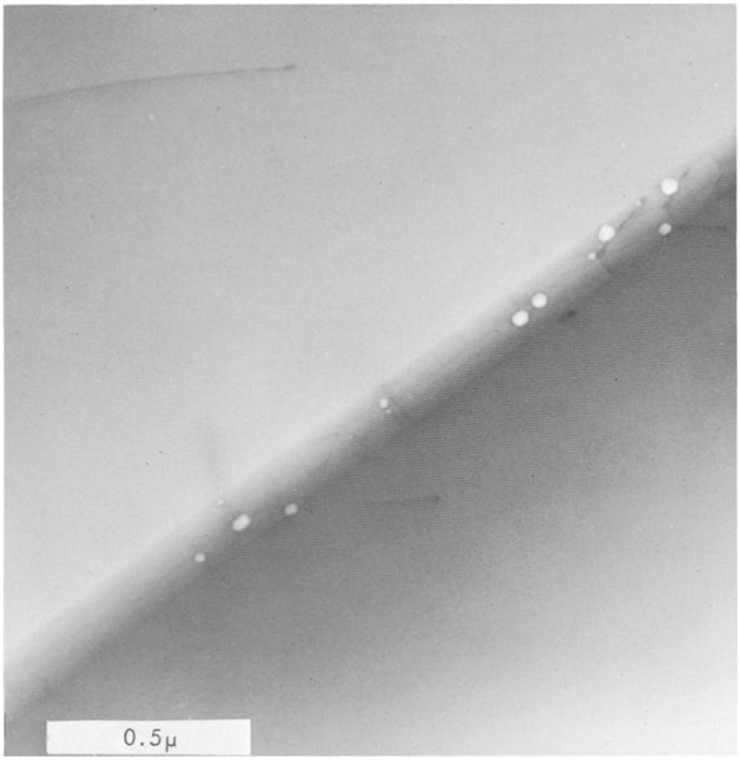

FIG. 27—*Transmission electron micrograph of irradiated Hastelloy N. Note helium bubbles at the grain boundary* (×*61,000*).

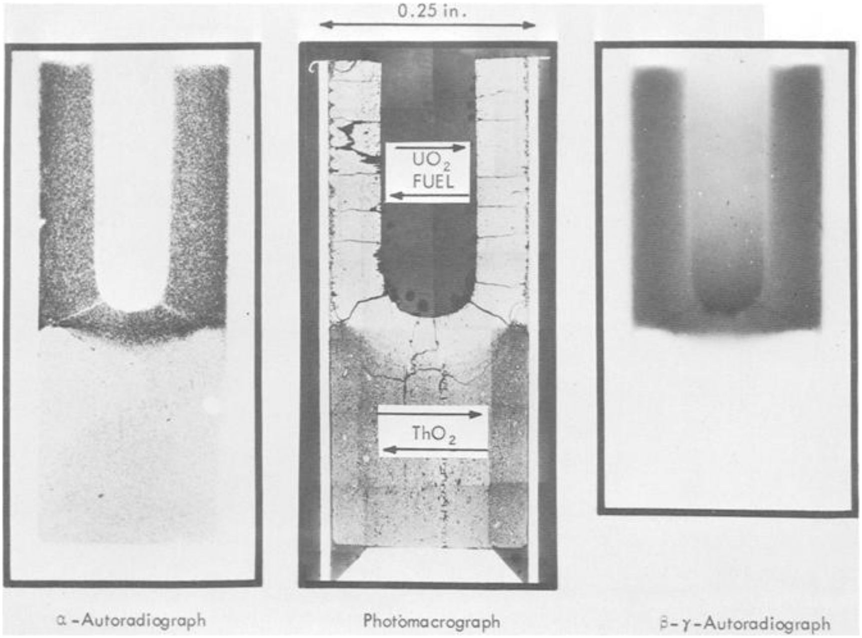

FIG. 28—*α-emitting oxides and β-γ fission products in a longitudinal section of a fuel pellet after irradiation.*

in irradiated fuels, considerable additional information with regard to the performance of the fuel can be obtained at very little additional expense with autoradiographic techniques. In autoradiography one simply places the radioactive specimen in contact with a suitable film for short periods of time, removes the exposed film from the glove box or the hot cells, and develops the image with proper solutions. Alpha activity is normally registered with plastics [*36*], such as cellulose nitrate,[10] and etched with a caustic solution to reveal alpha particle tracks. Latent images of β-γ activities can be recorded on photographic film and developed using ordinary darkroom techniques. A typical example of an autoradiographic examination is shown in Fig. 28. It is evident that uranium has much greater α activity than thorium and that thorium has no naturally occurring β-γ activity; furthermore, there was no general migration of fission products into the ThO_2, although a solid solution was formed at the interface of the UO_2 and ThO_2. The two very dark spots at the bottom of the β-γ autoradiograph are due to deposits of metallic fission products; one deposit survived polishing and can be seen in the photomacrograph.

[10] Kodak special film, Type 106-01-A, nonsilver radiation recording film, Eastman Kodak Co., Rochester, N. Y. 14650.

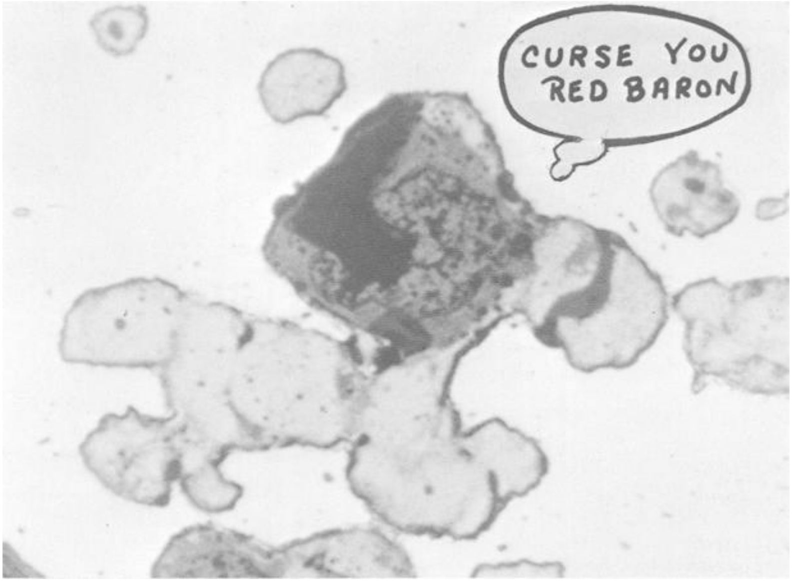

FIG. 29—*Snoopy in the reactor* (×*440*).

Reactor Characters

Just as "characters" can be found in the microstructure in conventional metallography, this added attraction can be discovered in working with radioactive materials. Snoopy has become a familiar character in papers and magazines, and he has played an important part in the Apollo 10 trip to the moon; so why shouldn't he show up in a reactor. Snoopy was found in the microstructure of a fuel plate of U_3O_8 fuel dispersed in an aluminum matrix and was reported as the cover feature in a nuclear magazine [*37*]. A chemical reaction between the fuel and the aluminum matrix formed the figure shown in Fig. 29. The dark areas are voids; the dark gray is remaining fuel, U_3O_8; the light gray was originally U_3O_8 but has reacted with the aluminum matrix. With such a sterling character working on the team, metallography will definitely carry a principal role in the development of better fuels and materials.

Summary

The value of metallography in the examination of radioactive materials is presented. Many of the responsibilities in this field are not covered; however, some of the equipment and working conditions required when working with radioactive materials are described. Some selected examples of the influence of neutron irradiation on the microstructure of fuels and structural materials are presented.

Acknowledgments

We are indebted to our excellent metallography and photography technicians, who have exercised great patience and high standards in performing their duties. We thank G. M. Slaughter, R. E. Gehlbach, and J. R. Weir, Jr., for their suggestions in reviewing the manuscript. Special thanks go to Mary Combs for her suggestions and preparation of the manuscript.

References

[*1*] Morgan, K. Z. and Turner, J. E., *Principles of Radiation Protection*, John Wiley & Sons, New York, 1967.

[*2*] Gray, R. J. and Leslie, B. C., "An Alpha Metallography Facility," Proceedings of 22nd AEC Metallography Group Meeting, Denver, Colo., 19–21 June 1968; Conf. No. 68-0614, Div. Tech. Inf. Ext., Atomic Energy Commission (to be published).

[*3*] "Health and Safety," *Plutonium Handbook, A Guide to the Technology*, Section VII, O. J. Wick, Ed., Gordon and Breach, New York, 1967, pp. 785–936.

[*4*] Krill, F. M., *Metal Progress*, MEPOA, Vol. 70, No. 1, July 1956, pp. 81–82.

[*5*] Long, E. L., Jr., and Gray, R. J., *Metal Progress*, MEPOA, Vol. 74, No. 4, Oct. 1958, pp. 145–148.

[*6*] Rothstein, P. and Turner, F. R. in *Methods of Metallographic Specimen Preparation, ASTM STP 285*, American Society for Testing and Materials, 1960, pp. 90–102.

[*7*] Gray, R. J. and Leslie, B. C., "A Metallograph for Glove Box Operations," Proceedings of First Annual Technical Meeting, International Metallographic Society, Denver, Colo., 11–13 Nov. 1968.

[*8*] Long, E. L., Jr., et al in *Methods of Metallographic Specimen Preparation, ASTM STP 285*, American Society for Testing and Materials, 1960, pp. 79–89.

[*9*] Jacobowitz, H., *Fundamentals of Nuclear Energy and Power Reactors*, John F. Rider New York, 1959.

[*10*] Winters, C. E., *Nuclear Science and Engineering*, NSENA, Vol. 17, No. 3, Nov. 1963, pp. 443–447.

[*11*] Holden, A. N., *Dispersion Fuel Elements*, ASM-AEC Monograph, Gordon and Breach, New York, 1967.

[*12*] Harms, W. O. et al in *Ceramic Matrix Fuels Containing Coated Particles*, TID-7654, Proceedings of a symposium held at Battelle Memorial Institute, 5 and 6 Nov. 1962, 1963, pp. 71–104.

[*13*] Bomar, E. S. and Gray, R. J. in *International Symposium on Compounds of Interest in Nuclear Reactor Technology*, J. T. Waber et al, Eds., Metallurgical Society, American Institute of Mining and Metallurgical Engineers, New York, 1964, pp. 703–728.

[*14*] "Coated-Particle Fuels," ORNL-4324, Oak Ridge National Laboratory, Oak Ridge, Tenn., Nov. 1968.

[*15*] Scott, J. L. and Weaver, S. C., "Fuels for Water Reactors," ORNL-TM-2357, Oak Ridge National Laboratory, Oak Ridge, Tenn., Dec. 1968.

[*16*] Bates, U. L. and Roake, W. E., "Irradiation of Fuel Elements Containing UO_2 Powder," Fifth Nuclear Engineering and Science Congress, Preprint V-90, April 1959.

[*17*] MacEwan, J. R. and Lawson, V. B., *Journal of the American Ceramic Society*, JACTA, Vol. 45, 1962, pp. 42–46.

[*18*] Kitts, F. G. et al, "Sol-Gel Urania-Plutonia Microsphere Preparation and Fabrication into Fuel Rods," Proceedings of International Symposium on Plutonium Fuels Technology, Scottsdale, Ariz., 1967; Nuclear Met 13, American Institute of Mining, Metallurgical and Petroleum Engineers, New York, 1968.

[*19*] Bierlein, T. K., Morgan, J. R. and Mallett, G. R., "The Metallography of Irradiated Uranium—Preparation, Cathodic Vacuum Etching, and Replication," HW 42184 (Rev.), 25 May 1956.

[*20*] Padden, T. R. in *Uranium Dioxide: Properties and Nuclear Applications*, J. Belle, Ed., U. S. Government Printing Office, Supt. of Documents, Washington, D. C., July 1961.

[*21*] Leighton, S. A., "Preparation of Radioactive Metallic Specimens for Replication," Technical Papers of the Nineteenth Metallography Group Meeting, 20–22 April 1965, ORNL-TM-1161, Oak Ridge National Laboratory, Oak Ridge, Tenn., Feb. 1966.

[*22*] McGrath, F. E., "One-Step Replication in the Hot Cell," Technical Papers of the Seventeenth Metallographic Group Meeting, 21–23 May 1963, NMI-4999, Los Alamos Scientific Laboratory, Los Alamos, N. M., April 1966.

[*23*] Miller, J. L., Jr., *Metallography, An International Journal*, Vol. 1, No. 3/4, Jan. 1969, pp. 443–447.

[*24*] DuBose, C. K. H. and Stiegler, J. O., "Semiautomatic Preparation of Specimens for Transmission Electron Microscopy," ORNL-4066, Oak Ridge National Laboratory, Oak Ridge, Tenn., Feb. 1967.

[*25*] DuBose, C. K. H. and Stiegler, J. O., *The Review of Scientific Instruments*, RSINA, Vol. 38, No. 5, May 1967, pp. 694–695.

[*26*] DuBose, C. K. H. and Jones, C., "Techniques for the Preparation of Transmission Electron Microscopy Specimens from Tubing," ORNL-TM-2408, Oak Ridge National Laboratory, Oak Ridge, Tenn., Jan. 1969.

[*27*] Katz, O. M., "Fission Gas Bubbles in Fractured UO_2," Proceedings of the Electron Microscopy Society of America 26th Annual Meeting, 16–19 Sept. 1968, C. J. Arceneaux, Ed., Clailors Pub. Div., Baton Rouge, La., 1968.

[*28*] Stiegler, J. O. et al, "High Fluence Neutron Irradiation Damage in Aluminum," Proceedings of the IAEA Symposium on Radiation Damage in Reactor Materials, Vienna, Austria, 2–6 June 1969 (to be published).

[*29*] Cunningham, J. E., "Severe Radiation Damage to Aluminum Alloys," ORNL-TM-2138, Oak Ridge National Laboratory, Oak Ridge, Tenn., March 1968.

[*30*] Yust, C. S. et al, in *Carbon*, Pergamon Press, Elmsford, N. J. (in press).

[*31*] MacPherson, H. G., *Journal of Power Engineering*, Vol. 71, 1967, p. 56.

[*32*] McCoy, H. E., *Journal of Nuclear Materials*, JNUMA, Vol. 31, 1969, p. 67.

[*33*] McCoy, H. E., "An Evaluation of the Molten-Salt Reactor Experiment Hastelloy N Surveillance Specimens—First Group," ORNL-TM-1997, Oak Ridge National Laboratory, Oak Ridge, Tenn., Nov. 1967.

[*34*] McCoy, H. E., "An Evaluation of the Molten-Salt Reactor Experiment Hastelloy N Surveillance Specimens—Second Group, " ORNL-TM-2359, Oak Ridge National Laboratory, Oak Ridge, Tenn., Feb. 1969.

[*35*] McCoy, H. E., "An Evaluation of the Molten-Salt Reactor Experiment Hastelloy N Surveillance Specimens—Third Group," ORNL-TM-2647, Oak Ridge National Laboratory, Oak Ridge, Tenn., Jan. 1970.

[*36*] Gruber, W. J., "Autoradiography of Irradiated Nuclear Ceramic Fuels," Proceedings of Fall Meeting of the American Ceramic Society, Pittsburgh, Pa., 6–9 Oct. 1968.

[*37*] *Nuclear News*, NUNWA, Vol. 12, No. 1, Jan. 1969.

J. L. Brimhall,[1] *B. Mastel,*[1] *and H. R. Brager*[1]

A Review of Some Techniques and Metallurgical Applications for Transmission Electron Microscopy*

REFERENCE: Brimhall, J. L., Mastel, B. and Brager, H. R., **"A Review of Some Techniques and Metallurgical Applications for Transmission Electron Microscopy,"** *Applications of Modern Metallographic Techniques, ASTM STP 480,* American Society for Testing and Materials, 1970, pp. 97–126.

ABSTRACT: The application of transmission electron microscopy in metallurgical studies is discussed. It is hoped that the reader will obtain an idea of what is involved in electron microscopy and some of the pitfalls to avoid. Specimen preparation techniques, analysis of the microstructure with specific examples, factors affecting quantitative analysis, and recent innovations are all discussed. Throughout, the recent advances and techniques will be emphasized. For a more complete description and background of the techniques, appropriate references are given at the end of the paper.

KEY WORDS: electrolytes, electron microscopy, evaluation, foils (materials), metallographic structures, metallography, metallurgical analysis, microstructures, thickness, transmissivity

Transmission electron microscopy is rapidly becoming a standard metallographic technique which few laboratories can do without. In fact, it is no longer adequate to merely take pictures with the microscope, since methods are now available for the detailed and complete analysis of microstructure. The technique is unique in that the internal microstructure is observed rather than just the surface. With the advent of ultrahigh voltage electron microscopy, thicker specimens can be studied and results will be more representative of the bulk microstructure.

Specimen Selection and Preparation

The study of materials by transmission electron microscopy generally requires thinning of the specimen to allow penetration by the electron beam.

---

[1] Senior research scientists, Pacific Northwest Laboratory, Battelle Memorial Laboratory, Richland, Wash. 99352.

* This paper is based on work performed under U. S. Atomic Energy Commission Contract AT(45-1)-1830.

The maximum thickness through which a beam can penetrate is given by a critical value for the product of physical thickness and density of the specimen. For aluminum specimens a thickness of 2000 Å is not excessive, while a specimen of uranium must be thinned to less than 500 Å for transmission by the conventional 100-keV beam. Thus, techniques are required for thinning specimens to proper dimensions without altering the microstructure during processing. To date electrolytic dissolution of the specimen has demonstrated itself as the best method of preparation.

In general, specimens for transmission electron microscopy can be categorized into two groups: (1) those involving thin foils, 100 μm or less in thickness, or (2) wafers cut from bulk specimens. Studies of quenched-in defects, irradiation effects, dislocation interactions, and diffusion can be performed with thin foils. Preparation of specimens for microscopy is relatively easy, as only one thinning step is required. Studies requiring direct comparisons between microstructure and physical properties generally require wafers to be cut from bulk material, as, for example, a failed pressure vessel, tubing, or structural supports. Specimens in this category require two stages of preparation, which, therefore, is more time consuming.

Preparation from Thin Specimens

The basic method of thinning specimens electrolytically, as described by Heidenreich [*1*][2] and subsequently refined by Bollmann [*2*], has not changed greatly. In all cases the specimen is made the anode in an electrolyte composed of an oxidizing agent and a carrier which removes metal ions from the specimen. Specialized polishing cells have been described to accommodate a wide variety of specimen sizes [*3*]. After painting the edge of the specimen with an insulting lacquer to prevent preferential attack,[3] a dc is impressed between the specimen and cathodes. Appropriate meters should be employed in the circuit to monitor and reproduce polishing conditions. The choice of electrolyte, temperature, and voltage is dictated by the material to be thinned. Excellent tabulations exist and should be consulted [*4*, *5*].

The shape of the cathodes has been modified by various investigators to control polishing rates [*6*, *7*]. Ginn and Brown [*8*] have shown that a uniform polishing rate can be obtained when a potential relative to a calomel electrode is supplied by a potentiostat. This addition to the circuitry is valuable when polishing specimens which contain large precipitates. A simpler potentiostat has been designed by Malone [*9*], who uses the feedback from a probe to control the output current and thus maintain the voltage between the anode and probe constant.

---

[2] Italic numbers in brackets refer to the list of references at the end of this paper.

[3] Microstop lacquer, Michigan Chrome and Chemical Co., Detroit, Mich. 48213.

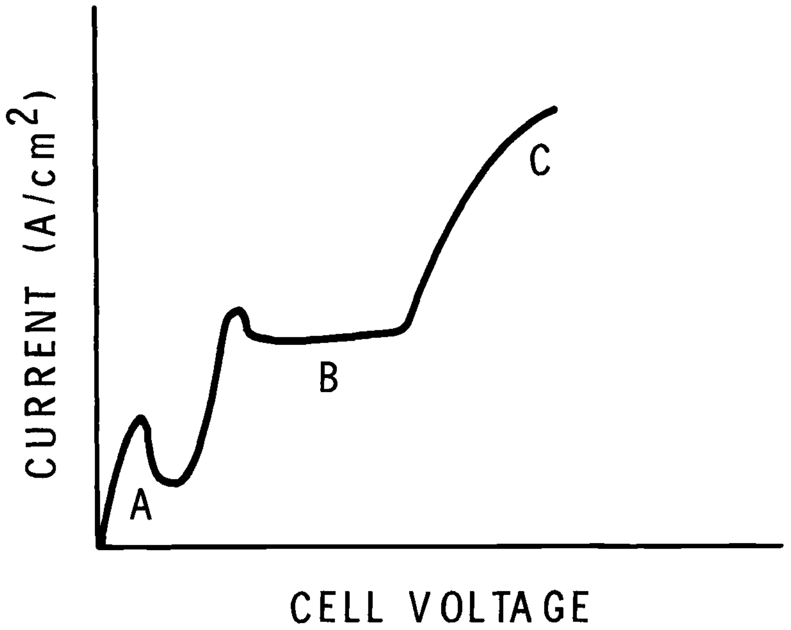

FIG. 1—*Schematic plot of current versus voltage in a standard electrolytic polishing apparatus. Etching takes place in region* A; *region* B *is the polishing range; in region* C *the specimen is pitted.*

During polishing the ratio of the voltage to the current will vary. To establish optimum polishing conditions a plot of the current and voltage is first prepared (Fig. 1). At lower voltages the current increases rapidly and the specimen is etching; a plateau is then reached where a further increase in voltage results in no increase in current. The best polishing takes place at the high end of the plateau. Increasing the voltage beyond the plateau will cause the current to increase again and pit the specimen.

Preparation from Bulk Sections

In an increasing number of cases it is necessary to study the microstructure of specimens which are in bulk form. This requires that small sections be cut from the bulk material so that they will fit into the specimen holder. These sections can be cut from the bulk in a variety of ways: by a diamond slitting saw, spark machining, acid saws, or by whatever method the investigator prefers. A diamond saw has been used routinely to section a wide variety of materials (Fig. 2). The samples are first embedded in plastic to prevent deformation during sawing and sections 0.50 mm thick are cut [*11*]. Although action of the saw does produce a cold-worked layer on the surface, tests have

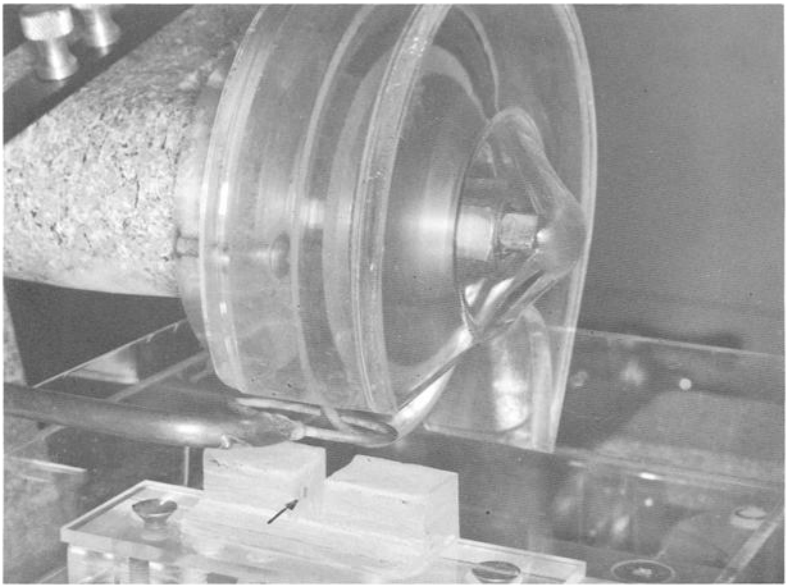

FIG. 2—*Diamond saw for sectioning bulk samples. Arrow indicates sample imbedded in plastic.*

demonstrated that this layer can be removed during subsequent polishing. Spark machining of sections can produce surfaces with a thinner disturbed layer on the surface, but this method is rather time consuming and the sides of the section are seldom parallel. Sections with the least amount of disturbed material on the surface are prepared with an acid saw. This process is slow; Hunt [*11*] has recently described a technique for prolonging the acid carrier life by rinsing the carrier with water.

After a small section has been obtained, the next stage in specimen preparation is the initial thinning, or dimpling, of both sides of the section. A number of jet dimpling devices have been described in the literature [*12*, *13*]. All the methods utilize the flow of an electrolyte through a jet against the specimen, which is made the anode (Fig. 3). The process is rapid and several mils of material can be removed each minute. A detailed analysis of the dimpling process has been investigated by Du Bose and Stiegler [*14*]. A polishing plateau is not observed during jet dimpling, the current and the electrolyte flow rate determine the shape of the dimple. The depth of the dimple is predicted from previously established calibration curves of specimen thickness versus time of jetting. A novel method of measuring the thickness of nonradioactive specimens during dimpling has been developed by Sharp [*15*]: the specimen is interposed between a source of Sr^{90}, a beta emitter, and a counting chamber; the thickness of the dimple is a function of the number of counts transmitted through the foil.

After the specimen has been dimpled, final polishing is performed in a specialized cell, as described by Du Bose [14] or Blankenburg [16]. In either case the specimen is positioned between a light source and a detector which will interrupt the polishing action when perforation takes place (Fig. 4). Both use a cadium sulfide cell to detect the transmitted light beam and special circuitry to stop polishing at the first perforation. In place of the cadium sulfide cell, a small microscope may be used to observe the specimen. Holes less than 5 μm in diameter in dimpled specimens can be detected and polishing can be stopped manually. The latter method has an advantage in that the operators can distinguish between bubbles in the electrolyte and an actual perforation.

Use of a special holder made of polytetrafluoroethylene (teflon), as described by Dewey and Lewis [17], permits polishing of sections without the

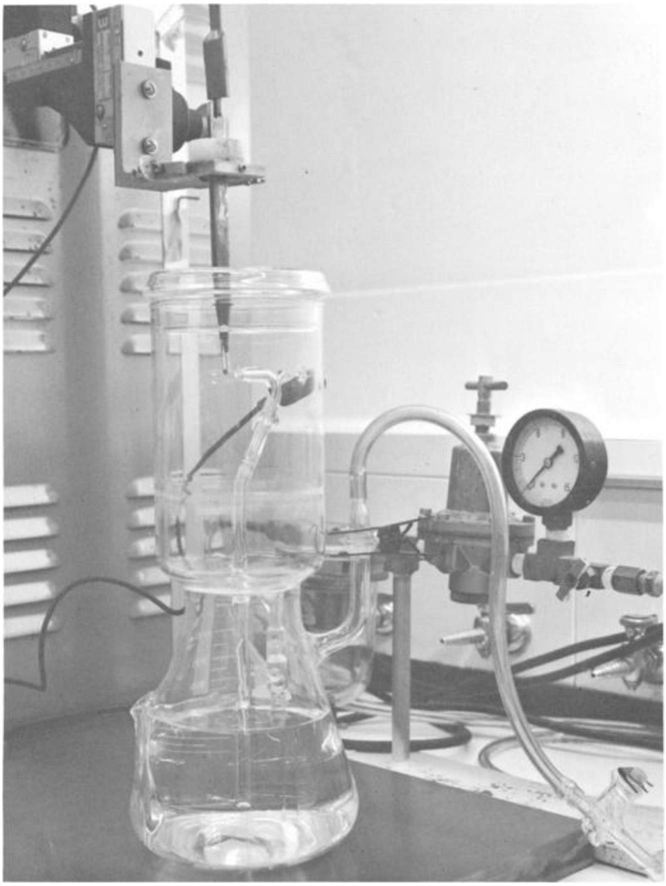

FIG. 3—*Apparatus for jet dimpling of bulk samples. Jet is controlled by air pressure.*

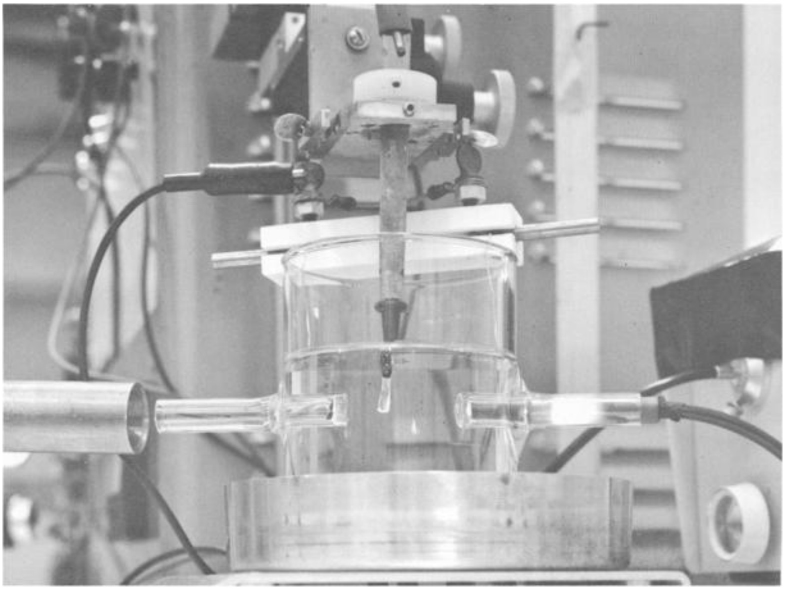

FIG. 4—*Apparatus for final polishing dimpled specimen. Specimen is immersed and positioned between the light beam and detector.*

dimpling operation. The holder is made of two covers which screw into the holder and enclose the specimen. One disadvantage of the technique is that the temperature of the specimen may rise to 120 C under certain polishing conditions [*18*]. If structural changes take place in this temperature range, the electrolyte must be circulated against the specimen. Such a device has been described by Schoone [*19*], who pumps the electrolyte through hollow plastic tubes which contain the cathodes. In this device the specimen in the teflon holder is positioned between a light source and a photo cell, and when perforation takes place the polishing is interrupted.

The methods outlined above can be made applicable to a wide variety of bulk samples. For example, transmission microscopy has been performed on thin wires which were ground or spark machined so that opposite sides were flat [*20, 21*]. These surfaces were then dimpled and polished as described. Techniques for studying thin-walled tubing in the microscope have been described by Du Bose and Jones [*22*]. Their method consists of sawing the supported sample, jet dimpling under controlled conditions, and final polishing. From the methods outlined above, specimens for transmission microscopy can be obtained from any sample geometry.

Other Specimen Preparation Techniques

A relatively new and completely different method of specimen preparation is that of ionic bombardment. The dimpled specimen is made the cathode in a vacuum chamber. After evacuation a rare gas at reduced pressure is admitted and a potential of several thousand volts is applied between the specimen and the two ion guns, the anodes. Specimen material is removed by a sputtering action from both sides of the specimen simultaneously. The process is relatively slow, removing about 1 μm/h depending on the sputtering rate of the specimen. This method does offer several advantages over electrolytic dissolution: (1) the specimen is free of corrosion products, (2) large areas of the specimen are transparent to electrons, and (3) the process can be greatly controlled and reproducible results thereby obtained. Specimens of electrical conductors as well as nonconducting ceramics have been successfully prepared for microscopy by this method. Two ion thinning machines are now commercially available,[4] and with the advent of high-voltage microscopy the use of this technique should become more popular.

Chemical polishing of metals has been investigated to some extent for specimen thinning. There are several inherent difficulties associated with chemical polishing which restrict the use of this technique. Since chemical polishing is usually carried out at elevated temperatures, polishing rates are high and difficult to control. Preferential attack on precipitates with consequent loss from the specimen is a common occurrence, and corrosion product contamination is difficult to remove from thinned specimens. The use of chemical polishing has been largely restricted to thinning ceramic and semiconductor materials. A small cell which circulates heated chemical reagents against the specimen has been used by Kirkpatrick and Amelinckx [*23*] to thin magnesium oxide crystals and barium titanate. The cell is made of glass and is small enough to fit under an optical microscope so that polishing can be observed. It is versatile and should provide a basis for chemical polishing of a wide variety of nonconducting materials. Semiconductor materials have been thinned by first sawing wafer sections from the bulk, followed by chemical dimpling on alternate sides. Silicon and germanium specimens 0.30 mm thick prepared in this manner show that deformation introduced by the wafering can be removed by polishing action. A simple chemical jetting device has been described by Booker [*24*] to thin silicon and germanium.

Sections of layered materials which have a plane of easy cleavage may be prepared by repeated cleavage. Natural and synthetic graphites have been cleaved between adhesive tape and studied extensively [*25*]. The technique is valuable but restrictive in that the cleaved surfaces are generally parallel

---

[4] Alba, Ingenieurs Constructeurs, Asnieres-Seine, France, and Commonwealth Scientific Corp., Alexandria, Va. 22314.

to one axis only and some deformation is introduced into the specimen during the operation. Fragments from large cleaved surfaces have been removed by flooding the cleaved surface with collodion and then stripping. These replicas containing the cleaved fragments are then examined in the microscope. This method has been successfully used by Hulse and Tice [*26*] to study MgO, TiO_2, Al_2O_3, and other ceramic materials.

Specimens containing internal cracks and pores cannot be prepared by the methods described. During chemical or electropolishing the cavities in a specimen will become enlarged and their geometry will change. Use of an ultramicrotome to cut sections thin enough without changing the internal porosity has been investigated by Phillips [*27*]. The specimen was in the form of a rod which was electropolished to a reduced diameter, embedded in plastic, and sectioned with a diamond knife. Internally oxidized copper was heated in hydrogen to form internal cavities. Upon sectioning there was some distortion of the cavities and it was necessary to make a correction parallel to cutting direction [*28*]. This technique is well suited for obtaining size and density distributions of cavities. In the same study it was demonstrated that second-phase particles as small as 20 Å could be observed in microtomed sections. Because the sectioning action does produce a high density of dislocations (10^{12} cm^{-2}) the technique is not suitable for the study of dislocation densities, interactions, etc.

Artifacts in Specimen Preparation

Soon after transmission microscopy studies were initiated it was recognized that artifacts can arise during specimen preparation. The origin of the artifacts may be attributed to polishing effects or changes which take place in the microstructure as thinning proceeds. The presence of oxide layers on highly reactive substances such as zirconium, uranium, and titanium may be verified by electron diffraction. The formation of hydride in thin foil specimens of zirconium has been attributed to hydrogen pickup during electropolishing [*29*]. Transformations of body centered cubic (bcc) niobium to face centered cubic (fcc) niobium oxide have been observed after storage of thin foils at room temperature [*30*]. In this case oxygen may have been picked up during specimen polishing and the local concentration became sufficiently high to cause the phase transformation. One should be aware of these artifacts when interpreting precipitate structures, making accurate calculations of foil thickness, and performing diffusion experiments in the microscope.

Direct comparison of the microstructure of thin specimens required for electron microscopy with that of the bulk sample is possible only if the effects of the thinning process are known. Rearrangements of dislocations during polishing are expected. It was first demonstrated by Wilsdorf and Schmitz [*31*] that the dislocation density will vary as the thickness of the specimen changes. They deformed single crystals of aluminum and observed dislocation densities in regions having different thicknesses, noted that the density was markedly reduced in sections of the foil which were less than 2000 Å thick and that the distribution of the dislocations present were altered, and concluded that dislocations escaped to the surface and that untangling of networks took place during thinning.

An attempt to establish quantitatively the number of dislocations lost during polishing was made by Ham [*32*]. He found that under certain conditions 60 percent of the dislocations were lost during specimen preparation but that their general arrangement was not greatly altered. Further evidence for the loss of dislocations during specimen preparation is furnished by Mader et al [*33*]. Deformed single nickel and nickel-copper crystals revealed few screw dislocations in the sections cut parallel to the glide plane. Assuming both edge and screw dislocations are formed in equal numbers, they concluded that screw dislocations had escaped from the specimen by cross slip during polishing and, as noted by Wilsdorf and Schmitz, the density of dislocations decreased noticeably when the foil thickness became less than 1000 Å.

Application of the Technique

In order to obtain the maximum amount of information from transmission electron microscopy, certain procedures or techniques which make microstructural features visible and identifiable must be employed. Since all of the techniques cannot be discussed in detail in this section of the report, only a few specific methods will be described and appropriate references covering the standard techniques will be cited. The specific methods described here will include the conditions which must be satisfied for obtaining useful information and the sources of errors and ambiguities in the techniques. Recent developments in interpretation and mechanical innovations not included in the standard reference books [*5*, *6*, *34–36*] will also be covered. The theory of diffraction contrast will not be covered except to point out some recent trends.

Specimen Manipulation

In order to get maximum information one must be able to control or change the specimen or foil orientation relative to the incident electron beam. Most electron microscopes today can be equipped with some type of goniometer stage. Valdré [*37*] has designed and built a number of precision stages. Several different, multipurpose, high-resolution stages which heat and cool as well as tilt on several axes have been built and are described in the literature [*38*, *39*]. Some stages have also been built that allow studies at temperatures near liquid helium with simultaneous ion bombardment [*40–42*]. It is important that the stage be adjustable so that the tilt axis and optic axis of the microscope can be made to intersect. In this way the field of view will not change and the focus should not be affected during tilting.

The specimen stage tilt mechanism should be smooth to allow tilting through very small angles for changing diffraction contrast and it should be accurate enough to measure differences in orientation for different diffracting conditions or to determine the precise angle of tilt for a stereopair [*43*]. The accuracy and range of tilt of a stage is best determined from analysis of Kikuchi lines. Since the positions of the Kikuchi lines on the diffraction pattern vary directly with specimen orientation, the shift of the Kikuchi lines during tilting can be converted to an angular motion and compared with the tilt read on the stage [*44*]. Sheinin [*45*] has described an alternate calibration method which uses the angular shift associated with the displacement of several orders of a particular Bragg reflection spot. In this case the diffraction spots of interest are perpendicular to the tilt axis and the rotation of the image with respect to the diffraction pattern and the position of the tilt axis relative to the diffraction patterns must be established. Calibrations for some microscopes are available [*46*, *47*]. The location of the tilt axis on the diffraction pattern can be marked on the screen or indicated by wires inserted into the microscope. Once the tilt axis has been located, specific orientations and positions of the foil or structural features in the foil can be selected. Makay [*48*] has described a unique method in which a reflecting mirror is used to image a graduated scale onto the microscope screen.

Determination of Specimen Orientation and Diffracting Conditions

An analysis of the microstructure requires that the crystallographic orientation of the specimen be known. Interpretation depends on the knowledge of the precise diffracting condition, which is provided only by a correct analysis of the diffraction pattern. Graphical and analytical methods are available for indexing diffraction patterns [*5*, *36*]. For standard crystal systems one generally compares the diffraction pattern with standard patterns drawn up for the most common orientations and deduces the orientation by inspection.

It must be realized that the orientation given by a spot diffraction pattern generally cannot be precise. A study of the maximum possible deviation of the orientation derived from a spot pattern from the actual orientation has shown that spots from a particular orientation can persist over a tilt of 20 deg [*46*]. This is due to several different factors: relaxation of the Laue conditions, plastic bending of the foil, elastic rumpling, and lattice curvature from dislocations. The orientation obtained by spot patterns is not only approximate but it is also not unique, that is, we cannot distinguish between $[hk\ell]$ and $[\bar{h}\bar{k}\bar{\ell}]$.

There are several ways for obtaining orientation information more accurately. One can visually optimize the intensity of spots corresponding to ideal orientation upon double tilting. Or, if one determines the range of tilt over which a particular spot pattern is observed, then the midpoint of this tilt range will give a fairly accurate measure of the orientation [*46*]. Ryder and Pitsch [*49, 50*] have outlined a method by which the unique and relatively accurate orientations can be determined if the spots which do not have a common zone can be indexed. By such a method orientations accurate to ±1 deg can be obtained. The most accurate method of obtaining crystal orientation utilizes Kikuchi lines. Von Heimendahl et al [*44*] have shown how the orientation may be determined from the analysis of three independent sets of Kikuchi lines. The poles representing the intersection of the diffracting planes are determined from the analysis of their Kikuchi lines, and their angular separation from the direction of the beam can be found analytically or by stereographic projection. Because this method does require Kikuchi lines, it can be applied only to materials which give rise to Kikuchi lines and not, for example, to highly irradiated or cold-worked materials.

The use of Kikuchi lines to obtain orientations has been made much more general through the development of Kikuchi maps. The Kikuchi pattern is unique for a particular structure and orientation, and, therefore, standard Kikuchi projections exist for all orientations encountered during tilting. The Kikuchi patterns corresponding to certain regions of reciprocal space such as [001], [011], [111] are brought together to form Kikuchi maps. The unknown pattern can then be compared to these Kikuchi maps in order to determine the precise crystal orientation. The Kikuchi maps and their use have been discussed by Thomas et al [*51, 52*]. Maps have been constructed for the fcc, bcc, and hcp lattice systems. Thomas [*53*] has further discussed the applicability of Kikuchi lines in the field of transmission electron microscopy. In addition to determining the orientation exactly and uniquely, Kikuchi maps can also be used to find the nearest suitable diffracting vector $\bar{g}$ for a particular analysis.

Dark-Field Electron Microscopy

Several advantages of dark-field over bright-field microscopy have been known for a considerable time. For attainment of maximum resolution in dark field, the diffracted beam must be coincident with the optical axis of the microscope. Originally this could only be done by tilting the gun, more recently, however, microscopes have been equipped with electromagnetic coils which deflect the beam and simplify achievement of high-resolution dark field. It must be realized that the operating reflection in dark field is the negative of that in bright field, so the beam must be tilted away from the

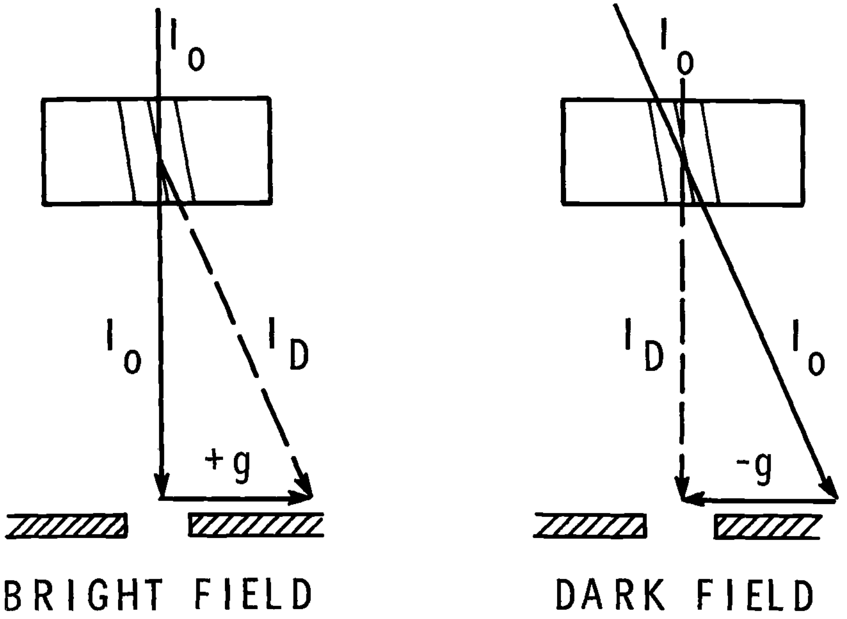

FIG. 5—*Schematic ray diagram illustrating the use of negative bright field* $\bar{g}$ *for operation in dark field.*

operating bright field $\bar{g}$. This is shown in the diagram in Fig. 5. To obtain maximum contrast conditions when using dark field one should also have two beam conditions. The advantages of dark-field microscopy are discussed by Hirsch et al [5] and include (1) indexing extinction contours, (2) identifying phases in a multiphase material, (3) revealing contrast associated with one particular diffracting condition, (4) improving image contrast for those features which show low contrast in bright field, such as small precipitates, and (5) obtaining additional contrast information where the bright-field and dark-field images are not complimentary. Bell and Thomas [*54*] have also shown that in dark field the defects have much better contrast if the defect is near the top or bottom of the foil whenever the foil is tilted to one side or the other of the Bragg condition, that is, s, the deviation parameter, is slightly positive or negative. This is helpful in determining the approximate distribution of defects in a thin foil and in making the presence of a large defect in the foil known. Examples of the use of dark field in the analysis of defects and precipitates are given in a later section.

Electron Stereomicroscopy

Electron stereomicroscopy permits the determination of the spatial configuration of microstructural features. Until recently, most applications were qualitative in nature and served only to differentiate surface features from internal features. The development of precision goniometer stages in which the optical axes can be aligned has permitted the quantitative analysis of the distribution of the structure in the foil. The technique of stereomicroscopy is quite straightforward. The specimen is positioned at some angle ϕ away from the horizontal reference plane of the foil and photographed; it is then tilted to $-\phi$ and the same area is rephotographed. These photographs constitute a stereopair. The angle ϕ is generally between 5 and 10 deg. Problems arise, however, in the quantitative evaluation of the elevation differences of various features, which may give rise to errors. This is particularly true in transmission microscopy where elevation differences of ±15 Å may be important. A detailed treatment of electron stereomicroscopy has been given by Nankivell [*55*] and others [*56–58*]. If one is imaging structures for stereomicroscopy employing diffraction contrast, the diffraction condition must remain the same when tilting through 2ϕ. This is achieved by keeping the operating **g** parallel to the tilt axis. For images produced by absorption contrast, as in the case of voids or certain precipitates, any tilt axis in the specimen plane can be used, provided the defects have good contrast in both micrographs. Several sources lead to errors in the elevation differences determined by electron stereomicroscopy. The tilt axis may not intersect the optical axis. This means that the specimen will move slightly out of its original plane; as a consequence, the objective lens must be refocused and hence the magnification will change. This is best solved by proper alignment of the optical and tilt axes and optical equalization of the magnification of the micrographs. The value of 2ϕ may be erroneous—tilt angles can be accurately determined by the use of Kikuchi lines as discussed previously [*44*]. Magnification calibration may have changed and may necessitate recalibration. Finally, there are measurement errors inherent in the determination of elevations using the parallax bar.

Identification of Features

Imaging of Structure—Familiarity with basic diffraction contrast theory is essential in the interpretation and identification of microstructural features. The development of the essential theory is beyond the scope of this paper, and the reader is referred to texts by Hirsch et al [*5*] or Heidenreich [*35*]. Although this paper refers to the results of some of the theoretical work, no derivations will be given. Much of the work in this area has been concerned with the theoretical calculation of the contrast expected from certain types of hypothetical defects, using computer techniques for plotting the intensity distribution of the defects as a function of various parameters, and then comparing the results with those obtained experimentally. Recently, contrasts for dislocations [*59–61*], stacking faults [*62–65*], and precipitates [*66, 67*] have been theoretically analyzed. This technique has been taken one step further by reconstructing the complete image of dislocations by computer techniques [*68*, *69*]. The images agree quite well with the experimentally observed images. Though one need not know all the ramifications of diffraction contrast, it is important to know how the various parameters are determined and the relationship between the nature of the image and the diffraction conditions.

Dislocation-Type Defects—Extensive information [*5*, *35*, *36*, *70*, *71*] has been published in recent years on the identification of dislocation structures and interface structures such as stacking faults, twin boundaries, and grain boundaries. The principles used to identify the structures are covered in detail. The microscopist essentially makes use of knowledge of how certain diffracting conditions can make a particular defect visible or invisible or give it particular contrast features, that is, fringes or "lines of no contrast." The specimen is manipulated in the microscope and the diffraction pattern is observed until the proper conditions are obtained. The nature of the image contrast is then observed for different sets of diffracting conditions until an unambiguous determination of the cause of the diffraction contrast is achieved.

An example of a recently developed technique which facilitates the identification of different possible Burgers vectors for dislocations in a deformed material is dark-field microscopy [*72*]. Rather than using the bright-field technique, where $\bar{\mathbf{g}}$ satisfies the $\bar{\mathbf{g}} \cdot \bar{\mathbf{b}} = 0$ criterion, one uses high-resolution dark-field microscopy, in which the particular $\bar{\mathbf{g}}$ is brought to the center of the diffraction pattern. The maximum intensity of the diffracting spot can be attained by bringing the extinction contour in the bright-field image that corresponds to the selected $\bar{\mathbf{g}}$ to the optical axis by adjustment of the tilting stage. The dark-field image then shows clearly which dislocations satisfy the $\bar{\mathbf{g}} \cdot \bar{\mathbf{b}} = 0$ criterion. An example of this is shown in the Fig. 6 for dislocation loops in neutron-irradiated molybdenum. The loops are known to have a Burgers vector of $\mathbf{a}/2\langle 111 \rangle$ or $\mathbf{a}\langle 001 \rangle$. Using the criterion that the loop is invisible when $\bar{\mathbf{g}} \cdot \bar{\mathbf{b}} = 0$, the loops cannot be $\langle 100 \rangle$ type. In this case the loops would have been invisible for one of the $\bar{\mathbf{g}}$'s. A $\langle 111 \rangle$ type would be visible in both cases, as is shown in Figs. 6*a* and *b*.

Another recent area of interest has been the identification of small defects, such as small dislocation loops, point defect clusters, voids, or precipitates, whose dimensions are generally less than 150 Å. The analysis of the contrast due to the strain fields from small defects was first treated by Ashby and Brown [*73*, *74*]. They calculated the contrast as a function of several different parameters and in particular showed that, when the defects were near the surface of the foil and the foil was oriented for Bragg diffraction, the contrast was asymmetric and produced a "black-white" image. From the nature of this black-white contrast, illustrated in Fig. 7, the sign and magnitude of the Burgers vector can be determined. Rühle [*75*] has shown that the sense of

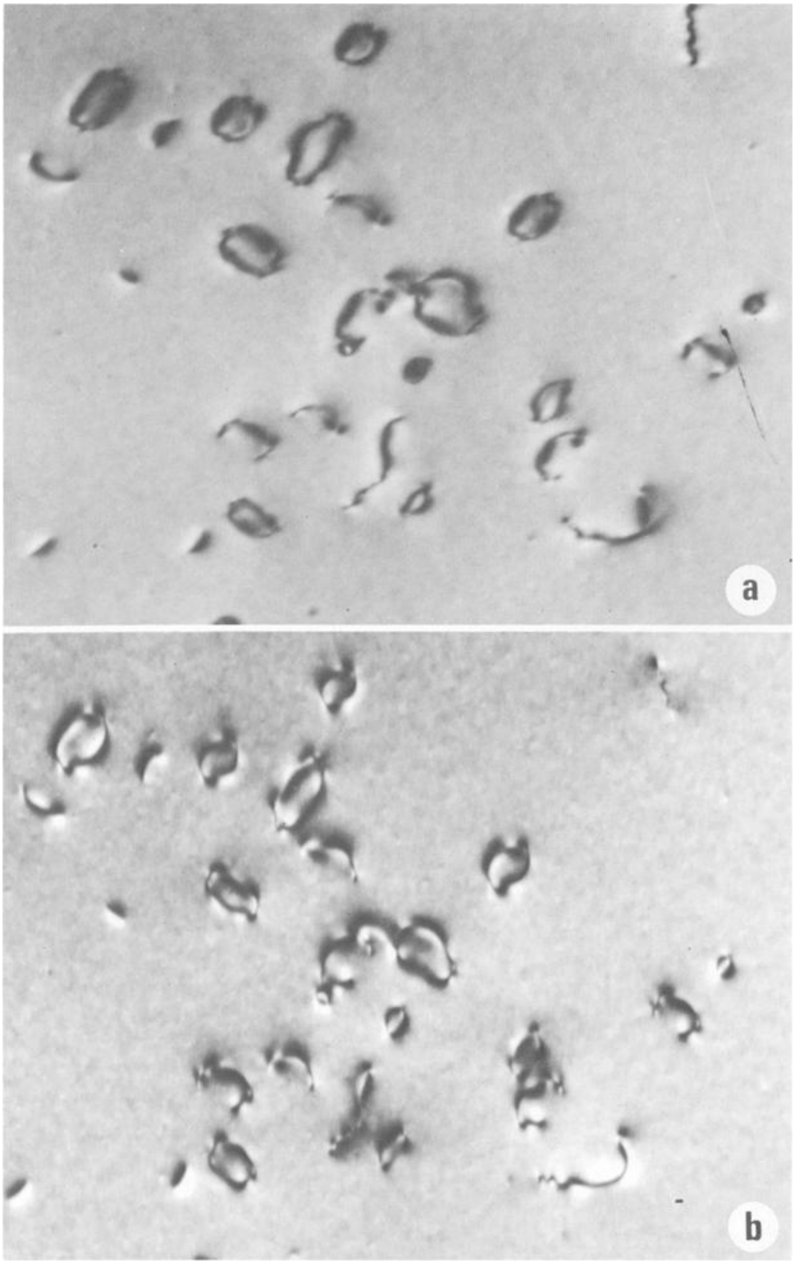

FIG. 6—*Dark-field micrographs of dislocation loops in molybdenum. Loops are visible for both dark-field reflections or* $\bar{\mathbf{g}}\cdot\bar{\mathbf{b}} \neq 0$*. Loops cannot be* **a**⟨100⟩ *type, because some would satisfy* $\bar{\mathbf{g}}\cdot\bar{\mathbf{b}} = 0$ *criterion.* (a) **g** = [*020*]; (b) **g** = [*200*] (×*102,000*).

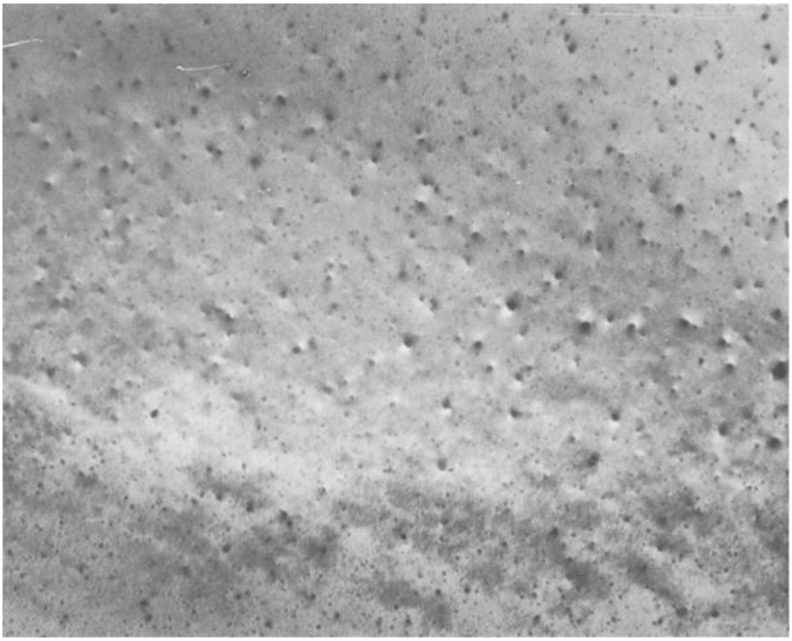

FIG. 7—*Defect clusters in neutron-irradiated rhenium showing the black-white nature of the contrast when the foil is oriented in exact Bragg diffraction and two beam conditions* (×*108,000*).

this black-white contrast varies periodically as a function of the depth of the defect in the foil. The effect of this periodic reversal of contrast, as well as other parameters on the black-white contrast, has been widely discussed [*76*].

An example of the use of this technique is given for the case of neutron-irradiated rhenium. The defects produced by the neutron irradiation are imaged in the Bragg condition to produce a black-white contrast shown in Fig. 7. Stereomicroscopy is used to determine the position of the defects in the foil relative to the surface. If gold is evaporated on the foil to decorate one surface, subsequent stereomeasurements are much easier to make. The defects in the bright-field stereopictures taken in the kinematical condition to produce black spots, as shown in Fig. 8, are correlated with the black-white or white-black contrast associated with the particular defects in the foil oriented for Bragg diffraction. The direction of the black-white contrast as a function of the distance of the responsible defect from the surface is plotted in Fig. 9. This diagram shows that within the layers indicated the sense of the white streak denoted by $\bar{\mathbf{g}}\cdot\bar{\ell}$ is predominantly in one direction. Thus from the rules established by Rühle, these defects are interstitial in type and, in fact, are interstitial loops with Burgers vector $\mathbf{a}[11\bar{2}0]$. These images can be

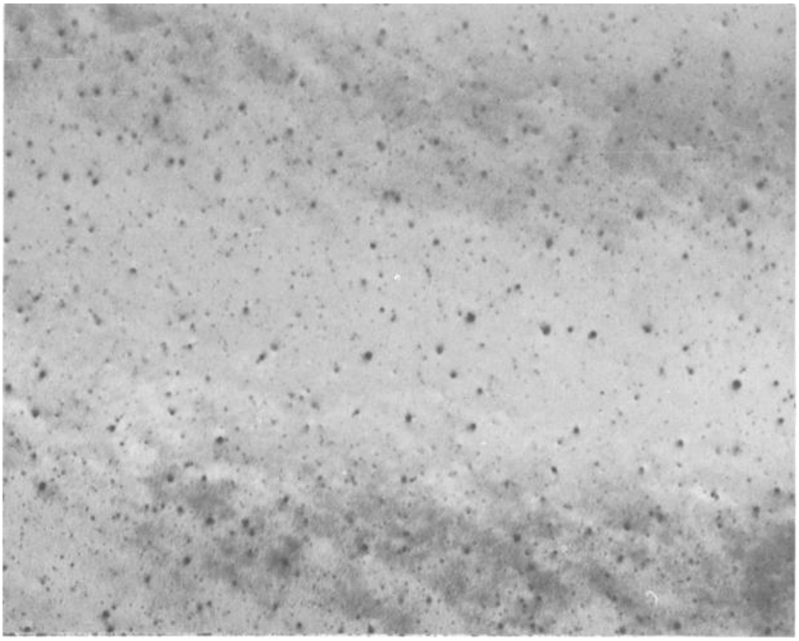

FIG. 8—*Same area as Fig. 7, but tilted away from the Bragg condition. Black-white contrast has now changed black spot contrast. Stereopictures are taken under these conditions* (×*108,000*).

formed in either bright or dark field. For images near the bottom, or electron exit, surface, the direction of the black-white streaks are complimentary in bright and dark field; for images near the top, or entrance, surfaces, the images are the same in bright and dark field. In this example both bright- and dark-field analyses were performed for defects near the bottom surfaces, and the images were indeed complimentary.

This technique has been used extensively to identify defects in quenched and irradiated materials. The technique can be used, in principle, for the identification of the nature of small precipitates as well. There are several sources of error in the analysis, however: the inaccuracies involved in the stereoanalysis, as discussed previously; the position of $\bar{\mathbf{g}}$ relative to the image must be correct; the possibility of misinterpretation due to a denuded layer of defects near the surface or due to a surface oxide. The maximum accuracy to which the position of the defects in the foil can be measured is 15 to 25 Å.

Precipitates—Of great interest to metallurgy is the study of second phases, or precipitates, in metals. It is important to know the size, shape, degree of coherency, strain field, and composition of the precipitate as well as its crystallographic relationship to the matrix. The ability to observe and dis-

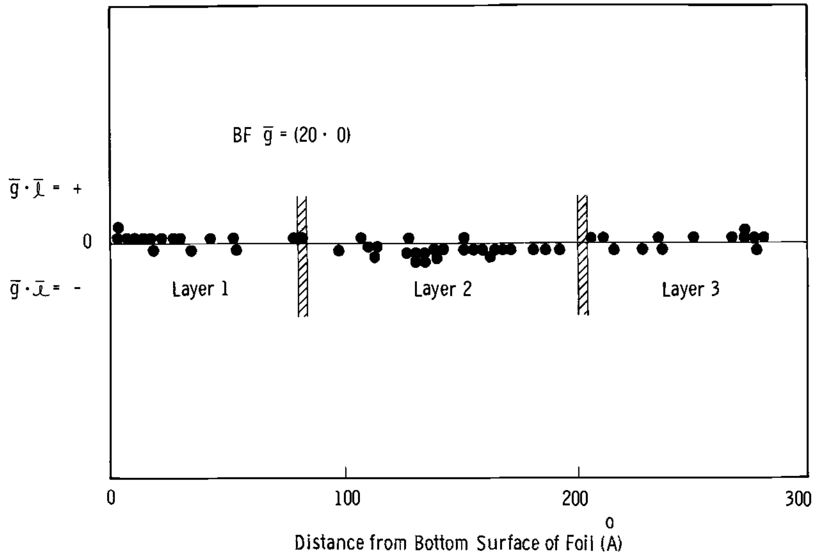

FIG. 9—*Distribution of the sense of the black-white images on Fig. 7 as a function of the distance of the defect from the surface of the foil.* $\bar{l}$ *is the direction of the black-white streak drawn from black to white part.*

tinguish precipitates in a matrix by transmission electron microscopy depends on one or both of two basic factors, matrix and precipitate contrast. Matrix contrast arises from displacements in the matrix due to the strain field of the precipitate. This is particularly useful for small precipitates and has been treated by Ashby and Brown [*73*, *74*]. Precipitate contrast is due to the selective diffraction of the beam when passing through the particle. Contrast can also arise strictly from differences in absorption when there is a significant difference in atomic number between the precipitate and the matrix. Precipitate contrast due to diffraction comes from several sources. Structure factor contrast is due to differences in structure factor of the precipitate and the matrix. This is important when observing solute-rich coherent precipitates such as Guinier-Preston zones. In this case there is an effective increase or decrease in foil thickness, so the bright-field and dark-field micrographs are complimentary. Orientation contrast occurs when the precipitate is oriented to give strong diffraction and the matrix is not. In this case the precipitates will appear dark on a light background on the screen. When the precipitate is diffracting, dark-field microscopy can be used to image the structure using a precipitate reflection. In this manner the precipitates are clearly resolved in the matrix, as shown by comparing Figs. 10*a* and 10*b*. This is very useful for locating and determining the presence of very small diffracting precipitates. A recent example is shown by the work of Brammer and Rhodes [*77*].

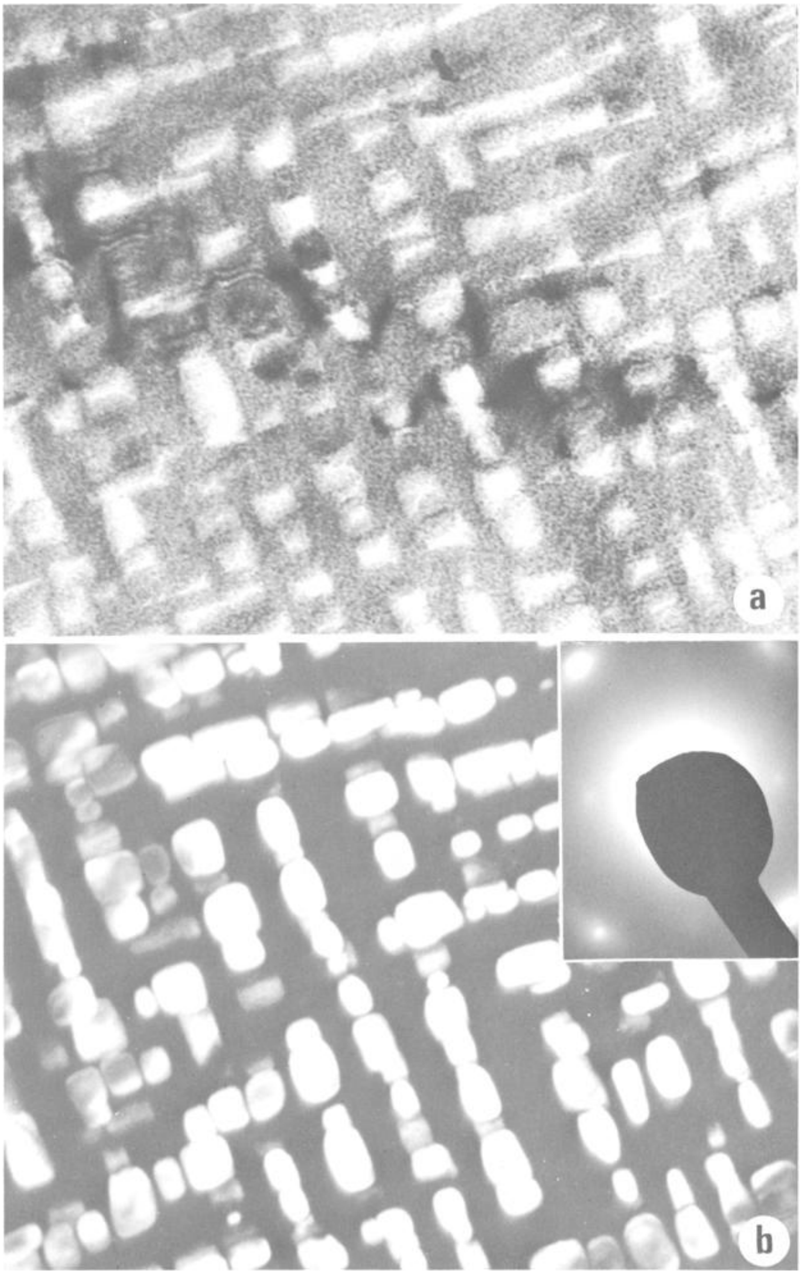

FIG. 10—*Imaging of coherent precipitates in a Ni-Al alloy:* (a) *bright field,* (b) *dark field from precipitate spot indicated on diffraction pattern* (×*81,000*).

Precipitate contrast can also produce displacement fringe contrast and Moiré fringe contrast. Displacement fringe contrast is analogous to stacking fault contrast and is due to a phase shift of the incident and diffracted beams. Ardell [*78*] has discussed this type of contrast at large coherent interfaces. Moiré fringes are a geometrical effect arising from differences in lattice spacing or orientation or both of the precipitate and matrix. In order to distinguish Moiré fringes from other types of fringes, it must be realized that the spacing in Moiré fringes is not a function of the wavelength of the incident beam and that the direction of the fringes is determined solely by the direction of the operating reflection. Other types of fringes will lie parallel to the line of intersection of the precipitate and the surface.

The inaccuracies involved in measurements of selected area diffraction patterns preclude the general use of transmission microscopy for the identification of unknown precipitates. It is almost mandatory that an internal standard such as evaporated thallium chloride or gold be used. Sumerling [*79*], however, has devised a method for using an external standard and claims an error of ±0.5 percent. Mackay [*48*] has also described methods for measuring dimensions on electron diffraction patterns. Selected area diffraction is, however, very useful if there are only a limited number of possibilities for a precipitate and the lattice spacings are not too close for these different possibilities.

Voids—Internal voids and gas bubbles are readily detected by transmission electron microscopy. These types of defects are most easily detected by absorption contrast, so it is not desirable to have the foil in a strong diffracting condition. Voids do give rise to unique diffraction contrast, a process that has been treated by Levy [*80*] and Van Landuyt et al [*81*]. In certain instances, strain fields can be associated with inert gas bubbles. The magnitude of this strain field and the magnitude of the surface energy have also been calculated [*82*].

Neutron-irradiated stainless steel is a good material for illustrating procedures used to identify microstructural features, because it contains most of the lattice defects which are encountered in metallurgical work. After irradiation, dislocations, dislocation loops, stacking faults, second-phase precipitates, and voids are present. Figure 11 illustrates the structure after exposure to neutrons in the reactor to a fluence of 10^{22} neutrons/cm^2 at 540 C. The specimen is oriented for strong diffraction and dislocation loops with stacking fault contrast are present. Crystallographic analysis showed them to lie on $\{111\}$ planes, so they are Frank-type dislocation loops. If the specimen is tilted so that strong Bragg diffraction does not occur, absorption contrast clearly reveals the voids (Fig. 12). Stereomicroscopy substantiated that voids were indeed within the foil and not just surface pits. Since the vacancies go into the voids, it was inferred that the interstitials are probably responsible

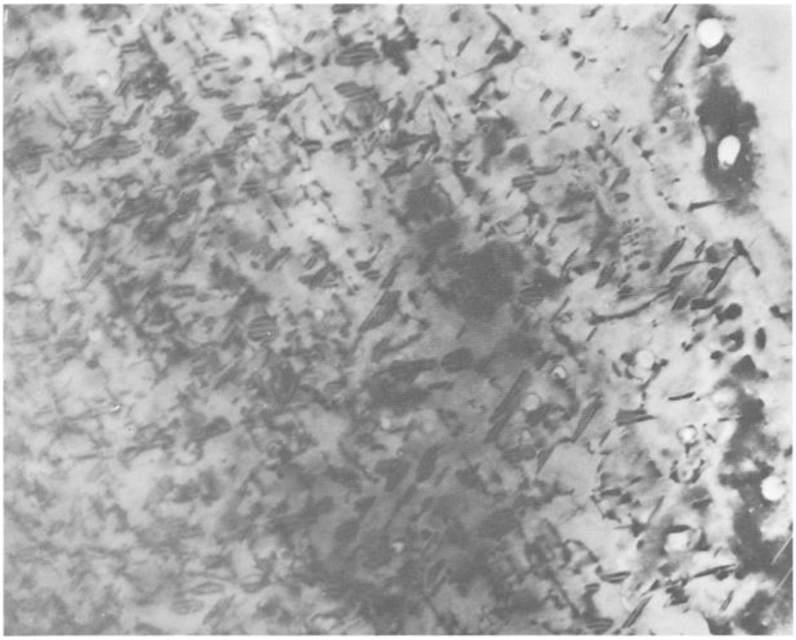

FIG. 11—*Stainless steel irradiated to 1 × 10^{22} neutrons/cm^2 at 540 C. Specimen oriented for strong diffraction contrast shows the faulted Frank dislocation loops* (×*101,000*).

for the Frank loops. This assignment was further substantiated by the fact that during an anneal at an elevated temperature the loops unfaulted and formed networks as shown in Fig. 13. The nature of the loops remaining after the anneal has been established by one of the methods outlined by Hirsch et al [*5*], and they were found to be interstitial in nature. In addition to voids and dislocation structures, precipitates are induced to form in the stainless steel under the proper irradiation conditions. Although these are visible in bright field (Fig. 14*a*), they are more clearly delineated under dark-field imaging using a precipitate reflection (Fig. 14*b*). This phase was identified from the diffraction pattern as $M_{23}C_6$. In many of the stainless steel alloys several different phases are present and, because of the limited number and low intensity of the precipitate diffraction spots and the closeness of the lattice parameters (*d* spacings), the precipitates cannot be identified with certainty. In such cases extraction replicas were studied by electron diffraction and X-ray diffraction to confirm the results on the foil itself.

The preceding example and discussion illustrate how individual components in a complex structure can be differentiated and identified when the proper techniques are used. As a further step, a structure can be analyzed quantitatively and used to explain the mechanical properties of the material. This has been done for the case of irradiated Type 304 stainless steel [*83*].

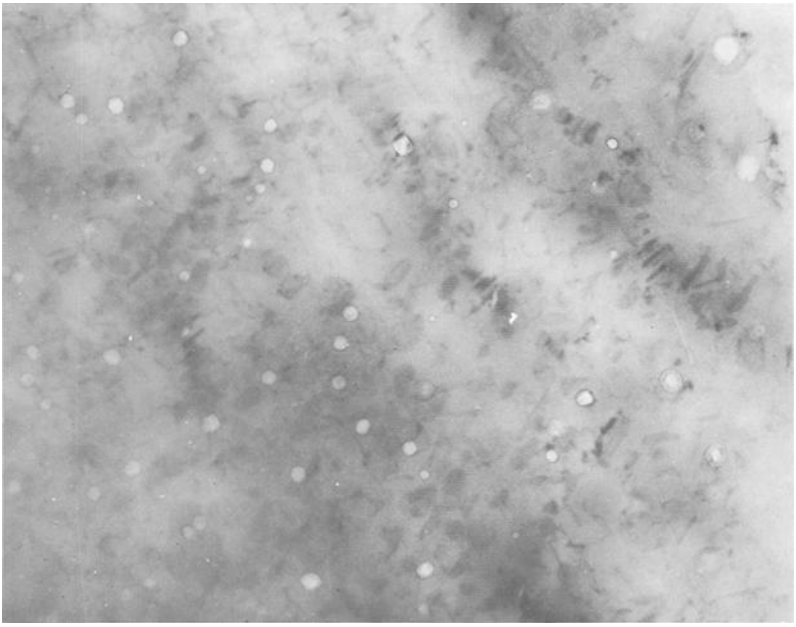

FIG. 12—*Same area as Fig. 11, but tilted away from strong diffraction conditions. Voids are now clearly shown in absorption contrast* (×*101,000*).

Factors Affecting Quantitative Analysis—The analysis of transmission electron micrographs requires certain quantitative information, determinations, and calculations. The limitation on the accuracy of quantitative results can be grouped into three categories: (1) dimensional uncertainties of the foil, (2) limitations in the visibility or of features within the foil, and (3) nonrepresentative results due to interactions of microstructural features with the foil surface.

The dimensional uncertainties are related to the accuracy of determining the thickness of the foil in the region being examined and the magnification of the micrographs. The magnification of the image and its rotation relative to the diffraction pattern can normally be calibrated by standard techniques to accuracies of 2 percent or less [*5*, *36*]. The analysis of the foil thickness is a more difficult problem. In most metal specimens the foil has a wedge-shaped cross section with a range of thicknesses normally greater than 10 percent of the mean thickness. The thicknesses of these foils are usually measured by one of three basic approaches: (1) slip trace analysis, (2) thickness contour analysis, and (3) stereomicroscopy measurements [*5*, *6*, *34*, *35*].

Foil thickness can be easily measured if slip traces, coherent twin boundaries, or other planar defects which have known crystallographic relationships intercept both surfaces of the foil. The foil thickness is directly related to the projected dimension of the detail feature (slip trace, etc.) and the tangent of the angle between the foil surface and the plane of the detail feature. Using normal specimen preparation techniques, slip traces are not normally produced in the region of the foil being examined. Various techniques such as localized contamination buildup or straining the foil have been devised to cause dislocation motion in the region examined.

The second technique widely used to estimate the foil thickness is the use of thickness contours. The thickness contour method can be used on grain or twin boundaries, since it is not necessary to know the angle between the boundary and the foil surfaces. The foil is first oriented for exact Bragg diffraction to get the most accurate results. The thickness of the foil is then determined at any point by counting the number of thickness fringes from the edge of the crystal and multiplying by the extinction distance. The assignment of a particular diffracting vector $\bar{g}$ which produces the extinction contours is easily made by imaging the structure using dark-field electron microscopy. The condition of exact Bragg diffraction is best determined by

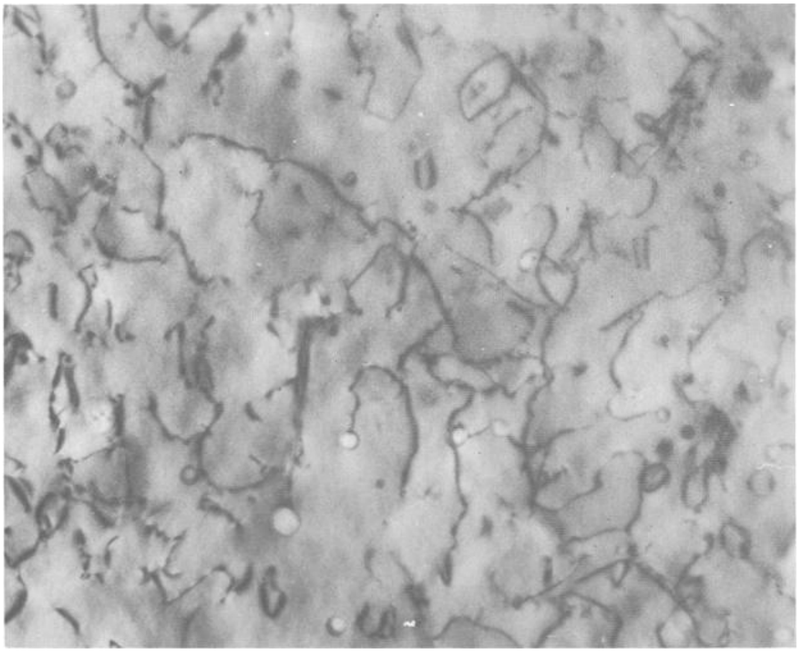

FIG. 13—*Same specimen as in Figs. 11 and 12, but annealed at 600 C for 1 h. Loops have unfaulted and in many cases have interacted to form a network. Analysis of these loops indicates that they were formed from an initial platelet of interstitial atoms* (×*101,000*).

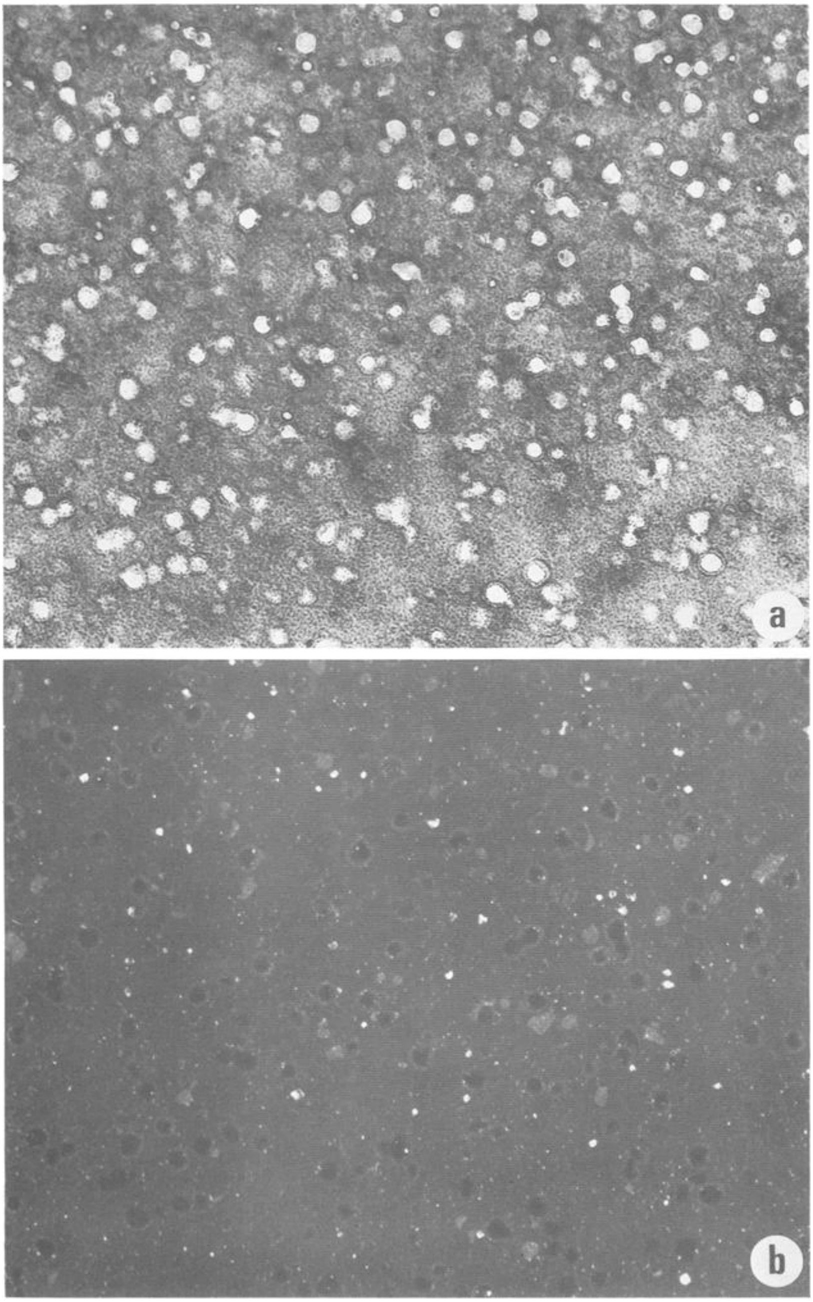

FIG. 14—*Irradiated stainless steel. Small precipitates identified as* $M_{23}C_6$ *have formed. Precipitates are practically indistinguishable in* (a) *bright field but are clearly delineated when imaged on* (b) *dark field, using a precipitate reflecting spot* (×*77,400*).

causing the Kikuchi line to intersect the diffraction spot. For recrystallized materials, Kikuchi lines are nonexistent in thin regions of the foil and are broad and very diffuse for all thicknesses of heavily cold-worked material. When the deviation from the exact Bragg condition cannot be accurately minimized, serious errors in the determination of the foil thickness can result.

A third versatile approach to estimating the foil thickness is by stereomicroscopy. This requires use of an accurately calibrated goniometer stage. Stereomicroscopy can be used on a wide variety of objects to determine the foil thickness, since only the parallax between stereopairs of specific sharp contrast points on each surface of the foil are used. The objects can be slip traces, single dislocations intercepting both surfaces, grain boundaries, individual particles observed to be on each surface, or small particles formed by evaporation of metal on both surfaces of the foil. The evaporation of metal on the foil surface reduces the resolution of the image but provides a standard for determining the camera constant.

Foil thickness has been approximated relatively simply by measurements of dislocations randomly distributed within the foil [*84*]. In addition, a simple geometric relationship has been devised for alloys containing a precipitated second phase of platelets or needles which are regularly oriented and of a scale equivalent to the foil thickness [*85*].

Quantitative analysis requires knowledge of the factors which affect the visibility of objects within the foil. For dislocations or loops some of the dislocations may be invisible if only one reflection is operating. For individual strong reflections the percentage of visible dislocations in cubic materials has been determined [*5, 35, 36, 70, 71*]. However, due to dislocations interacting with the free surface during specimen preparation, the percentage of dislocations observed in deformed metals appears to be inversely related to the amount of cold work [*86*].

Voids have been recently observed in pure metals and alloys irradiated by fast neutrons. The small voids (< 100 Å) are best resolved by optimizing their contrast by imaging with the foil oriented to produce thickness contours near the field of interest. As previously stated for diffraction conditions other than Bragg conditions, the size and visibility of voids in metals changes with void size, foil thickness, and depth of void in the foil [*80, 81*]. The voids can also be observed in absorption contrast. The observed distribution of the voids in the absorption contrast condition will change with the thickness of the foil. In the thinner portion of the foil a larger percentage of larger voids will intercept the surface than of smaller voids and will not be counted. The distribution of voids in the foil will then be biased toward a smaller size. Conversely, in thicker regions of the foil, the absorption contrast due to smaller voids will be difficult to resolve, resulting in the void distribution being shifted towards larger void sizes. Therefore, in determining void size and density, measurements should be made in foils of varying thickness to remove the bias introduced by very thin and very thick foils.

Recent Advances

A recent innovation in transmission microscopy is the use of an energy analyzer. In this technique, the plasmon loss in the electron beam is measured, and since this loss varies for different elements the composition of a region can be determined. Such an instrument has been built and described by Cundy et al [*87*]. Briefly, the energy analyzer is placed beneath the fluorescent screen. A fine slit allows a certain band of electrons from the region of interest to pass into the analyzer. The plasmon loss in the electrons going through this slit is subsequently analyzed and compared to standards. This has been used to determine the composition of amorphous silica particles in an internally oxidized Ni-Si alloy [*88*]. Analysis of precipitate phases has also been done in Al-Cu and Al-Mg alloys [*89*, *90*]. This appears to be a promising technique for true microanalysis, that is, analysis of very small regions in a material. It does require a major modification to the microscope, however.

Recently, much interest has been directed to high-voltage electron microscopy in which accelerating voltages of over 500 keV are used. High-voltage microscopy offers several distinct advantages. The penetrating power of the electron is increased so that thicker specimens may be studied. This is important where the preparation of very thin foils is extremely difficult. The results will also be more representative of behavior of a bulk material if thicker films are studied. Resolution is increased because of reduction in spherical aberration errors and the chromatic aberration introduced by the specimen. Also, electron irradiation damage can be studied *in situ* by use of the electron beam. The extent of damage in a high-voltage microscope has been studied by Makin [*91*]. Thomas [*92*] has reviewed the results from some of the existing high-voltage microscopes and compared the structures as a function of accelerating voltage. Changes in the theory of diffraction contrast, which may be necessary in the interpretation of structures obtained in high-voltage microscopes, are currently being developed.

References

[*1*] Heidenreich, R. D., *Journal of Applied Physics*, JAPIA, Vol. 20, Oct. 1949, pp. 993–1010.

[*2*] Bollman, W., *Physical Review*, PHRVA, Vol. 103, Sept. 1956, pp. 1588–1589.

[*3*] Gidley, J. A. F. and Davies, R. A., *Journal of Scientific Instruments*, JSINA, Vol. 44, April 1967, pp. 297–299.

[*4*] Brammar, I. S. and Dewey, M. A. P., *Specimen Preparation for Electron Metallography*, American Elsevier, New York, 1966, p. 58.

[*5*] Hirsch, P. B., Howie, A., Nicholson, R. B., Pashley, D. W. and Whelan, M. J., *Electron Microscopy of Thin Crystals*, Butterworths, Washington, D. C., 1965, p. 455.

[*6*] Kay, D. H., *Techniques for Electron Microscopy*, Blackwell Scientific Publications, Oxford, 1965, p. 375.

[7] Hirsch, P. B. et al, *Electron Microscopy of Thin Crystals*, Butterworths, Washington, D. C., 1965, p. 377.
[8] Ginn, B. J. and Brown, E. D., *British Welding Journal*, BRWJA, Vol. 12, Jan. 1965, p. 90.
[9] Malone, M., *Journal of Scientific Instruments*, JSINA, Vol. 43, Sept. 1966, pp. 666–667.
[10] Mastel, B. and Kissinger, H. E., *Journal of Scientific Instruments*, JSINA, Vol. 41, Aug. 1964, pp. 510–511.
[11] Hunt, M. D., Spittle, J. A. and Smith, R. W., *Journal of Scientific Instruments*, JSINA, Vol. 44, March 1967, pp. 230–231.
[12] Strutt, P. R., *Review of Scientific Instruments*, RSINA, Vol. 32, April 1961, pp. 411–414.
[13] Riesz, R. P. and Bjorling, C. G., *Review of Scientific Instruments*, RSINA, Vol. 32, Aug. 1961, pp. 889–892.
[14] DuBose, C. K. H. and Stiegler, J. O., "Semiautomatic Preparation of Specimens for Transmission Electron Microscopy," ORNL-4066, Oak Ridge National Laboratory, Feb. 1967.
[15] Sharp, J. V., *Journal of Scientific Instruments*, JSINA, Vol. 44, April 1967, pp. 292–293.
[16] Blankenburgs, G. and Wheeler, M. J., *Journal of the Institute of Metals*, JIMEA, Vol. 92, 1964, pp. 337–338.
[17] Dewey, M. A. P. and Lewis, T. G., *Journal of Scientific Instruments*, JSINA, Vol. 40, Aug. 1963, pp. 385–387.
[18] Cox, A. R. and Mountford, M. D., *Journal of the Institute of Metals*, JIMEA, Vol. 95, 1967, pp. 347–349.
[19] Schoone, R. D. and Fischione, E. A., *Review of Scientific Instruments*, RSINA, Vol. 37, Oct. 1966, pp. 1351–1354.
[20] Lindbo, J., *Journal of Scientific Instruments*, JSINA, Vol. 43, May 1966, pp. 319–320.
[21] Gidley, J. A. F. and Richards, P. N., *Journal of Scientific Instruments*, JSINA, Vol. 2, Series 2, 1969, p. 297.
[22] DuBose, C. K. H. and Jones, C. *Metallography*, MEIJA, Vol. 2, March 1969, pp. 31–40.
[23] Kirkpatrick, H. B. and Amelinckx, S., *Review of Scientific Instruments*, RSINA, Vol. 33, April 1962, pp. 488–490.
[24] Booker, G. R. and Strickler, R., *British Journal of Applied Physics*, BJAPA, Vol. 13, Sept. 1962, pp. 446–448.
[25] Williamson, G. K., *Proceedings of the Royal Society of London*, Series A, PRSLA, Vol. 257, Sept. 1960, pp. 457–463.
[26] Hulse, C. O. and Tice, W. K., *Journal of the American Ceramic Society*, JACTA, Vol. 49, April 1966, pp. 190–193.
[27] Phillips, V. A. in *Symposium on Advances in Electron Metallography and Electron Microanalysis, ASTM STP 317*, American Society for Testing and Materials, 1962, p. 34.
[28] Phillips, V. A., *Praktische Metallographie*, PMTLA, Vol. 4, 1967, p. 637.
[29] Bailey, J. E., *Acta Metallurgica*, AMETA, Vol. 11, April 1963, pp. 267–280.
[30] Van Torne, L. I. and Thomas, G., *Acta Metallurgica*, AMETA, Vol. 12, May 1964, pp. 601–616.
[31] Wilsdorf, H. G. F. and Schmitz, J., *Journal of Applied Physics*, JAPIA, Vol. 33, May 1962, pp. 1750–1754.
[32] Ham, R. K., *Philosophical Magazine*, PHMAA, Vol. 7, July 1962, pp. 1177–1182.
[33] Mader, S. and Seeger, A., *Journal of Applied Physics*, JAPIA, Vol. 34, Nov. 1963, pp. 3376–3386.
[34] Thomas, G., *Transmission Electron Microscopy of Metals*, Wiley, New York, 1962.
[35] Heidenreich, R., *Fundamentals of Transmission Electron Microscopy*, Interscience, New York, 1964.
[36] Andrews, K. W., Dyson, D. J. and Keown, S. R., *Interpretation of Electron Diffraction Patterns*, Hilger and Watts, London, 1967.
[37] Valdré, V., *Nuovo Cimento*, NUCIA, Vol. 53B, Jan. 1968, pp. 157–173.

[*38*] Mills, J. C. and Moodie, A. F., *Review of Scientific Instruments*, RSINA, Vol. 39, July 1968, pp. 962–970.
[*39*] Lehtinen, B., Broberg, E. and Dahne, L., *Journal of Scientific Instruments*, JSINA, Vol. 44, April 1967, pp. 289–296.
[*40*] Schulze, K. J. and Schimmel, G. S., *Proceedings of the 6th International Congress for Electron Microscopy*, Kyoto, 1966, p. 173.
[*41*] Watanabe, H. and Ishikawa, I., *Japan Journal of Applied Physics*, JJAPA, Vol. 6, Jan. 1967, pp. 83–88.
[*42*] Venables, J. A. and Thomas, G. J., *Journal of Scientific Instruments*, JSINA, Vol. 1, Series 2, Feb. 1968, pp. 121–127.
[*43*] Bollman, W., *Proceedings of International Symposium on Electron Diffraction and Nature of Defects in Crystals*, Melbourne, 1965, Pergamon Press, New York, 1966, pp. 1p–c.
[*44*] von Heimendahl, M., Bell, W. and Thomas G., *Journal of Applied Physics*, JAPIA, Vol. 35, Dec. 1964, pp. 3614–3616.
[*45*] Sheinin, S. S., *Review of Scientific Instruments*, RSINA, Vol. 37, Feb. 1966, pp. 232–234.
[*46*] Laird, C., Eichen, E. and Bitler, W. R., *Journal of Applied Physics*, JAPIA, Vol. 37, May 1966, pp. 2225–2231.
[*47*] Eyre, B. L., Maher, D. M. and Robertson, D. H., *Journal of Scientific Instruments*, JSINA, Vol. 1, Series 2, Aug. 1968, pp. 851–855.
[*48*] Makay, A. C., *Journal of Scientific Instruments*, JSINA, Vol. 1, Series 2, Sept. 1968, pp. 907–911.
[*49*] Ryder, P. L. and Pitsch, W., *Philosophical Magazine*, PHMAA, Vol. 15, March 1967, pp. 437–446.
[*50*] Ryder, P. L. and Pitsch, W., *Philosophical Magazine*, PHMAA, Vol. 18, Oct. 1968, pp. 807–816.
[*51*] Levine, E., Bell, W. L. and Thomas G., *Journal of Applied Physics*, JAPIA, Vol. 37, April 1966, pp. 2141–2148.
[*52*] Okamoto, P. R., Levine, E. and Thomas, G., *Journal of Applied Physics*, JAPIA, Vol. 38, Jan. 1967, pp. 289–296.
[*53*] Thomas, G., *Transactions of the Metallurgical Society*, AIME, TMSAA, Vol. 233, Aug. 1965, pp. 1608–1619.
[*54*] Bell, W. L. and Thomas, G., *Physica Status Solidi*, PHSSA, Vol. 12, Dec. 1965, pp. 843–852.
[*55*] Nankivell, J. F., *Optik*, OPTKA, Vol. 20, April 1963, pp. 177–198.
[*56*] Garrod, R. I. and Nankivell, J. F., *British Journal of Applied Physics*, BJAPA, Vol. 9, June 1958, pp. 214–217.
[*57*] Wells, D. C., *British Journal of Applied Physics*, BJAPA, Vol. 11, May 1966, pp. 199–201.
[*58*] Pankratz, J. M., "Theory and Errors in Electron Stereomicroscopy," Proceedings of Electron Microscope Society of America, New Orleans, 1968.
[*59*] Head, A. K., Loretto, M. H. and Humble, P., *Physica Status Solidi*, Vol. 20, April 1967, pp. 505–519.
[*60*] Head, A. K., Loretto, M. H. and Humble, P., *Physica Status Solidi*, PHSSA, Vol. 20, April 1967, pp. 521–536.
[*61*] Humble, P., *Physica Status Solidi*, PHSSA, Vol. 21, June 1967, pp. 733–740.
[*62*] Hauserman, F. and Wilkens, M., *Physica Status Solidi*, PHSSA, Vol. 18, Dec. 1966, pp. 609–624.
[*63*] Booker, G. R. and Hazzledine, P. M., *Philosophical Magazine*, PHMAA, Vol. 15, March 1967, pp. 523–528.
[*64*] Steeds, J. W., *Philosophical Magazine*, PHMAA, Vol. 16, Oct. 1967, pp. 785–804.
[*65*] Humphreys, C. J., Howie, A. and Booker, G. R., *Philosophical Magazine*, PHMAA, Vol. 15, March 1967, pp. 507–522.
[*66*] Sass, S. L., Mura, T. and Cohen, J. B., *Philosophical Magazine*, PHMAA, Vol. 16, Oct. 1967, pp. 679–690.

[*67*] Guyot, P., *Physica Status Solidi*, PHSSA, Vol. 28, July 1968, pp. 349–354.

[*68*] Humble, P., *Australian Journal of Physics*, AUJPA, Vol. 21, June 1968, pp. 325–336.

[*69*] Loretto, M. H. and France, L. K., *Philosophical Magazine*, PHMAA, Vol. 19, Jan. 1969, p. 141.

[*70*] Bell, W. L. and Thomas, G., *Philosophical Magazine*, PHMAA, Vol. 13, Feb. 1966, pp. 395–420.

[*71*] Bollman, W., *Philosophical Magazine*, PHMAA, Vol. 13, May 1966, pp. 935–944.

[*72*] Hale, K. F. and Hendersen-Brown, *Proceedings of the International Conference on Electron Diffraction and Nature of Defects in Crystals*, Melbourne, 1965, Pergamon Press, New York, 1966, p. 10.

[*73*] Ashby, M. F. and Brown, L. M., *Philosophical Magazine*, PHMAA, Vol. 8, July 1964, pp. 1083–1103.

[*74*] Ashby, M. F. and Brown, L. M., *Philosophical Magazine*, PHMAA, Vol. 8, Oct. 1964, pp. 1649–1666.

[*75*] Rühle, M., *Physica Status Solidi*, PHSSA, Vol. 19, Jan. 1967, pp. 263–295.

[*76*] *Symposium on the Nature of Small Defect Clusters*, AERE-R-5269, M. J. Makin, Ed., Her Majesty's Stationery Office, London, 1966.

[*77*] Brammer, W. C. and Rhodes, C. G., *Philosophical Magazine*, PHMAA, Vol. 16, Sept. 1967, pp. 477–486.

[*78*] Ardell, A. J., *Philosophical Magazine*, PHMAA, Vol. 16, July 1967, pp. 147–158.

[*79*] Sumerling, R., *Journal of Scientific Instruments*, JSINA, Vol. 43, March 1966, pp. 169–172.

[*80*] Levy, V., "Transmission Electron Microscope Examination of Rare Gas Bubbles in Metals; Analysis of Observed Contrast Effects," CEA Rep. 2431, Commissariat a l'Energie Atomique, France.

[*81*] Van Landuyt, V., Gevers, R. and Amelinckx, S., *Physica Status Solidi*, PHSSA, Vol. 10, July 1965, pp. 319–335.

[*82*] Brown, L. M. and Mazey, D. J., *Philosophical Magazine*, PHMAA, Vol. 8, June 1964, pp. 1081–1082.

[*83*] Holmes, J. J., Robbins, R. E., Brimhall, J. L. and Mastel, B., *Acta Metallurgica*, AMETA, Vol. 16, July 1968, pp. 955–968.

[*84*] Ishida, Y., *Philosophical Magazine*, PHMAA, Vol. 14, Aug. 1966, pp. 411–412.

[*85*] von Heimendahl, M., *Journal of Applied Physics*, JAPIA, Vol. 35, Feb. 1964, pp. 457–458.

[*86*] Foxon, C. T. B. and Rider, J. G., *Philosophical Magazine*, PHMAA, Vol. 14, July 1966, pp. 185–188.

[*87*] Cundy, S. L., Metherell, A. J. F. and Whelan, M. J., *Journal of Scientific Instruments*, JSINA, Vol. 43, Oct. 1966, pp. 712–716.

[*88*] Cundy, S. L. and Grundy, P. S., *Philosophical Magazine*, PHMAA, Vol. 14, Dec. 1966, pp. 1233–1242.

[*89*] Cundy, S. L., Metherell, A. J. F. and Whelan, M. J., *Philosophical Magazine*, PHMAA, Vol. 17, Jan. 1968, pp. 141–148.

[*90*] Spalding, D. R. and Metherell, A. J. F., *Philosophical Magazine*, PHMAA, Vol. 18, July 1968, pp. 41–48.

[*91*] Makin, M. J., *Philosophical Magazine*, PHMAA, Vol. 18, Sept. 1968, pp. 637–654.

[*92*] Thomas, G., *Philosophical Magazine*, PHMAA, Vol. 17, June 1968, pp. 1097–1108.

DISCUSSION

J. C. Russ[1] (*written discussion*)—In discussion of the Brimhall, Mastel, and Brager paper it should be pointed out that when stereotilt is used it is not necessary that the angle of tilt be ± the same amount with respect to the horizontal. The tilt angle can be selected anywhere throughout the range of motion of the specimen stage, provided the stage does not change focal distance or magnification during tilt. Thus the angle can be selected to suit other conditions, such as achieving the desired diffraction condition in both stereoimages.

J. L. Brimhall (*author's closure*)—Dr. Russ' statement that stereoimages can be obtained within any selected tilt angle of sufficient magnitude is certainly true. One should realize, however, that when the tilt angles are not equal the foil will appear to be inclined if viewed in stereo. For precise measurements of elevation differences this inclination must taken be into account.

---

[1] Applications consultant, JEOLCO, Inc., Medford, Mass. 02155.

R. M. Pelloux[1]

Replicating Techniques for Electron Fractography

REFERENCE: Pelloux, R. M., "**Replicating Techniques for Electron Fractography,**" *Applications of Modern Metallographic Techniques, ASTM STP 480*, American Society for Testing and Materials, 1970, pp. 127–130.

ABSTRACT: The different replicating techniques used in electron fractography are reviewed briefly and general guidelines are given to judge the advantages and difficulties of each technique.

KEY WORDS: fractography, metallography, replicas

Replicating techniques and the interpretation of replicas have been reviewed recently [*1*, *2*].[2] This report, within the context of the conference, will deal only with the basic techniques of replication. The review of the techniques given by Plateau [*3*] will be followed very closely.

Replicating Techniques

Carbon Evaporation

Although carbon evaporation was first used in 1954 by Bradley [*4*], it is still one of the main stumbling blocks in the replicating technique. The carbon should be spectrographically pure graphite. The point source is best obtained by sharpening one of the rods in a pencil sharpener and maintaining it in contact with the flat face of the other rod by means of a spring. The evaporation time should not exceed a few seconds (3 or 4 s). Consequently, the vacuum should be better than 10^{-5} mm of mercury and the power required for evaporation of the order of 40 to 50 A under 20 V. It is necessary to have a 2-kW power supply and a step-down transformer. A distance of 4 in. between the source and specimen is sufficient to avoid any melting or

---

[1] Professor, Department of Metallurgy and Materials Science, Massachusetts Institute of Technology, Cambridge, Mass. 02139.

[2] Italic numbers in brackets refer to the list of references at the end of this paper.

softening of the details of the plastic replicas if the evaporation time is less than 5 s. Long evaporation times should be avoided.

One-Step Replicas

This is the most accurate and faithful technique (Fig. 1*a*) and should be used as much as possible for research with laboratory test fractures. The carbon film is evaporated directly onto the fracture surface and released by dissolving the base metal. The shadowing angle is usually not critical because of the roughness of the surface. The continuity of the carbon film is assured by the surface diffusion of the evaporated carbon.

Electrolytic Extraction of the Replicas—The replicas can be extracted by using electropolishing or etching solutions. After scribing the surface to make the shape of the replicas, electroetch the specimen for 20 s. Transfer the specimen to distilled water or alcohol and let the carbon film float off to the surface. Repeat if it does not work the first time. The second-phase particles can be extracted with the replicas if the voltage is properly adjusted. The proper voltage can be found by recording the polarization curves of the different phases of the alloy. The inclusions can also be released from the matrix prior to electroetching by chemical etching through the carbon film.

Chemical Extraction of the Replicas—This is obtained by dissolving the base metal without having a gas reaction which could tear the carbon film. The best reagent was found to be a solution of 10 percent bromine in alcohol. The reaction takes from 10 to 15 h. The specimen is washed in pure methanol and the replicas should float off to the surface.

Oxide Replicas—These one-step replicas are rarely used and should be attempted only by the experienced technician if he feels that they are the only way to replicate the surface. The structure of the oxide may lead to some confusing observations.

Two-Step Replicas (Fig. 1*b*)

In the two-step replicas (Fig. 1*b*) the details of the fracture surface are transferred to a plastic mold which is easy and convenient to dissolve to release the final carbon replica. The plastic mold can be obtained by applying successive layers of a varnish or formwar or by simply pressing a softened piece of cellulose acetate to the fracture surface.

The preparation of the two-step replicas includes metal shadowing to enhance the contrast. The shadowing angle should coincide with the macroscopic direction of crack propagation to facilitate the orientation of the replica in the electron microscope. The shadowing angle and direction of the carbon film is not critical. If it is available, rotary shadowing is recommended.

Extraction—I have found that the best technique is to dissolve the acetate film in pure acetone. The replica is placed, carbon side facing down, on a

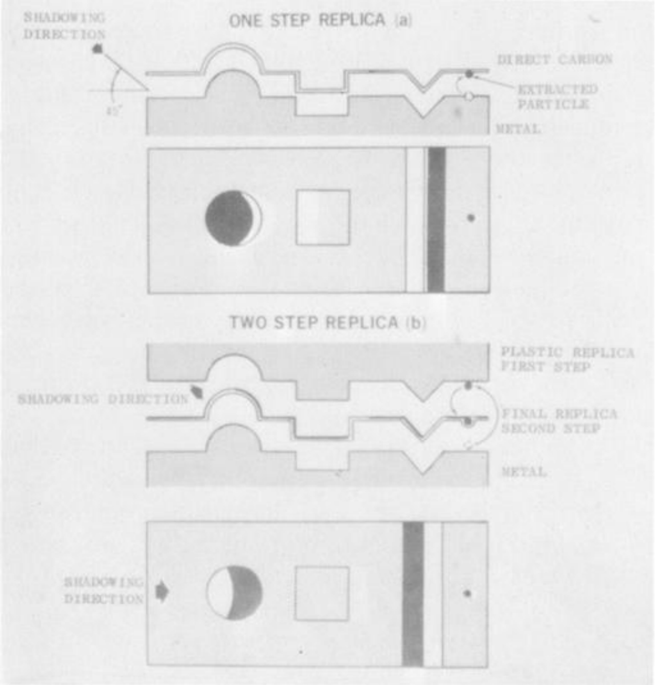

FIG. 1—*One-step and two-step replicas.*

small piece of filter paper in a Petri dish. Acetone is added slowly and the wetting action of the filter paper is such that the film will float easily. Most of the problems related to cracking of the replicas are due to a poor carbon film (too thin or too thick); however, if cracking is experienced the wax technique should be used. The carbon side of the replica is stuck face down on a glass slide coated with a thin film of molten bee's wax. The acetate film is then dissolved in pure acetone. The swelling of the acetate cannot crack or break the carbon film which is held by the wax. When the acetate is all dissolved the temperature of the acetate bath is raised to 150 F to melt the wax and free the carbon replica.

Two-Step Replicas Using Electrolytic Nickel—Plateau [*3*] suggests that a two-step replica can be obtained with a layer of electrolytic nickel serving as the first-step mold. The nickel is stripped off and the carbon evaporated. The extraction of the carbon replica is achieved by dissolving the nickel in bromine alcohol.

General Recommendations

The interpretation of the replicas requires the knowledge of some basic ground rules and some judgment. The interpretation of the shadows of the one-step and two-step replicas is straightforward once the direction of shadowing and the type of replica are known [*1*, *2*]. As a consequence it is always possible to differentiate a hill from a valley without any ambiguity. Electron stereomicroscopy should be used as much as possible to understand the profile of the fracture surface. The relative orientation of the two micrographs (left or right) is given by the previous ground rule on contrast.

Bowles[3] recently suggested that tilting the replica to very large angles (±45 deg) can improve the contrast of some details such as fatigue striations. This technique should be evaluated further; however, I feel that the contrast given by a replica is best improved by using the smallest objective aperture available (20 μm if possible).

The artifacts have been well identified by Beachem [*5*] and should not be confused with the real fracture details.

By now the techniques of replicating fracture surfaces are well established, and in spite of their limitations they represent a valuable and permanent tool. As long as the resolving power of the scanning electron microscope is limited to 200 or 300 Å, the transmission microscope will be required to analyze the fine details of a fracture surface.

References

[*1*] Spitzig, W. A. et al in *Electron Fractography*, *ASTM STP 436*, American Society for Testing and Materials, 1967, pp. 13–29.

[*2*] Phillips, A., *Electron Fractography Handbook*, AFML TDR 64-416, Air Force Materials Laboratory, 1965.

[*3*] Plateau, J., Henry, G. and Roesch, L., *La Microfractographie*, Editions Metaux, Paris, 1966.

[*4*] Bradley, D. E., *Journal of Applied Physics*, JAPIA, Vol. 5, 1954, pp. 96–97.

[*5*] Beachem, C. A. and Dahlberg, E. P., Naval Research Laboratories Memo Report 1457, Sept. 1963.

---

[3] Private communication with Q. Bowles.

Y. E. Smith[1] *and C. A. Siebert*[2]

Transformation Kinetics of Thermomechanically Worked Austenite by Deformation Dilatometry*

REFERENCE: Smith, Y. E. and Siebert, C. A., "**Transformation Kinetics of Thermomechanically Worked Austenite by Deformation Dilatometry,**" *Applications of Modern Metallographic Techniques, ASTM STP 480*, American Society for Testing and Materials, 1970, pp. 131–151.

ABSTRACT: A method was developed for monitoring the continuous cooling transformation of thermomechanically worked austenite by dilatometry. A commercially available, induction-heated, gas-quenching dilatometer was modified by the addition of a compression device that permitted the deformation of dilatometer specimens at high temperature. Continuous cooling transformation data were obtained on undeformed and thermomechanically worked specimens of a 0.1C-0.4Mo-B structural steel. The results clearly indicate the need for data on transformation kinetics in the selection of steel compositions for processing by thermomechanical working schedules.

KEY WORDS: cooling, deformation, dilatometry, boron-containing alloys, molybdenum-containing alloys, phase transformations, strain hardening, structural steels, austenite, evaluation

Thermomechanical working processes include a multiplicity of processing schedules of combined thermal and mechanical working treatments that have been developed to optimize the resulting mechanical properties of metals. The terms thermomechanical working and thermomechanical treatment, as applied to steels, generally imply strain hardening of the austenite by deformation that takes place prior to or during the gamma-to-alpha transformation [*1–3*].[3] The extensive amount of development that has been done on such processes in recent years has generated a need for quantitative information

---

[1] Research supervisor, Research Laboratory, Climax Molybdenum Co., Ann Arbor, Mich. 48105. Personal member ASTM.

[2] Professor, Department of Chemical and Metallurgical Engineering, University of Michigan, Ann Arbor, Mich. 48105. Personal member ASTM.

* This paper is based on a PhD dissertation submitted by Y. E. Smith to the University of Michigan.

[3] Italic numbers in brackets refer to the list of references at the end of this paper.

summarizing the effects of the deformation of the austenite on transformation kinetics. Thus far only limited efforts have been expended toward the accumulation of data on the transformation kinetics of thermomechanically worked austenite.

Grange and Mitchell [*4*] conducted a study of the effects on transformation kinetics of austenite deformation in a nickel-chromium-molybdenum steel. They obtained isothermal transformation data on material in three conditions: (1) undeformed, (2) deformed to 50 percent reduction by rolling at 816 C (1500 F), and (3) deformed to 50 percent reduction by rolling at isothermal temperatures between 260 C (500 F) and 704 C (1300 F). Deformation at the isothermal holding temperature was found to accelerate the beginning of both the pearlite and bainite reactions by as much as one order of magnitude. Deformation at the higher temperature had a significant, but somewhat lesser, effect on the pearlite reaction and only a very small effect on the bainite reaction.

Gidon et al [*5*] investigated the effect of austenite deformation at 550 C (1022 F) on the kinetics of isothermal transformation between 300 C (572 F) and 700 C (1292 F). The transformation rate was progressively accelerated by increasing degrees of deformation up to 93 percent reduction, the highest level investigated. Korneyev and Estrin [*6*] studied the influence of 25 percent reduction at 900 C (1652 F) on the isothermal transformation kinetics of a nickel-chromium-silicon steel and a high chromium-nickel iron. Isothermal transformation in the range of 550 C (1022 F) to 660 C (1220 F) was significantly accelerated in both materials.

Isothermal transformation data can be used for studying the fundamental characteristics of the effect of deformation on transformation kinetics and for the classification of various compositions with respect to the degree of this effect. On the other hand, for the application of thermomechanical working to hardening of heavy sections and to controlled rolling on the hot-rolling mill, continuous cooling transformation data have somewhat greater utility. Studies of the continuous cooling transformation of thermomechanically worked steels have not been reported in the literature.

In this investigation a method was developed for studying the continuous cooling transformation kinetics of thermomechanically worked austenite by dilatometry. Specimens can be subjected to rapid heating and cooling rates. They can be deformed up to 50 percent reduction of area by compression, in one or more steps, while the temperature is being automatically controlled. As an example of the large effects upon transformation kinetics brought about by thermomechanical working, data are presented for a molybdenum-boron structural steel that is designed to be produced by controlled rolling and transformed to a bainitic microstructure. Transformation rate data, which can be produced by the technique described in this paper, would take much of the guesswork out of the design of thermomechanical processing schedules.

Experimental Method

Dilatometer

The dilatometer used in this study is a commercially available, induction-heated, gas-quenching dilatometer modified to a unique design such that it is capable of a broad range of heating and cooling rates. The specimen is heated in a vacuum chamber by an induction coil, which is energized by a high-frequency oscillator at 1.7 megacycles. A gas cooling coil is wound integrally on the inside of the induction heating coil. This cooling coil is perforated to allow for an even distribution of cooling gas around the specimen. Therefore, the specimen can be cooled rapidly from a high temperature with no mechanical movements of the specimen or external apparatus being required.

The specimen temperature is continuously measured by a platinum-13 percent rhodium thermocouple that is welded to the specimen. The temperature is maintained at a constant or continuously varying level by the automatic proportioning control system. The system is designed for four types of cooling cycles:

1. *Gas Quenching*—The induction heater is turned off and the cooling gas is simultaneously turned on.
2. *Linear Cooling*—Heater power is continuously reduced by the control system as the programming unit generates an approximately linear cooling curve.
3. *Accelerated Linear Cooling*—The same as the linear cooling cycle above, except that a limited flow of gas impinges on the specimen, making it possible to cool the specimen at a controlled rate that is faster than its natural cooling rate.
4. *Step Cooling*—The specimen is gas quenched to a predetermined intermediate temperature, at which the control system turns on heater power and holds indefinitely. This cycle is ideal for the determination of isothermal transformation data.

Dimensional changes of the specimen are monitored by a differential transformer. A schematic diagram of the differential transformer and specimen assembly is presented in Fig. 1. As the specimen expands or contracts as a result of thermal or phase changes, the fused silica rod moves relative to the outer fused silica tube. The rod is attached to the core of the differential transformer and the tube is attached, via the inner case, to the coil. The corresponding relative motion of the core relative to the coil produces a millivolt signal that is proportional to the movement. This signal is recorded as a

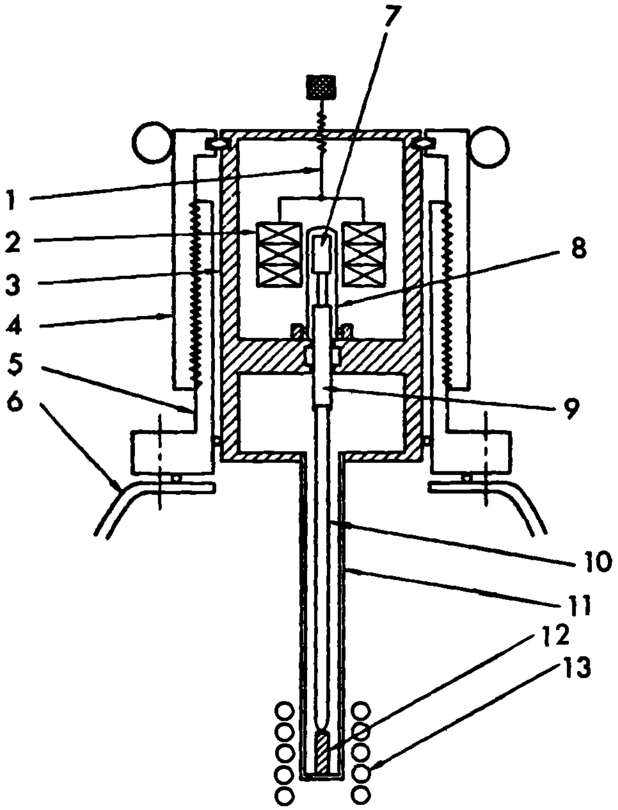

(1) Zero-setting mechanism.
(2) Differential transformer coil.
(3) Inner movable case.
(4) Outer movable case.
(5) Fixed base.
(6) Vacuum Chamber.
(7) Differential transformer core.
(8) Vacuum-seal fused silica tube.
(9) Slide pin.
(10) Dilatation detecting fused silica rod.
(11) Outer fused silica tube.
(12) Specimen.
(13) Heating/cooling coil.

FIG. 1—*Standard specimen assembly for Formastor-F dilatometer.*

function of time on a fast dual-pen recorder, along with the specimen temperature. The most sensitive of the four differential transformer scales distributes a 0.05-mm dimensional change over the full 25-cm width of the strip chart.

Compression Device

To investigate the effect of the thermomechanical working of the austenite on transformation kinetics, a modification of the dilatometer was needed to provide for a means of deforming the specimen while it was being maintained at a high temperature. Furthermore, it was necessary to provide for measurement of the dilatation of the deformed specimen immediately after deformation as the cooling cycle was started. Figure 2 presents a sketch of the compression device that was designed for this purpose. The device attaches to the vacuum chamber of the dilatometer by means of the external flange and

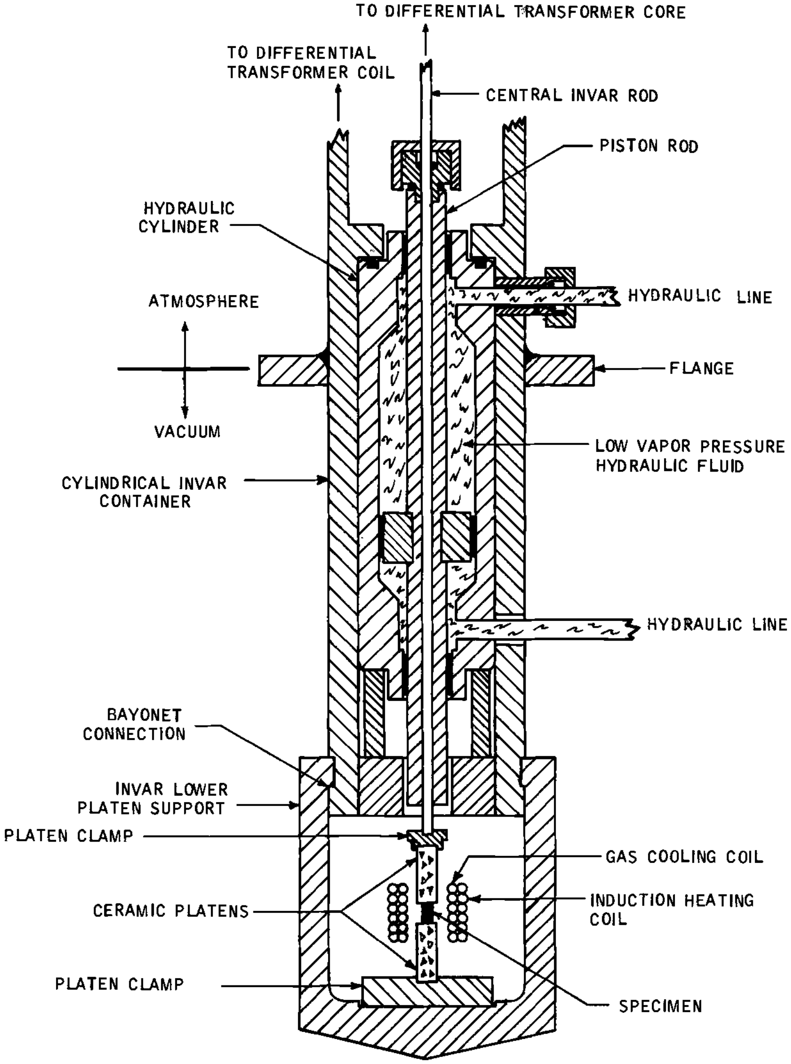

FIG. 2—*Simplified sketch of compression device.*

occupies the normal position of the differential transformer, as shown by the photograph of Fig. 3. The new position of the differential transformer is immediately above the compression device.

The cylindrical specimen occupies its usual position within the heating-cooling coil. It rests on the stationary ceramic lower platen, which is held by a clamp. The upper platen clamp is attached by a screw thread to the central rod, which extends through the assembly to the differential transformer at the upper end. A double-ended, double-acting hydraulic cylinder of 1½-in. (38-mm) internal diameter provides the force required for deformation. At the rated pressure of 1500 psi (10.3 MN/m^2), a maximum force of 2000 lb (8900 N) is available. Deformation of the specimen is accomplished

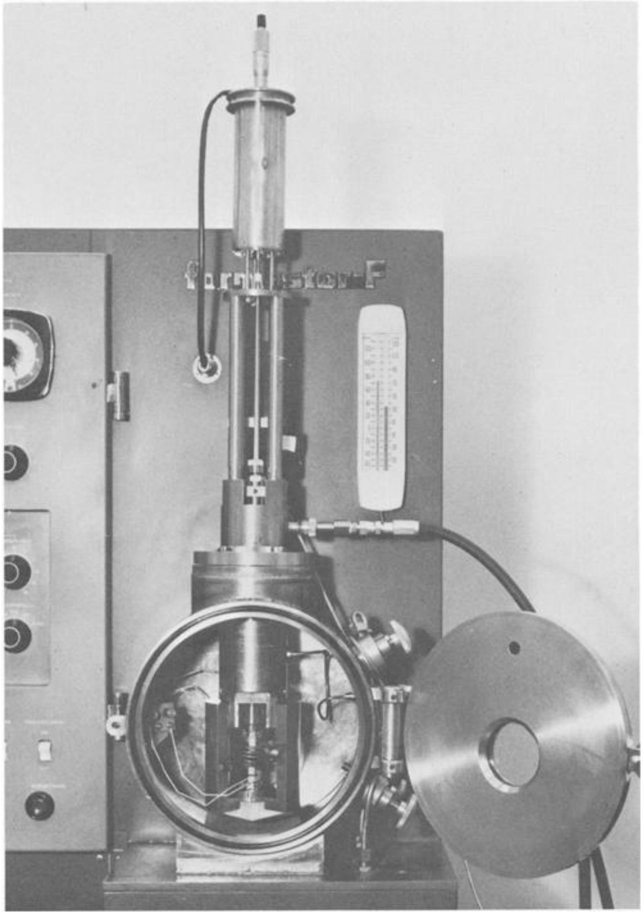

FIG. 3—*Vacuum chamber of the dilatometer showing the attached compression device.*

by driving the piston downward. The piston rod slides freely over the central rod, which is supported by the specimen via the upper platen and clamp. The freedom of relative motion between these two coaxial elements is permitted by the O-ring seal at the upper contact point and a brass bushing at the lower contact point (not shown). After the piston rod contacts the upper platen clamp, further downward motion deforms the specimen in axisymmetric compression. The piston needs only to be backed off a small amount, prior to cooling, for specimen dilatation to be transmitted to the differential transformer via the central rod during the cooling cycle.

The amount of specimen deformation may be monitored in two ways. It may be recorded on the strip chart by means of the differential transformer if it does not exceed about 0.060 in. (1.5 mm). Otherwise, the measurement may be taken from the voltage output of a resistance-type displacement transducer that indicates the position of the piston.

All critical metal components of the compression device that might contribute to extraneous expansion due to thermal effects were made of Invar 36. These include the outer frame, lower platen support and clamp, upper platen clamp, and central rod. The ceramic platen material, cordierite, was carefully selected to optimize the compressive strength at as high a level as possible and the thermal conductivity and thermal coefficient of expansion at as low a level as possible.

Design of Undeformed Specimens

The specimens that were used to establish the normal continuous cooling transformation characteristics of the steel were 10 mm long and 3 by 3 mm square. The thermocouples for all specimens except those cooled at the three highest cooling rates were percussion welded at the bottom of a 1.5-mm hole in the bottom of the specimen, approximately 5 mm deep, as shown in Fig. 4*a*. Preliminary temperature measurement tests were conducted on specimens cooled at the highest rate to be used in the study, 1200 C/min. The bainite start temperature of a specimen was measured with the thermocouple first on the inside and then on the outside. It was established that there was less than a 10 C difference in the results obtained by the two methods when accelerated linear cooling was used rather than simple gas quenching. To minimize the error in the data due to this temperature gradient between center and surface, the technique illustrated in Fig. 4*b* was used. The thermocouple was split between center and surface to average the temperatures at the two points.

Design of Deformed Specimens

To minimize the complexity of the deformation pattern, cylindrical specimens were used for thermomechanical working prior to transformation.

However, lubrication was not used at the specimen-platen interface because of the problems involved with the reaction of the platen material and the lubricant. The specimens were 0.160 in. (4.7 mm) in diameter and 0.250 in. (6.4 mm) high, as shown in Fig. 5, Specimen A. Specimen B is deformed to 25 percent reduction. The existence of sliding friction at the specimen-platen interface limited the barreling to a moderate extent.

The thermocouple was attached to the specimen by percussion welding at the location shown by Fig. 4*c*. Since accelerated cooling rates were to be used in the study, a test was conducted to determine the error in temperature measurement resulting from having the thermocouple on the surface of the specimen. A specimen was prepared in a manner illustrated by Fig. 4*d*. The platinum-rhodium control thermocouple occupied its normal position on the surface. Two chromel-alumel thermocouples, one in the center and one on the surface, were connected to form a differential thermocouple. The output

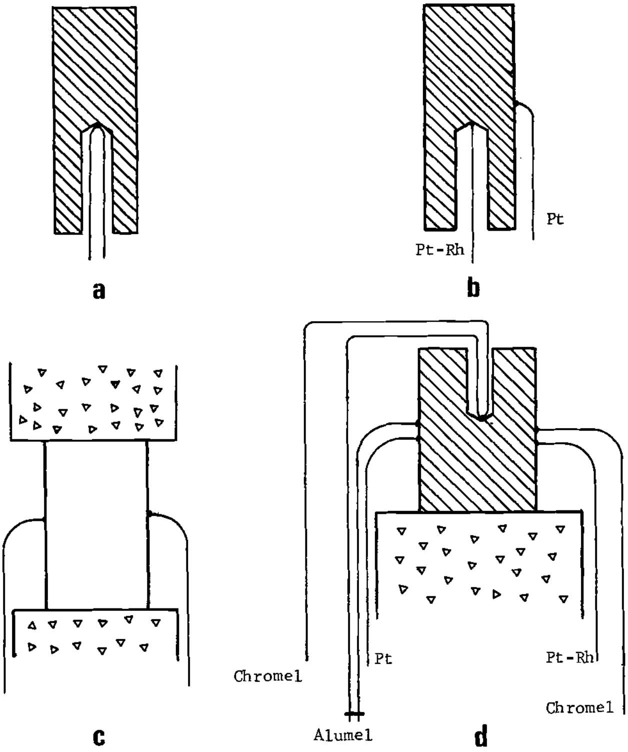

FIG. 4—*Thermocouple configurations for dilatometer specimens:* (a) *standard undeformed specimen,* (b) *undeformed specimen for fast cooling rates,* (c) *standard deformed specimen, and* (d) *specimen temperature distribution test.*

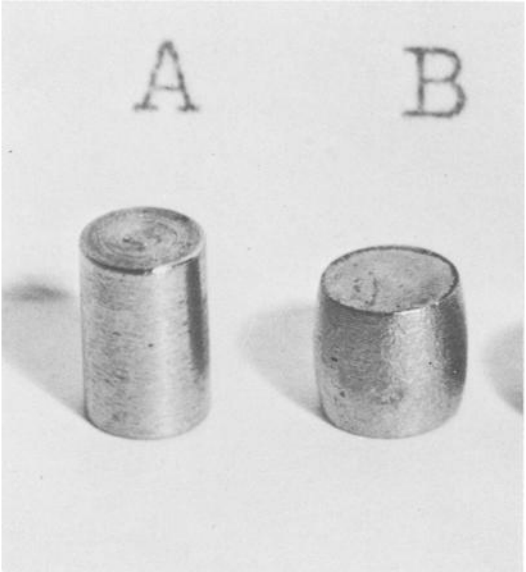

FIG. 5—*Deformation dilatometer specimens.*

of this differential thermocouple was recorded during accelerated linear cooling cycles at 1200 C/min using helium as the cooling gas. The maximum center-to-surface temperature difference was 6 C. Therefore it was concluded that the average temperature of the specimen never deviated more than 3 C from the indicated temperature. No corrections were made to the indicated temperatures.

The small temperature gradient between center and surface is made possible by the 1.7-megacycle induction heating source, which generates over 90 percent of the heat within about 0.3 mm of the surface.

Continuous Cooling Transformation Diagrams

The chemical composition of the molybdenum-boron structural steel, for which transformation kinetic data were obtained, was in percent by weight:

C	Mo	Mn	Si	Zr	N	B	P	S
0.10	0.39	0.88	0.34	0.046	0.005	0.003	0.014	0.024

The upper and lower critical temperatures of this steel, 892 C (1638 F) and 706 C (1303 F), respectively, were determined by heating a specimen in the dilatometer at 2.5 C/min. The austenitizing temperature selected for the transformation study was 930 C (1706 F).

To study the transformation kinetics of deformed, but unrecrystallized, austenite, it is necessary to determine a temperature for deformation that satisfies the following conditions:

1. Recrystallization must not take place in the time required to deform the specimen and begin the cooling cycle (30 s).

2. Transformation must begin at a temperature significantly below the deformation temperature. Since the initiation of transformation is detected by the deviation of the dilatation curve from an established pattern, there must be a sufficient length of dilatation curve to create a pattern before the transformation begins.

A preliminary investigation of the transformation to polygonal ferrite showed that it began as high as 810 C (1490 F). Recrystallization data for carbon and low-alloy austenites from various sources suggested that temperatures significantly above 830 C (1526 F) would not satisfy the first of the above conditions. Therefore, 830 C (1526 F) was tentatively selected as the deformation temperature.

When the Mo-B steel is cooled from the austenitic condition at an appropriate rate to form a coarse, upper bainitic structure, the prior austenite grain boundaries are readily observable in the optical microstructure. They are marked by the extremities of the bainite plates, since the plates do not cross austenite boundaries, and also by carbide precipitation.

Figure 6 presents an example of the microstructure. The specimen was austenitized at 930 C (1706 F), cooled to 830 C (1526 F), held for 30 s, and cooled at 300 C/min. Most of the prior austenite boundaries are detectable. The grain boundary carbide outline may be concentrated by increasing the austenite grain size. This technique was used during testing for recrystallization in a deformed specimen. A specimen was austenitized at 1040 C (1904 F), the temperature was reduced to 830 C (1526 F), and the specimen was deformed to 50 percent reduction in 10 s. It was held for 20 s more at the deformation temperature and then cooled at 300 C/min. The optical photomicrograph is presented in Fig. 7. The large, elongated prior austenite grains indicate the absence of recrystallization.

On the basis of these preliminary tests, the thermomechanical schedule for the deformed specimens was established as follows:

1. Austenitize at 930 C (1706 F) for 9 min and 20 s.

2. Reduce the temperature to 830 C (1526 F) in 10 s.

3. Deform the specimen, reset the chart speed, and zero the differential transformer within 30 s.

4. Cool at an approximately linear rate. (Since the cooling curves were generated by a millivolt signal from the programmer which was reduced at a constant rate, the cooling curves deviated from linearity identically as the Pt-13Rh temperature versus millivolt curve deviated from linearity.)

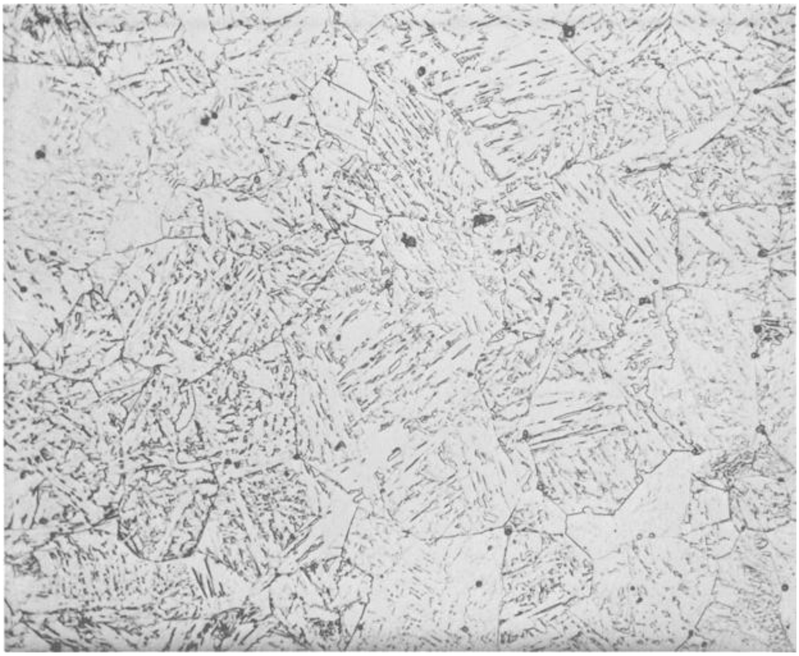

FIG. 6—*Microstructure of Mo-B steel austenitized at 930 C (1706 F) and cooled at 300 C/min (×460).*

The undeformed continuous cooling transformation specimens were subjected to the same thermal cycle, including the intermediate hold at 830 C (1526 F), to determine the effects of deformation as accurately as possible.

The cooling rates for the continuous cooling transformation specimens were 1200, 600, 300, 150, 75, 40, 20, 10, 5, 2, and 1 C/min. The two slowest cooling rates were omitted from the diagram for deformed specimens. It was assumed that specimens cooled too slowly from the deformation temperature would have time to recrystallize.

As discussed earlier, some of the cooling curves required only programmed cooling while the highest cooling rates required simultaneous gas cooling. The particular mode of operation for each cooling rate was as follows:

Cooling Rates, deg C/min	Mode of Cooling
1200	Helium-accelerated linear cooling
600, 300, 150	Argon-accelerated linear cooling
75, 40	Linear cooling in argon atmosphere
all other slower rates	Linear cooling in vacuum

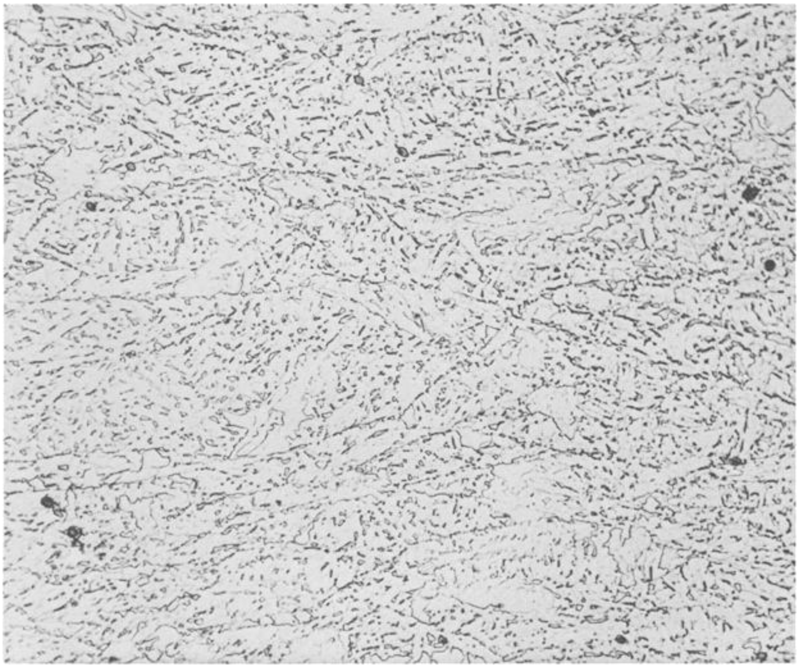

FIG. 7—*Microstructure of Mo-B steel austenitized at 1040 C (1904 F), deformed to 50 percent reduction at 830 C (1526 F) and cooled at 300 C/min* (×*460*).

Each specimen was austenitized in a vacuum at approximately 10^{-4} torr (0.013 N/m^2). The low pressure was maintained for slow cooling. For cooling in still argon the main vacuum valve was closed just before lowering the temperature from the austenitizing level. A fraction of an atmosphere of argon was bled in at the initiation of the cooling cycle. For accelerated cooling the system was switched from the oil diffusion pump to the rotary pump just before the end of austenitizing, and the gas flow was started simultaneously with the cooling cycle. Gas flows were carefully selected and controlled with the aid of pressure regulation and flowmeters.

Results

Interpretation of Dilatometer Data

As discussed above, considerable modification of the dilatation detecting mechanism was necessary to facilitate the in-place deformation of a specimen at high temperature. This modification made it nceessary to deviate somewhat from the normal procedure in the interpretation of the dilatation curves.

Therefore, it is worthwhile to discuss the specific techniques that were used to interpret the dilatation curves for both undeformed and thermomechanically worked specimens. Two deviations from the normal procedure were necessary:

1. The transformation start and finish points were at 2.5 and 97.5 percent, respectively, as opposed to 1 and 99 percent, which are more common. This modification reduced the scatter in the start and finish points.

2. The start of the high-temperature transformation in deformed specimens cooled at slow rates was located by an inflection point rather than by deviation from a straight line. This was necessary because of the expansion of the Invar components in the vicinity of the induction heating coil when operating at a high power level. This extraneous expansion component, which was initiated while austenitizing and holding at the deformation temperature, did not completely subside until the specimen temperature was reduced below 740 C (1364 F).

Specimen dilatation and specimen temperature were both recorded by the dual-pen recorder as functions of time. The dilatation versus temperature curve, which is a cross plot of the recorded data, was used to determine the start and finish points of transformation. Figure 8 is a representative example of a dilatation curve for an undeformed specimen. It summarizes the transformation of the 0.1C-0.4Mo-B steel when cooled from 830 C (1526 F) at 2 C/min. The extreme high-temperature and low-temperature portions of the curve represent normal thermal contraction during cooling for metastable

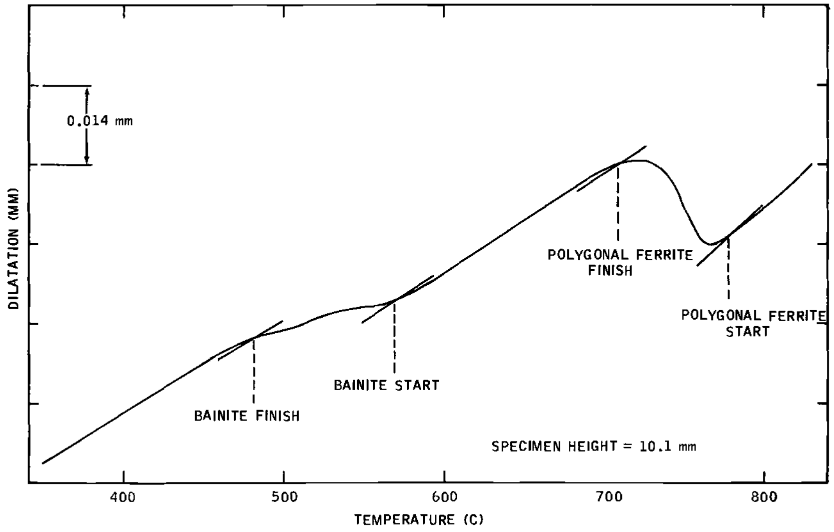

FIG. 8—*Dilatation curve of undeformed 0.1C-4Mo-B steel cooled at 2 C/min.*

austenite and transformation products, respectively. Transformation is indicated by the tendency of the specimen to expand against the normal cooling contraction. This results in a lesser rate of contraction, or even expansion, if transformation is sufficiently rapid. The transformation product can be identified by the temperature range in which transformation takes place. The expansion that takes place in the high-temperature range of Fig. 8 is an indication of partial transformation to polygonal ferrite. The lesser disturbance in the cooling contraction, which appears between about 480 and 580 C (896 and 1076 F), indicates that the remainder of the specimen has transformed to bainite. The transformation start and finish points were obtained by means of an offset technique, using an offset increment equal to 2 to 2.5 percent of transformation.

The slope of the intermediate straight section of the curve is also of significance. The effective coefficient of thermal expansion of the partially transformed material is less than that of the austenite and greater than that of the final transformation products. Therefore, if transformation to polygonal ferrite stops before transformation to bainite starts, the slope of the intermediate section of the curve should be less than that of the upper straight section but greater than that of the lower straight section. If the slope of the intermediate section is less than that of the lower section, it must be concluded that transformation to polygonal ferrite continues until the beginning of transformation to bainite. It may be observed in Fig. 8 that transformation to polygonal ferrite in this specimen stops before bainite begins to form.

Figure 9 presents the dilatation curve of an undeformed specimen cooled at 5 C/min. Transformation in this specimen differs from that of Fig. 8 in two respects: (1) a smaller fraction of the specimen transforms to polygonal ferrite, as would be expected from the faster cooling rate, and (2) polygonal ferrite continues to form until the bainite transformation begins.

The dilatation curve of a deformed specimen which was cooled at 300 C/min is presented in Fig. 10. The specimen completely transformed to bainite. The dilatation of a deformed specimen that was cooled at 40 C/min is represented by the curve of Fig. 11. As discussed above, deformed specimens that are cooled at slow rates are subject to an error in the dilatation curve due to thermal expansion of the Invar components of the compression device. However, the existence of this component of thermal expansion in the dilatation indication at the beginning of the cooling cycle does not significantly complicate the detection of the beginning of polygonal ferrite formation. As the specimen is cooled, the polygonal ferrite reaction starts rather abruptly, and the resulting change in slope of the dilatation curve is readily noticeable. Figure 12 presents a dilatation curve for a deformed specimen cooled at 10 C/min. The high-temperature dilatation error for this very slow cooling rate is somewhat greater than in the previous example, but there is still no difficulty in detecting the initiation of transformation.

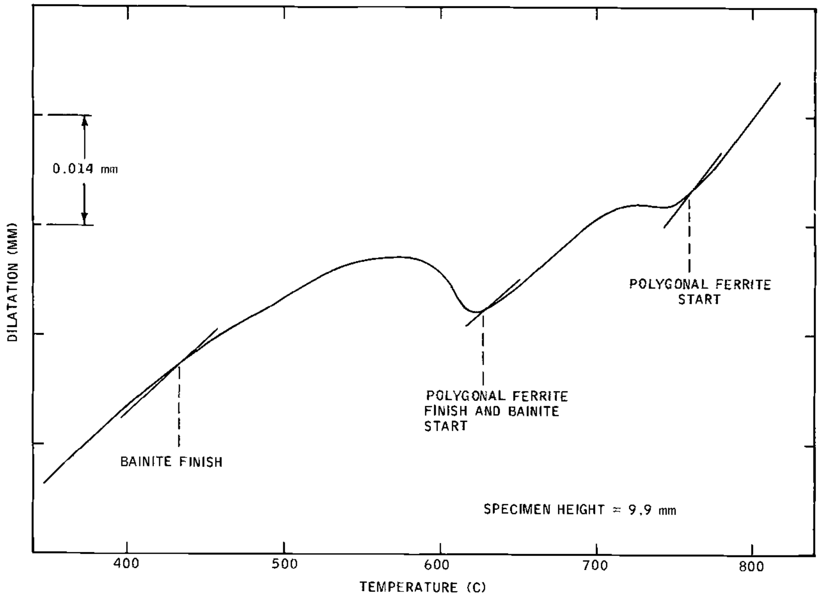

FIG. 9—*Dilatation curve of undeformed 0.1C-4Mo-B steel cooled at 5 C/min.*

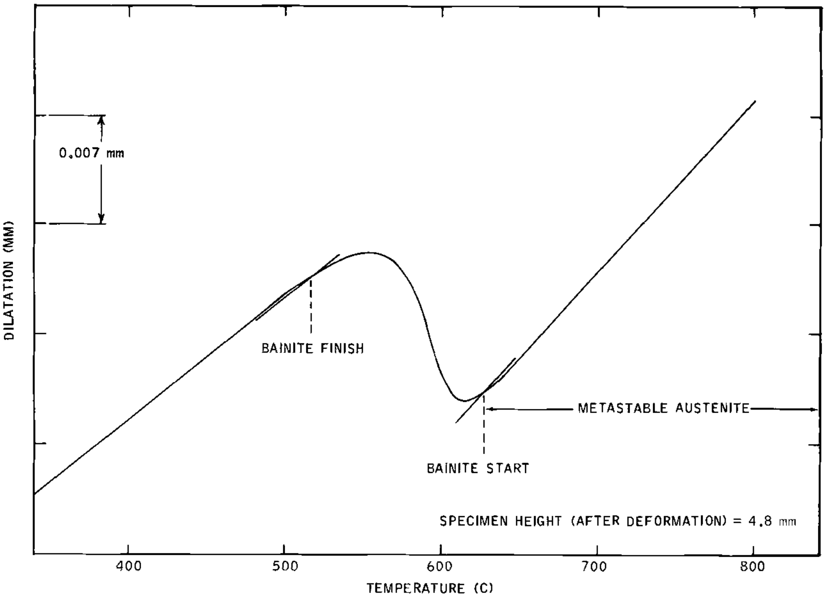

FIG. 10—*Dilatation curve of 0.1C-0.4Mo-B steel thermomechanically worked to 25 percent reduction and cooled at 300 C/min.*

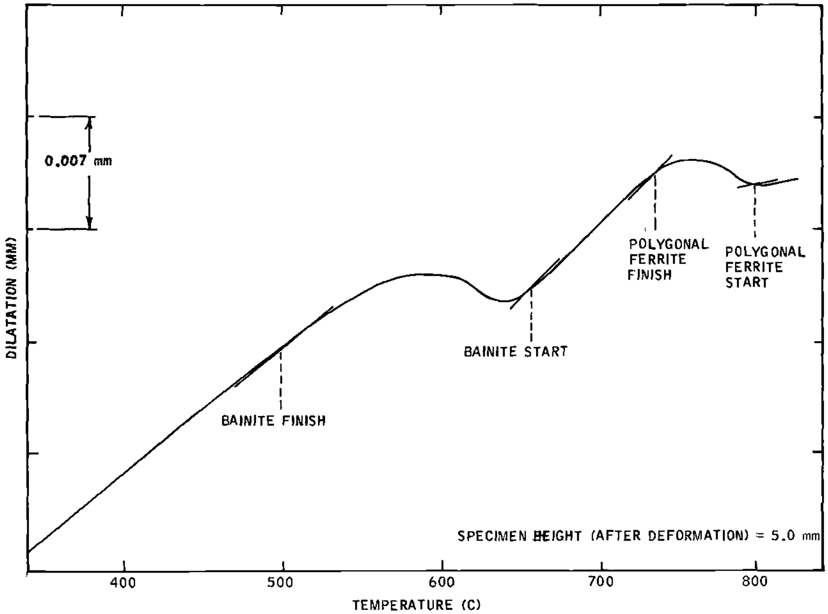

FIG. 11—*Dilatation curve of 0.1C-0.4Mo-B steel thermomechanically worked to 25 percent reduction and cooled at 40 C/min.*

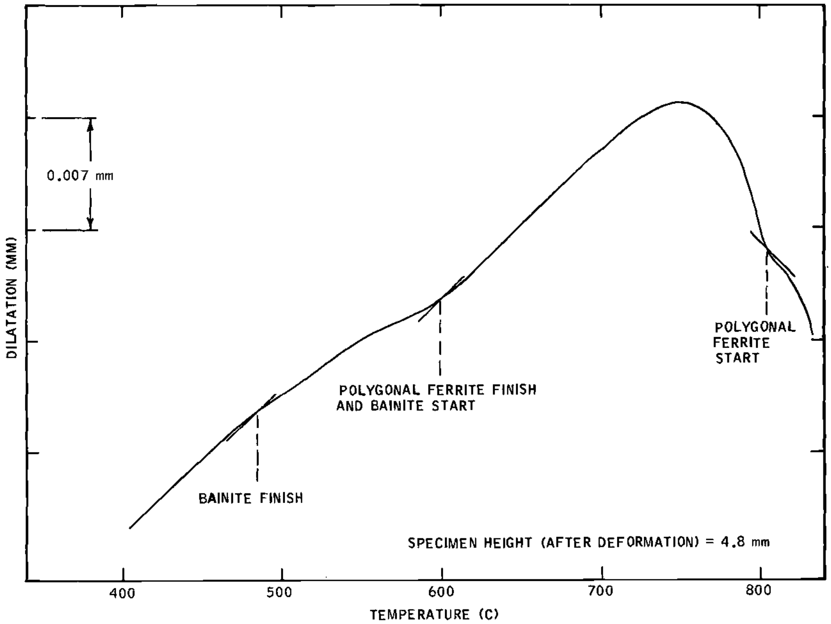

FIG. 12—*Dilatation curve of 0.1C-0.4Mo-B steel thermomechanically worked to 25 percent reduction and cooled at 10 C/min.*

Continuous Cooling Transformation Diagrams

Continuous cooling transformation diagrams of undeformed and thermomechanically worked 0.1C-0.4Mo-B steel are presented in Figs. 13 and 14, respectively. The diagrams show the start and finish points for both high-temperature and low-temperature transformation products. The high-temperature transformation product is primarily polygonal ferrite. Only the two undeformed specimens cooled at the slowest rates contain a small amount of pearlite; there is no pearlite in the deformed specimens. The low-temperature transformation product is predominantly bainite.

Intermediate degrees of transformation are denoted by horizontal marks on the cooling curves at 10, 50, and 90 percent transformation. The intermediate markers are omitted for deformed specimens that formed polygonal ferrite, because the extraneous expansion of the Invar components that occurred in the high-temperature range made it impossible to accurately determine their location. The extent of partial transformation at the completion of the high-temperature transformation was estimated by both metallographic and dilatometric methods. The estimates of percentage austenite transformed, which appear on the diagrams at the high-temperature transformation finish points, were determined by comparing the results of both methods.

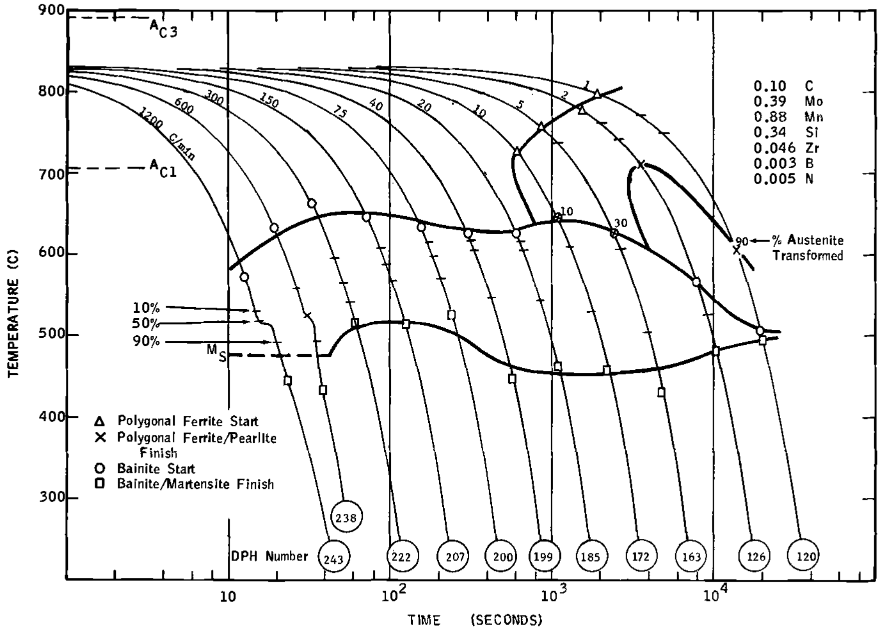

FIG. 13—*Continuous cooling transformation diagram of 0.1C-0.4Mo-B steel in the undeformed condition.*

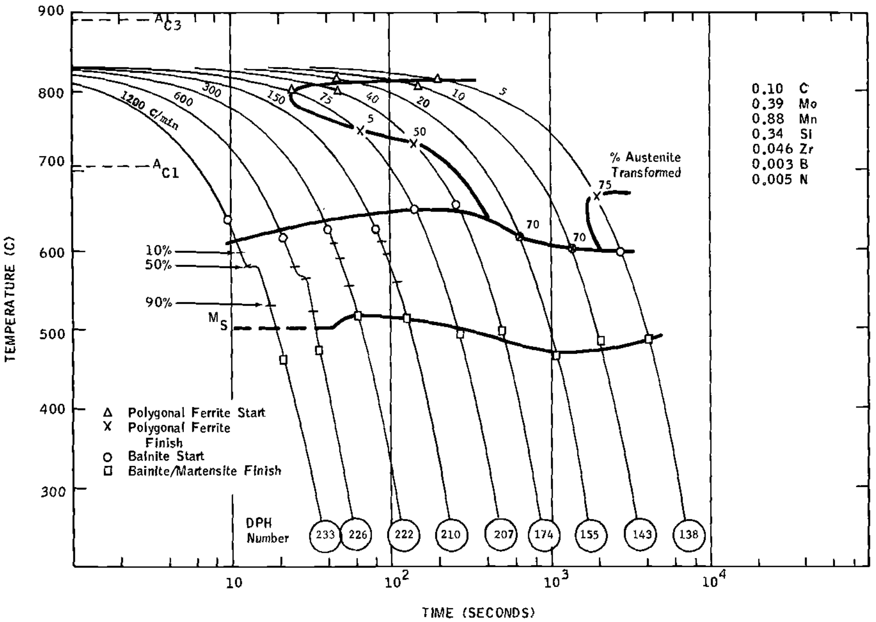

FIG. 14—*Continuous cooling transformation diagram or 0.1C-0.4Mo-B steel thermomechanically worked to 25 percent reduction.*

The beginning of martensite transformation in this steel does not result in a significant change in slope of the dilatation curve when it starts at the end of the bainite reaction. Therefore, the martensite start temperature is not readily determined dilatometrically. The martensite start temperature for the undeformed steel was calculated from the formula of Stevens and Haynes [7]. For the thermomechanically worked material it was estimated by comparing the optical microstructure with the dilatation curve.

Discussion and Summary

For this steel the thermomechanical working to only 25 percent reduction had a strong effect on the kinetics of the gamma-to-alpha transformation in the high-temperature region. The limiting cooling rate for avoiding the formation of polygonal ferrite was shifted by almost one order of magnitude. Other effects of prior deformation of the austenite on the transformation kinetics were minor by comparison. However, a steel with higher bainitic hardenability might have exhibited a much greater shift in the bainite start curve as a result of thermomechanical treatment. The noteworthy change in the kinetics of transformation of this steel during continuous cooling underscores the need for kinetic data on other thermomechanically treated steels.

It also emphasizes the necessity for giving due consideration to the effects of processing steps when selecting a steel composition for thermomechanical treatment. Higher initial hardenability, that is, higher alloy content, may be necessary to facilitate the realization of the benefits of thermomechanical processing.

The technique that has been developed makes it possible to monitor the continuous cooling transformation of specimens subjected to thermomechanical treatments. A wide range of cooling rates is attainable, with good temperature measurement and control over the whole range. The processing schedule may be more complex than the single deformation used in this study. A few seconds are needed to prepare for the measurement of specimen dilatation after deformation has taken place. Additional limitations on the method at its current stage of development are the practical limits of about 50 percent reduction and the extraneous expansion component, which appears during slow cooling in the high-temperature range. This extraneous expansion causes the technique to be unsuitable for isothermal studies. Consideration has been given to replacing certain critical Invar components with nonmetallic pieces that would not generate heat as a result of being near the induction coil. Meanwhile, any doubts raised by the expansion component during transformation studies can be allayed by interrupting the cooling cycle by quenching and observing the microstructure.

The inability to deform specimens to high levels is also a limitation of some significance. Thermomechanical processing treatments may call for 75 to 90 percent reduction. It is believed that this problem can be overcome by extrapolation techniques. Another paper [*8*] will present the bulk of the continuous cooling transformation data obtained on thermomechanically worked material (considerable photomicrographic evidence will be included). These data support the feasibility of extrapolation to higher levels of deformation.

Acknowledgments

The contributions of the members of the doctoral committee, W. F. Hosford, M. J. Sinnott, D. K. Felbeck, and O. F. Kimball, of the University of Michigan, and M. Semchyshen of the Climax Molybdenum Company are gratefully acknowledged.

References

[*1*] Marschall, C. W., "Hot-Cold Working of Steel to Improve Strength," DMIC 192, Defence Metals Information Center, Oct. 1963.

[*2*] Koppenaal, T. J., *Transactions*, American Society for Metals, TASEA, Vol. 62, 1969, p. 24.

[*3*] Duckworth, W. E., *Journal of Metals*, JOMTA, Vol. 18, Aug. 1966, p. 915.

[4] Grange, R. A. and Mitchell, J. B., *Metals Engineering Quarterly*, MENQA, Feb. 1961, p. 41.

[5] Gidon, E. D., Malyshevskii, V. A., Prus., A. A., Shuvalova, N. A. and Pomerants, D. M., *Metal Science and Heat Treatment of Metals*, MSHTJA, Feb. 1965, p. 105.

[6] Korneyev, G. M. and Estrin, E. I., *Physics of Metals and Metallography*, PHMMA, Vol. 23, No. 1, 1967, p. 188.

[7] Stevens, W. and Haynes, A. G., *Journal of the Iron and Steel Institute*, JISIA, Vol. 183, 1956, p. 349.

[8] Smith, Y. E. and Siebert, C. A., "Continuous Cooling Transformation Kinetics of Thermomechanically Worked Austenite," to be published in the *Transactions*, American Society for Metals, 1970.

DISCUSSION

J. C. Russ[1] (*written discussion*)—The author should take care to point out that he has used a convention in drawing his CCT diagrams that differs from those presented by many other authors, in particular, those presented in *Metal Progress.* The author shows the nose of the high-temperature transformation protruding in such a way that some cooling lines enter the field and then leave it again. This would imply a retransformation to austenite if taken literally. A less confusing convention is to bring the lower side of the nose parallel to cooling lines and use percent transformation lines to indicate the degree of transformation.

Y. E. Smith (*author's closure*)—I appreciate Dr. Russ' remarks, since he makes a point which is quite worthwhile, and because, in so doing, he offers Professor Siebert and myself an opportunity to take note of another item concerning the published CCT data which is somewhat overdue for discussion. Dr. Russ has indirectly called attention to the fact that there has been no effort to standardize the presentation of transformation diagrams. Perhaps some effort by ASTM in this direction would be helpful. The convention that we chose was selected on the basis of simplicity. The areas which are formed by connecting the points picked off the dilatation curves are regions of microconstituent *formation*, rather than microconstituent *presence*, as in the diagrams referred to by Dr. Russ. This should be obvious, since the points which define the boundaries of these regions are designated "polygonal ferrite start" and "polygonal ferrite finish."

The second point concerns the amount of scatter that is inherently present in transformation data. When a plotted curve is published for any set of data which involves significant scatter, it is an injustice to the reader to exclude the data points from the published curve. The individual determinations are the facts and the line between the points is, to some degree, fiction. The engineer who is attempting to make use of the transformation data should have the opportunity to distinguish between the facts and the fiction.

---

[1] Applications consultant, JEOLCO, Inc., Medford, Mass. 02155.

J. B. Newkirk[1]

Advances in X-ray Metallography

REFERENCE: Newkirk, J. B., "**Advances in X-ray Metallography,**" *Applications of Modern Metallographic Techniques, ASTM STP 480,* American Society for Testing and Materials, 1970, pp. 152–182.

ABSTRACT: X-ray metallography, as defined for this review, consists of the application of X-rays to the microstructural characterization of solids. Basic crystal structure analysis is excluded, though the identification of phases whose crystal structures are known is not: the subject is briefly reviewed, using examples taken mostly from recently published works. The principles and typical applications of X-ray diffraction topography are emphasized. Other methods to which specific references are made include microradiography, macrostrain measurement, Kossel pattern analysis, and applications of long wavelength X-ray analysis.

KEY WORDS: crystals, metallography, metallurgy, microstructure, X-ray analysis, evaluation

The large and continuing outpouring of new applications for X-ray technology in metallurgy leaves no doubt that a section on X-ray methods in metallography deserves a place in this symposium. It is instructive to review the types of metallographic information that can be had through the study of X-ray emission, scattering, or absorption. Such a list would include at least the subjects given in Table 1. Also, a respectable number of new techniques and instruments have emerged in the field of X-ray metallography during the past few years. The items in Table 2 would have to be among these, though most of the entries in Table 1 are also associated with specialty devices, some of which are available commercially. To discuss in a meaningful way all of the items listed in Tables 1 and 2 would require a sizeable book. Therefore this review will emphasize only those subjects which have enjoyed especially active development during the past few years.

Several very good text and reference books on subjects directly related to X-ray metallography are now available (for example, see Refs *1–3*[2]). Fortunately, a disproportionately large fraction of the progress in X-ray metallography is reported in a relatively few monographs and journals, making

---

[1] Brainerd F. Phillipson professor, Department of Metallurgy and Materials Science, University of Denver, Denver, Colo. 80210.

[2] Italic numbers (in brackets) refer to the list of references at the end of this paper.

TABLE 1—*Types of metallographic information obtainable by X-ray analysis.*

Crystal structures	Crystallographic parameters
	Phase identification
Phase diagrams	. . .
Strain measurement	Macrostrains
	Microstrains
	Topographical display
Defects in crystals	By Debye-Scherrer line profile
	Topographical
	Point defects
	Line and planar defects
Grain size	. . .
Preferred orientation in polycrystalline aggregates	. . .
Recrystallization kinetics	. . .
Thickness measurement	Plating
	Ultrathin film layers
Degree of crystallinity in glasses	. . .
Liquid structures	. . .
Ordered structures	Determination of long-range order
	Determination of short-range order
Magnetic domain structures	. . .
Wear and abrasion studies	. . .
Fatigue studies	. . .
Solid phase transformations	Mechanism
	Kinetics
Lang wavelength X-ray applications	Atomic binding
	X-ray astronomy
	Light element fluorescence analysis
X radiation treatment of materials (nonbiological)	. . .
Chemical analysis	Relative amounts of phases in mixture (diffraction)
	Fluorescence analysis

it relatively easy to locate articles of special interest. The continuing series of symposia entitled *Applications of X-ray Analysis,* with which I have been privileged to be associated for several years, has been active in bringing together current developments in many phases of X-ray metallography. This series, sponsored by the Metallurgy Division of the University of Denver Research Institute, is published under the title *Advances in X-ray Analysis* [*4*]. The influence of contributors to the Denver X-ray Conference will be found throughout this survey.

TABLE 2—*Metallographic devices and methods involving X-ray analysis.*

Powder methods	Focusing
	Automated
	High temperature
	Low temperature
	Precision parameter determination
Special diffractometer methods	Precision lattice constants
	High temperature
	Low temperature
Radiography	Macroscale
	Neutron macroscale
	Microscale, contact
	Microscale, projection
	Flash
Small-angle X-ray scattering	...
X-ray topography	...
Divergent beam (Kossel) method	...
X-ray fluorescence analysis	Dispersive
	Nondispersive
	X-ray microprobe
X-ray absorption analysis	Topographical
	Absorption spectroscopy
Isotopic X-ray sources	...
High-brillance sources	Fine focus
	Rotating anode
Image intensification	TV display
Totally reflecting X-ray spectrograph	...

X-ray Diffraction Topography

About 10 years ago several workers independently, and nearly concurrently, developed methods by which the microstructure of a crystal could be imaged by diffracted X-rays. These methods have come to be grouped under the general heading *X-ray diffraction topography*, to distinguish them from the older microradiographic methods in which diffraction plays no part. In principle all of the diffraction topographical methods are related, in that an actual image of a single crystal specimen is produced on a photographic plate by a bundle of diffracted X-rays that vary in intensity from place to place, depending on the nature of the crystal. Some of the methods display the surface of the specimen crystal only, whereas others show microstructural detail throughout its thickness.

The essential features of several basic methods in X-ray topography are described in Ref *5*. Refinements of the theory of image contrast and of variations of the principal techniques are reported in several reviews and

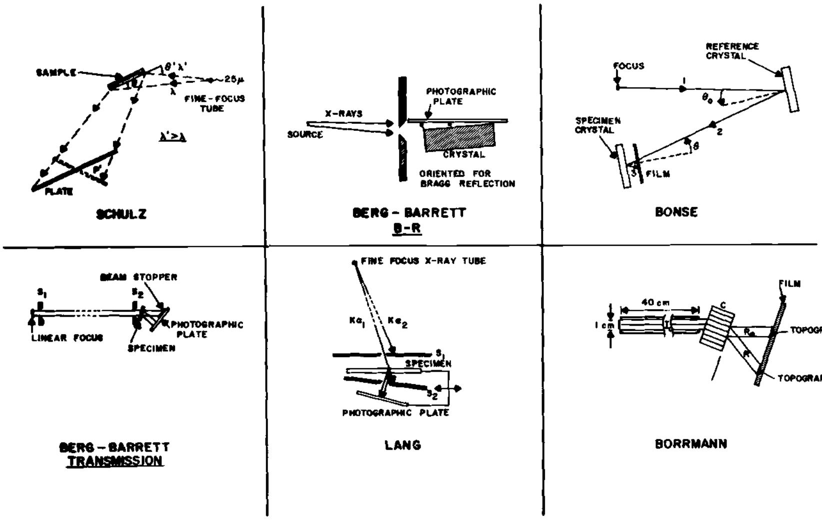

FIG. 1—*The basic methods for making X-ray diffraction topographs are sketched here. Details are given in Ref* 30d *and others.*

original papers [*6*]. Therefore, in this survey, description of the basic techniques will be limited to the sketches given in Fig. 1 and to Table 3, in which the features of the various basic methods are compared. In the rest of this section, examples of microstructure made visible by X-ray topography are given for several classes of materials. Also, several refinements of the basic X-ray topographical methods are described and practical examples of their uses are given.

Polycrystalline Metal Aggregates

Weissmann and Evans [*7*] have developed a technique based on the original Berg-Barrett geometry by which the grains seen on a metallographically prepared surface of a polycrystalline aggregate can be made to diffract white X radiation to a film placed close to the metal surface (see Fig. 2). The spots on the "multiple Laue" pattern can be related to the grains seen on the metal surface by their corresponding sizes and shapes. The relative orientations of the grains can also be estimated if needed by tracing the strong reflections to identifiable Debye-Scherrer lines, thereby determining the Miller indexes of the particular reflection. Using this somewhat laborious method it is possible to determine the relative grain orientations, the approximate sizes and shapes of grains, and, to some extent, the size and relative disorientation of the subgrains. Nakayama et al [*8*] have applied this method to the study of tungsten crystals, from 10 μm to 2 mm in size, which are disoriented at angles ranging from 10 seconds to 16 minutes of arc.

TABLE 3—*Summary of the features of the basic techniques for X-ray diffraction topography* [5].

Technique	Schulz, Guinier, and Tennevin	Berg-Barrett	Double Crystal	Wide-Beam Transmission (Barth and Hosemann)		Scanning Transmission (Lang)	
Apparatus	Simple	Simple	Complicated	$\mu_0 t > 10$ Simple	$\mu_0 t < 1$ Simple	$\mu_0 t \sim 3$ Complicated	$\mu_0 t < 1$ Complicated
Exposure time	1 to 25 h	Short (~1 h)	Short (~1 h)	Long (~10 h)	Short (~1 h)	10 to 30 h	2 to 10 h
Defect for which technique is most suited with kind of contrast[a]	Grain dis-orientation, subgrains(1)	Subgrains(1) Dislocations(2)	Subgrains(1) Dislocations(1) Stacking faults	Dislocations(3)	Subgrains(1) Dislocations(2) Stacking faults	Dislocations (2) (3)	Subgrains(1) Dislocations(2) Stacking faults
Best geometric resolution, μm	50	1	1	1	1	1	1
Sensitivity to deformations	Low	Low	High	High	Low	High	Low

Sensitive to the *sense* of deformations	Tilts: Yes Inhomogeneous deformation: No	Subgrains: Yes Dislocations: No	Yes	Yes	No	Yes	No
Thickness t of specimen contributing to topograph[b]	Schulz: $\leq$ G. + T. 50 to 1000 μm	$\leq 5\ \mu$m	$\leq 5\ \mu$m (back reflection) $\leq 300\ \mu$m (transmission)	1 to 5 mm	0 to 2 mm	0.1 to 5 mm	0 to 2 mm
Dislocation image width,[c] μm	. . .	1 to 5	Up to 150	≤ 50	~ 5	Up to 150	1 to 10
Upper limit of dislocation density, lines/cm^2	. . .	5×10^6	10^5	5×10^3	5×10^6	5×10^3	5×10^6

---

[a] (1) homogeneous dilation and tilt contrast, (2) extinction contrast, (3) dynamical contrast.

[b] This is determined, in the Bragg case, by the extinction depth and, in the Laue case, by the value of μ_0 (the absorption coefficient) for the material and the value of t imposed by the technique.

[c] Based on the assumption that this is determined by normal image overlap.

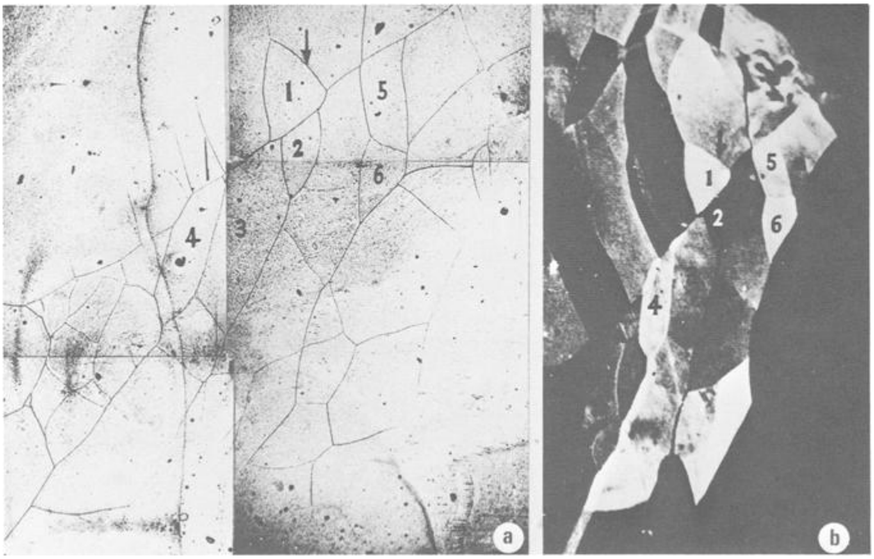

FIG. 2—*Correlation of substructure in tungsten crystals:* (a) *light micrograph of substructure disclosed by etching with 3 percent boiling H_2O_2;* (b) *Berg-Barrett X-ray micrograph. Unfiltered radiation; copper target; effective size of focal spot 40 μm* [7] (*×16*).

Application of Diffraction Topographic Techniques to the Study of Metallic and Nonmetallic Crystals

The first, and still the largest, application of the Lang scanning transmission technique has been with nonmetallic and semiconductor crystals of relatively low density. It has not been as successfully applied to the study of dislocations in metal crystals. Since optimum image contrast is obtained with the Lang technique when $\mu t \sim 1$, it is necessary to thin the crystal, say copper, to about 0.002 in. in thickness without introducing any new crystal imperfections. This is a delicate operation and is a limitation of transmission X-ray topographical techniques when examining any but low-density materials with a high modulus of elasticity.

Transmission topography of thick copper crystals has been accomplished by Young and Sherrill [9] using the Borrmann anomalous transmission technique. An example of their work, showing dislocations in copper, is given in Fig. 3.

Single-Crystal Semiconductors

Perhaps the greatest application of X-ray topography has been in the semiconductor industry, where line defects can lead to short circuiting and to electrical failure of transistor and other microcircuitry devices. The Lang technique has been popular for revealing dislocations, stacking faults, and other crystals [*10*]. Figure 4 shows a topograph of silicon made by Lang using the method he developed. The various defects are described in the figure caption. Other workers, notably Schwuttke [*11*], have developed the Lang technique to a point where it is a common tool for characterizing semiconductor crystals with and without associated microcircuit overlayers.

The stacking faults found in annealed silicon web dendrites (Fig. 5) are interesting and dramatic. The stacking faults are bounded by ⟨112⟩ partial dislocations and may be either extrinsic or intrinsic. As Fig. 5 clearly shows, the details of the topographic image are strongly dependent upon the specific set of (*hkl*) planes that is used to make the topograph. Details about the analysis of these and other topographs showing stacking faults and dislocations are given in Ref *10*. Recent comparative studies of semiconductor crystals by X-ray topography, electron microscopy, and etching methods have led to remarkably consistent conclusions about the dislocation and stacking fault structures. X-ray topographs can therefore be accepted as reliable sources of data for the microstructural characterization of large crystals of this type.

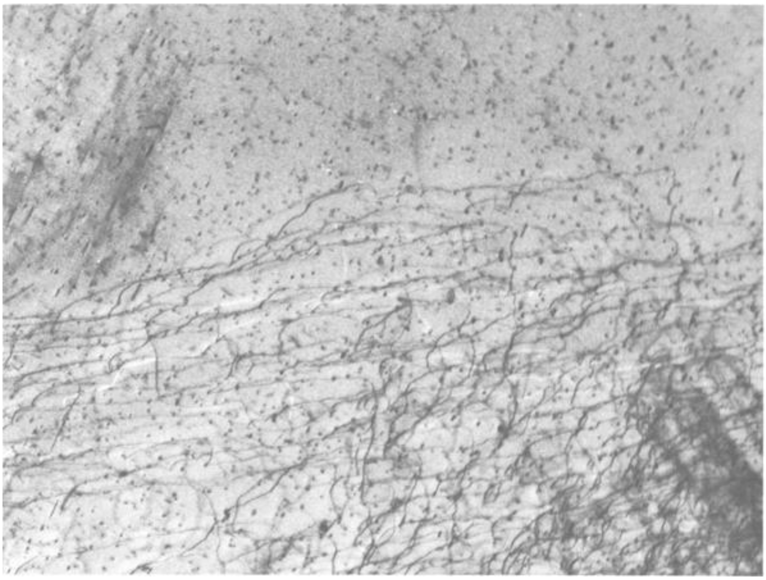

FIG. 3—*Borrmann-type (111) topograph of a copper crystal about 0.4 mm thick using Mo K_α radiation. The dark lines are dislocations that were produced in a previously dislocation-free crystal by an applied resolved stress of about 10 g/mm^2. The black spots are due to vacancy clusters and the smears to dislocations on other slip systems. Courtesy of F. W. Young, Jr.* (×*20*).

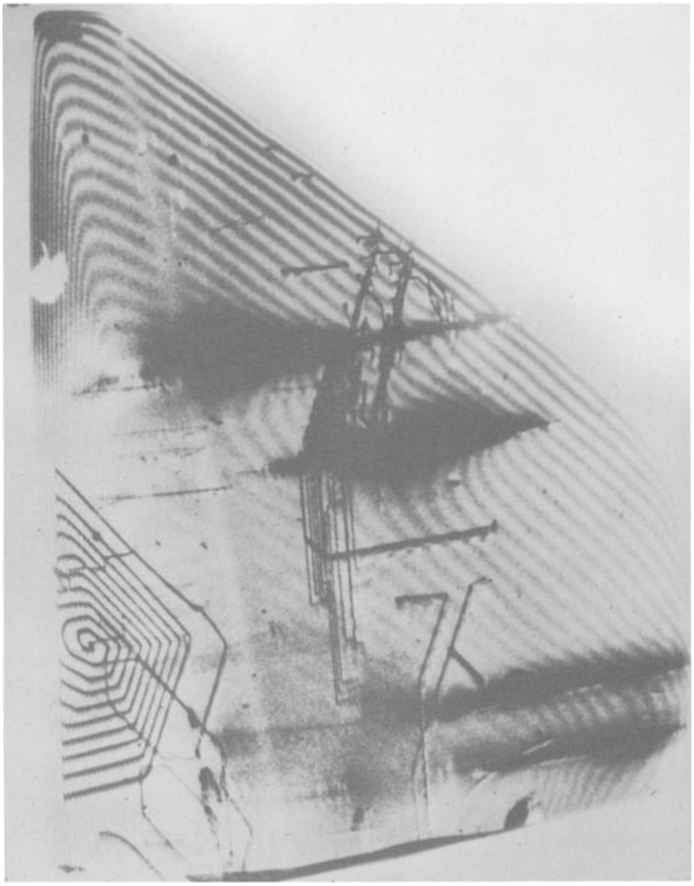

FIG. 4—*Lang-type (111) topograph of a wedge-shaped silicon crystal using Ag K_α radiation. The spiral and straight dislocation lines, the Pendellösung fringes, and unorganized surface damage effects are clearly visible. Courtesy of A. R. Lang.*

An analytical description of characteristic four-lobed rosette patterns found in {111} and {110} X-ray topographs of monocrystalline Si has recently been worked out by Walford and Carron [*12*]. They have proposed a stress model which leads quantitatively to the X-ray topographical patterns that have been observed. This is an example of the development of a qualitative X-ray topographic method into a reliable quantitative tool.

X-ray Topography of Other Nonmetallic Materials

An interesting revelation about the microstructure of large flux-grown beryllium oxide crystals was achieved through the application of Lang-type X-ray topography [*13*]. Figure 6 is an (0002) Lang topograph of a pyramidal

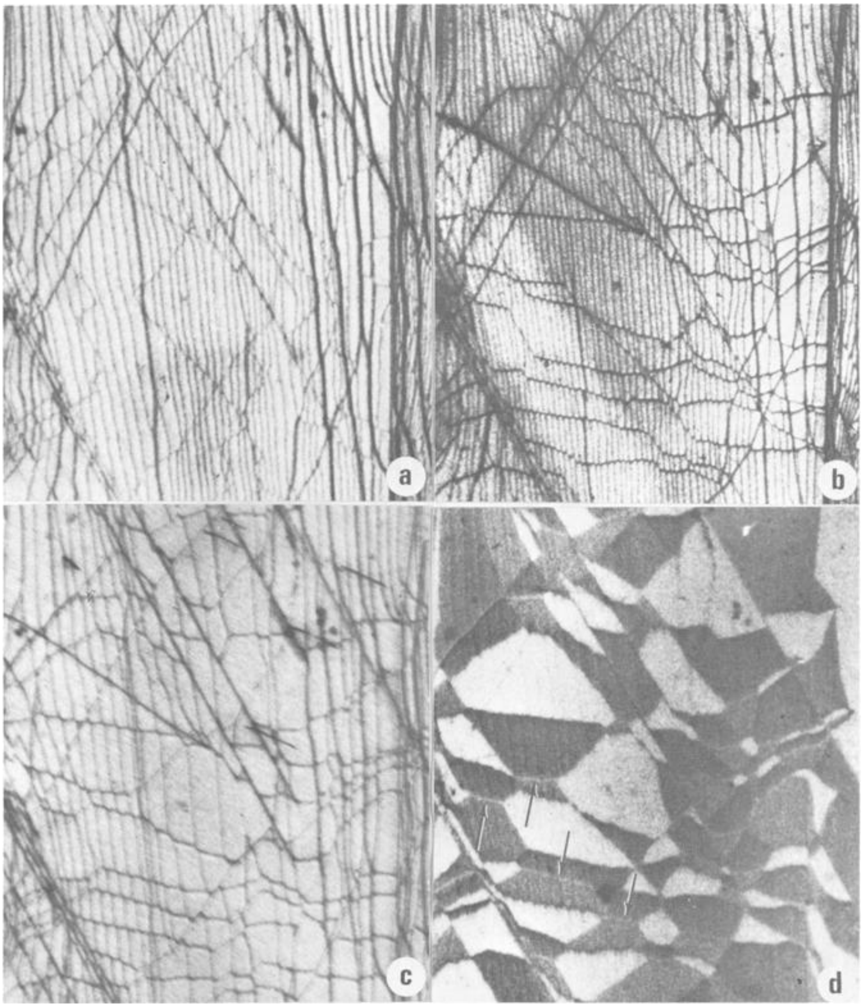

(*a*) [2$\bar{2}$0] topograph, dislocation contrast.

(*b*) [20$\bar{2}$] topograph, dislocation contrast.

(*c*) [02$\bar{2}$] topograph, dislocation contrast.

(*d*) [11$\bar{1}$] topograph, stacking fault contrast. Note inverted dislocation contrast (arrows) in regions separating extrinsic faults from intrinsic faults.

FIG. 5—*These X-ray topographs of an annealed silicon web show the effects of the diffraction vector direction on the dislocation or stacking fault contrast. Each dislocation bounding a fault is a partial and can be made to disappear by proper choice of diffraction vector. After Meieran and Bleck,* Journal of Applied Physics, *Vol. 38, 1967, pp. 3495ff* (×*45*).

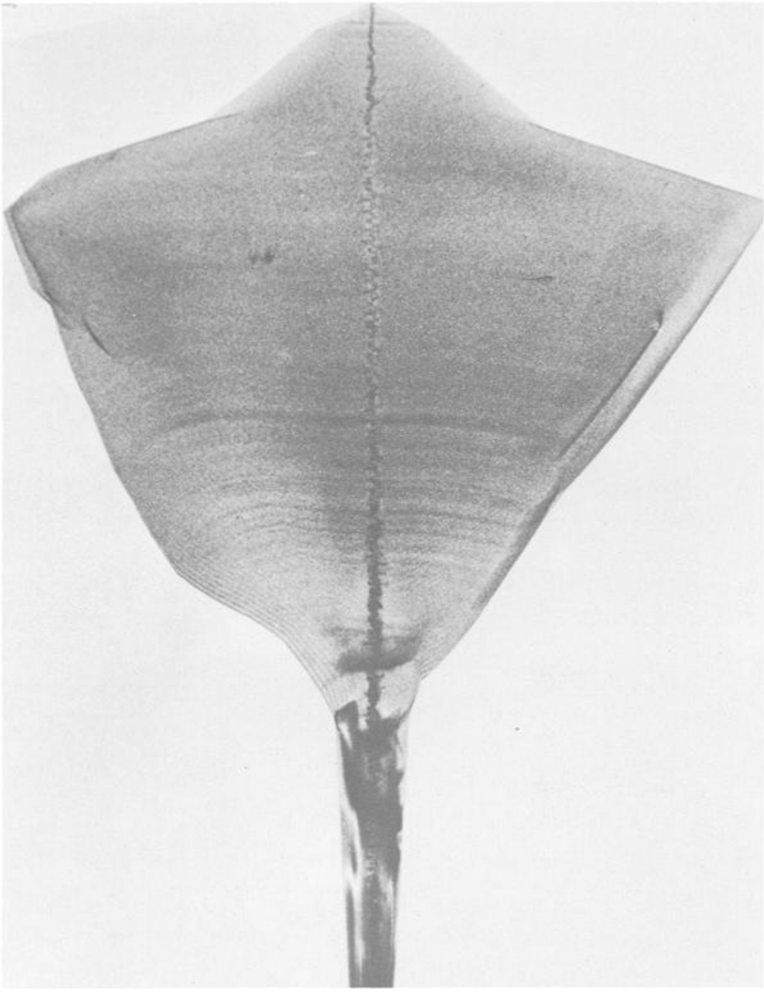

FIG. 6—*This Lang-type (0002) topograph of an etched BeO crystal shows the axial screw dislocation impurity bands and Pendellösung fringes* [13] (×*50*).

BeO crystal about 5 mm in total length. The topograph clearly shows a screw dislocation at the axis of the crystal. Close examination of the axial image reveals detail (not visible in the published figure) which suggests that degeneration of the screw dislocation has occurred, resulting in a spiral form of the dislocation core. This idea is consistent with the theory of point defect interaction with screw dislocations.

Spectacular X-ray topographs of quartz crystal slabs in resonant oscillation have been made by Wagner and Young [*14*] and by Spencer [*15*]. Since the diffracted intensity is dependent upon the strain gradient within the crystal, the standing wave patterns at the various resonant frequencies that characterize a given crystal can be made visible (see Fig. 7).

Sources of Image Contrast

Strain Gradients

The intensity of diffracted X-rays depends upon many factors, including the wavelength of the rays, the geometrical conditions of diffraction, and the perfection of the diffracting crystal. It is beyond the scope of this paper to describe these factors in detail. Other reviews are available where this subject is discussed in depth [*16–18*]. For the present purpose it is sufficient to say that any local reduction in ideal crystal periodicity results in a corresponding *increase* in diffracted intensity from that region. Thus, total and partial dislocations are usually seen as lines of higher intensity having a width between 0.1 and 50 μm, sometimes more, depending on the particular technique used to form the X-ray image. Stacking faults are visible as planes of uniform intensity different from that of the background. On the other hand, strain gradients are seen as bands which are always of higher intensity than that of the background. These localized aperiodic entities are in part characterized by directionality. It is a very useful property of diffraction topography

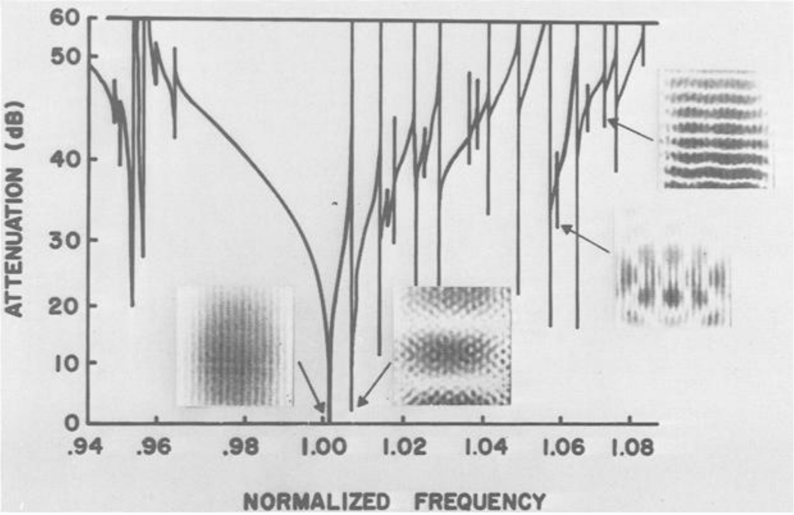

FIG. 7—*Diffraction topographs can make visible the coupled thickness-shear, twist, and flexural vibration modes in rectangular AT-cut quartz plates. The X-ray topographs shown were made with* ($2\bar{1}\bar{1}0$) *reflections. The ordinate is calibrated in frequency normalized to the infinite plate thickness-shear frequency. Courtesy of W. J. Spencer.*

that the direction of a strain gradient can be experimentally determined by judicious choice of the specific set of crystallographic planes used to make one or more topographic images of the defect. By applying the criterion that diffracted intensity varies directly with the component of strain normal to the diffracting planes, one can usually deduce the strain gradient direction which is associated with a given defect. Thus the relative intensity of a defect image, as seen in topographs made with various (*hkl*) crystallographic planes, constitutes the data from which may be deduced the direction of the maximum strain gradient that is associated with that defect.

Point Defects

Some crystal defects, for example point defects, are not directional. They may, however, introduce sufficient crystalline aperiodicity to enhance the diffracted intensity locally. Thus, impurity layers in crystals can appear in topographs as corresponding bands of extrahigh intensity, as seen in Fig. 6. Reference *19* describes in detail the effects of small concentrations (as low as 10^{14} atoms per cubic centimeter) of impurities on the integrated X-ray diffracted intensity. In summary one can say that the presence of impurity traces in crystalline materials can cause small changes in lattice parameters and large changes (usually an increase) in the intensity of X-rays diffracted by that material. If the identity of a uniformly dissolved impurity is known, a meaningful estimate of its concentration can be made from precise measurements of crystallographic lattice parameters or the structure factor F of its host. X-ray diffraction topography, on the other hand, is an effective method for observing the distribution of trace impurities in relatively large crystals if those crystals are otherwise highly perfect. However, at its present state of development, diffraction topography cannot identify the impurity nor measure quantitatively its concentration level.

Moiré Patterns

When grids of similar periodicity are placed in close contact and nearly parallel with one another, they produce a Moiré, or "difference," pattern when viewed in transmission. The Moiré pattern depends upon the relative periodicities of the original grids and their orientation relative to one another [*20*]. For original grids of spacing d_1 and d_2, respectively, the pattern consists of fringes of spacing $D_c = d_1d_2/(d_1 - d_2)$, for a so-called compression Moiré pattern, or $D_t = d/\epsilon$ for a twist Moiré pattern (d = actual periodic spacing of both of the grids; ϵ = twist angle between two grids of equal d spacing). An example of a Moiré pattern, which varies from a twist to a compression Moiré, is shown in Fig. 8. Chikawa [*19*] has used Moiré fringes in Lang topographs to detect extremely small concentrations of impurities in CdS

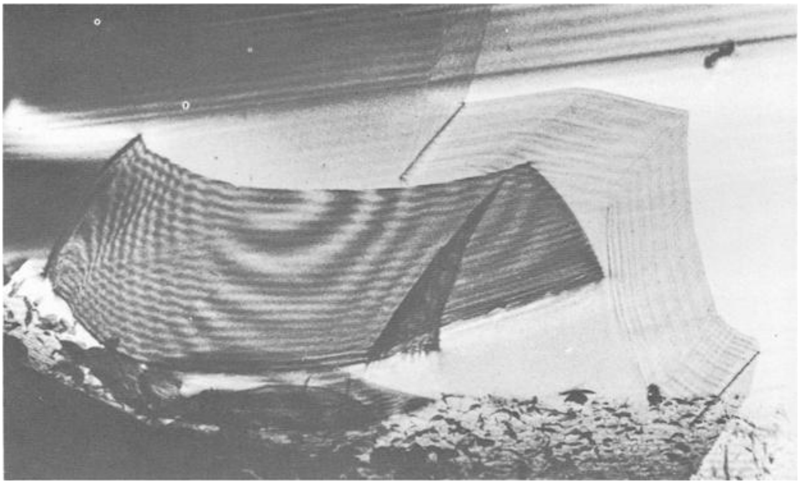

FIG. 8—*Lang-type topograph of a quartz plate 1 mm thick showing X-ray Moiré fringes at a crack in the plate. $10\bar{1}0$ reflection, Ag K_α radiation. Courtesy of A. R. Lang* (×*15*).

crystals. By means of X-ray Moiré patterns, Bonse and Hart [*21*] have measured controllable translations of less than 1 Å, rotations of a few thousandths of a second of arc, and relative dilations of $(d_1 - d_2)/d = 10^{-8}$.

Pendellösung Fringes

According to dynamical diffraction theory, as X-rays pass through a crystal at the Bragg angle the energy of the diffracted beam varies with the thickness traversed. As a consequence of this effect, intensity fringes called Pendellösung fringes, are seen in the transmission diffraction topographic image of a specimen whose thickness is nonuniform, analogous to optical interference fringes that form when light is reflected from nonparallel surfaces that are very close together. An example of Pendellösung fringes is seen in Fig. 4. Since the spacing of Pendellösung fringes is dependent upon the structure factor F in the diffracted intensity equation, the fringe pattern can be used to make an accurate and absolute measurement of F [*22a*].

Variations and Extensions of Basic X-ray Topographic Methods— Modified B-B Techniques

Young and Wagner, following a method used by Shetty et al [*22b*], have refined the transmission Berg-Barrett (B-B) technique by placing moving soller slits (MSS) between the X-ray line source and the specimen. This arrangement limits the extent of the X-ray source which can illuminate any given part of the specimen and partially collimates the beam. One beneficial result of this geometry is an improvement in the image resolution, since the $K\alpha_1\alpha_2$ overlap which occurs in the ordinary transmission Berg-Barrett arrangement can be avoided. The technique permits topographical imaging of macroscopic strains in the specimen crystal as well as other defects commonly seen by the Lang method. Figure 9 shows topographs of a quartz crystal made by the (*a*) conventional Lang method and (*b*) the MSS method. The geometric resolution is about 7.1 μm in the MSS case and about 2.3 in the Lang case, with exposure times of 2 and 5 h, respectively. The MSS method is much simpler than the Lang method with respect to equipment required and ease of setup. Armstrong and Schultz [*23*] have found hexagonally shaped prismatic dislocation loops and shallow half-loops near the surface of cleaved pure zinc crystals using the standard reflection Berg-Barrett technique. Transmission topographic techniques would show such loops throughout the bulk of the specimen if they existed there. However these methods require expensive and complicated equipment and may require prohibitively long exposure times to produce high-resolution single-image topographs. On the other hand, the transmission B-B technique, while permitting a much shorter exposure time and requiring simpler equipment, produces double images as a result of the doublet structure of the characteristic K_α radiation that is usually used to make the picture. Dionne [*24*] has demonstrated that the disadvantages of both methods can be avoided if the K_β characteristic radiation is used with the transmission B-B geometry. Using Ilford L-4 nuclear plates (50-μm

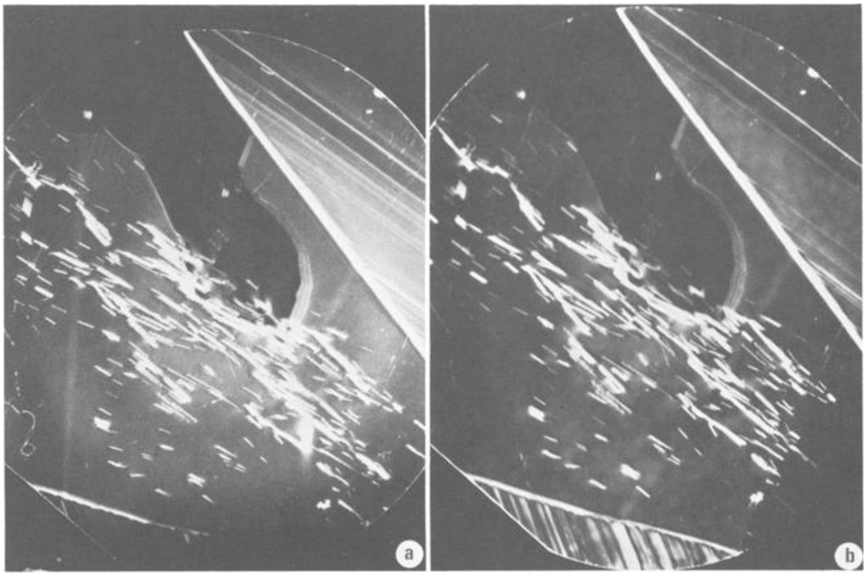

FIG. 9—*Diffraction topographs of the same quartz crystal by* (a) *the conventional Lang method and* (b) *the moving soller slit method. Courtesy of R. A. Young.*

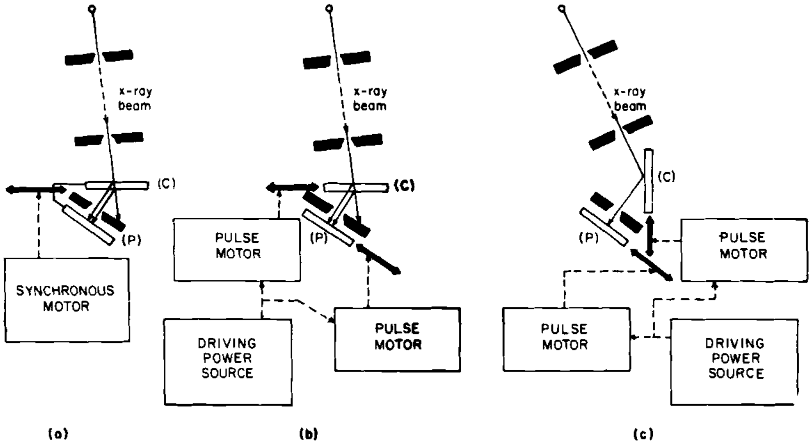

FIG. 10—*Comparison of the* (a) *Lang method with the modifications*, (b) *and* (c), *suggested by Yoshimatsu et al* [25]. *The dark arrows indicate traversing motions.*

emulsion thickness) and copper K_β radiation, Dionne was able, in a ½-h exposure, to make a high-resolution 220 transmission topograph of an 80-μm-thick wafer of silicon 3 cm^2 in area. Furthermore, the use of K_β radiation made it possible to sample a much larger specimen area, without the necessity of scanning, than is otherwise possible.

Modified Lang Techniques

Usually the topographical image obtained with a Lang or Berg-Barrett camera is badly distorted geometrically with respect to the object crystal. Kohra and his co-workers [25] have shown that image distortion can be reduced and sometimes eliminated by causing the specimen and the film to traverse in manners other than that of the original Lang method (see Fig. 10). Thus the (200) Lang reflection, which may be drastically foreshortened with respect to the specimen itself, can be restored in shape to correspond approximately with the crystal, as shown in Fig. 11.

A major application of the Lang geometry has been for the examination of silicon wafers containing surface microcircuitry patterns. Often a crystal slice with, for example, several hundred planar diodes has considerable warps and bends. When this happens only part of the wafer can be in suitable orientation to satisfy Bragg's law, and thus only part of the wafer can contribute to a topographic image by the Lang technique. To avoid this limitation Schwuttke [26] has added an oscillating motion to the specimen, as shown in Fig. 12. If the angular oscillation range is larger than the maximum warp angle, the entire specimen can usually be made to diffract with more or less uniform background intensity. Figure 13 is a topograph of a silicon wafer

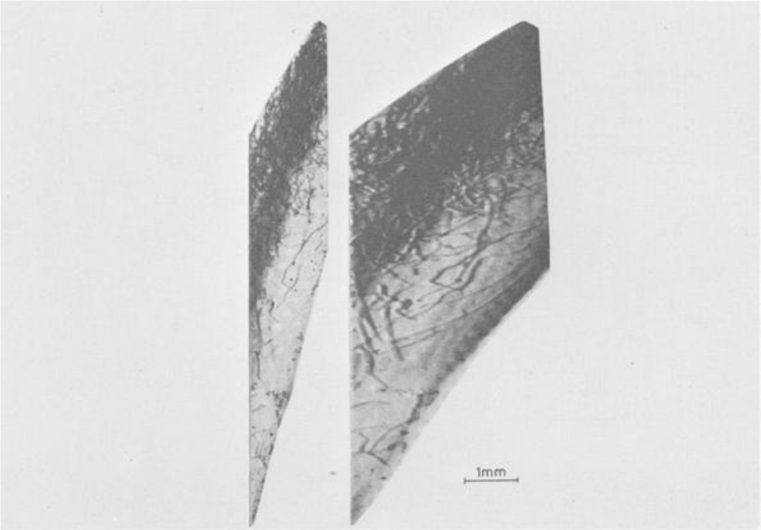

FIG. 11—*Transmission 220 topographs of a silicon crystal made by the* (a) *Lang method and* (b) *a modified method* [25].

6 in. in diameter made by this so-called scanning oscillating topographic (SOT) method.

Traversing Laue Method

Very recently Mateer [*27*] published a note describing a simple and direct method for qualitatively estimating the perfection of large crystals making up a 2-mm-diameter wire specimen. The specimen and film are traversed in a direction that is normal to a polychromatic X-ray beam (see Fig. 14). The resulting Laue pattern consists of streaks instead of the usual spots. Figure 15 shows an example of this type of photograph made with a relatively imperfect aluminum crystal wire. All streaks are shorter than the trace of the primary beam, showing that grain boundaries were crossed in the traverse. The waviness and nonuniform thickness of the streaks indicate that plastic deformation has occurred, probably by bending and twisting during handling.

An X-ray Interferometer

The Borrmann effect, relating to the anomolously low absorption of X-rays by a defect-free crystal when set at a Bragg angle, permits the construction of an interferometer, an example of which is shown diagramatically in Fig. 16. The first of these was made by Bonse and Hart [*28*]. Channels were cut in a large, low-defect silicon crystal several centimeters long, leaving slabs which stand in perfect crystallographic alignment with one another.

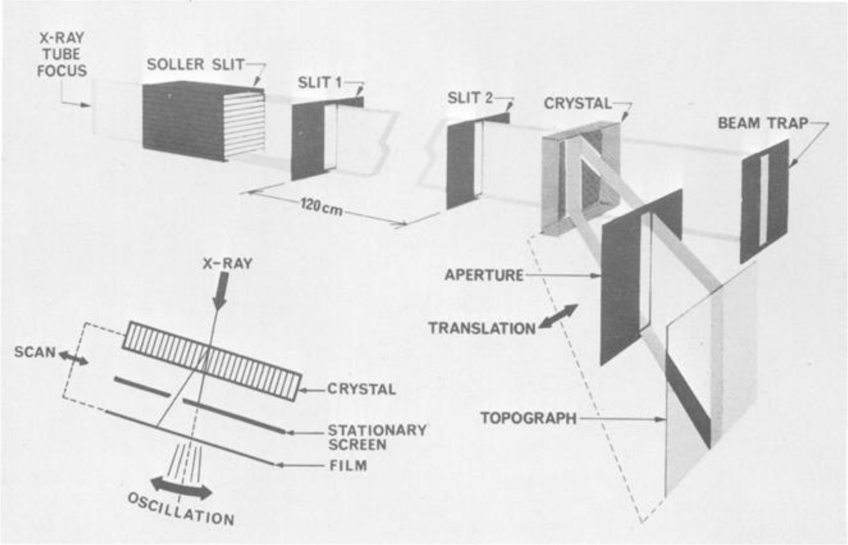

FIG. 12—*Possible geometry of scanning oscillating technique (SOT). Courtesy of G. H. Schwuttke.*

When the device is placed at the proper angle in an X-ray beam to diffract wavelength λ, two beams, D_o^{I} and D_o^{II}, of the same intensity emerge from the far side of the crystal. The rays in these two beams are in phase with one another. The beams that are shaded in the figure are rediffracted by the second and third slabs as shown, with the result that the final beams D_o and D_h are formed by the recombination of two twice-diffracted beams. Ideally the phase relation is maintained throughout the sequence of diffraction events so that the rays in D_h^{I} and D_o^{II} recombine with the same phase relationship across the entire beam at the last slab, A, of the interferometer. However, if the phase in one leg is altered locally with respect to the other, inhomogeneous interference will occur, resulting in areas of varying intensity in beams D_o and D_h. The total intensity of either of these beams can be measured with a counter, or a photographic plate can be placed in D_o or D_h. The latter arrangement produces topographs which show variations of phase differences, therefore interference contrast effects from point to point within the beam. The device is extremely sensitive to slight differences in density of materials. For example a geiger counter can be made to fluctuate full scale by gently wafting air through the channels of the interferometer. Apparently the air density differences account for the wide swings of emitted beam intensity. Several geometrical variations of the original design have been proposed [*28*].

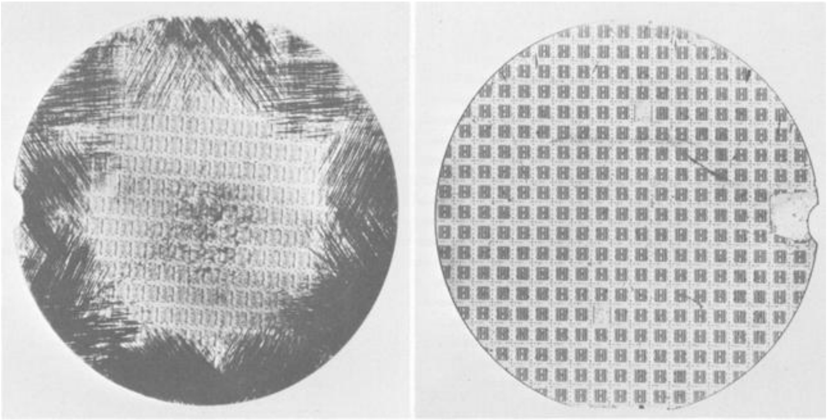

FIG. 13—*SOT topograph of a 6-in.-diameter integrated silicon device structure at the left shows crystal damage around the periphery of the 2-in. wafer. Better manufacturing control gives a wafer with minimal damage like the one shown on the right. Courtesy of G. H. Schwuttke.*

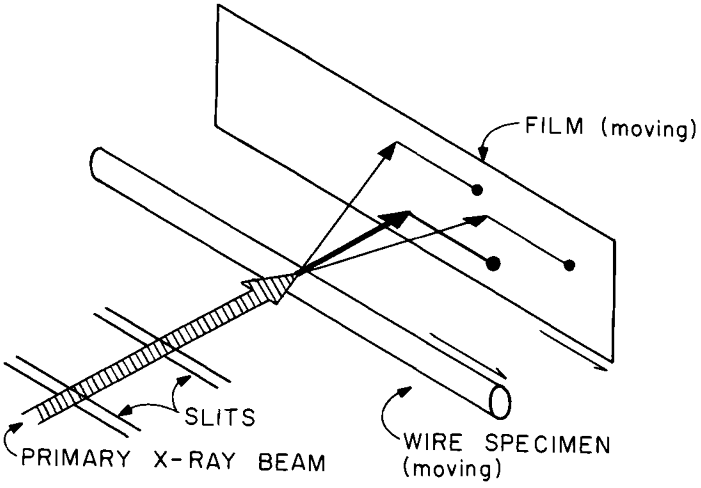

FIG. 14—*Arrangement for examining crystal perfection by Mateer's method. The heavy spots at the start of each streak are caused by stationary exposure at the initial position on the specimen* [27].

The X-ray interferometer is a very promising development with respect to useful applications, some of which are:

1. Precise measurement of the refractive index of substances for X-rays.
2. Precise measurements of thickness of small and complicated objects.
3. X-ray phase contrast topography, especially of biological materials.

4. Observation and measurement of extremely small lattice distortions.
5. Possible solution of phase angle problems in X-ray crystallography.

Diffraction Topography with a Television Pickup and Image System

One of the limitations of X-ray diffraction topography is the time required to make a photographic image and to process the image for visual display. Chikawa and Fujimoto [*29*] have shown that a television image system,

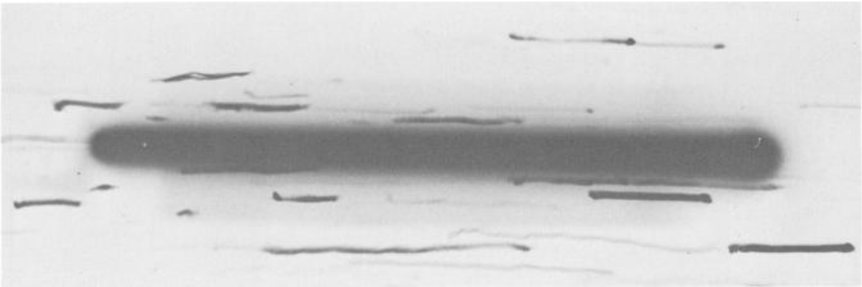

FIG. 15—*The waviness and nonuniform thickness of streaks indicate plastic deformation by bending and twisting. This Mateer-type photogram was made of an aluminum wire 2 mm in diameter* [27].

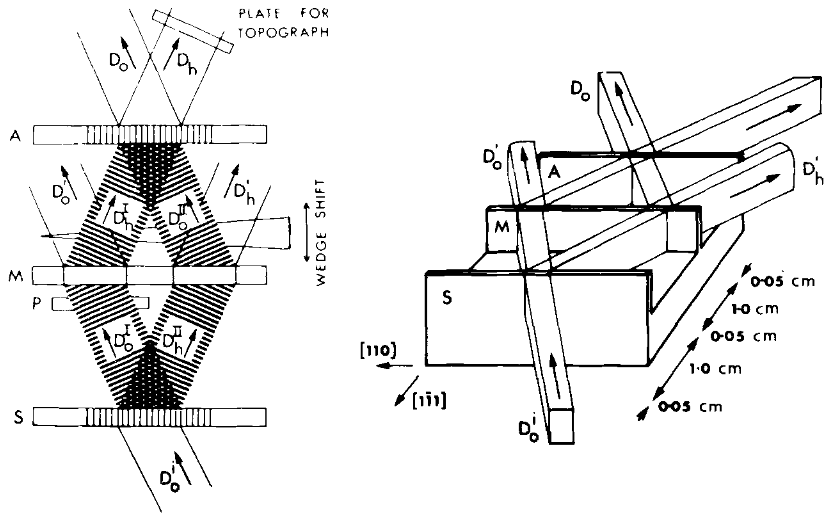

FIG. 16—*This basic design of the X-ray interferometer shows the beam splitters, the transmission mirror* M, *the analyzer crystal* A, *the beam paths, and approximate distances for an X-ray interferometer cut from a single crystal of silicon (for Cu K_α radiation)* [28].

using an X-ray-sensing vidicon tube, is suitable for rapid observations of strong topographic image detail. At present the resolution (about 30 μm) is inferior to that of the photographic method, and a high-intensity X-ray source (rotating target fine focus) is usually required. At the time of this writing, the maximum useful enlargement of the television readout image is about 25 times.

The foregoing remarks have touched upon only a small fraction of large numbers of papers on X-ray topography that have appeared in the past ten years. Much of the current work in this subject is published in the *Journal of Applied Physics*, *Acta Crystallographica*, the *Journal of the Physical Society of Japan*, and the *Philips Research Reports*. Also, there are several monographs where reviews as well as current work can be found [*30*].

Other X-ray Metallographic Methods

In this section several X-ray radiographic and diffraction metallographic methods are described. They are singled out from Table 1 partly because of their intrinsic interest and partly because of their recent arrival. Unlike some of the X-ray topographical methods just described, most of the following methods do not require any more complex equipment than the standard X-ray generator itself.

Micro and Macroradiography

In its simplest form a microradiograph, made either by contact or by projection [*32*],[3] is merely a photographically recorded shadowgraph of a wafer specimen. The wafer should be thin enough to (1) permit a reasonably short exposure and (2) contain an amount of detail sufficiently small to not confuse the image. The contrast from point to point in the image is given by the expression:

$$\text{Contrast} = \log (I_C/I_A) = (\mu_A - \mu_B)X$$

The meanings of the terms are given in Fig. 17.

If several X-ray tubes are available, each with a different target element, it is possible to make a qualitative analysis of microconstituents by a differential absorption method. An example of this technique is given in Fig. 18. The radiographic image of an inclusion stringer in a low-alloy steel is seen to be lighter than the background in the top radiograph, made with cobalt radiation, and darker than the background in the bottom radiograph, which was made with iron radiation.[4] Only manganese has an absorption edge

---

[3] An extensive bibliography, "Microradiography and Soft X-ray Radiography," has been prepared by the X-ray Division and Kodak Research Laboratories, Eastman Kodak Co., Rochester, N. Y. (1955).

[4] Private communication. I am indebted to H. J. Beattie, General Electric Co., for the use of Figs. 19*a* and 19*b*.

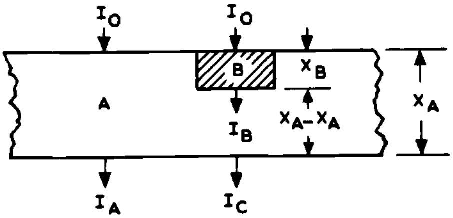

FIG. 17—*Intensity relationships: microradiography of inclusions* [31].

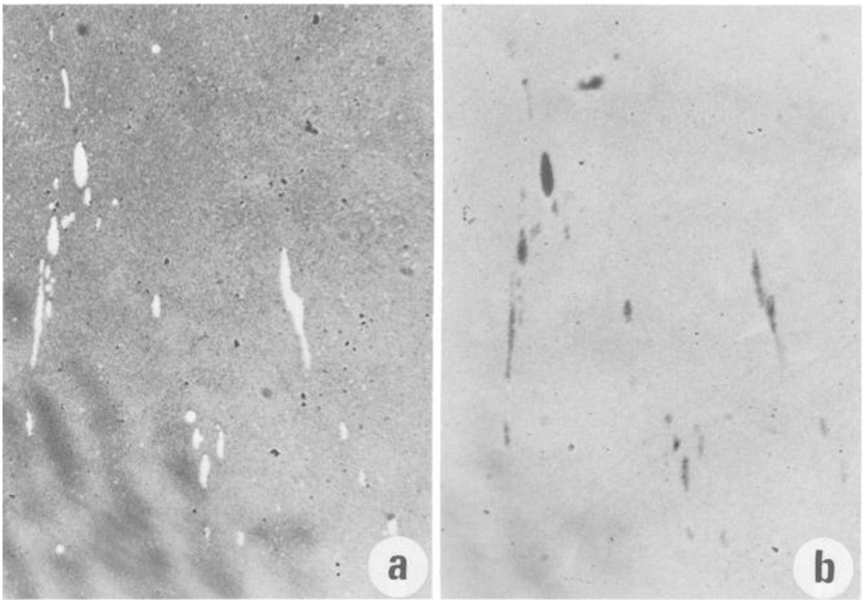

FIG. 18—*Microradiographs showing MnS inclusions in a 0.002-in.-thick sheet of low-alloy Ni-Cr-Mo-V steel:* (a) *cobalt K_α radiation;* (b) *same area as* a *but with iron K_α radiation*[4] *(×100).*

lying between the strong K_α emission wavelengths of Co and Fe (see Fig. 19). Therefore the inclusions must be rich in Mn, suggesting that they consist primarily of MnS. A comprehensive description of this method, with many illustrative examples, is given in Ref *31*. Absorption analysis of microconstituents can sometimes be supplemented by other methods of X-ray microanalysis. These methods are summarized and discussed in a recent review by Mertins [*32*].

A new dimension has been added to macroradiography with the development of ultrahigh-intensity, flash X radiation sources.[5] By means of a burst

---

[5] Information of flash X-ray radiography can be obtained from Field Emission Corp., Melrose Ave. at Linke St., McMinnville, Ore. 97128.

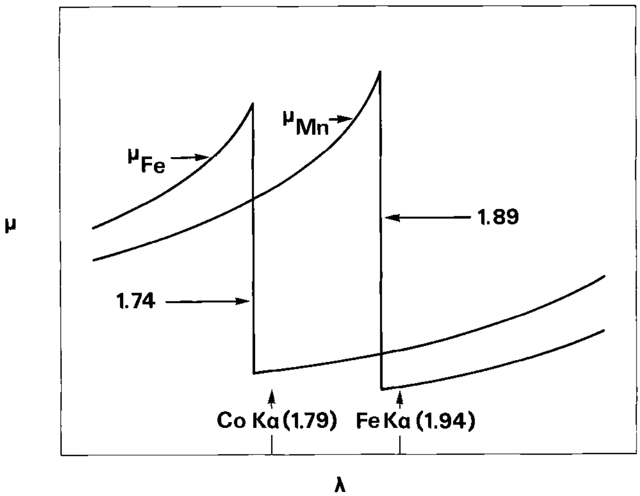

FIG. 19—*X-ray absorption curves for iron and for manganese. Note that the absorption edge for manganese lies between the K_α emission lines for cobalt and iron.*

of X-rays as short as 2 ns, it is said to be possible to record transient phenomena within thick casings. In this way it may be possible to monitor metal flow during casting, explosive welding, and other encased metallurgical processes.

Related to X-ray macroradiography, and complementing its capabilities, is a relatively new technique known as neutron radiography [*33*]. This testing method gives shadowgraphs which are much the same as X-ray radiographs in general appearance. However, neutrons are absorbed much more strongly by hydrogenous materials and by certain other light elements such as boron and lithium than they are by many dense elements which strongly absorb X-rays. Thus it is possible for a neutron beam to penetrate many dense metals and form a good radiographic image of rubber, plastics, and other hydrogen-containing objects even though they geometrically overlap much denser material. An example of this very useful method is given in Fig. 20. A newsletter devoted to neutron radiography is now available for persons who are actively working in that field.[6]

Temperature Gradient Debye-Scherrer Specimen

For metallographic applications where one is investigating a reaction that occurs over a range of temperatures, it is sometimes useful to examine specimens which have been heat-treated in a temperature gradient. After

---

[6] *Neutron Radiography Newsletter*, J. P. Barton and H. Berger, Eds., Argonne National Laboratory, Argonne, Ill. 60439.

the gradient treatment the specimen is quenched to room temperature, where Debye-Scherrer examination of the microstructure can be performed at various points along the specimen. The most convenient specimen for this method is a polycrystalline wire. Failing this possibility, the material may be packed in powdered form in a thin-walled quartz capillary tube which can then be held in the temperature gradient. In this way one can produce in a single specimen all the crystal structures that are associated with that composition over the range of temperatures covered by the gradient treatment. The method offers the further advantage that there are no gaps in temperature where one might miss an important phenomenon.

An example of the temperature gradient method for X-ray metallographic examination is given in Ref *34*. The purpose of the study was two-fold: (1) to locate, in copper-gold alloys near the composition CuAu, the narrow temperature range between the fields of long-range order and of disorder and (2) to establish whether the equilibrium through the transition range is a heterogeneous (two-phase) or a homogeneous (single-phase) one. A few wires of composition near CuAu were sealed in evacuated quartz tubes and

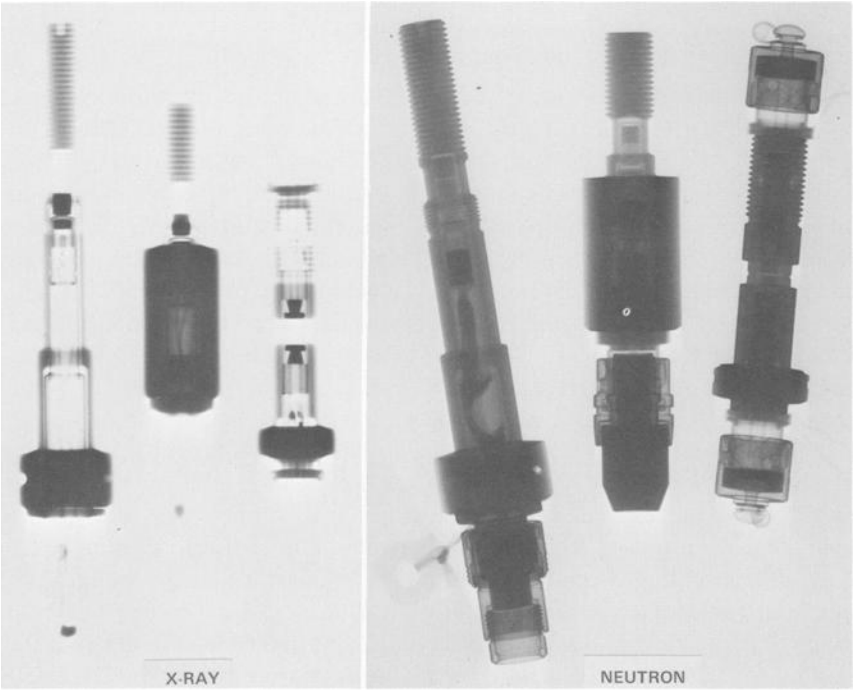

FIG. 20—*These two radiographs of explosive bolts show the metal parts in the X-ray radiograph and the plastic and explosive parts in the neutron radiograph.*

equilibrated in temperature gradients which spanned the temperature range of interest. After the equilibration treatment the wires were quenched to retain the high-temperature microstructure. Debye-Scherrer X-ray photographs were then made at room temperature at various places along the length of the wires (see Fig. 21). The transition temperature range was quickly found, since each point on the wire corresponded to a known treatment temperature. The Debye-Scherrer patterns given by the part of the wire lying within the transformation range clearly showed the ordered as well as the disordered phases, proving the heterogeneous nature of the equilibrium.

The temperature gradient method is especially useful for the determination of phase boundaries by the disappearing phase method [*35*]. In the study of the Cu-Au system just mentioned, the lines bounding the (order + disorder) field were located by establishing (through Vegard's law) the compositions of the conjugate phases through the temperature range of two-phase equilibrium (Fig. 22). Thus, the temperature gradient method, utilizing the Debye-Scherrer method for characterizing the phases present, is a useful X-ray metallographic tool for materials which can be formed to a wire or to a powder and which either retain their high-temperature structures on quenching or transform to recognizable room temperature products.

Strain Measurement in Multiphase Systems

Cuka [*36*] has shown that the usual X-ray methods for determining stresses in dispersed particles near the surface of a solid may lead to gross errors due to failure to take into account the nonuniformity of stress in the particles themselves. He demonstrates that, for a continuous matrix containing dispersed crystalline phases, the apparent measured strains in the dispersed particles may depend on the wavelength of the radiation used and on the size of the particles, even though the actual strains in particles below the penetration depth are not dependent on particle size. The apparent strains may differ by as much as three times the known strains in particles that are far removed from the surface. It is therefore necessary, when measuring nonuniform strains in a metal surface by an X-ray metallographic method, to take into account the wavelength and, for dispersed systems, the particle size effects. Cuka's method is based on a simple model system in which the discontinuous phase is assumed to be a random dispersion of equal spheres, simulated by a random placement of balls in a box. This model implies that there is less of the dispersed phase in the immediate neighborhood of the specimen surface than deeper in the body. Due to this matrix-particle interaction at the surface, one of the basic assumptions in the usual "two-exposure" method for strain measurement by X-ray diffraction is invalidated, especially if the particle size of the dispersed phase is small. The standard two-exposure method, otherwise known as the "normal-inclined beam" method, involves

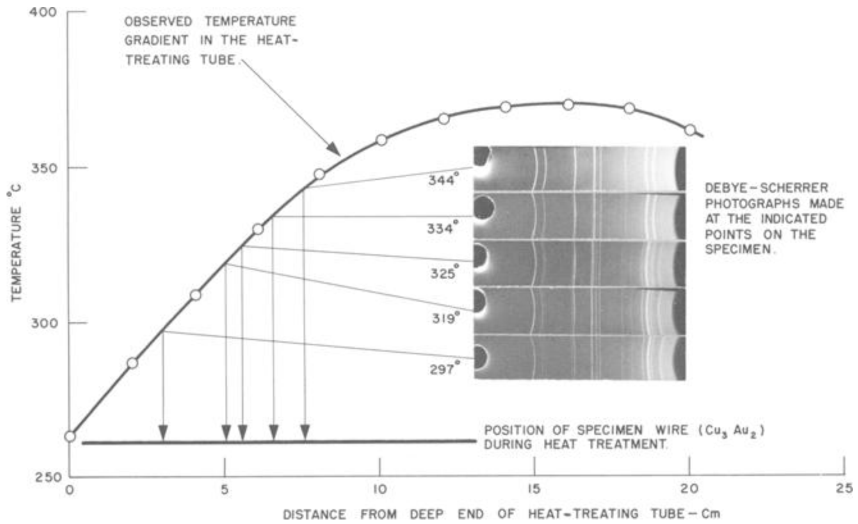

FIG. 21—*Composite diagram showing the location of the wire specimen in a temperature gradient and the Debye-Scherrer patterns corresponding to several places (temperatures) on the wire* [34].

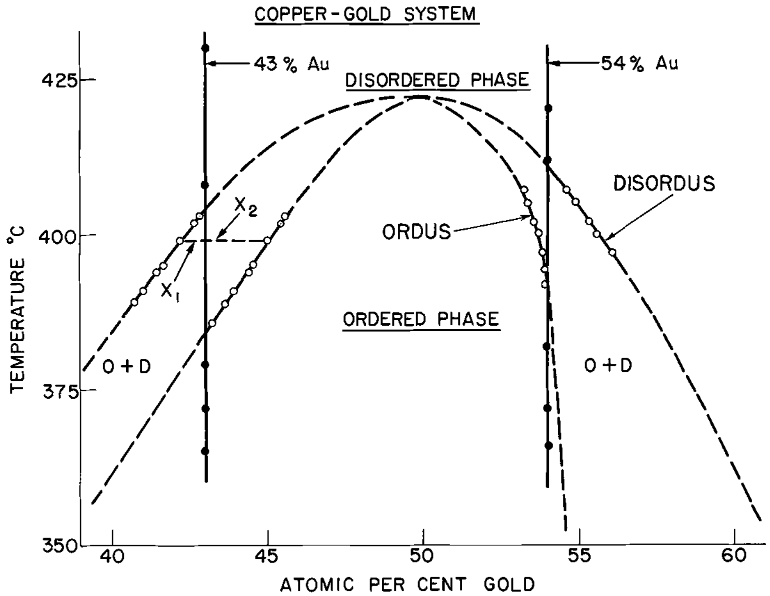

FIG. 22—*By means of Debye-Scherrer patterns made at various places along gradient-treated Cu-Au wires, the locations of the ordus and the disordus lines could be established* [34].

the assumption that the stress component in a direction perpendicular to the specimen surface is zero in the material exposed to the X-rays. Where finely dispersed phases are present, however, it must be assumed that some degree of mutual straining of the matrix and particles always occurs as a result of different thermal expansion, differential residual plastic effects, phase changes, precipitation stresses, and other causes. This mutual straining may have a significant component normal to the specimen surface and may occur well within the reach of the X-ray beam. One cannot, therefore, confidently assume that the stress observed by the X-rays is zero in the direction normal to the surface when dispersed phases are present.

Application of X-ray Analysis to Studies of Friction and Wear

Two solid surfaces sliding over each other make physical contact at relatively few places and over much less actual area than the apparent macroarea of contact. In some metals, particularly steels, it is thought that the wear which occurs as surfaces slide over one another can be directly related to the local oxidation which occurs at the asperities of contact while they are briefly heated by the sliding friction under load. Following a series of preliminary experiments, Quinn [37] reported a theory for the prediction of rate of wear in terms of (1) the thickness ξ of oxide film which forms locally during frictional heating and (2) the distance d along which real contact is made during sliding friction. He proposed that the wear debris contains oxide crystallites, the size of which could provide a minimum possible value for ξ, and that the crystallography of the worn remaining surface should provide some indication of the temperature to which it has been raised during the sliding process. Thus, by investigating the crystalline nature of the worn surfaces and of the wear debris, it is possible to get independent checks on the oxidational wear hypothesis. The X-ray data were obtained by standard Debye-Scherrer methods. Quinn found that at low sliding speeds (a rounded steel pin sliding on a steel plate) large amounts of α-Fe or α-Fe_2O_3 or both were formed, whereas at high speeds large amounts of α-Fe_2O_3 or FeO or both were formed. Comparison of these results with wear rates and frictional drag demonstrated that high wear rates and high frictional force are associated with large amounts of α-Fe or α-Fe_2O_3 or both in the wear debris. The data appear to be reproducible and show the value of standard X-ray diffraction methods in the study of friction and wear.

The Kossel Technique

This method has been receiving considerable attention during the past few years for precise orientation of single crystals and as a simple means for determining lattice parameters in single-crystal specimens with relatively good precision. Also, some idea of the crystalline perfection can be deduced from the Kossel pattern. To make a Kossel pattern a sharply divergent beam of characteristic X-rays is needed whose apex, ideally, is just at the surface of the thin single-crystal specimen. The most satisfactory way to produce the required divergent conditions is to direct a fine beam of electrons onto the specimen surface, as in electron probe microanalysis. The X-rays which are generated spread in all directions. It is also possible to produce a strongly divergent X-ray beam by secondary radiation within the specimen or by means of an auxiliary fluorescent radiator placed in direct contact with it [*38*]. The strong characteristic X-rays which penetrate the specimen participate in forming the Kossel pattern. Whenever rays in the divergent beam fall upon a family of crystallographic planes at the Bragg angle, diffraction occurs, producing a cone of diffracted X-rays. The cone of diffraction is recorded on a photographic film, with varying geometry, placement, and intensity as shown in Fig. 23. Standard methods have been worked out for analyzing Kossel patterns [*39*]. If the crystal structure is known, it is usually a straightforward matter to identify the conic section traces in terms of the Miller indexes on the planes causing them. One can then deduce the orientation of the specimen crystal with respect to the film. The optimum thickness of

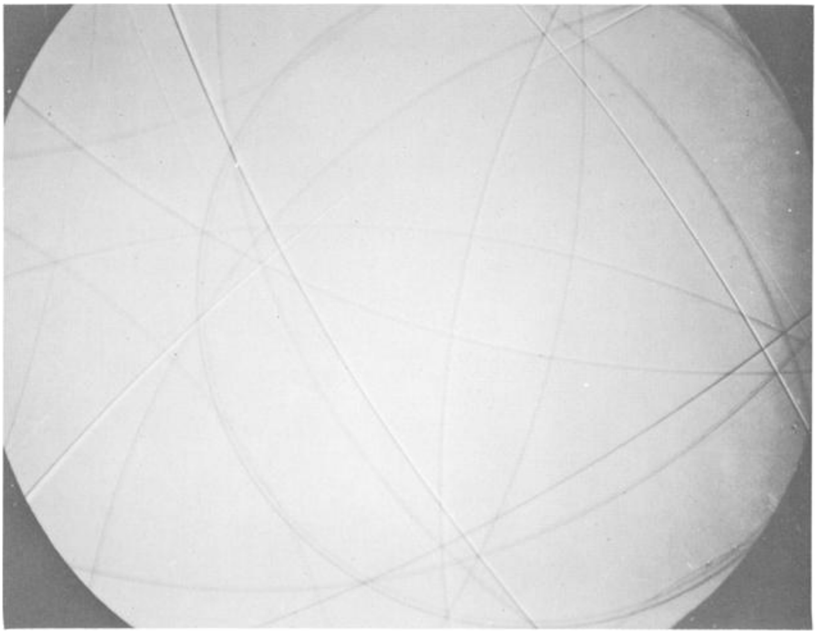

FIG. 23—*Kossel pattern of a cubic crystal with a* ⟨*100*⟩ *direction within a few degrees of the camera axis.*

specimen has been shown to be $1/0.2L$, where L is the linear absorption coefficient. Specimens thinner than this do not diffract efficiently, whereas thicker specimens absorb so strongly that the required exposure time becomes too long.

It has been shown [*40*] that the angular distance between certain points where the arcs intersect is a very sensitive measure of the lattice parameter. It is a favorable characteristic of the method that a precise knowledge of the specimen-to-film distance is not needed because the pattern contains self-calibrating features. For example, the angular relations between the conics corresponding to the K_α and K_β radiations are known purely from the geometry of the diffraction restrictions; therefore, their traces can be used for a precise standardization of each film. It has been stated that under controlled conditions the lattice parameter can be determined to a precision of 1 in 400,000. This level of precision, together with the fact that the pattern originates from a point on the specimen as small as a few micrometers, makes the method useful for measuring composition gradients (via Vegard's law) across dendrites on a microscopic scale.

The Kossel pattern is of course directly related to the crystallographic orientation of the specimen crystal. It therefore provides a direct and convenient method by which to determine (1) the orientations of adjoining crystallites in a polycrystalline aggregate, (2) the twin matrix orientation relationship, and (3) the relative orientations of conjugate phases in a polyphase alloy. One simply brings the required area of the thin specimen under the excitation beam and observes the transmission Kossel pattern recorded on a standard X-ray photographic film. Some of the commercial electron probe microanalyzers are designed to permit convenient Kossel photography in the electron probe instrument.

Metallurgical Application of Long Wavelength Analysis

Perhaps distantly related to metallography in its usual sense is the subject of atomic bonding in metals and alloys. The effects of bonding on soft, that is long wavelength, X-ray emission spectra have been observed for many years. However, only recently have systematic studies of these effects been made.[7] The effects can be classified as follows: (1) changes in relative intensities of the various emission lines, (2) gross changes in line shape, (3) significant shifts in the position of the wavelength maxima, and (4) the appearance or disappearance of satellite lines. The basic causes of spectral alterations are changes in electron distribution around the atoms and the amount of ionic character of the bond. Since the elements comprising an insulating compound undergo a greater change in electron distribution with chemical

---

[7] Holliday, J. E., "Chemical Bonding and Valance State—Conducting Materials," invited lecture at the 18th Annual Conference on Applications of X-ray Analysis, Denver, Colo., 1969.

combination than do elements making up an alloy or a conducting compound, soft X-ray emission spectra from insulators show a greater change relative to the pure elements than do spectra from conductors. However, it has been found that there can also be large changes in the soft X-ray emission spectra given by alloys and conducting compounds. The general rule is that, the greater the electronegative difference between the combining elements, the greater is the change in the soft X-ray emission band when the alloy or compound is formed. There is no doubt that future application of recently developed techniques and instruments relating to long wavelength X-ray analysis will greatly extend our understanding of bonding and valence and that this knowledge will expand our understanding of metallurgical processes. The subject of *Long wavelength X-ray analysis* was emphasized at the annual Denver X-ray Conference for 1969, the proceedings of which will soon be published [*41*].

Summary

Because of space restrictions it has been necessary to omit many important subjects within the field of X-ray metallography. It is clear that this branch of metallurgy is still growing actively, challenging the most competent, yet providing useful information to novice, metallographers. Now, modern metallographic laboratories include the classical X-ray methods as routine services. The more specialized techniques, some of which are described here, are finding increasing applications as new materials are put to practical use.

References

[*1*] Barrett, C. S. and Massalski, T. B., *Structure of Metals*, 3rd ed., McGraw-Hill, New York, 1966.

[*2*] Cullity, B. D., *Elements of X-ray Diffraction*, Addison-Wesley, Reading, Mass, 1956.

[*3*] Taylor, A., *X-ray Metallography*, John Wiley and Sons, New York, 1961.

[*4*] *Advances in X-ray Analysis*, AXRAA, Vol. 12, 1968.

[*5*] Bonse, U. K., Hart, M. and Newkirk, J. B., *Advances in X-ray Analysis*, AXRAA, Vol. 10, 1966, pp. 1–8.

[*6*] Azaroff, L. V., *Progress in Solid State Chemistry*, PSSTA, Vol. 1, 1964, pp. 347–379.

[*7*] Weissmann, S. in *Fifty Years of Progress in Metallographic Techniques*, *ASTM STP 430*, American Society for Testing and Materials, p. 142.

[*8*] Nakayama, Y., Weissmann, S. and Imura, T. in *Direct Observation of Imperfections in Crystals*, J. B. Newkirk and J. H. Wernick, Eds., John Wiley and Sons, N. Y., 1962, pp. 573–592.

[*9*] Young, F. W., Jr., and Sherrill, F. A., *Canadian Journal of Physics*, CJPHA, Vol. 45, 1967, pp. 757–763.

[*10*] Meieran, E. S., "The Application of X-ray Topographical Techniques to the Study of Semiconductor Crystals and Devices," submitted for publication in *Siemens Review*, SZTEA, 1969.

[*11*] Howard, J. K. and Schwuttke, G. H., *Advances in X-ray Analysis*, AXRAA, Vol. 10, 1966, pp. 118–133.

[*12*] Walford, L. K. and Carron, G. J., *Journal of Applied Physics*, JAPIA, Vol. 39, 1968, pp. 5802–5804.

[*13*] Austerman, S. B., Newkirk, J. B. and Smith, D. K., *Journal of Applied Physics*, JAPIA, Vol. 36, No. 12, Dec. 1965, pp. 3815–3822.

[*14*] Wagner, C. E. and Young, R. A., "X-ray Topographic Description of Mode in a Vibrating Crystal," to be published in *Journal of Applied Crystallography*, 1969.

[*15*] Spencer, W. J., *Journal of the Acoustical Society of America*, JASMA, Vol. 41, No. 4 (Part 2), April 1967, pp. 994–1001.

[*16*] Azaroff, L. V. in *Crystallography and Crystal Perfection*, Academic Press, London, pp. 109–124.

[*17*] Penning, P., *Advances in X-ray Analysis*, AXRAA, Vol. 10, 1966, pp. 67–79.

[*18*] Kato, N. in *Crystallography and Crystal Perfection*, Academic Press, London, pp. 153–173.

[*19*] Chikawa, J. and Newkirk, J. B. in *Trace Characterization, Chemical and Physical*, National Bureau of Standards Monograph 100, Meinke and Scribner, Eds., April 1967, pp. 165–202.

[*20*] Lang, A. R., *Nature*, NATUA, Vol. 220, No. 5168, 16 Nov. 1968, pp. 652–657.

[*21*] Bonse, J. and Hart, M., *Zeitschrift fuer Physik*, ZEPYA, Vol. 190, 1966, pp. 455–467.

[*22*] *a*. Hattori, H., Kuriyama, H., Katagawa, T. and Kato, N., *Journal of the Physical Society of Japan*, Vol. 20, No. 6, June 1965, pp. 988–996.
b. Shetty, N. N., Taylor, J. B. and Calvert, L. D., *Review of Scientific Instruments*, RSINA, Vol. 36, 1965, pp. 1888–1890.

[*23*] Armstrong, R. W. and Schultz, J. M., *Surface Science*, SUSCA, Vol. 12, 1968, pp. 19–26.

[*24*] Dionne, G., *Journal of Applied Physics*, JAPIA, Vol. 38, No. 10, 1967, pp. 4094(c)–4096.

[*25*] Yoshimatsu, M., Shibato, A. and Kohra, K., *Advances in X-ray Analysis*, AXRAA, Vol. 9, 1966, pp. 14–22.

[*26*] Schwuttke, G. H., *Journal of Applied Physics*, JAPIA, Vol. 36, 1965, pp. 2712ff.

[*27*] Mateer, R. S., *Transactions*, American Society for Metals, TASEA, Vol. 62, 1969, pp. 293–297.

[*28*] Bonse, U. and Hart, M., *Acta Crystallographica*, ACCRA, Vol. A24, 1968, pp. 240–245.

[*29*] Chikawa, J. and Fujimoto, I., *Applied Physics Letters*, APPLA, Vol. 13, No. 11, Dec. 1968, pp. 387–389.

[*30*] *a*. *The Direct Observation of Imperfections in Crystals*, J. B. Newkirk and J. H. Wernick, Eds., John Wiley and Sons, 1962.
b. *Direct Observation of Dislocations*, Amelinckx, Ed., Academic Press, 1964.
c. *Advances in X-ray Analysis*, AXRAA, Vol. 10, 1966.
d. Bonse, U. K., Hart, M. and Newkirk, J. B. in *Encyclopaedic Dictionary of Physics*, Pergamon Press, New York.

[*31*] Bertin, E. P. and Longobucco, R. J., *Scientific Instruments News*, SINSA, Vol. 6, No. 1, 1961, pp. 1–13.

[*32*] Mertins, K., *Practische Metallographie*, PMTLA, Vol. 5, 1968, pp. 669–685.

[*33*] Berger, H., *Neutron Radiography, Methods, Capabilities and Applications*, Elsevier Publishing Co., Amsterdam, Netherlands, p. 175.

[*34*] Newkirk, J. B., *Review of Scientific Instruments*, RSINA, Vol. 24, No. 12, 1953, pp. 1116–1121.

[*35*] Barrett, C. S. and Massalski, T. B., *Structure of Metals*, 3rd ed., McGraw-Hill, New York, 1966, p. 160.

[*36*] Cuka, P., *Journal of Applied Physics*, JAPIA, Vol. 38, 1967, pp. 3959–3964.

[*37*] Quin, T. F. J., *Advances in X-ray Analysis*, AXRAA, Vol. 10, 1966, pp. 311–327.

[*38*] Geisler, A. H., Hill, J. K. and Newkirk, J. B., *The Physical Review*, PHRVA, Vol. 72, No. 10, 1947, pp. 983–984.

[*39*] Frazer, J. and Arrhenius, G. in *Optique des Rayons X et Microanalyse* (in English), R. Castaing et al, Eds., Editions Scientifiques Hermann, Paris, 1966, p. 16.

[*40*] Gielen, P., Yakowitz, H., Ganow, D. and Ogilvie, R. E., *Journal of Applied Physics*, JAPIA, Vol. 36, No. 3 (Part 1), 1965, pp. 773–782.

[*41*] "Proceedings of the 18th Annual Conference on Applications of X-ray Analysis," Denver, Colo., 1969, *Advances in X-ray Analysis*, AXRAA, B. Henke, G. R. Mallett, and J. B. Newkirk, Eds., Vol. 13, 1970.

Erwin Eichen,[1] *Frank Kunz*,[1] *and Jack Tabock*[1]

The Electron Microprobe Analyzer as a Research Instrument

REFERENCE: Eichen, Erwin, Kunz, Frank and Tabock, Jack, "**The Electron Microprobe Analyzer as a Research Instrument,**" *Applications of Modern Metallographic Techniques, ASTM STP 480*, American Society for Testing and Materials, 1970, pp. 183–213.

ABSTRACT: The use of an electron microprobe as a research tool will be considered. The theory of operation of this instrument will be briefly discussed. The different possible modes of data presentation will be given. These will include graphical representation on a recorder, video representation of scanned area using backscattered electrons, absorbed electrons, and X-rays, and the accumulation of quantitative data on scalers. Qualitative, semiquantitative, and quantitative analysis will be included in the discussion. Also included will be the importance of specimen preparation in microprobe analysis, and a number of different examples for various types of specimens will be given. These will include such materials as metals, glasses, ceramics, and semiconductors. Consideration will be given to the analysis of thin films as well as bulk materials. Some of the problems encountered in the analysis of thin films will be discussed as well as ways of circumventing these problems. Examples will be given to illustrate the type of problems and the means of approach in cases where qualitative analysis, semiquantitative analysis, and quantitative analysis are desired. In the latter case, the different types of corrective procedures which can be used will be discussed. These include correction for absorption, fluorescence, and atomic number.

KEY WORDS: electron beams, electron probes, metallography, X-ray analysis, evaluation

The electron microprobe X-ray analyzer was first developed as a practical research tool in the early fifties by Castaing [*1*].[2] Since that time much research has been done on this instrument both to gain an understanding of the technique itself and to extend the methods to cover a broader spectral range and a much wider capability of performance. The microprobe has been the subject of a number of previous ASTM symposia and meetings [*2*–*7*] as well as numerous articles on both techniques and applications. Heinrich [*8*] has

---

[1] Scientific research staff, Electron and X-ray Optics Section, Ford Motor Co., Dearborn, Mich. 48121.

[2] Italic numbers in brackets refer to the list of references at the end of this paper.

prepared a comprehensive bibliography which can be referred to by those who wish to gain additional knowledge in this field.

The purpose of the present paper is not to reiterate the work reported during past symposia but to discuss the more practical aspects of microprobe analysis, such as specimen preparation of different materials, different means of data presentation, and the means for doing qualitative, semiquantitative, and quantitative analysis. The emphasis will be placed on the use of the microprobe as a metallographic research tool.

Theory of Operation

The electron microprobe analyzer theory of operation is shown schematically in Fig. 1. An electron optical lens system produces an electron beam which is capable of being focused to a point 1000 to 3000 Å in diameter. The impinging of the beam on a specimen will cause bound electrons to be ejected from the atoms and subsequent generation of characteristic X-rays. The X-rays are made to impinge on a crystal grating of known *d* (lattice) spacing and will be diffracted from the crystal in accordance with Bragg's law.

The X-rays are detected generally by use of a proportional counter, either of the flow or sealed type. The specimen, crystal, and detector are placed so that they are on the circumference of the Rowland circle; the crystal and detector can be moved in relation to the specimen so that X-rays of different wavelengths can be detected; and the total system can be calibrated so that the wavelength of the X-rays being detected can be determined. Since every atom produces a unique characteristic X-ray, determining the wavelength of

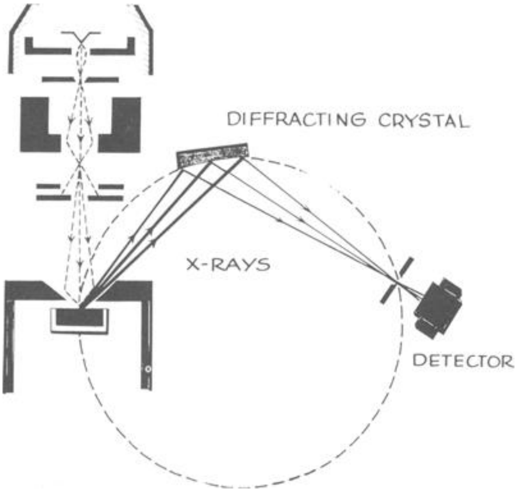

FIG. 1—*Schematic representation of the operation of an electron microprobe analyzer.*

the X-rays unequivocally identifies the atoms present in the specimen. The number of X-ray photons produced at a given wavelength is related to the number of atoms present in the specimen. It will be seen in a later section on corrective procedures that the way in which the number of photons produced and measured is related to the composition can be very complex. This complexity will depend largely on the specific elements present in the specimens. The range of elements which can be identified with this technique is determined by the geometry of the instrument and the *d* spacing of the diffracting crystal. Most instruments can detect all elements from boron on up, while a few can also detect beryllium.

Even though the diameter of the electron beam used in the microprobe is usually in the order of a quarter of a micrometer, the area from which X-rays are produced is much larger; it is usually taken to be from 1 to 2 μm. This results from the fact that X-rays produced in the specimen will be emitted in all directions and an X-ray photon generated by an electron at the periphery of the beam can emerge from the surface of the specimen at some distance outside of the beam. Also, we have the so-called electron diffusion or scattering effects [9]. The depth of electron penetration in a specimen depends on the accelerating voltage applied to the electron beam and the density of specimen. Electrons accelerated at 25 kV into a specimen such as iron will penetrate about 2 μm.

Modern electron microprobes have the means for moving the incident electron beam before it impinges on the specimen in both the x and y directions either by electrostatic or by electromagnetic means. The purpose for being able to accomplish this will become evident in the next section when the different modes of data presentation are discussed.

Modes of Data Presentation

The first item that must be considered under data presentation is the type of data which is available for evaluation. When a beam of electrons strikes a target (in this case the specimen) a number of things may occur. Some of the electrons from the beam will be reflected or backscattered from the target. While these electrons have a spectrum of energies, their energies will be close to that of the incident electron beam. The electrons which are not backscattered will be absorbed by the specimen. These are the electrons which produce X-ray photons by interacting with the atoms present in the specimen. These interactions also yield secondary electrons with energies less than 50 eV.

Therefore, four possible kinds of information are obtainable from a material which is being bombarded by a beam of electrons. Of these means, direct compositional information can only be obtained from the X-ray photons. Backscattered electrons, absorbed electrons (usually called sample current), and secondary electrons can only be used directly to form a video picture on a cathode-ray tube by scanning an area in both the x and y directions. This picture can be extremely useful, since it gives a metallographic-type picture of the area being analyzed.

There are a number of different ways to describe the type of analysis which can be performed with a microprobe. For example, it is possible to talk in terms of whether an analysis is qualitative, semiquantitative, or quantitative or whether it is desirable to have a point analysis (an analysis at a single point), an analysis along a line, or an area analysis. Both of these classification systems will to a large extent determine the mode of data presentation used. The manner in which this is determined will be discussed in later sections of this paper.

There are essentially three ways in which data may be handled with the equipment. The first may be termed a counting technique. In this case any X-ray entering the detector is converted into an energy pulse. It is in turn amplified, passed through a pulse height analyzer, and stored in a scaling unit. Data are usually accumulated by counting X-ray photons for a fixed length of time or by determining the length of time necessary to accumulate a fixed number of counts. This technique is generally used when quantitative or semiquantitative results are required.

The second method involves the use of a strip chart or x-y recorder. In this case the intensity of X radiation is plotted against a second parameter. For example, to determine the elements present in a specimen at a fixed point, one spectrometer would be varied while recording X-ray intensity as a function of spectrometer position (wavelength). From this plot it would be possible to determine the wavelength of all X-rays present and in that manner identify all of the elements present. Another way of using this technique is for the determination of how the quantity of a single element varies with distance across the specimen. This would be achieved by plotting the X-ray intensity from a spectrometer adjusted to the wavelength of the element desired versus the specimen position. The latter can be varied mechanically by driving the specimen stage under a fixed electron beam position at a constant rate or by electronically sweeping the electron beam across the specimen. The specific procedure chosen is usually determined by the experimental variables, such as length of traverse required, or the need for extreme accuracy in traversing a portion of the specimen. This technique is restricted for use with semiquantitative or qualitative analysis.

The third means for data presentation involves an area scan which yields a video- or metallographic-type representation. This is accomplished by scanning an area of the specimen with the beam deflection system available on the microprobe and simultaneously synchronizing the deflection of the beam in a cathode-ray tube so there is a point to point correlation of the microprobe electron beam on the specimen and the cathode-ray beam on the face of the tube. Most generally pictures can be obtained using X-ray information, backscattered electrons, absorbed electrons, and secondary electrons as long as suitable systems are available in the microprobe for their detection and amplification. The pictures are produced by supplying information at every point in the scan as to the number of X-rays of electrons present and applying this information to the *z* axis, or beam intensity control, of the cathode-ray tube. At a point where there is a large number of X-rays or electrons the intensity of the cathode-ray tube is high, and where the number is low the intensity is low. In this manner it is possible to build a point-by-point scanned picture whose brightness at any point is directly proportional to the number of X-rays or electrons present at that point. It can be seen, therefore, that besides the metallographic or positional information which can be obtained from these pictures, qualitative compositional information can also be directly obtained. In the case of the electron pictures additional electronic processing of the signals is possible, for example, it is possible to obtain negative pictures (ones in which the intensity of the cathode-ray tube is inversely proportional to the number of electrons present at that point). This procedure can be useful in studying phases where the compositional variation is not very great and contrast between the phases is minimal. By going to a negative image it is sometimes possible to markedly increase the contrast between the phases.

Special Types of Data Presentation

While we have already considered the usual means for handling and presenting data with an electron microprobe, a number of specialized methods have been developed which extend the usefulness of the technique. These methods generally require additional equipment and only satisfy very specific needs.

The first technique to be considered is used primarily with backscattered electron presentations to differentiate as to whether contrast information represents compositional or topological effects. In cases where there is surface relief on the specimen it is not possible to tell unequivocally whether a change in electron intensity is due to a change of composition or a change in surface elevation. The technique requires the use of two detectors placed 180 deg from each other in proximity to the cone. The signals from these detectors can be used either individually or together. When used together the signals can be added or subtracted. When the backscattered electron picture of the analyzed specimen contains contrast effects due to compositional differences, adding the signals from the two detectors will enhance these contrast effects while subtraction of the signals will minimize or eliminate these effects entirely. When the contrast is the result of topographical relief, the subtraction of signals from the two detectors will enhance contrast while the addition of signals will cause the contrast to be minimized.

Another type of presentation was developed by Heinrich and his co-workers [*10*] to allow a concentration map for one or more elements to be determined for a specimen. It is based on a matrix generator, which can position the beam on the specimen at any point in a n by n matrix (where n can be as large as 100). At each point a small area is scanned and the average composition of one or more elements is obtained. The composition of the total matrix can be plotted and the elemental distribution of the entire area can be obtained. Isoconcentration lines for the area can be formed by joining points of the same composition.

A useful method for presenting information on how more than one element varies in an area was developed by Yakowitz and Heinrich [*11*]. Their method involves taking the usual X-ray scanning Polaroid photographs for three elements. Each element is then assigned a color and all three black-and-white photographs are retaken on a single sheet of color Polaroid film. Before each exposure the proper color filter is placed over the lens of the copying camera so that only that color which represents the specific element will be exposed to light. After the three exposures the film is processed in the normal manner. The color print will thus represent the distribution of the three elements in the area photographed. Different mixtures of the primary colors, representing different amounts of elements present, will be readily discernible in the print. The most important factor in this technique is the necessity for achieving perfect registry when rephotographing each picture. This can be achieved by constructing a jig to hold each print in the exact same position.

Another technique that holds much promise in microprobe analysis is the so-called nondispersive detection, or energy analysis, of X-rays reported on by Fitzgerald et al [*12*]. Here, instead of identifying the X-rays by diffracting them with a crystal of known interatomic spacing and determining their wavelength from the diffracting angle, the energy of the X-ray is determined directly and the X-ray identified by its energy. Such a system consists of a detector, a means of amplifying the pulses from the detector, an energy analyzer, and a means of storing and recording the number of pulses of each energy. One such type of system is shown in Fig. 2. It includes a solid state crystal detector (lithium-drifted silicon) which must be liquid nitrogen cooled, a field-effect transistor preamplifier (which also must be cooled), a linear amplifier, a multichannel analyzer to determine the energy of the pulses and to store the pulses according to their energy, and a readout system. In this type of system all X-rays regardless of energy are analyzed at the same time. A total analysis can be completed in a very short time, usually in a matter of minutes. At present only qualitative analysis can be done. Because of some practical limitations imposed by the experimental setup (including resolution limitations of the detector), there is a low energy limit below which it is not possible to detect or analyze the X-rays. At present this lower limit is in the

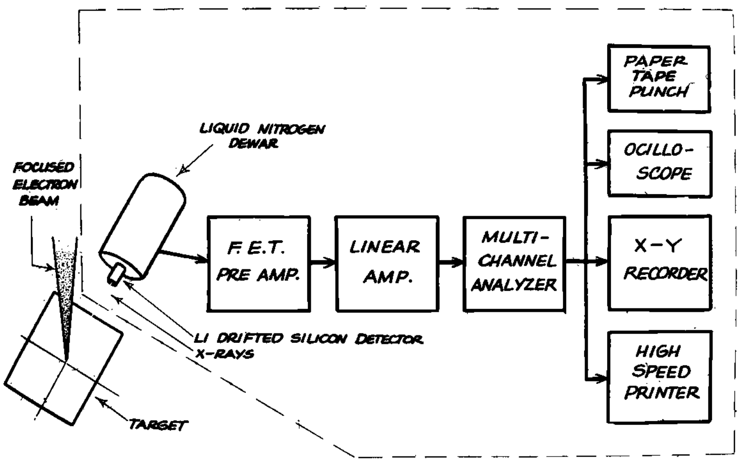

FIG. 2—*Schematic representation of a nondispersive X-ray detection system.*

vicinity of the energy represented by magnesium characteristic X radiation; the exact lower limit will vary from system to system. This method of analysis is being used as a very quick means for qualitatively determining what elements (above the low energy limit) are present in the specimen. Much work is now being done to determine the extent to which this form of analysis can be made quantitative.

The above techniques represent only some of the special techniques which are at present available and were chosen primarily as examples of what can be done and, in some cases, because of the metallographic type of information that they provide.

Classification of Analysis

The types of analysis which can be done with a microprobe can be classified in a number of different ways. One of the most common ways of classification is in terms of whether the analysis is qualitative, semiquantitative, or quantitative. Let us now consider what is required both in terms of data and procedure to accomplish each one of these types of analysis. Examples of various types of analysis will be given in a later section of this paper.

Qualitative Analysis

The most simple type of analysis to perform is of course the qualitative analysis, where all that is necessary is the establishment of the presence of an element by determination of the wavelengths of the X-rays being detected. After determining the wavelength, care must be taken to insure that the number of X-rays above background are statistically significant. One use for this form of analysis is the identification of inclusions or foreign particles in a known matrix. Usually the size and shape of the inclusion can be obtained and documented by taking an X-ray scanning micrograph. It should be remembered, however, that there is a finite lower limit to the size of inclusion that can be identified. A practical method for calculating this lower limit for various accelerating voltages and different elements is given by Reed [*9*]. Castaing [*13*] also offers a method for calculating the X-ray spread which exceeds the electron beam diameter from a few tenths of to several micrometers.

Semiquantitative Analysis

Semiquantitative analysis will provide an approximate evaluation of the amount of an element which is present, to arrive at which the following procedure should be followed. The presence of an element in the specimen should be established as in the case of the qualitative analysis. The number of X-rays generated under a given set of conditions (such as the accelerating voltage of the electron beam, the beam diameter, and the beam current) should be determined for the specimen. Under the same conditions, the number of X-rays generated from a standard which contains a known amount of the element being analyzed is determined. After correcting both of these values for background and instrumental errors such as dead time (the time when an X-ray entering the detector will not be counted) and beam drift (the change in beam current during the analysis), the ratio of the specimen's to the standard's X-ray intensity is calculated. To a first approximation this simple, uncorrected probe ratio may be considered to be a semiquantitative analysis. Its actual accuracy varies widely depending on the elements present in the specimen being analyzed. Under the best circumstances it could be as close as 10 percent of the amount present, while in other cases it could be in error by as much as 100 percent.

In regard to the use of standards a number of comments should be made. For most work (at least for metallurgical and physics applications) the pure elements are usually most desirable for standards. In cases where this is not possible (where the element is a liquid or a gas or not conveniently obtainable) a stoichiometric compound can be used. If neither of the above are available, a homogeneous, single-phase, well-analyzed nonstoichiometric compound or an alloy can be used. In geological or biological applications it is generally preferable to use pure compounds of the type being analyzed, for example, an oxide, sulfide, carbonate, or phosphate.

Quantitative Analysis

For quantitative analysis there are two techniques for converting X-ray intensity data into actual concentration. The first is an empirical approach which uses the direct conversion of intensity into concentration, and the second involves the use of a correction procedure which converts the measured X-ray intensities into true intensities. The true intensities derived from the elements present in the specimen (unknown concentration) are then compared to the true intensities obtained on standards of known elemental concentrations, and a concentration of the element in the specimen can be calculated. In practice both of the steps involved in the second method are combined into one step, since the probe ratio (defined above in the section on Semiquantitative Analysis) is first calculated and the correction procedure is applied to this ratio.

The empirical method used in the direct determination of concentration is an old technique which is still used in X-ray fluorescence analysis. It is a simple procedure and yet it can be a most accurate method for converting X-ray intensities into concentrations. The technique requires the use of calibration curves, which are obtained by plotting X-ray intensity versus concentration for a number of well-analyzed (by other analytical techniques), homogeneous (on a microscale) standards. The intensity of the unknown can then be referred to the calibration curve and the concentration determined directly from this curve. This technique is especially useful for dilute solutions (since they are easily made homogeneous) of alloys which require frequent analysis. Carbon analysis in steel is routinely performed in this manner. There are a number of drawbacks, however, to this approach to quantitative analysis. In the first place, a laboratory which has very diverse analytical problems would require a very large number of standards to meet its requirements. The costs in both time and money to build a library of standards would probably be prohibitive. Every time a new type of specimen was received the length of time necessary to make and check standards would mean a large delay in obtaining an analysis. Finally, the difficulty and sometimes the impossibility of preparing suitable and homogeneous standards, especially in multiphase alloys and nonmetallic systems, would preclude the use of this technique.

The use of a correction procedure to obtain quantitative analysis with a microprobe was first elucidated by Castaing [*1*]. The technique is based on the principles of X-ray generation and the behavior of electrons in solids. These principles will not be covered here since they are comprehensively discussed elsewhere [*1*, *14*, *15*]. The greatest advantage of this technique is that a single standard, usually the pure element, is needed for the analysis. In essence, as has been previously mentioned, the problem is initially approached in exactly the same manner as the semiquantitative analysis, by the determination of a probe ratio. The corrections are then applied to this probe ratio. Assuming the determination of a good probe ratio, the accuracy of the analysis will be determined by the validity of the applied corrections.

The usual means for arriving at a quantitative value for the analysis of one or more elements in a specimen is to apply to the probe ratio a secondary fluorescence, an absorption, and an atomic number correction. Depending on the elements present in the specimen, one or more of the corrections may not be needed.

Secondary fluorescence arises from two sources, the characteristic line radiation and the continuous spectrum. When it is present, fluorescence has the effect of increasing the X-ray intensities measured, since additional X-rays are generated. Therefore, the correction must have the effect of reducing the intensity of the measured radiation by the increased amount. Generally the fluorescence due to the continuous radiation is small, from 0.2 to 0.7 percent, and is ignored [*16*]; there are a few times, however, where it must be included [*17*]. Several mathematical models are available that can be used to correct for characteristic fluorescence [*1, 14, 18, 19*]; the procedure suggested by Reed [*19*] appears to be the most versatile.

The absorption correction arises from the fact that X-rays are generated below the surface of the specimen. The detector sees an intensity which is diminished by the amount absorbed while traveling to the surface. Therefore, it can be seen that this correction should have the effect of increasing the measured intensities. The model suggested by Philibert [*20*] and modified by Duncumb and Shields [*21*] appears to be accurate within wide limits of applicability.

The atomic number correction is probably the most difficult to quantitatively evaluate. It is usually the last correction to be made and is used to correct for any remaining nonlinearity between the measured intensity of the X-rays and the actual concentration. The effect is attributed to two sources, both of which are a function of the atomic numbers of the elements present in the specimen. These are the electron stopping power and electron backscattering, which decreases and increases, respectively, with atomic number. Several procedures are suggested for the correction of the atomic number effect [*22–26*], and evaluations of some of these procedures have been published [*27, 28*]. The correction procedures suggested by Thomas [*22*] and by Duncumb and Reed [*23*] are the most encouraging.

The whole correction procedure technique can be best summarized by the following equation

$$C_A = K_A \times F_A \times A_A \times Z_A \ldots\ldots\ldots\ldots\ldots\ldots (1)$$

where C_A is the concentration of element A, K_A is the probe ratio of element A, and F_A, A_A, and Z_A are the fluorescence, absorption, and atomic number corrections, respectively. This equation is usually present in a somewhat different form given as Eq 2.

$$C_A = K_A \left[\frac{1}{1 + (I_F/I_D)}\right]\left[\frac{F(\chi_A)}{F(\chi_{AB})}\right]\left[\frac{R_A}{\overline{R}_{AB}} \times \frac{\overline{S}_{AB}}{S_A}\right] \ldots\ldots\ldots\ldots (2)$$

Where:

C_A = mass concentration of element A in a complex target of A, B, C, ... ,
K_A = first approximate weight fraction of element A corrected for dead time and background,
I_F = fluorescence intensity from element A,
I_D = intensity of primary radiation,
$F(\chi_A)$ = absorption correction for standard A,
$F(\chi_{AB})$ = absorption correction for complex target,
R_A = backscatter coefficient for standard A,
$\overline{R}_{AB}$ = backscatter coefficient for complex target,
$\overline{S}_{AB}$ = stopping power for complex target, and
S_A = stopping power for standard A.

The constituents which comprise each one of the above correction factors are many and are extremely complex. They include such properties as absorption edge jump ratios, fluorescent yields, atomic weight of the elements, excitation potential, mass absorption coefficients, electron mass absorption coefficients, backscatter coefficients, average electron stopping power, and ionizations potentials. They also require instrumental factors such as the accelerating voltage of the electrons and the X-ray takeoff angle. The purpose of pointing out these factors is to emphasize the complexity of the correction procedures. Also, the corrective procedures are basically iterative processes. For these reasons, application of these procedures in any but the most simple cases requires the use of a computer.

Much work has been done by many investigators on the development of computer programs for the application of the correction procedures. They include programs for both time-sharing and batch-type computers. Beaman and Isasi [*29*] have made an evaluation of a large number of these computer programs for a number of alloy systems. Attempts are now being made to develop module-type programs for these corrections so that they will be amenable to use with a small, on-line computer and people not having large computers available will be able to do quantitative analysis. The on-line minicomputers will be able to also serve a second, and probably equally important, function of controlling the operation and data accumulation of the microprobe. Figure 3 is a schematic representation of an automated readout and control system for an electron microprobe.

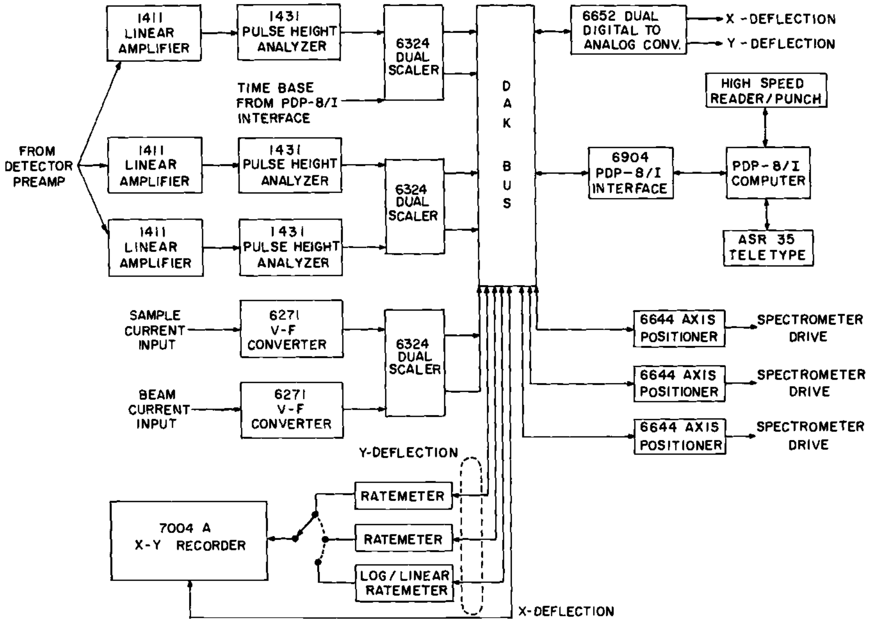

FIG. 3—*An automated electron microprobe readout and control system.*

Specimen Preparation

The preparation of specimens for electron microprobe analysis can play an extremely important part in the results that can be achieved with the instrument. Because of the wide number of materials that can be investigated, and because of the different kinds of information which can be obtained, one or even relatively few methods of specimen preparation cannot be specified. Usually the actual method employed will be largely influenced by the type of investigation and the specific information desired. However, there are some general rules which can be followed and some general pitfalls which should be avoided.

Most generally, and whenever possible, it is desirable to use the best metallographic polishing techniques in the preparation of the specimen. Polishing materials that contain the same elements as those being investigated in the specimen should be avoided. For example, it is not desirable to use carborundum paper and alumina polishing powder when analyzing the specimen for aluminum, silicon, or carbon. Another example would be the use of diamond paste when analyzing for carbides. Where it is not possible to avoid contamination from the metallographic preparation because of the elements being analyzed, it may be necessary to adopt a two-stage polishing and analyzing procedure. If a specimen is being analyzed for aluminum, magnesium, silicon, and carbon, for example, it could initially be polished with alumina-containing materials and analyzed for all elements except aluminum. It would then be necessary to repolish the specimen using silicon carbide papers and magnesium oxide polishing powder and analyze the specimen for aluminum. Ultrasonic cleaning of the specimen between each polishing step is generally advantageous.

A specimen should not be stored at atmospheric pressure for any length of time, and it should be repolished just before it is put into the microprobe. In the case of quantitative analysis it is desirable (but it may not always be practical) to have the standards in the same mount as the specimen, whenever possible, to insure the same surface conditions on them. Etched specimens should not be used for quantitative analysis, since topographic effects or selective attack can lead to inaccurate results. If it is necessary to analyze a specific phase or area in the specimen, it should be located prior to its being placed into the instrument. (It can be marked using diamond impressions or other suitable means by looking at an etched specimen in an optical microscope.) The specimen should then be repolished to remove all traces of the etched structure before it is placed in the microprobe for analysis. If it is necessary to analyze the edge of a transverse specimen or a surface layer at the edge of the specimen, plating the specimen before mounting will insure that the edge or the layer is not removed during the polishing of the specimen. Obviously a plating should be used which will not interfere with the analysis.

In dealing with nonconducting specimens the same general polishing pro cedures apply; however, before the specimen is placed in the microprobe a conductive coating must be placed on the specimen surface to prevent the specimen from charging and the electron beam from being deflected. There are a number of coatings which can be used. A thin film of carbon or a metal such as aluminum (no more than 100 Å) can be evaporated onto the surface. Conductive sprays are commercially available and can readily be used for this purpose. The important thing to remember is to choose a conductive coating that will not interfere with the analysis being performed.

There are a number of types of specimens which are studied on which no surface preparation can be performed, since it is the surface itself which is of interest. One such specimen is the fracture surface. Generally for specimens of this type the interest is in a surface film or an inclusion on the surface. Specimens of this type can only be evaluated qualitatively. The prime reason for this is that the surface is usually very rough and it would be very difficult (if not impossible) to apply correction programs to the specimen. In preparing for the microprobe, the specimen should be mounted so that the area of interest is as close to being normal to the electron beam as is possible. It must also be insured that no part of the specimen will block the area of interest from the detector.

Another type of specimen on which there is usually no surface preparation is the integrated circuit. For specimens of this type the main reason for investigation is circuit failure, and therefore qualitative results are sufficient. Specimens of this kind must be coated for surface conductivity in the probe.

The use of a microprobe for the analysis of thin films can present a number of problems depending on the thickness of film and the type of information desired. Let it be assumed that a concentration profile is desired. If the film is thick enough the specimen can be coated to preserve the film and a transverse specimen prepared. The analysis can then be performed in the usual manner by indexing the beam across the film and measuring the concentration of the desired element. For the case when the film is not thick enough to perform the analysis in this manner, another approach must be taken. One means of achieving this is to polish the specimen at a small angle (from 1 to 5 deg) to its surface. This technique produces a specimen with an apparent increased film thickness. Thus, at an angle of 5 deg, the apparent film thickness is increased by eleven and a half times. From the geometry of the specimen it is easy to relate any position in the film to its true position. A means for preparing a specimen of this kind is shown in Fig. 4. It consists of a cylinder into which a piston, ground at the desired polishing, fits. The specimen is glued to the piston, and the piston is then inserted into the cylinder. The entire holder is metallographically polished until the specimen is absolutely flat.

In the case of very thin films, where all that is needed is an overall analysis of the film, a number of approaches can be taken. The main problem involves the penetration of the film by the electron beam so that the substrate is also yielding X-rays. One approach is to lower the accelerating voltage to decrease penetration. When this is done it may be necessary to use L or M X radiation rather than K radiation, since the accelerating potential may not be high enough to excite the latter radiation. Another possibility is to use a substrate

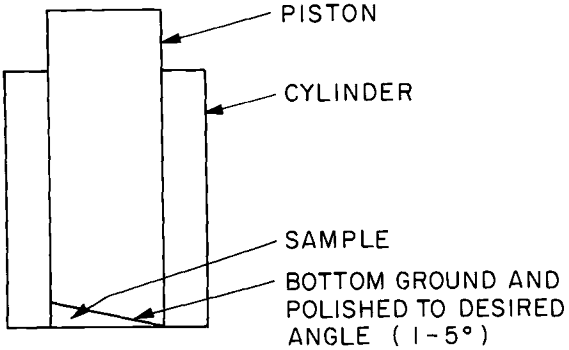

FIG. 4—*An angle lapping holder for polishing thin film specimens.*

which will not interfere with the analysis of the film. At best, highly accurate analyses of thin films are difficult, because the films are very difficult to prepare with a uniform thickness, and changes in thickness will affect the results.

Examples

A number of examples using different types of specimens and data presentation methods will be given. Figure 5 is a x-y recorder scan of intensity versus wavelength at a fixed point on two specimens. The problem involved the identification of an inclusion in a steel ingot. Since it was suspected that the inclusion might be slag, a specimen of the slag was run in the same manner. From the results of these spectrometer scans it was possible to identify the inclusion as slag.

Another area in which it is very often necessary to identify inclusions is glass. Specimens of this type have to be carbon coated before they can be analyzed. Figure 6 shows the results of analysis of a defect (oval-shaped inclusion, one of many in the glass) in a piece of "float" glass. The backscattered electron pictures show a metallographic view of the defect. From the X-ray photographs the inclusion was identified as an iron nickel sulfide. It was possible to eliminate these defects by replacing some stainless steel implements used in the furnace. Another type of glass inclusion is shown in Fig. 7. It was found to be zirconium rich and traced to the furnace lining.

Another area of interest is in high-temperature nickel-base alloys. Figure 8 shows the identification of an aluminum inclusion. The sample current, or absorbed electron, picture gives a metallographic view of the inclusion, while the X-ray micrographs show the presence of the different elements. Figure 9 shows the presence of a chromium carbide inclusion in a similar alloy, as evidenced by the high X-ray fluorescence of the inclusions in the Cr and C X-ray raster micrographs. The Al and Ni X-ray raster micrographs show corresponding depletion areas. Figures 10*A* and *B* allow a microprobe study of an oxidation problem in a nickel-base alloy. To maintain the oxide at the edge the specimen was nickel plated prior to polishing. While the oxide was viewed in the optical microscope it looked uniform. However, as can be seen from the absorbed electron picture in Fig. 10*A*, it is actually a dual oxide. This is confirmed by X-ray photographs, which show the oxide on the right is predominantly aluminum while that on the left contains chromium, titanium, cobalt, and nickel. The line scans in Fig. 10*B* also substantiate these results but in a more quantitative manner.

Another area in which the electron microprobe can be very useful is in the examination of fracture surfaces. Its use for this purpose will be shown in the group of micrographs. Figure 11 is a group of micrographs of a crack in a wire. The top micrographs are optical micrographs in the etched and unetched condition. During the optical examination, it was observed that there appeared

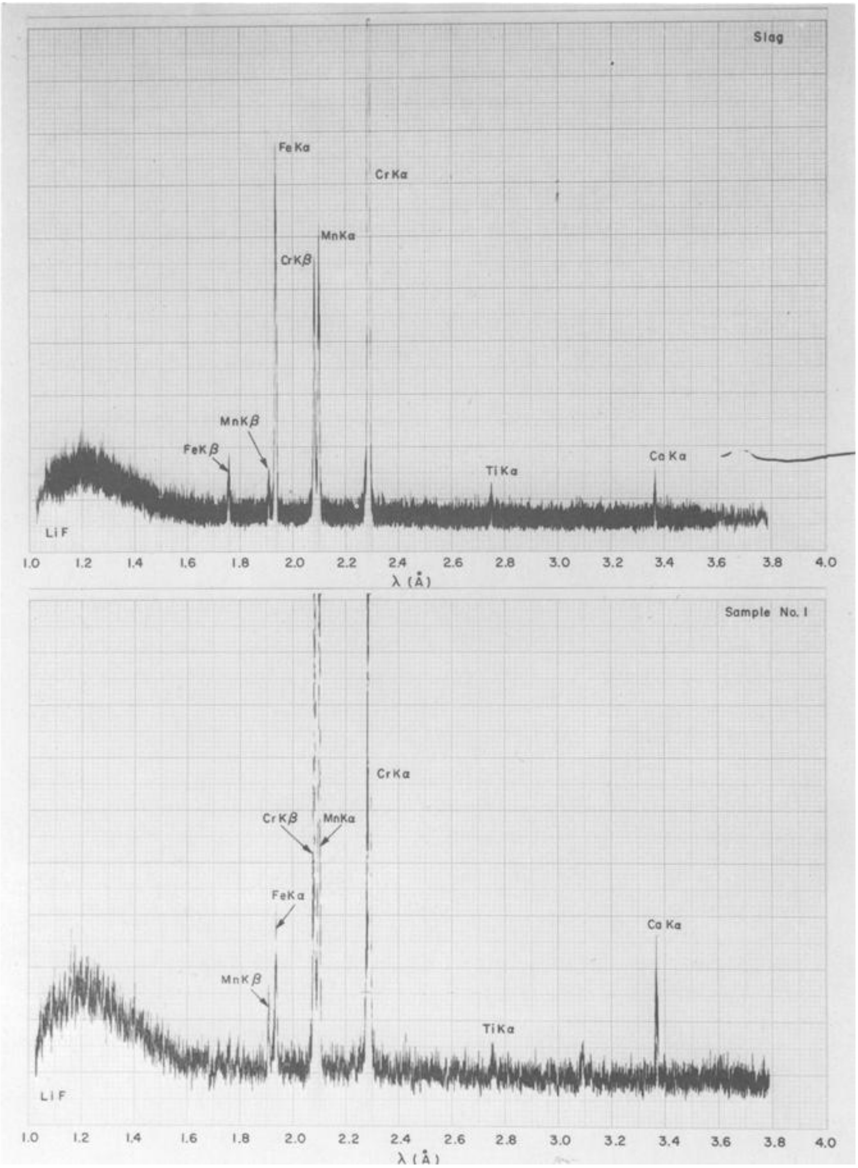

FIG. 5—*Spectral scan of slag* (top) *and inclusion* (bottom) *using an LiF diffracting crystal.*

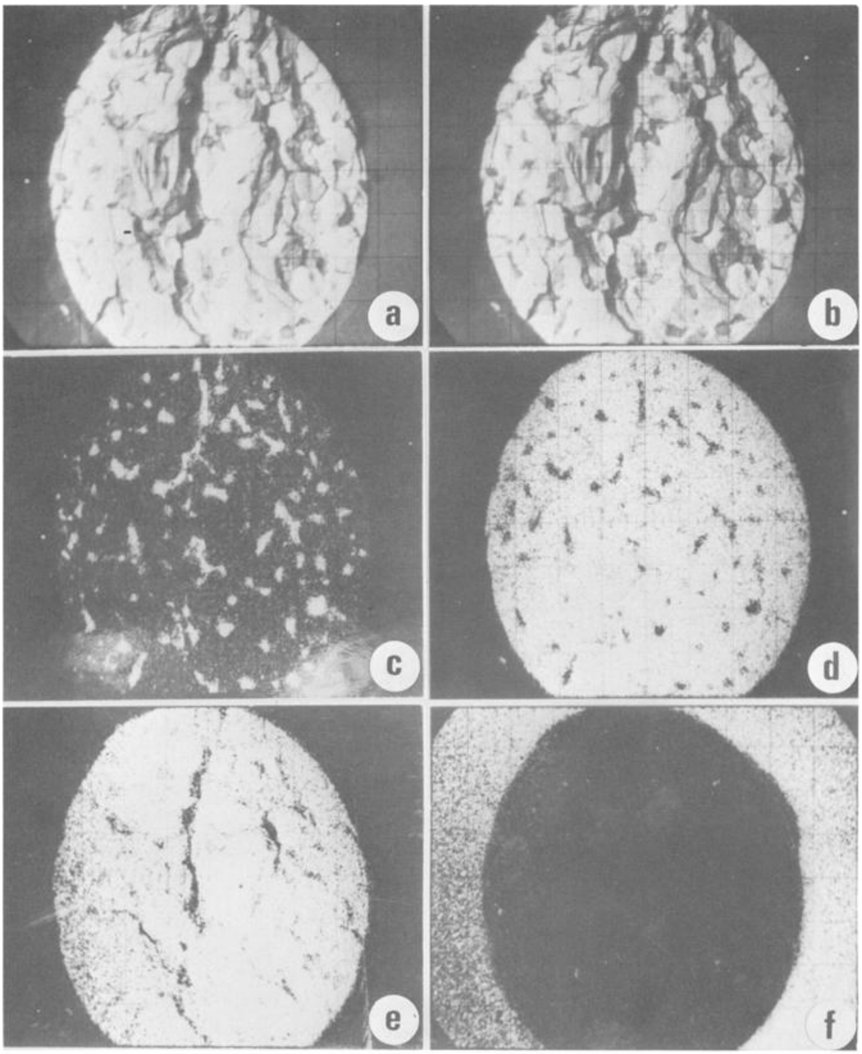

(a) and (b) Backscattered electrons.
(c) Iron Kα.
(d) Nickel Kα.
(e) Sulfur Kα.
(f) Silicon Kα.

FIG. 6—*Micrographs of an inclusion in a float glass windshield* (×*410*).

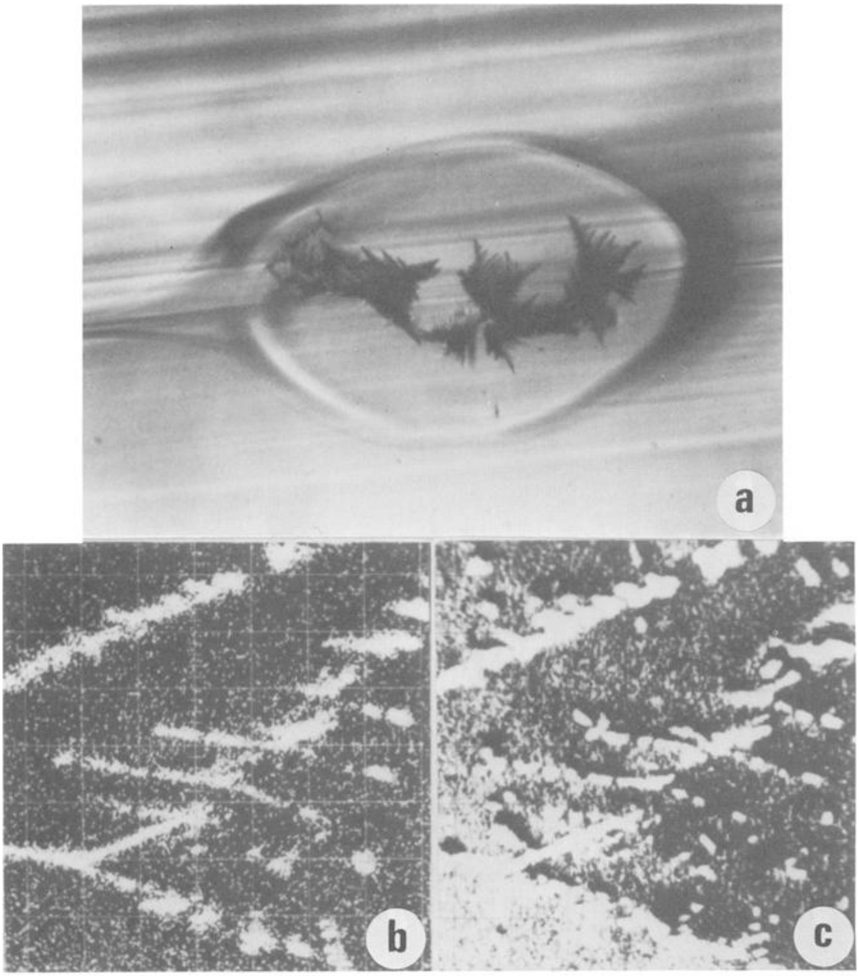

(a) Photomicrograph (×100).
(b) Zirconium (×400).
(c) Electron backscatter (×400).

FIG. 7—*Micrographs of a stone in sheet glass indicating a zirconium impurity.*

to be some foreign matter in the crack. The specimen was analyzed using the microprobe and lead was identified in the crack. It was decided to investigate this further and a piece of wire was fractured by notching it on the opposite side from the crack and bending it around the notch. Figure 12 is a photomicrograph of the fractured surface; the letters indicate portions of the fracture surface which were analyzed by Pb X-ray micrographs, shown in Fig. 13.

As can be seen, lead is present throughout area *D*, and partially in areas *A* and *B*, and it is totally absent from area *C*. A further investigation revealed that the steel, during processing to wire, was annealed in a lead bath. Therefore, this wire must have been cracked initially during the wire forming operation and picked up lead during the annealing process (areas *A*, *B*, and *D*). After being processed to a final part and put into operation, the crack began to grow (area C) until the piece finally failed.

Figure 14 is a microprobe study of a corrosion problem on an exhaust valve. The composition of an alloy used for this purpose is typically given

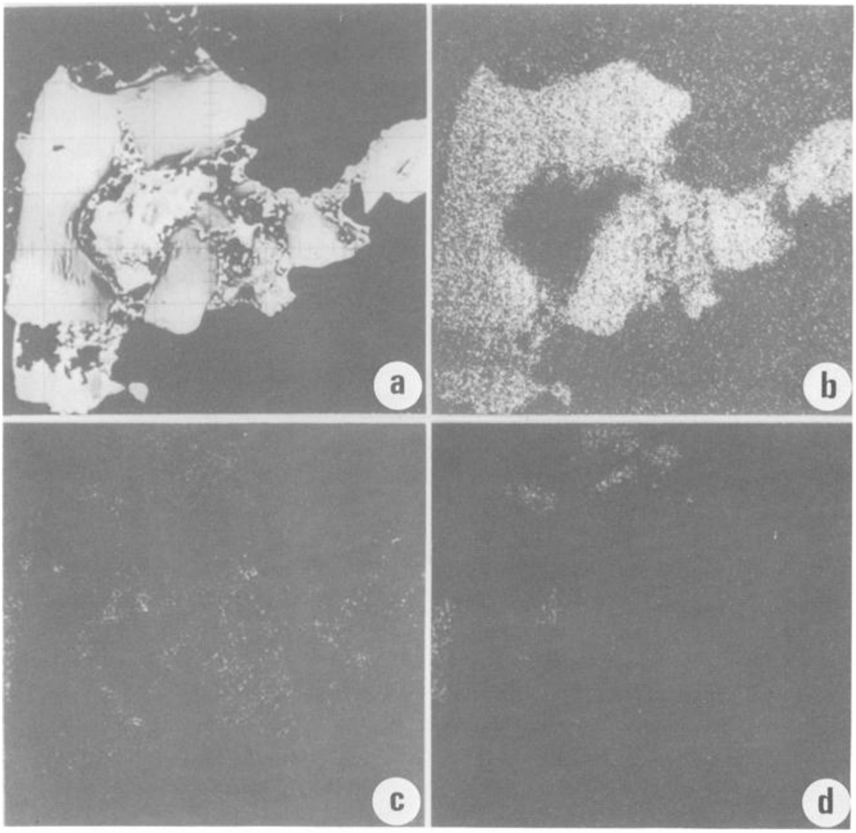

(a) Absorbed electron picture (sample current).
(b) Aluminum X-ray picture.
(c) Silicon X-ray picture.
(d) Zirconium X-ray picture.

FIG. 8—*Micrographs of an aluminum inclusion in a high-temperature nickel-base alloy* (×*160*).

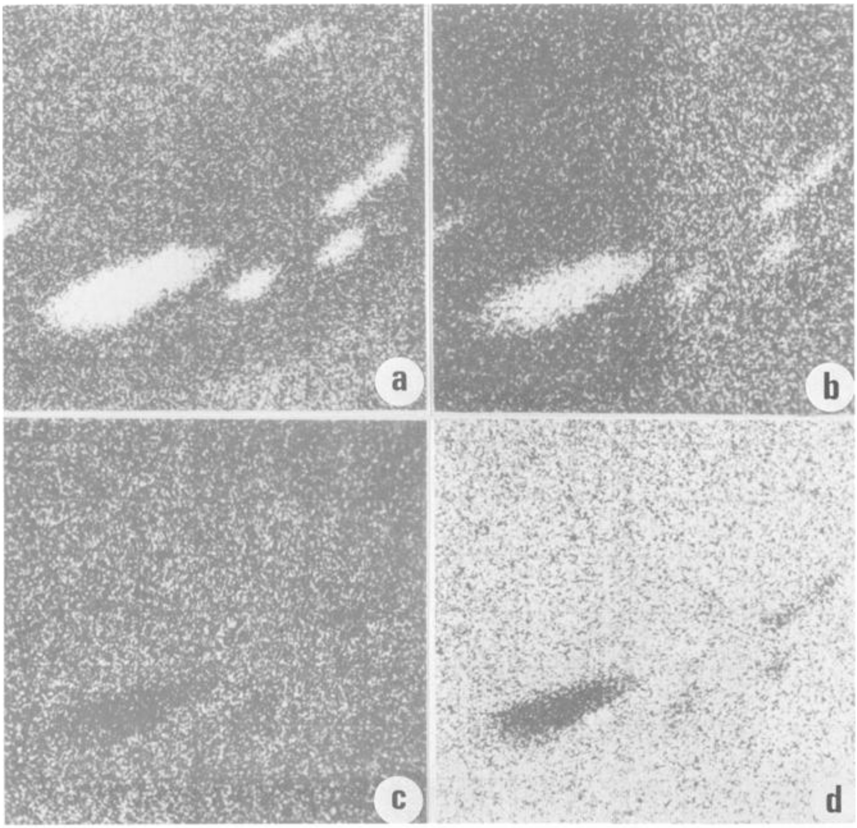

(a) Chromium.
(b) Carbon.
(c) Aluminum.
(d) Nickel.

FIG. 9—*Micrographs of a chromium carbide inclusion in a nickel-base alloy* (×*12*).

as 15 percent chromium, 15 percent nickel, 3 percent silicon, 1 percent carbon, and the balance iron. As can be seen by the high intensity of nickel radiation at the left of the nickel X-ray micrograph, the specimen was nickel plated to retain the corrosion products during specimen preparation. The X-ray micrographs clearly show what elements are associated with the corrosion products. The lead present in the corrosion product, shown at the bottom right, comes from the gasoline.

The next group of micrographs are examples of work on thin films. The first two represent two different types of diffusion studies in brasses. In the first example, where the film was extremely thin (less than 1 μm), we wished

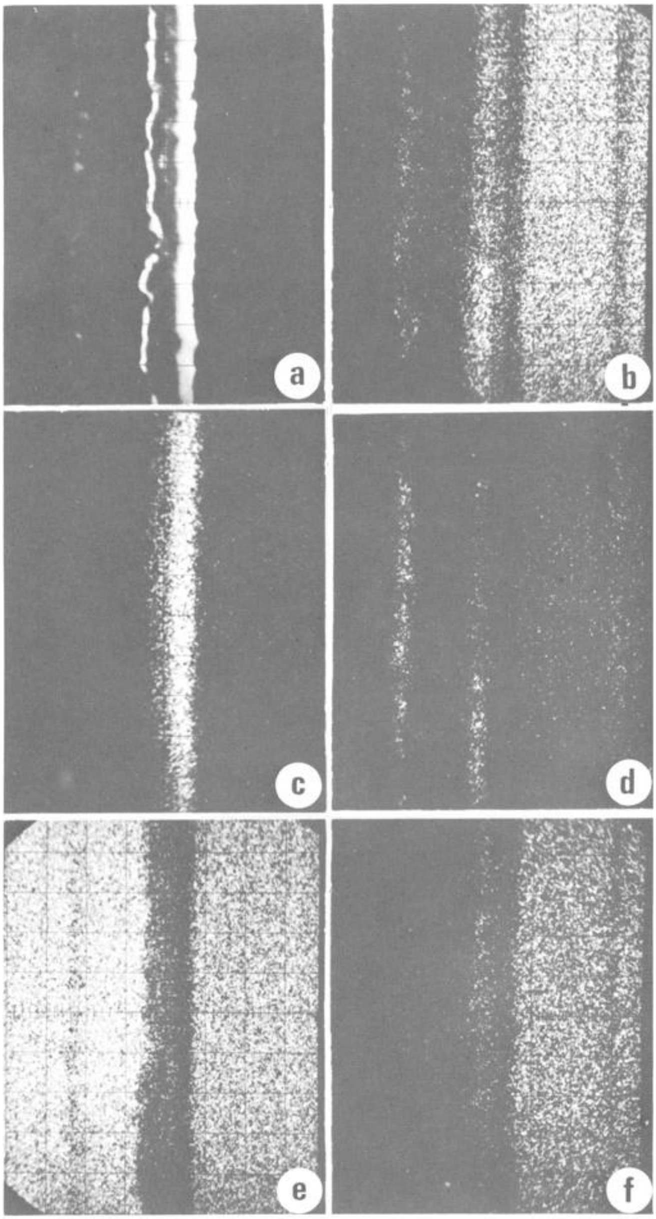

(a) Absorbed electrons.
(b) Chromium.
(c) Aluminum.
(d) Titanium.
(e) Nickel.
(f) Cobalt.

FIG. 10—(A) *Micrographs of area scans for absorbed electrons and various X-ray showing the results of a study of the oxidation of a nickel base alloy* (×2500).

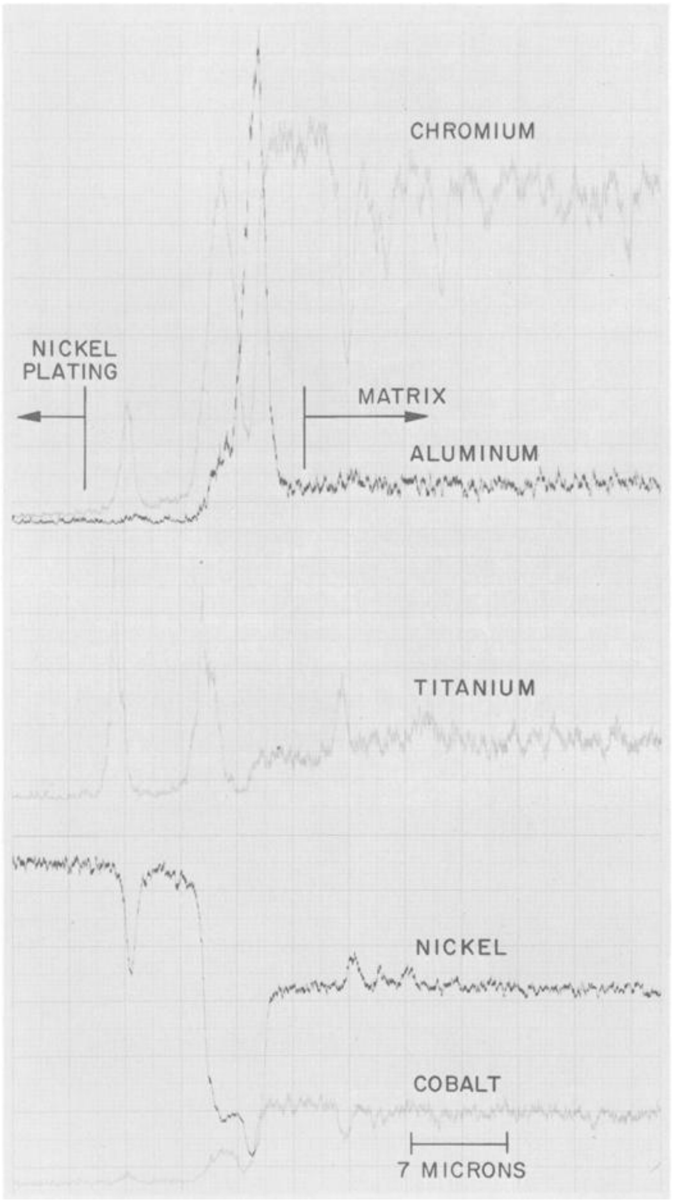

FIG. 10 (Continued)—(B) *Line scans for the same elements taken from the same area.*

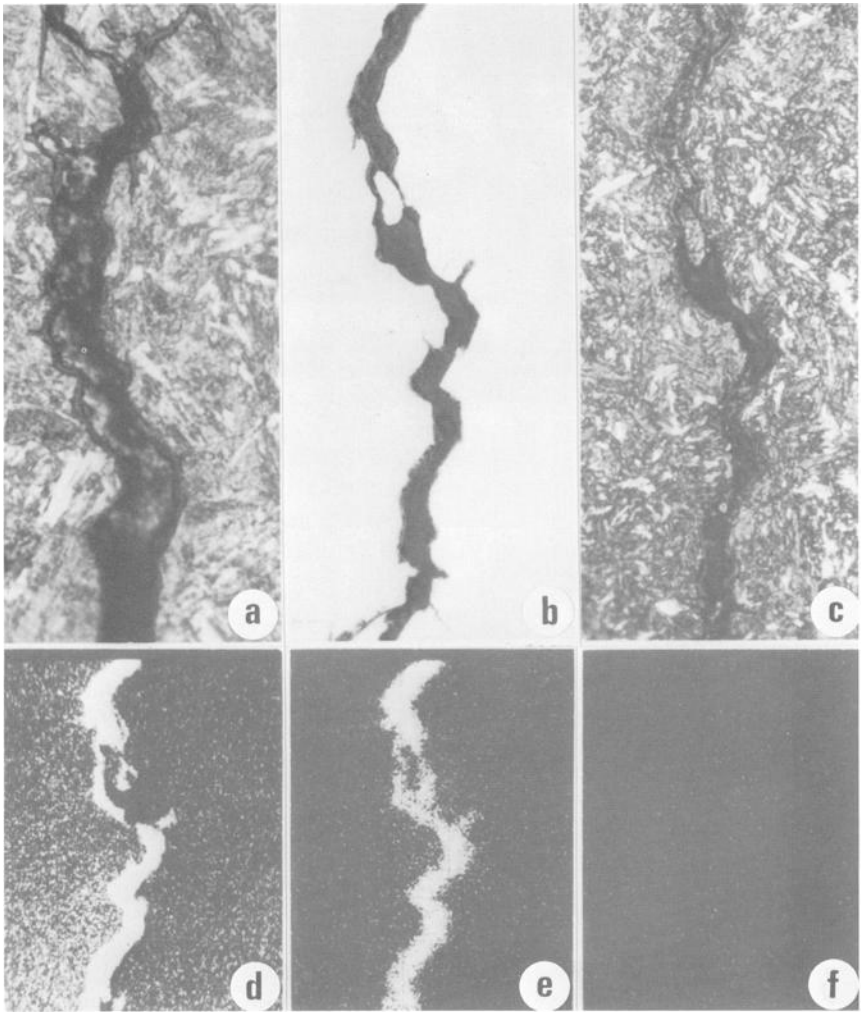

(a) Section through crack near midlength. Etched 2 percent nital, 10 s (×1200).
(b) Section through crack. Area used for electron microprobe. Unetched (×650).
(c) Same area as (b). Etched 2 percent nital, 15 s (×650).
(d) Electron backscatter micrograph of area (×450).
(e) Radiation from Pb in area (×450).
(f) Radiation from Ti in area (X450).

FIG. 11—*Micrographs of a polished section of a wire indicating the presence of lead in a crack.*

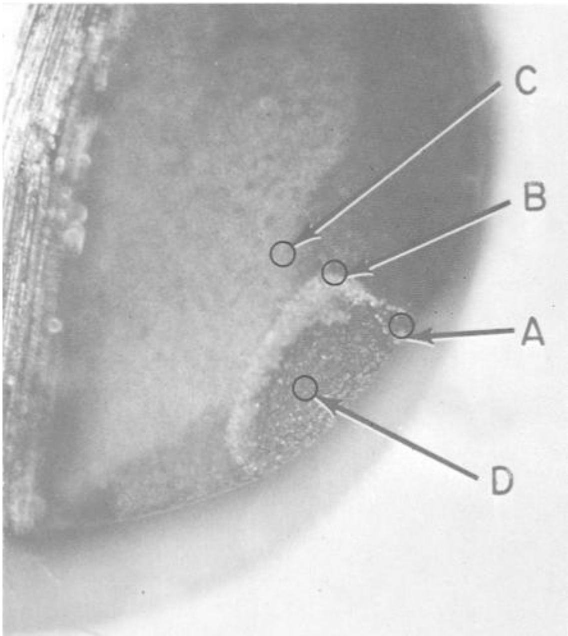

FIG. 12—*Photomicrograph of a fracture surface of the wire* (×*50*).

to trace the course of a diffusion of zinc into a copper layer, and because we were interested in diffusion in such a thin layer, it was not possible to use conventional techniques. Considering the situation in two dimensions, the film thickness in this case is less than the area from which X-rays are generated using the finest electron beam possible. Therefore any attempt to look at a transverse section across the thickness of the film could not possibly yield results to show the progress of the zinc diffusion.

It was previously mentioned that the depth of penetration of electrons into a given specimen is dependent only on the accelerating voltage. This fact was finally used to handle the problem. A longitudinal specimen was taken and a beam applied perpendicular to the film thickness. By reducing the voltage in continuous steps it was found that at some voltage the zinc X radiation did not appear. This voltage could be related to the thickness of copper into which the zinc had not diffused. However, it was not until voltages less than 10 kV were used that a condition was reached in which no zinc was present. Since the binding energy of K shell electrons is approximately 10 keV for both copper and zinc, no K X radiation will be generated for either element. However, the binding energy for L shell electrons is about 1 keV for both elements, and therefore the experiment can be done by measuring the L spectrum for them. Figure 15 gives the L spectrum for a brass consisting of approximately 50 percent of each element, from which it should be easy to monitor the zinc wavelengths and determine when zinc is no longer present.

Figure 16 shows the second example of a thin film, copper-zinc diffusion study. Here electron microprobe line profiling techniques could be used because the film thickness was much greater than the area from which the X-rays came. Previous diffusion studies of the copper-zinc matrix were carried out by Birks et al [*30*]; however, these studies were conducted at relatively high temperatures (550 C), whereas this study is confined to more moderate temperatures and to thin films. The experimental specimen configuration consisted of a 25-μm copper substrate, a 12.5-μm copper-zinc alloy layer, and a "variable" 0.05, 1.0, or 2.0-μm copper layer. The variable layer was used to insure proper instrumental parameters for each analysis. Since the

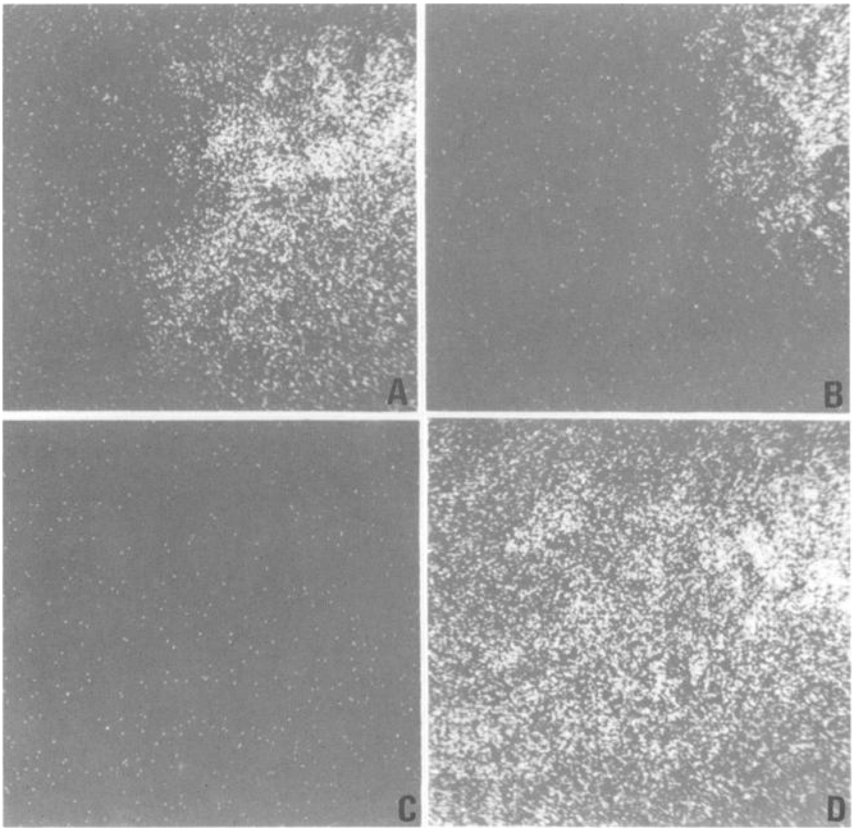

FIG. 13—*Micrographs showing the lead distribution at points* A *through* D *of Fig. 12* (×*150*).

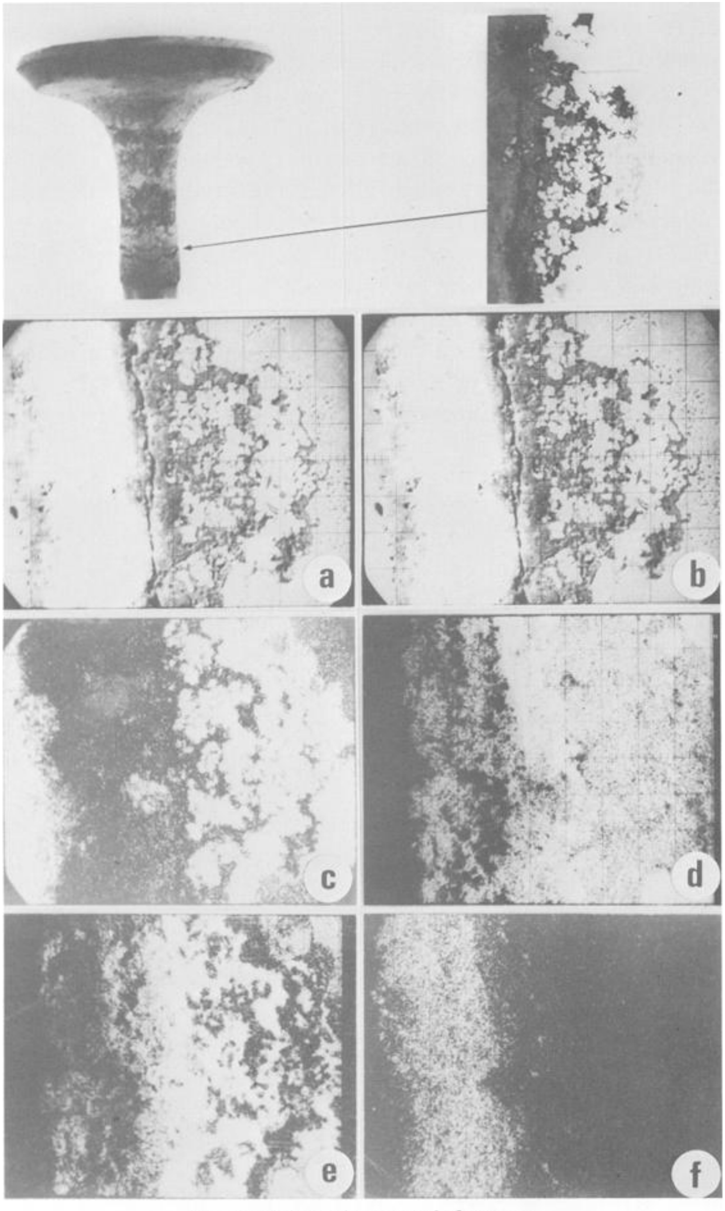

(a) and (b) Backscattered electrons.
(c) Nickel Kα.
(d) Iron Kα.
(e) Chromium Kα.
(f) Lead Mβ.

FIG. 14—*Micrographs showing a corrosion study on an exhaust valve* (×*400*).

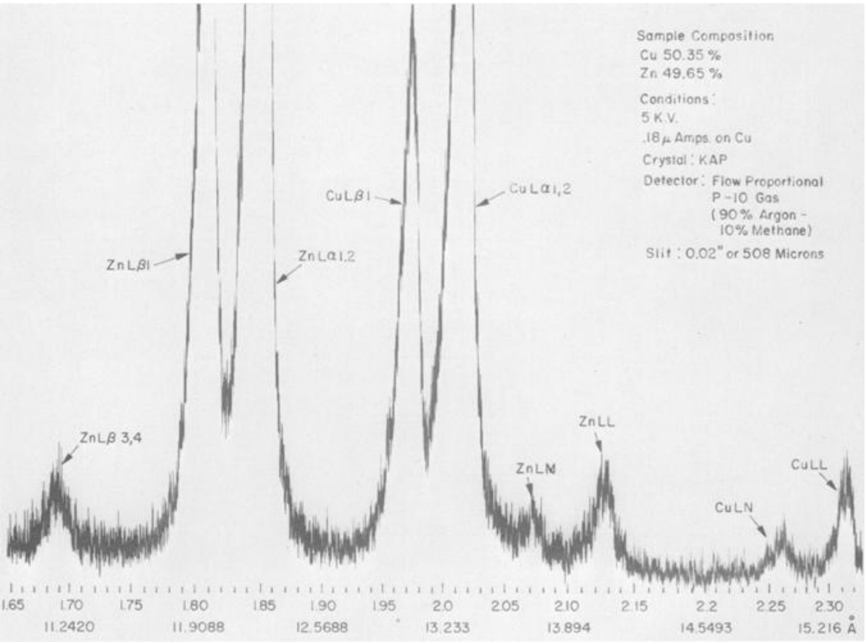

FIG. 15—*L spectrum for a Cu-Zn alloy.*

absorption, fluorescence, and atomic number effects for the copper-zinc matrix were somewhat minimized, a calibration curve was derived and is shown in Fig. 17. The curve was used to relate zinc and copper concentrations to the number of counts recorded from each specimen.

The use of the angle lapping technique to study diffusion in thin films is illustrated in Figs. 18 and 19. Specifically, we wished to study the concentration of phosphorus diffused in an oxidized layer of a silicon wafer to the depth of about 1 μm. The specimens were angle lapped to 3 and 5 deg. Calculations of actual depth could be made not only from the geometry but also from the presence of interference fringes in the optical microscope. The probe data were taken in 3 and 5-μm steps and are shown in these figures along with a schematic representation of the specimen and fringe pattern.

Summary

The use of an electron microprobe as a research instrument has been considered. Different ways in which the instrument can be used have been discussed. As new means of data accumulation and presentation are developed, the use of the microprobe will be still further broadened.

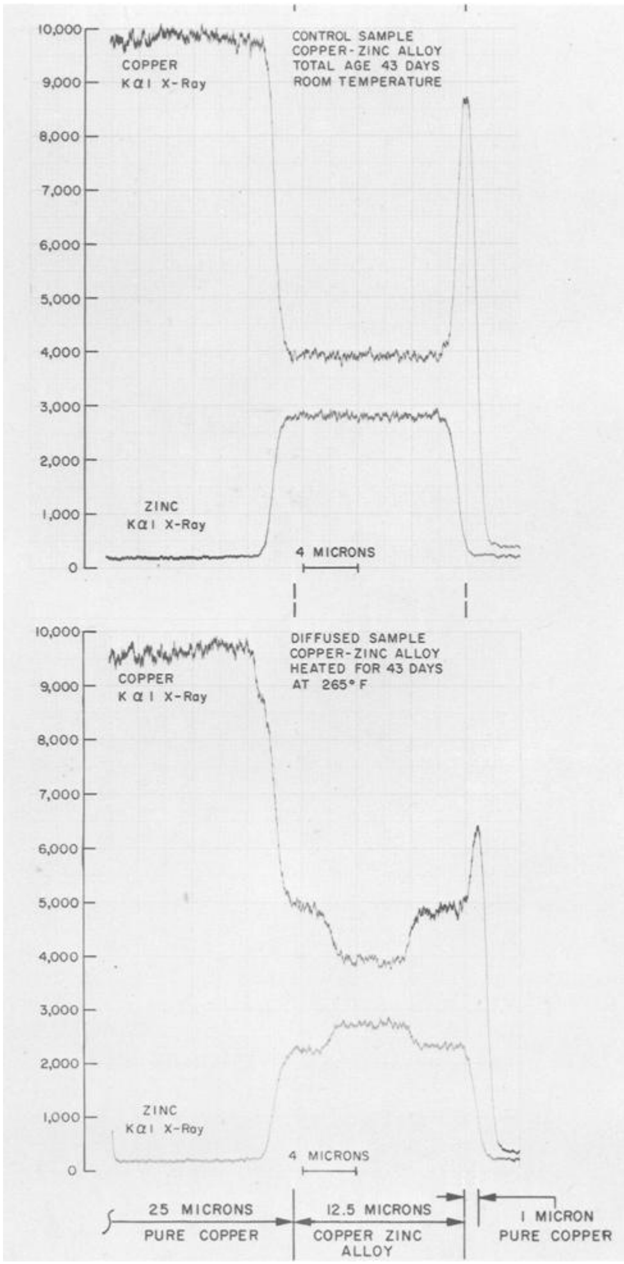

FIG. 16—*Electron microprobe determination of zinc diffusion coefficient in copper.*

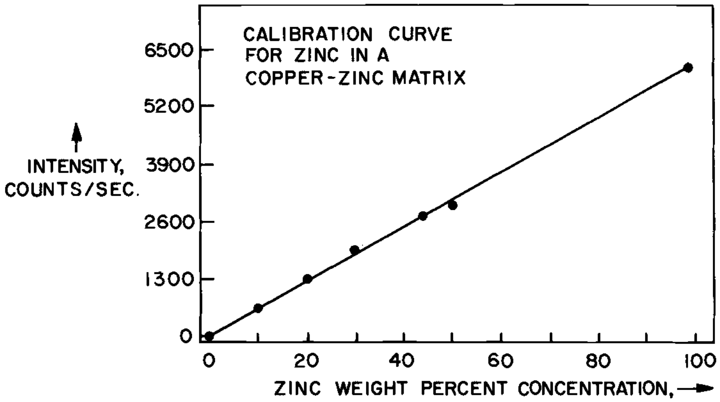

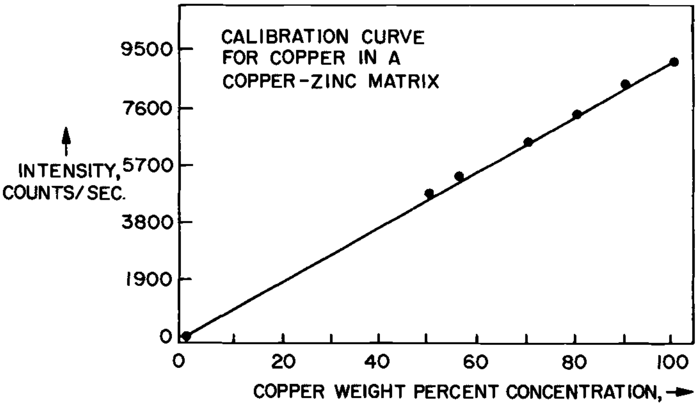

FIG. 17—*Electron microprobe calibration curves for copper-zinc at 15 keV.*

Acknowledgments

We wish to thank F. Borile, who generated much of the data presented in this paper.

References

[1] Castaing, R., PhD thesis, University of Paris, Paris, 1951, ONERA, No. 55.

[2] *X-ray and Electron Probe Analysis, ASTM STP 349*, American Society for Testing and Materials, 1964.

[3] Birks, L. S. in *X-ray and Electron Probe Analysis, ASTM STP 349*, American Society for Testing and Materials, 1964, p. 158.

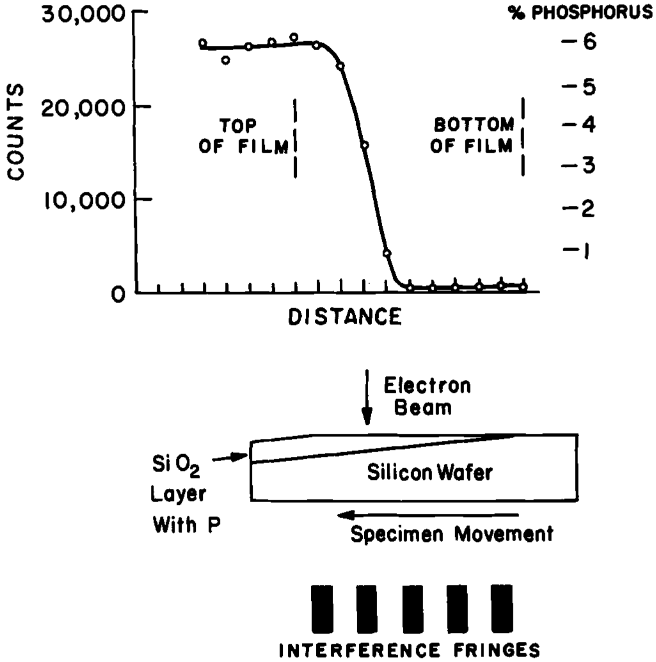

FIG. 18—*Concentration plot of phosphorus in silicon made on a thin wafer. Interface fringes indicate depth of film at each position.*

[4] Heinrich, K. F. J. in *X-ray and Electron Probe Analysis, ASTM STP 349*, American Society for Testing and Materials, 1964, p. 171.

[5] Brown, J. D. in *Fifty Years of Progress in Metallographic Techniques, ASTM STP 430*, American Society for Testing and Materials, 1968, p. 354.

[6] Heinrich, K. F. J. in *Fifty Years of Progress in Metallographic Techniques, ASTM STP 430*, American Society for Testing and Materials, 1968, p. 315.

[7] Criss, J., "Advances in Quantitative Electron Probe Microanalysis," 72nd Annual Meeting, American Society for Testing and Materials, Atlantic City, N. J., June 1966.

[8] Heinrich K. F. J. in *The Electron Microprobe*, T. D. McKinley et al, Eds., John Wiley, New York, 1966, p. 841.

[9] Reed, S. J. B. in *X-ray Optics and Microanalysis*, R. Castaing et al, Eds., Hermann, Paris, 1966, p. 339.

[10] Yakowitz, H. and Heinrich, K. F. J., *Journal of Research of the National Bureau of Standards*, Section A, JNBAA, Vol. 73A, 1969, p. 113.

[11] Heinrich, K. F. J., *Review of Scientific Instruments*, RSINA, Vol. 33, 1962, p. 884.

[12] Fitzgerald, R., Keil, K. and Heinrich, K. F. J., *Science*, SCIEA, Vol. 159, 1968, p. 528.

[13] Castaing, R., *Advances in Electronics and Electron Physics*, Vol. 13, L. Marton, Ed., Academic Press, New York, 1960, p. 317.

[14] Wittry, D. B., PhD thesis, California Institute of Technology, 1957.

[15] Duncumb, P. and Shields, P. K., *British Journal of Applied Physics*, BJAPA, Vol. 14, 1963, p. 617.

[16] Henoc, J., "Fluorescence by the Continuum," presented at Midwestern Probe Users Group Meeting, Rochester, Minn., June 1969.

[17] Brown J. D., "Continuum Fluorescence: Is it Important?," presented at the Fourth National Conference on Electron Microprobe Analysis, Electron Probe Analysis Society of America, Pasadena, Calif., 1969.

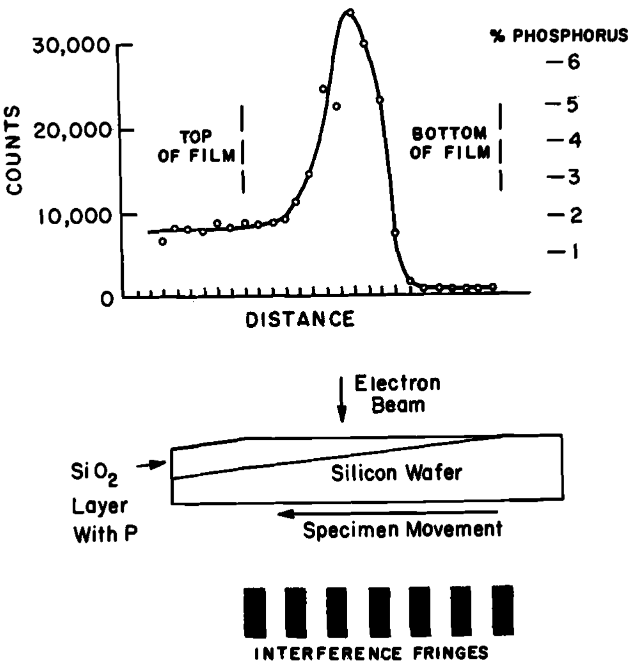

FIG. 19—*Same as Fig. 18. Note surface depleted zone.*

[18] Wittry, D. B., "Fluorescence by Characteristic Radiation in Electron Probe Microanalysis," USCEC Report 84-204, University of Southern California, July 1962.

[19] Reed, S. J. B., *British Journal of Applied Physics*, BJAPA, Vol. 16, 1965, p. 913.

[20] Philibert, J. in *X-ray Optics and X-ray Microanalysis*, H. H. Patee et al, Eds., Academic Press, New York, 1963, p. 379.

[21] Duncumb, P. and Shields, P. K. in *The Electron Microprobe*, T. D. McKinley et al, Eds., John Wiley, New York, 1966, p. 284.

[22] Thomas, P. M., "A Method for Correcting for Atomic Number Effects in Electron Probe Microanalysis," AERE Report 4593, Atomic Energy Research Establishment, Berkshire, England, April 1964.

[23] Duncumb, P. and Reed, S. J. B., National Bureau of Standards, Special Publ. No. 298, Seminar on Electron Probe Microanalysis, *Proceedings*, Washington, D. C., 1968.

[24] Belk, J. A. in *X-ray Optics and Microanalysis*, R. Castaing et al, Eds., Hermann, Paris, 1966, p. 214.

[25] Philibert, J. and Tixier, R., *British Journal of Applied Physics*, BJAPA, Vol. 19, 1968, p. 685.

[26] Ziebold, T. O. and Ogilvie, R. E., *Analytical Chemistry*, ANCHA, Vol. 35, 1963, p. 621.

[27] Beaman, D. R., *Analytical Chemistry*, ANCHA, Vol. 39, 1967, p. 418.

[28] Poole, D. M., Special Publ. No. 298, Seminar on Electron Probe Microanalysis, *Proceedings*, National Bureau of Standards, Washington, D. C., 1968.

[29] Beaman, D. R. and Isasi, J., "A Critical Examination of Computer Programs Used in Quantitative Electron Microprobe Analysis," presented at the Fourth National Conference on Electron Microprobe Analysis, Electron Probe Analysis Society of America, Pasadena, Calif., 1969.

[30] Achter, M. R., Birks, L. S. and Brooks, E. J., *Journal of Applied Physics*, JAPIA, Vol. 30, 1959, p. 1825.

J. C. Russ[1]

Use of the Scanning Electron Microscope in the Materials Sciences

---

REFERENCE: Russ, J. C., "**Use of The Scanning Electron Microscope in the Materials Sciences,**" *Applications of Modern Metallographic Techniques, ASTM STP 480*, American Society for Testing and Materials, 1970, pp. 214–248.

ABSTRACT: The scanning electron microscope is a relatively new instrument now finding rapidly growing use in the materials sciences. It scans a fine beam of electrons across the specimen surface and displays an image of that surface on a cathode-ray tube using any of the radiations that are generated by incident electrons. The characteristics of each of the images that can be formed using the different signals available are described, as well as its particular use for different types of specimens.

Many types of materials specimens can be examined in the scanning electron microscope with no preparation, but to obtain optimum results it is often necessary or desirable to coat the surface with a thin conductive layer. This and other steps of specimen preparation and handling techniques for solid and powder samples are outlined. Finally the interpretation of the various types of images and the dynamic observation of changes produced in the specimen by heating, straining, etc., are considered.

KEY WORDS: scanning, electron microscopy, metals, microstructure, fractography, corrosion, metal powders, plastics, elastomers, fibers

The scanning electron microscope (SEM) is a comparatively new instrument, quite different in principle and application from the conventional transmission electron microscope (TEM), and has been commercially available for only the past few years. It is now finding a rapidly expanding use in the diverse fields of biology, geology, metallurgy, semiconductor technology, and the general area of surface studies. Our present concern is with its use in the materials sciences, including studies of metal structure, fractography, worn or corroded surfaces, powders, and nonmetals such as fibers, rubbers, and plastics.

The history of the SEM goes back nearly as far as the TEM. Knoll, in Germany, suggested in 1935 the possibility of an instrument much like the present-day scanning microscope, and three years later Von Ardenne built

---

[1] Consultant, JEOLCO (U.S.A.), Inc., Medford, Mass. 02155. Personal member ASTM.

an instrument that was used to record transmission micrographs in a scanning mode. A more practical microscope was built at RCA by Zworykin and Hillier, who demonstrated 500-Å resolution in 1942, but this work was dropped.

After the war Bernard and Davoine in France, who reported 2-μm resolution in 1957, and Oatley and his co-workers in England, who introduced the photomultiplier tube to improve image quality, began development of the SEM. The work continued at Cambridge in England and at Japan Electron Optics Laboratories in Tokyo and culminated in the commercial introduction of instruments with about 250-Å resolution in 1965.

General Construction

A specimen in the SEM is bombarded with a fine probe of electrons, generally on the order of 100 Å in diameter or less. Since the probe strikes only one point on the specimen at a time, data must be accumulated from many points to build up a representation of an area of the specimen. Figure 1 illustrates the types of information that are generated and can be used for forming this representation. We will see what use each of these types of data can be put to.

The normal mode of operation is to scan the electron probe over an area of the specimen in a raster pattern. At the same time a cathode-ray or a television tube is scanned in synchronization with the electron beam so that each point on the display tube corresponds to a point on the specimen. Then the intensity of the spot on the tube is modulated in proportion to the intensity of one or the other of the types of data shown in Fig. 1. That this should produce an image that can be easily interpreted as a representation of the specimen is not obvious, but in fact this is the case, as we shall see.

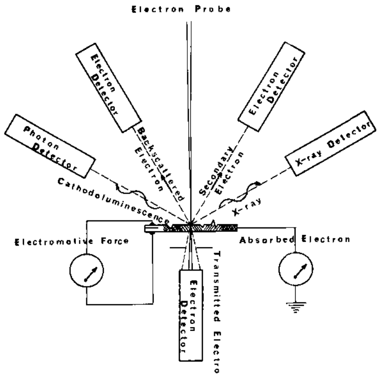

FIG. 1—*Types of information generated by impingement of electron probe on sample.*

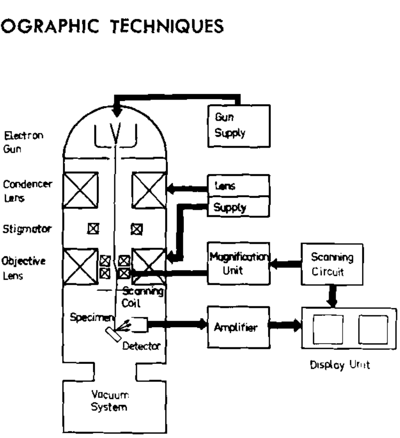

FIG. 2—*Block diagram of typical scanning electron microscope.*

The selection of the operating parameters, such as the number of lines scanned, the speed of scan, etc., is made to optimize the resulting image. Enough lines must be used to provide good coverage, without overlapping; and the speed of scan must be low enough to permit counting high numbers of electrons or photons for each point, since the signal-to-noise ratio improves in a manner proportional to the square root of the total number counted. Typical operating values are 500 to 1000 lines of scan, with times from a few seconds to a few minutes to accumulate a picture. With some instruments it is also possible to scan the beam rapidly to produce a real-time TV image of thirty frames per second for continuous viewing. The cathode-ray tube display is generally recorded photographically, although it is also possible to record it on video tape or to treat it as a flying spot and directly computer process it.

A historical review of the operating and design parameters of the early scanning microscopes can be found in Oatley et al [*1*],[2] and a general review of operation and applications in Kimoto and Russ [*2*]. Figure 2 shows the general features of construction of a modern scanning electron microscope. The electron source in the commercially available instruments is a heated hairpin tungsten filament, although experimental work with other sources is underway. Early instruments used three electrostatic lenses to demagnify the gun crossover to a probe under 100 Å in diameter. By improving the gun design and by using electromagnetic lenses which achieve slightly higher demagnification with less aberration, instruments can now be made with only two lenses, which makes operation and alignment simpler, capable of producing probe diameters down to 12 Å.

The probe is scanned by electromagnetic deflection coils in synchronization with the display tubes. Magnification is simply the ratio of the size of the display area on the cathode-ray tube to the distance the probe is scanned.

---

[2] Italic numbers in brackets refer to the list of references at the end of this paper.

The minimum magnification obtainable is generally about 20 for easy orientation to make the operator's transition from low-power optical microscopes easy. The limit on maximum magnification depends on the resolving power of the instrument, which will be discussed below. Detectors for several or all types of information available are provided, and two or more cathode-ray tubes can be used to present side-by-side images of different displays, greatly enhancing the ease of interpretation.

Figure 3 shows a typical commercial instrument, with one console containing the electron column, specimen chamber, and vacuum system, the second containing controls, displays, and power supply. Operation at accelerating voltages up to 50 kV is commercially available. The higher voltages are used to gain extra penetration, to generate X-rays from high atomic number elements, and because finer probes and better resolution can be obtained with some types of specimens.

A stage that can tilt and rotate the specimen, in addition to translating it, is advantageous as it facilitates the examination of rough surfaces and also because tilt effects image contrast. The tilt motions should ideally take place about a pivot point that coincides with the center of the area being examined on the specimen so that the same area can be kept in view and in focus. A specimen airlock, which permits rapid specimen exchange and maintains the cleanliness of the column and detectors, is likewise beneficial.

When the probe is properly focused on the specimen, changing magnification or specimen orientation does not require any change in focus. This is quite different from the conventional transmission microscope.

Resolution and Depth of Field

The resolution of an image with the SEM is limited to the size of the area emitting photons or electrons at any moment. When the electron probe hits the specimen, scattering causes the probe to spread so that the final volume

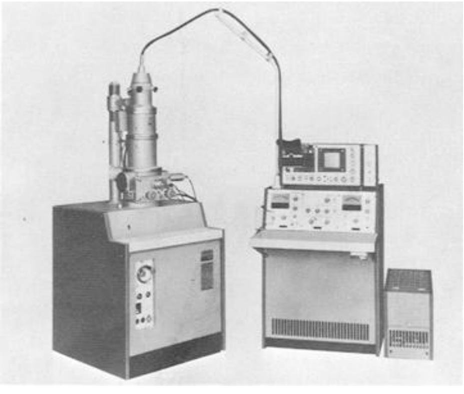

FIG. 3—*Overall view of typical scanning electron microscope.*

of electron capture is much larger than the incident probe, as shown in Fig. 4. Secondary electrons, with energies up to about 50 eV, are produced throughout this volume; however, most are reabsorbed after traveling only about 100 Å, so it is only the volume within 100 Å or less of the surface that emits secondary electrons which can be detected. This volume is only a few tens of angstroms larger than the diameter of the incident probe. Hence the secondary electron image provides the highest resolution.

Backscattered electrons come from a greater depth—and hence from a larger source area encompassed by the spread of the probe—so the resolution of the backscattered image is poorer than the sceondary electron image. Furthermore, the resolution of the backscattered image depends strongly on the degree of probe spread. As the accelerating voltage is increased the capture volume becomes larger and deeper; thus the neck becomes longer and narrower and the secondary electron resolution improves. Photons of X-rays or visible light come from essentially the entire capture volume and hence give the poorest resolution. Figure 5 shows the dependence of the spatial resolution of the X-ray image on accelerating voltage and beam current. As beam current drops, the beam diameter decreases and the capture volume grows smaller until it reaches a point where it depends only on the accelerating voltage, which controls how far the electrons can scatter in the material before being captured. Results for materials other than steel are similar but shift according to the average atomic number of the specimen—smaller source diameters for the higher atomic numbers.

In the case of a transmitted electron image of a thin section, which will be discussed below, no appreciable spreading of the beam occurs and the resolution is as good or better than the secondary image.

The further reduction of the diameter of the incident beam might be expected to provide better resolution in the secondary electron image. However, even with a beam of zero cross section, spreading in the specimen will still

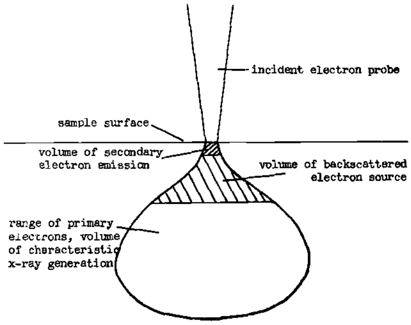

FIG. 4—*Penetration of incident electron probe into specimen.*

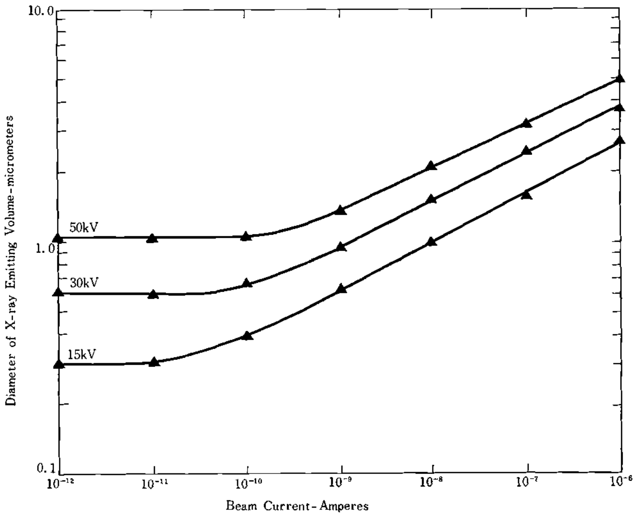

FIG. 5—*Spatial resolution of X-ray signal, showing variation with beam current and accelerating voltage (Fe Kα X-rays from steel specimen).*

limit the resolution to about 50 to 80 Å depending on the material. Also, the reduction of probe diameter requires the reduction of probe current (diameter is proportional to the 8/3 power of current); this reduces the number of secondary electrons produced per incident electron and decreases the signal-to-noise ratio in the output signal. With a beam current of 10^{-12} A at 25-kV accelerating voltage, a 38-Å beam can be achieved. This drops to 12 Å at 50 kV, as a higher accelerating voltage increases gun brightness. Further improvement below the current resolution levels (200 Å guaranteed, better than 100 Å obtainable) will probably be gradual because of the fundamental limitations mentioned.

It is worthwhile to note that the typical probe currents of 10^{-10} to 10^{-12} A are far below the 10^{-5} to 10^{-7} A of a conventional transmission electron microscope or the 10^{-7} to 10^{-9} A of a conventional electron microprobe. This reduces specimen contamination and specimen damage due to heating.

With a resolution of about 100 Å, the maximum useful magnification can be determined by considering the resolving power of the human eye on the final displayed image, which is about 0.2 mm. Displaying 100-Å spacings on the specimen as 0.2-mm spacings on the visual image gives a magnification of 20,000. Further magnification up to perhaps 50,000 may be useful to make examination easier, but beyond this point further enlargement is empty.

However, even in a magnification range of less than 1000 tò 2000, the SEM offers an important advantage over optical microscopes—namely, greater depth of field. The long working distance (typically 10 to 25 mm) and small

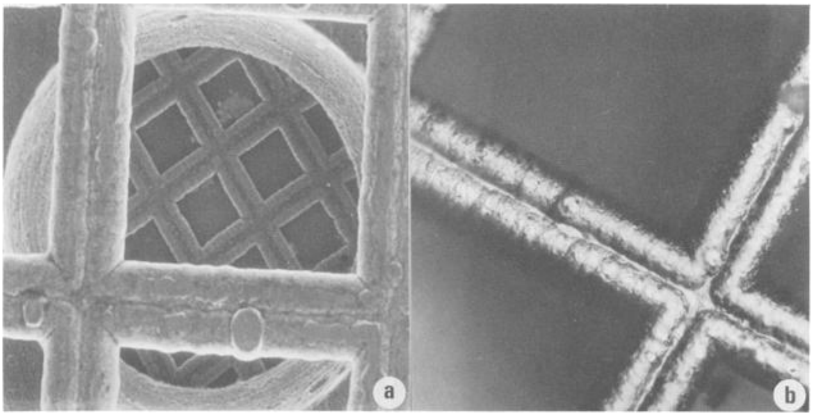

FIG. 6—*Depth of field of SEM far exceeds that of optical microscope:* (a) *secondary electron image* (×*300*)*;* (b) *image with optical microscope* (×*400*).

aperture of the final lens produces a highly parallel, uniform, and in-focus probe over a considerable distance so that, wherever in that distance the probe intersects the specimen, the image is in focus. The depth of field varies inversely with magnification, from over 1000 μm at ×100 to over 10 μm at ×10,000.

By comparison, the binocular optical microscope has a depth of field of about 150 μm at ×100, and the compound optical microscope has a depth of field of about 1 μm at ×1000. Figure 6 illustrates the depth of field of the scanning electron microscope. The stack of three specimens grids totals over 90 μm in thickness, and the optical microscope sees only part of the topmost grid.

For the examination of rough surfaces the SEM is indispensable. Furthermore, it requires no specimen preparation or at most a thin (100 to 500-Å) evaporated metal coating to provide conductivity on an insulating surface. Time-consuming replica techniques for the TEM do not provide any better resolution and frequently introduce artifacts. Also, they cannot be used for very rough, fragile, or multiply connected surfaces.

Examination of Rough Surfaces

The secondary electron image shown in Fig. 6 illustrates the usefulness of the SEM—the image is easily interpretable because it looks very much like things we normally see with the naked eye. To understand why this is so we must consider the causes of contrast in the secondary electron image, which is the image we normally use for examining the topography of rough surfaces.

Everhart [*3*] has shown that changing the surface inclination of the beam by only a few degrees produces an appreciable change in the number of secondary electrons produced. This is because the number produced is roughly proportional to the area of the teardrop-shaped capture volume exposed to the surface, which increases as the angle between the probe and the surface varies from 90 deg.

By the same argument, a sharp edge on the specimen surface will expose much more area and produce a greater number of secondary electrons. In the case of edges, there is also a strong effect of the electrical field of the detector. A high voltage (for example, 10 kV) is customarily applied to a grid in front of the detector to collect the low-energy secondary electrons and to accelerate them so that they can excite a scintillator. A photomultiplier tube then produces an electrical signal that can be amplified. The high voltage of the grid produces a field in the specimen chamber, and this field is concentrated at sharp edges on the specimen to reduce the surface work function and the space charge effect and to further enhance the production of secondary electrons.

The high voltage on the detector grid causes the low-energy secondary electrons leaving the specimen to travel in curved trajectories, so a signal can be obtained even from surfaces tilted away from the detector. This is not the case for the backscattered high-energy electrons, which travel in straight lines and so produce very definite dark shadows, as shown in Fig. 7.

The combination of variation of brightness with surface angle and edge enhancement produces an image on the secondary electron display that is easily interpretable as surface topography by the human eye. When visually examining a rough surface we find that with diffuse lighting the brightness varies in a gradual way with local surface angle, and the brain normally characterizes images by edges anyway, which is why line drawings and sketches are meaningful.

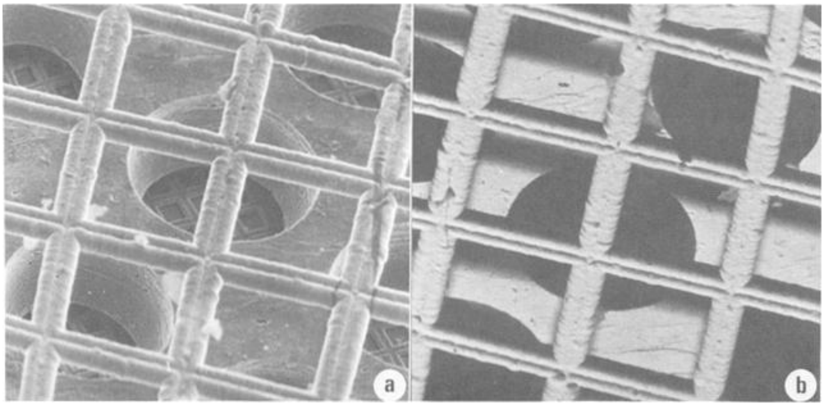

FIG. 7—*Secondary electron image of three specimen grids, tilted 45 deg, shows detail in shadow areas. Backscattered image has sharp, dark shadows* (×*215*)*:* (a) *secondary electron image;* (b) *backscattered electron image.*

To better understand the illumination effect of the secondary and backscattered electron images in Fig. 7, it is useful to consider the observer's position to be at the top of the electron column, looking down on the specimen, and the light source to be located where the detector is, generally at one side of the specimen chamber. In the case of the secondary electron image the light source is diffuse so that shadows are not sharp, but for the backscattered electron image the light source is well collimated and produces sharp shadows.

Figure 8 shows a fracture surface imaged with both secondary and backscattered electrons. In the secondary electron image, detail can be seen in the shadow areas and, in addition, the resolution is much better. For rough surfaces the magnification derived from the distance the probe is scanned is obviously incorrect. The true magnification varies with the orientation of the surface both on a local and an average scale. Fortunately, the human eye is accustomed to looking at rough surfaces obliquely and can compensate for this to a great degree. Correction devices that change the scanning pattern to a trapezoid make a first-order correction but introduce other distortions in projections or indentations on the surface that are very troublesome. For quantitative work it is necessary to use stereopairs, made by tilting the specimen a few degrees between pictures, as shown in Fig. 9. Then measurements can be made or contour maps plotted (Fig. 10). In making stereopairs it is particularly important to design the stage so that the tilt axis coincides with the point of examination. For reasonably flat specimens where large angles of tilt (for example, 15 deg) can be used, vertical resolution of a few hundred angstroms can be achieved.

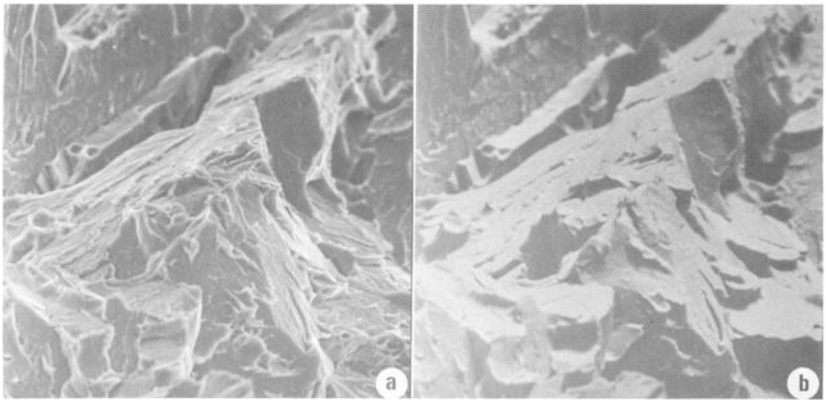

FIG. 8—*Secondary and backscattered electron images of metal fracture surface* (×*1600*): (a) *secondary electron image;* (b) *backscattered electron image.*

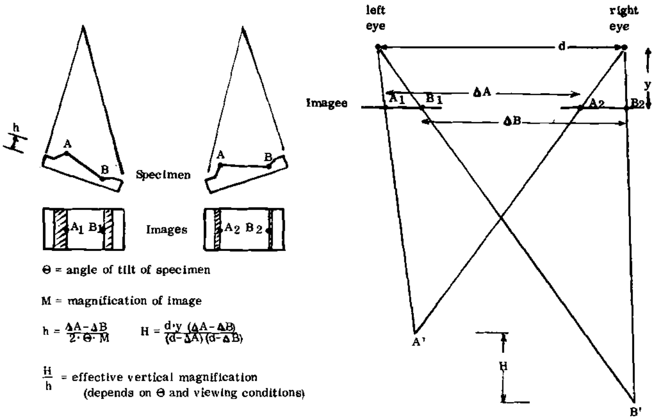

FIG. 9—*Principle of stereoscopic image reconstruction. The effective vertical magnification can be made the same as the image magnification or increased to enhance small elevation differences.*

Because the scanning microscope is parfocal (focus is achieved by varying the strength of the final lens to bring the narrowest portion of the beam to the surface of the specimen, and this is independent of the scanning distance which determines magnification), it is easy to change magnification. A convenient method of examining rough surfaces is thus to scan them at low magnification, locating features of interest, and then zoom in for closer examination. A rapidly scanned display on a TV monitor makes this operation very easy and also facilitates positioning the specimen when necessary to see particular areas of interest.

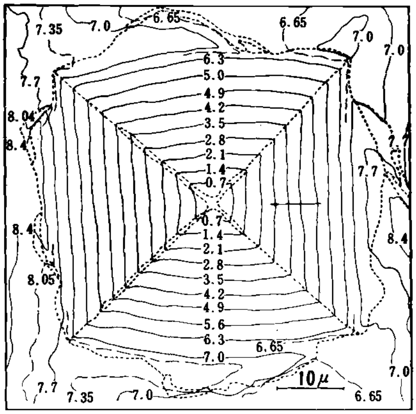

FIG. 10—*Contour map of impression of Vickers hardness indentation in metal, made from measurements on a pair of stereographic pictures of the surface. Vertical step in the diagram is 0.7 μm.*

Effects of Chemical Composition

It has been known for many years by electron microprobe users that elements with high atomic numbers backscatter a greater fraction of incident electrons than do ones with low atomic numbers. Thus contrast in the backscattered electron image can be used to obtain qualitative information on the average atomic number distribution in a specimen. Figure 11 shows this effect and also a somewhat similar contrast in the secondary electron image. This latter effect arises for two reasons. First, the efficiency of production of secondary electrons also varies from element to element, but not in a simple way. It depends on the binding energies of the various orbital electrons and shows surprising variations both from one element to the next or with different chemical combinations for an element. Second, there is a lesser effect of indirect production of secondary electrons by backscattered electrons. Increased backscattered electron intensity due to atomic number differences will increase the production of secondary electrons near the surface.

Cathodoluminescence

Fortunately, there are better ways of examining the composition of specimens. One of these of particular interest to biologists and geologists is cathodoluminescence. Some compounds emit visible or near-visible light when bombarded with electrons. This light can be detected with a photomultiplier (through suitable filters, if desired), and the signal used to modulate the cathode-ray tube display. Figure 12 shows the use of this mode of operation for a polished specimen. The secondary electron image shows only the roughness of the surface, and the backscattered electron image shows some

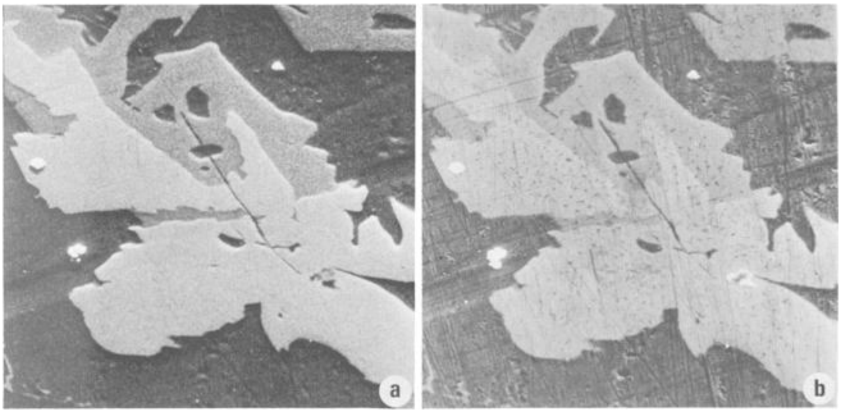

FIG. 11—*Polished cross section of Al-Mn alloy containing intermetallic phase and small tungsten carbides (×1400):* (a) *backscattered electron image;* (b) *secondary electron image.*

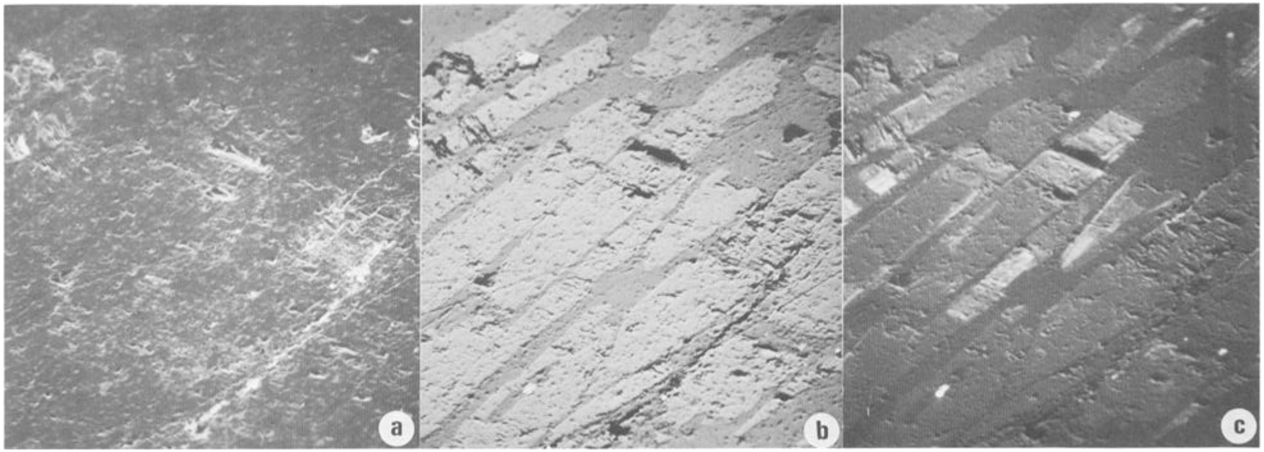

FIG. 12—*Cathodoluminescence image shows location of anhydrite in polished mineral specimen* (×*460*)*:* (a) *secondary electron image;* (b) *backscattered electron image;* (c) *cathodoluminescence image.*

contrast based on average atomic number differences. The cathodoluminescence image clearly shows the location of the fluorescing anhydrite phase.

X-ray Spectrometers

Even more precise identification of composition can, of course, be made by identifying the wavelengths or energies of the X-rays emitted from the specimen. In a conventional electron microprobe, which is similar in general principles of construction to a scanning microscope, this is accomplished by using one or more X-ray spectrometers with a crystal of known *d* spacing and a mechanism for moving it and a detector over a range of 2θ values [*4*]. Wavelength-dispersing spectrometers are now available for most SEM's.

Another type of detector particularly useful on the scanning microscope is the energy-dispersing type, consisting of a solid crystal detector and a multichannel analyzer [*5*]. The crystal detector can be placed close to the specimen to cover a large solid angle and collect many X-rays and is virtually 100 percent efficient for X-rays of aluminum and heavier elements. The use of this type detector is well suited, therefore, to the low probe currents of the SEM, and in general the attachment of such a detector does not limit the use of other features of the instrument. Since this type of spectrometer is very new and completely different from those used in conventional microprobe analysis, a description of the basic principle of operation is given below.

Figure 13 shows the spectrometer schematically. X-rays entering the lithium-drifted silicon semiconductor *p-i-n* device lose their energy by ionizing

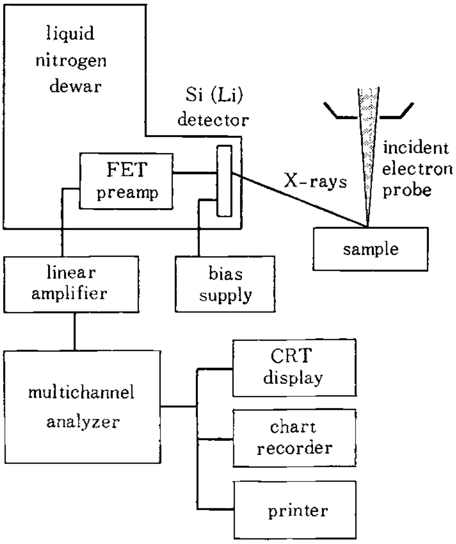

FIG. 13—*Schematic diagram of energy-dispersive X-ray spectrometer.*

the silicon in the broad depletion layer, creating electron-hole pairs. An applied bias voltage (typically 700 to 1000 V) collects the charge, and since each electron-hole pair requires 3.6 eV the total charge $Q = E/3.6 \times 1.6 \times 10^{-19}$ C is linearly proportional to E, the energy of the X-ray. A field-effect-transistor (FET) preamplifier integrates the charge into a current pulse which is amplified, converted to a voltage pulse, and fed to a multichannel pulse height analyzer. The diode and preamp are cooled with liquid nitrogen to stabilize the diode and reduce the dark current in the FET.

The analyzer sorts the pulses by height and counts the number of pulses in each energy band, producing an energy spectrum. It does this by using the voltage pulse to charge up a capacitor, and while the capacitor discharges it counts through the memory channels. When the discharge is complete the analyzer adds one to the count in whichever channel it has come to. Each X-ray is similarly processed so that a complete, simultaneous spectrum of all the emission peaks is obtained. The energy spectrum is linear and can be easily calibrated in terms of X-ray energy (for instance 50 or 100 eV per channel). It can be displayed on a cathode-ray tube, plotted on a recorder, or printed out numerically.

Since the spectrum obtained is in terms of X-ray energy rather than wavelength, it is necessary to think in terms of energy. Figure 14 shows the variation of the X-ray emission energies of the various electron transitions through the periodic table, and for reference purposes the table lists the X-ray emission energies up to 50 keV (maximum energy available in commercial scanning microscopes). The most efficient X-ray excitation is obtained with an excitation voltage at least twice the X-ray energy.

The light element detection limit is set by the difficulty of getting soft (low-energy) X-rays through the protective window and resolving them from zero energy (noise). At the present state of the art resolution (full width at half maximum) of the peaks is 250 eV or better, which would make it possible to do elements down to nitrogen. However, with a 1-mil-thick beryllium window virtually no nitrogen X-rays enter the diode. Oxygen and fluorine can be detected and elements from sodium and heavier are routine. Minimum detectable limits of about 0.1 percent or better are possible for most elements in the abscence of conflicting lines from other elements.

Electrical Effects

Another cause of contrast in the secondary electron image is the presence of voltages applied to various parts of a specimen. The early workers in the field, such as Everhart et al [*3*], considered the effect of the changes in the trajectories of the secondary electrons produced by the applied voltages. The change of trajectories with applied voltage would bring either more or fewer of the emitted electrons to the detector and produce a variation in the signal.

Kimoto [6] has since shown that a major cause of the contrast lies in the suppression of secondry electron emission in positively biased regions, independent of specimen arrangement. The other effect is the change of trajectories of secondary electrons between specimen and detector, and this depends strongly on the specimen orientation.

Figure 15 shows the contrast in an integrated circuit operated in the microscope. The applied voltages produce a voltage contrast that is useful for showing defects in fabrication or interactions between circuit elements. Voltage differences of as little as 0.1 V can be observed, and quantitative estimation of potential distribution is possible. No effect of applied voltages is seen, of course, in the backscattered electrons, since their energy is too great to be affected by small applied voltages.

Special Techniques

For *p-n* junctions or similar semiconductor devices it is possible to display the electromotive force produced across the junction by the passage of the incident electrons producing carriers. This mode is also called electron-beam-induced conductivity, since the carriers produced in the junction cause a local breakdown in the applied voltage. Figure 16 shows the location of the

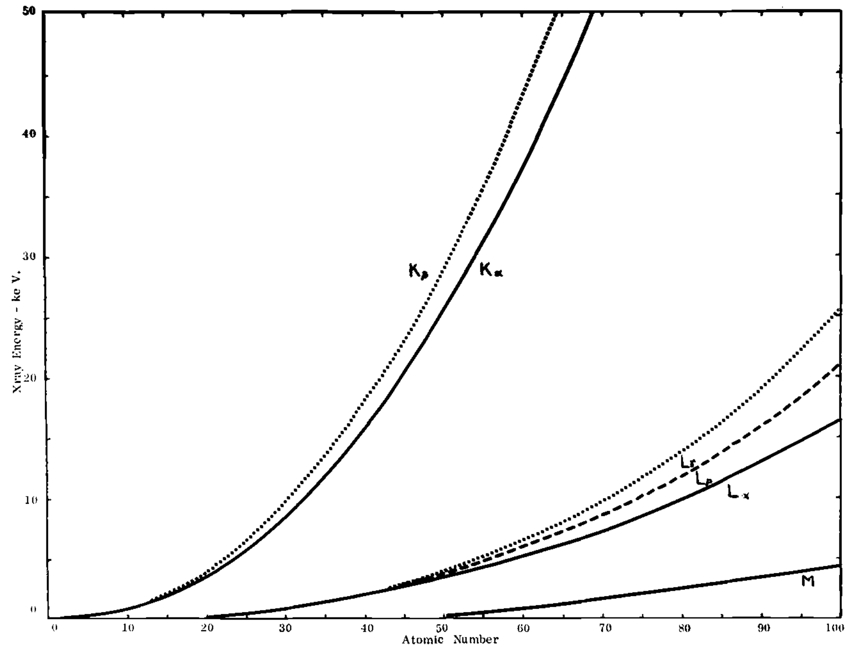

FIG. 14—*X-ray emission energies as a function of atomic number.*

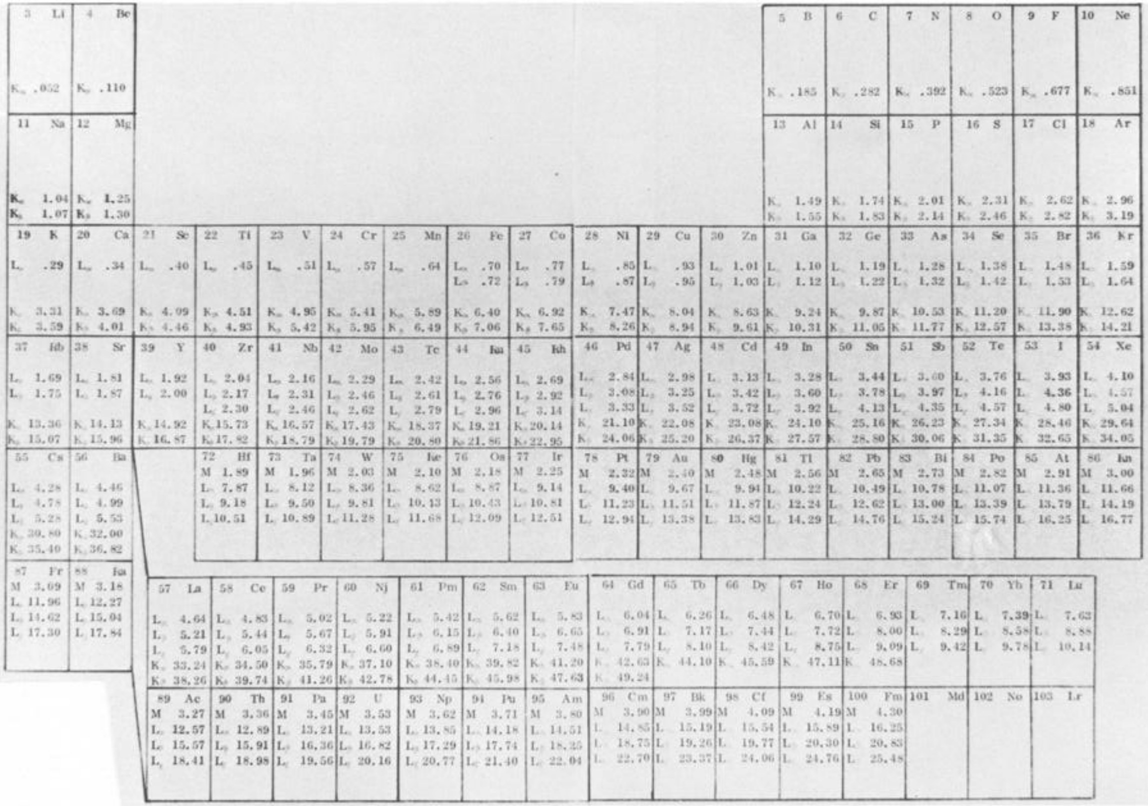

3 Li K .052	4 Be K .110											5 B K .185	6 C K .282	7 N K .392	8 O K .523	9 F K .677	10 Ne K .851
11 Na K 1.04 K 1.07	12 Mg K 1.25 K 1.30											13 Al K 1.49 K 1.55	14 Si K 1.74 K 1.83	15 P K 2.01 K 2.14	16 S K 2.31 K 2.46	17 Cl K 2.62 K 2.82	18 Ar K 2.96 K 3.19
19 K L .29 K 3.31 K 3.59	20 Ca L .34 K 3.69 K 4.01	21 Sc L .40 K 4.09 K 4.46	22 Ti L .45 K 4.51 K 4.93	23 V L .51 K 4.95 K 5.42	24 Cr L .57 K 5.41 K 5.95	25 Mn L .64 K 5.89 K 6.49	26 Fe L .70 L .72 K 6.40 K 7.06	27 Co L .77 L .79 K 6.92 K 7.65	28 Ni L .85 L .87 K 7.47 K 8.26	29 Cu L .93 L .95 K 8.04 K 8.94	30 Zn L 1.01 L 1.03 K 8.63 K 9.61	31 Ga L 1.10 L 1.12 K 9.24 K 10.31	32 Ge L 1.19 L 1.22 K 9.87 K 11.05	33 As L 1.28 L 1.32 K 10.53 K 11.77	34 Se L 1.38 L 1.42 K 11.20 K 12.57	35 Br L 1.48 L 1.53 K 11.90 K 13.38	36 Kr L 1.59 L 1.64 K 12.62 K 14.21
37 Rb L 1.69 L 1.75 K 13.36 K 15.07	38 Sr L 1.81 L 1.87 K 14.13 K 15.96	39 Y L 1.92 L 2.00 K 14.92 K 16.87	40 Zr L 2.04 L 2.17 L 2.30 K 15.73 K 17.82	41 Nb L 2.16 L 2.31 L 2.46 K 16.57 K 18.79	42 Mo L 2.29 L 2.46 L 2.62 K 17.43 K 19.79	43 Tc L 2.42 L 2.61 L 2.79 K 18.37 K 20.80	44 Ru L 2.56 L 2.76 L 2.96 K 19.21 K 21.86	45 Rh L 2.69 L 2.92 L 3.14 K 20.14 K 22.95	46 Pd L 2.84 L 3.08 L 3.33 K 21.10 K 24.06	47 Ag L 2.98 L 3.25 L 3.52 K 22.08 K 25.20	48 Cd L 3.13 L 3.42 L 3.72 K 23.08 K 26.37	49 In L 3.28 L 3.60 L 3.92 K 24.10 K 27.57	50 Sn L 3.44 L 3.78 L 4.13 K 25.16 K 28.80	51 Sb L 3.60 L 3.97 L 4.35 K 26.23 K 30.06	52 Te L 3.76 L 4.16 L 4.57 K 27.34 K 31.35	53 I L 3.93 L 4.36 L 4.80 K 28.46 K 32.65	54 Xe L 4.10 L 4.57 L 5.04 K 29.64 K 34.05
55 Cs L 4.28 L 4.78 L 5.28 K 30.80 K 35.40	56 Ba L 4.46 L 4.99 L 5.53 K 32.00 K 36.82		72 Hf M 1.89 L 7.87 L 9.18 L 10.51	73 Ta M 1.96 L 8.12 L 9.50 L 10.89	74 W M 2.03 L 8.36 L 9.81 L 11.28	75 Re M 2.10 L 8.62 L 10.13 L 11.68	76 Os M 2.18 L 8.87 L 10.43 L 12.09	77 Ir M 2.25 L 9.14 L 10.81 L 12.51	78 Pt M 2.32 L 9.40 L 11.23 L 12.94	79 Au M 2.40 L 9.67 L 11.51 L 13.38	80 Hg M 2.48 L 9.94 L 11.87 L 13.83	81 Tl M 2.56 L 10.22 L 12.24 L 14.29	82 Pb M 2.65 L 10.49 L 12.62 L 14.76	83 Bi M 2.73 L 10.78 L 13.00 L 15.24	84 Po M 2.82 L 11.07 L 13.39 L 15.74	85 At M 2.91 L 11.36 L 13.79 L 16.25	86 Rn M 3.00 L 11.66 L 14.19 L 16.77
87 Fr M 3.09 L 11.96 L 14.62 L 17.30	88 Ra M 3.18 L 12.27 L 15.04 L 17.84																

57 La L 4.64 L 5.21 L 5.79 K 33.24 K 38.26	58 Ce L 4.83 L 5.44 L 6.05 K 34.50 K 39.74	59 Pr L 5.02 L 5.67 L 6.32 K 35.79 K 41.26	60 Nd L 5.22 L 5.91 L 6.60 K 37.10 K 42.78	61 Pm L 5.42 L 6.15 L 6.89 K 38.40 K 44.45	62 Sm L 5.62 L 6.40 L 7.18 K 39.82 K 45.98	63 Eu L 5.83 L 6.65 L 7.48 K 41.20 K 47.63	64 Gd L 6.04 L 6.91 L 7.79 K 42.63 K 49.24	65 Tb L 6.26 L 7.17 L 8.10 K 44.10	66 Dy L 6.48 L 7.44 L 8.42 K 45.59	67 Ho L 6.70 L 7.72 L 8.75 K 47.11	68 Er L 6.93 L 8.00 L 9.09 K 48.68	69 Tm L 7.16 L 8.29 L 9.42	70 Yb L 7.39 L 8.58 L 9.78	71 Lu L 7.63 L 8.88 L 10.14
89 Ac M 3.27 L 12.57 L 15.57 L 18.41	90 Th M 3.36 L 12.89 L 15.91 L 18.98	91 Pa M 3.45 L 13.21 L 16.36 L 19.56	92 U M 3.53 L 13.53 L 16.82 L 20.16	93 Np M 3.62 L 13.85 L 17.29 L 20.77	94 Pu M 3.71 L 14.18 L 17.74 L 21.40	95 Am M 3.80 L 14.51 L 18.25 L 22.04	96 Cm M 3.90 L 14.85 L 18.75 L 22.70	97 Bk M 3.99 L 15.19 L 19.26 L 23.37	98 Cf M 4.09 L 15.54 L 19.77 L 24.06	99 Es M 4.19 L 15.89 L 20.30 L 24.76	100 Fm M 4.30 L 16.25 L 20.83 L 25.48	101 Md	102 No	103 Lr

FIG. 14 (Continued)—*Table of X-ray emission energies in keV.*

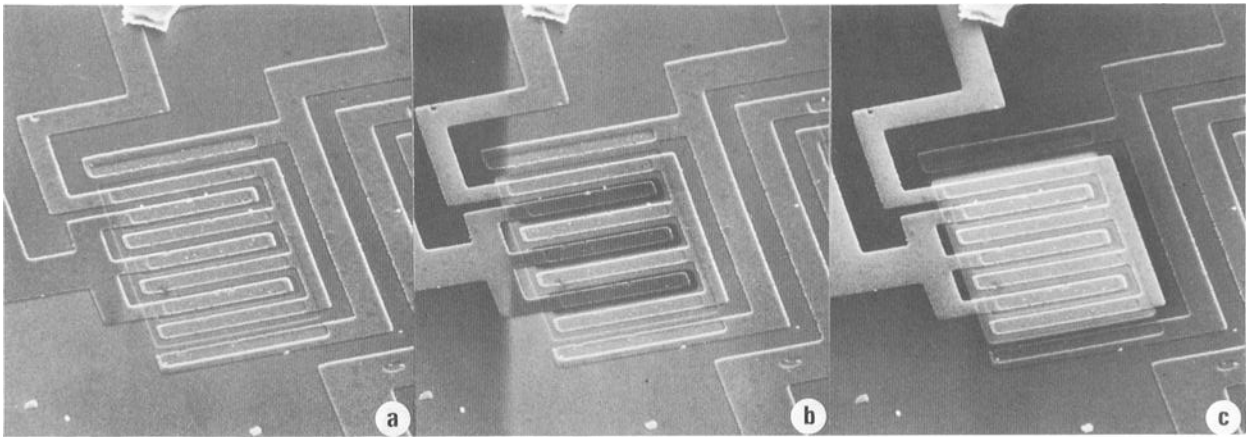

FIG. 15—*Voltage contrast in the secondary electron image of a semiconductor device to which bias voltages are applied while it is examined in the SEM* (×*170*): (a) *no bias applied;* (b) *emitter bias 5 V;* (c) *collector bias 20 V.*

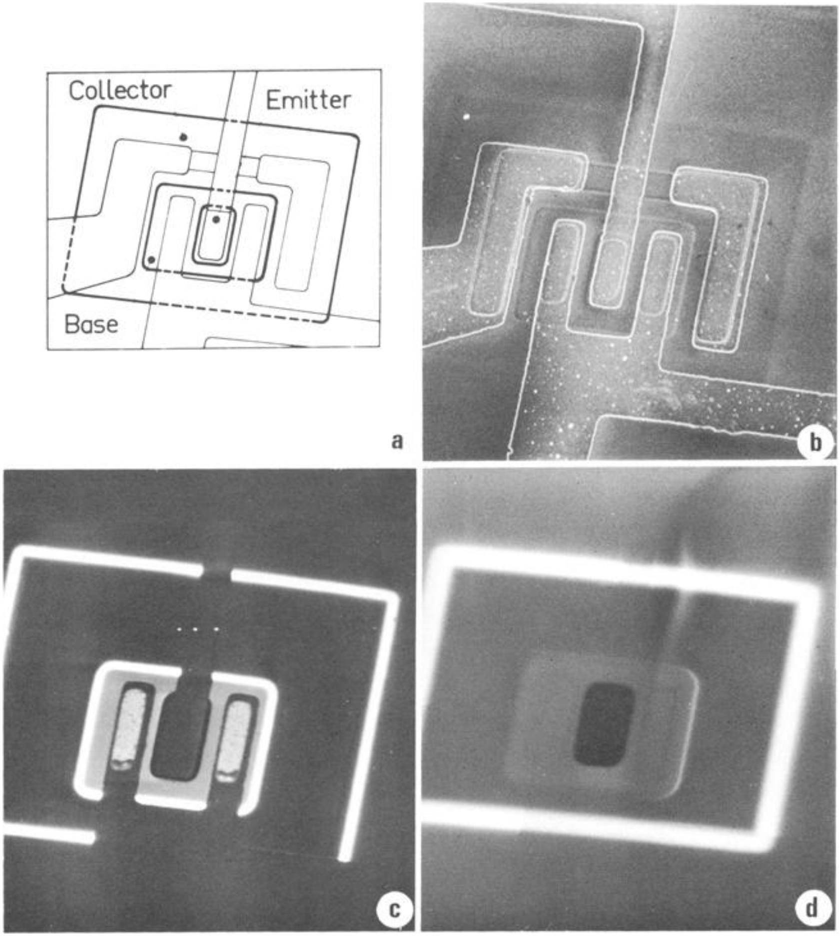

FIG. 16—*Use of electromotive force image to show collector-base junction and isolation junction in transistor. Note that the 10-kV picture* (c) *shows shadows of the connecting leads, which are fully penetrated at 25 kV:* (a) *diagram of transistor;* (b) *secondary electron image* (×*295);* (c) *electromotive force image, 10 kV;* (d) *electromotive force image, 25 kV.*

junctions in a transistor at various depths below the surface, achieved by varying the accelerating voltage of the incident probe and hence its depth of penetration.

There are also other specialized techniques developed for special purposes, including bias contour mapping of photoconductors [7] and mirror or retarding field biasing of the specimen to reveal surface defects in integrated circuits [*8*].

Transmitted Electron Image

Additional information on internal structure can be obtained with specimens thin enough to permit complete penetration of some of the incident electrons. By installing a scintillator and photomultiplier tube below the specimen, a transmitted electron signal can be detected and displayed on the cathode-ray tubes. Normally an aperture is used to reject any diffracted electrons and admit only those that penetrate in a direct line. It is also possible to do dark-field work by placing the aperture off center, deflecting the diffraction pattern, or using an annular aperture, as shown in Fig. 17.

The images that one obtains are similar in most respects to the images in a conventional transmission electron microscope. Figure 18 shows transmission micrographs of a biological thin section taken with the SEM and the TEM. The scanning electron microscope's transmission image has, first of all, much higher inherent contrast. This results partly from the nature of point-by-point examination, since electrons scattered from one point on the specimen cannot contribute to background at another point. Also, since the image is electronically amplified, the contrast can be controlled and enhanced as desired. This feature is quite useful for noncrystalline material where contrast in the TEM images is generally low. Another advantage for soft specimens is that the very low beam current (10^{-10} to 10^{-12} A compared to 10^{-5} to 10^{-7} A in the TEM) produces negligible specimen heating or damage.

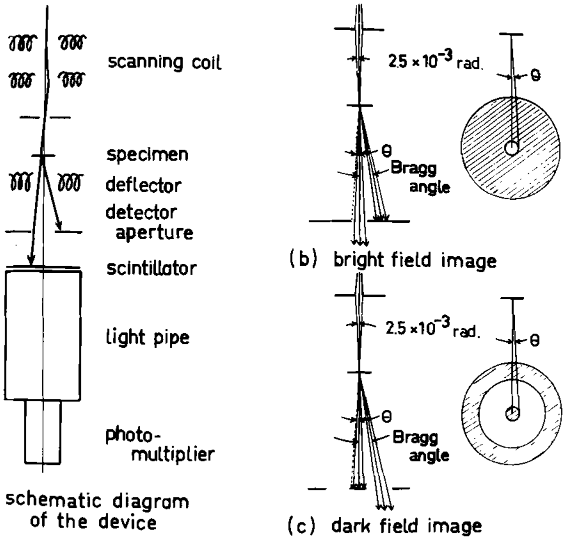

(a) schematic diagram of the device

(b) bright field image

(c) dark field image

FIG. 17—*Transmitted electron detector for the scanning electron microscope.*

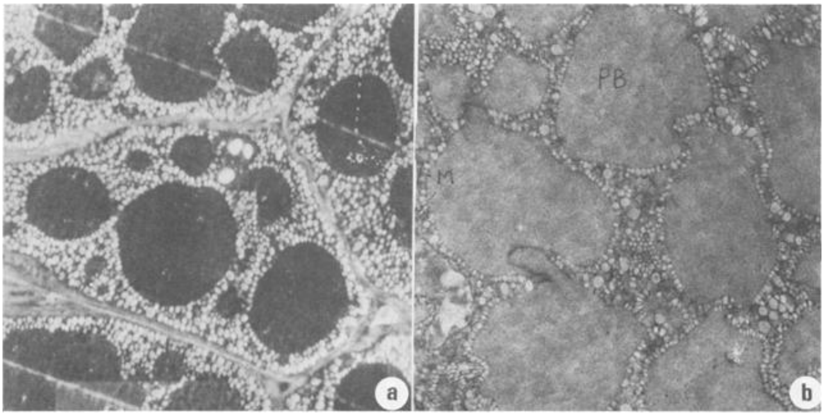

FIG. 18—*Transmission images with scanning electron microscope and conventional transmission electron microscope of same specimen of cotyledon cell of soybean seed:* (a) *with a scanning electron microscope* (×*190*); (b) *with a conventional electron microscope* (×*400*).

The transmission scanning electron microscope technique can also be used to some advantage for metal thin foil specimens. Figure 19 shows bright- and dark-field images of the same area of a crystalline specimen. The dark field image is obtained by offsetting the aperture to a diffracted beam, and this image covers exactly the same area as the bright-field image with no distortion or loss of resolution.

Also, the SEM transmission method can produce images of specimens from 2 to 5 times thicker than those used in a conventional TEM of the same accelerating voltage. The detector functions as an image intensifier to enhance

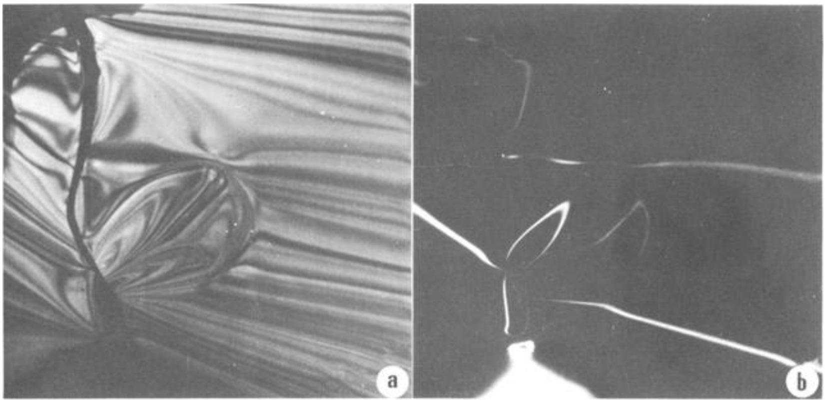

FIG. 19—(a) *bright- and* (b) *dark-field transmission scanning electron microscope images of a bend contour in a mica crystal* (×*1600*).

the brightness of even a very faint image. Image intensifiers in the TEM do not allow the use of very thick specimens, because in the TEM the electrons that penetrate through a thick specimen have lost varying amounts of energy due to scattering and are no longer monochromatic. The inherent chromatic aberrations of the electromagnetic image-forming lenses of the TEM then cause a loss of resolution that degrades the image.

In the SEM, however, no image-forming lenses are used, and image sharpness is not limited by these aberrations. The energy losses of the scattered electrons are not important, and image resolution is not impaired. The formation of the image without lenses also makes possible the distortion-free, dark-field technique discussed above, since spherical aberration is avoided.

In the transmission mode, the resolution of the SEM is the same as the diameter of the incident probe, generally under 100 Å. Better resolution is given by conventional transmission electron microscopes, which are now commercially available with a resolution down to 2 Å; but for relatively low-magnification work, up to ×20,000, the scanning electron microscope's advantages can be more important. The limit on resolution of secondary electron images discussed above does not apply in the case of transmission scanning electron microscope work, and it is possible to further improve resolution by reducing probe diameter without any limitation caused by spreading of the probe. (It is still necessary to reduce probe current, which requires longer counting to obtain an adequate signal-to-noise ratio.) Experimental work with instruments, such as that of A. V. Crewe [9] at the University of Chicago, has shown resolution of 3.4 Å in a transmission scanning electron microscope image.

Pseudo-Kikuchi Patterns

Another type of image particularly useful for the metallurgist is the psuedo-Kikuchi (or Coates) pattern that reveals crystallographic orientation. In the simplest case when a large single crystal is scanned by the beam, its angle of incidence varies from place to place, and internal diffraction takes place whenever a Bragg condition is satisfied. This causes a variation in the fraction of electrons that are absorbed or backscattered, as well as in the other signals generated by the impingement of the beam [*10*].

Figure 20 shows a backscattered electron image of the psuedo-Kikuchi pattern obtained with a large single crystal of silicon. In this image the important parameter is not distance of scan along the specimen but angle of incidence. This shows an extent of 3.5 deg from the central [111] pole (the surface of the crystal is normal to the [111] direction). Some of the various bands are identified with the planes that produced them.

A modified technique, called the rocking beam technique, can be used with specimens that are not single crystals to obtain selected area psuedo-Kikuchi

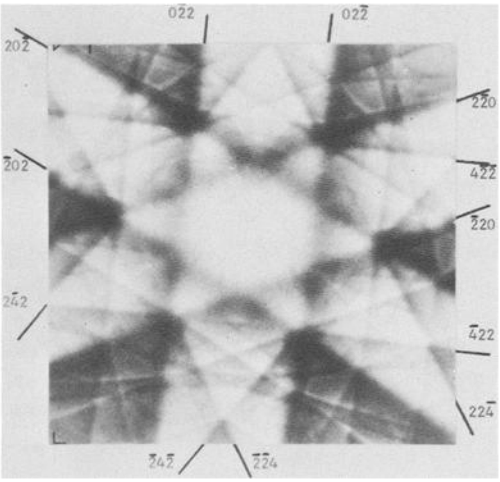

Fig. 20—*Pseudo-Kikuchi pattern from [111] orientation of silicon single crystal.*

patterns from grains as small as 1 μm in diameter. A supplementary deflection coil is used so that the angle of incidence of the beam can be varied while resting on a single point of the specimen. Using Kikuchi maps it is possible to identify the specimen's crystal structure and orientation.

Specimen Selection and Preparation

Specimens for the SEM must, of course, meet the usual criteria for any specimens in being representative and significant. Because the instrument can accommodate specimens up to several inches in size, and because of the wide range of magnification from very low to very high, it is practical to survey a large specimen area and zoom in on features of interest. This greatly relaxes the need for precise selection of specimens prior to examination, as is needed for instance with the TEM. And, of course, the usual requirements of cleanliness must be met—dust particles in particular can often be misinterpreted as fractures. Generally, cleaning with a gas jet or with solvent in a sonic cleaner is adequate.

Fractures, Worn and Corroded Surfaces

Surfaces that are very rough or very fragile can be mounted using conductive silver paint to provide an electrical contact to the stage. Then if the specimen itself is conductive, no further preparation may be necessary. Figure 21 shows an example of a metal fracture. For nonconducting specimens such as the plastic in Fig. 22 an electrical pathway to ground must be provided or the incident electron beam will quickly charge up the surface

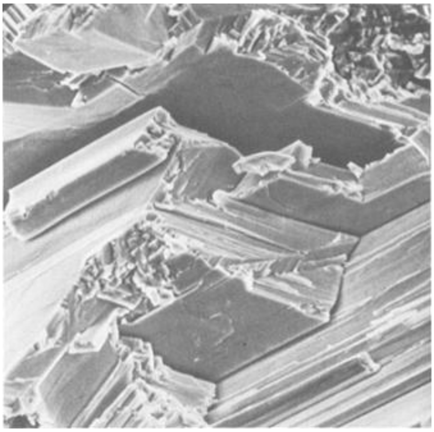

FIG. 21—*Cleavage fracture in zinc at −196 C (×540).*

to the full potential of the accelerating voltage, which will deflect the beam away and destroy the image. With specimens that conduct slightly, it is possible to overcome this problem by using a low (such as 5 kV) accelerating voltage and low beam current (such as 1 pA). Usually, however, it is necessary to apply a very thin conducting coating to the specimen. This is conveniently done by evaporating a thin layer of carbon or metal, which will be discussed in detail below. For some purposes the use of antistatic sprays is also practical [*11*], but these are useful only at low magnification because of the artifacts they introduce.

Coating is also sometimes useful on conducting specimens. The purpose is not to provide conductivity but either to produce a surface with better

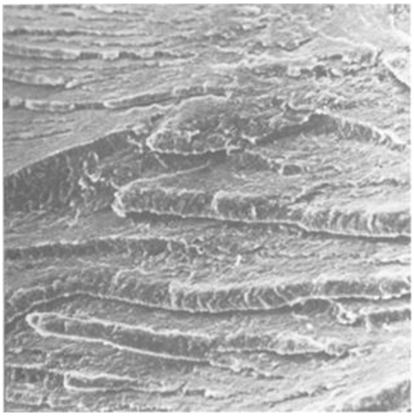

FIG. 22—*Fracture in high-impact polystyrene (×160).*

secondary electron emissitivity or to suppress the confusing effects of surface contaminants (oil, etc.) or internal structure (such as carbides just under a fracture surface which may appear as dark regions even though there is no surface depression).

Surfaces that are rough on a coarse scale and have many protrusions or edges, such as the crystal in Fig. 23, are best examined at relatively low accelerating voltages (say, 15 kV). The use of high voltages produces a finer incident beam but causes a larger capture volume which intersects the surface near the point of the protrusion or the sides of the ridges near the peak. The resulting image has relatively broad, bright lines at edges that obscure detail.

Metallographic Specimens

The SEM also offers a useful extension to the light-optical metallurgical microscope. Figure 24 shows a polished and etched surface of pearlite in steel at higher magnification and resolution than possible with the light microscope. Specimen preparation is generally the same as for the light microscope, except that the best etching practice may be different. For work with very small details and near edges a much lighter etch can be used because of the better resolution of the SEM. Also the composition contrast in the secondary electron image (possibly enhanced by using other images) sometimes permits examination of polished and unetched (or very slightly etched) surfaces, since the phases can still be recognized. On the other hand, the very large depth of field of the SEM makes it possible to keep very deeply etched surfaces in focus. Figure 25 is a cross section through a coating in which a deep etch was used to reveal the crystallinity of portions of the coating.

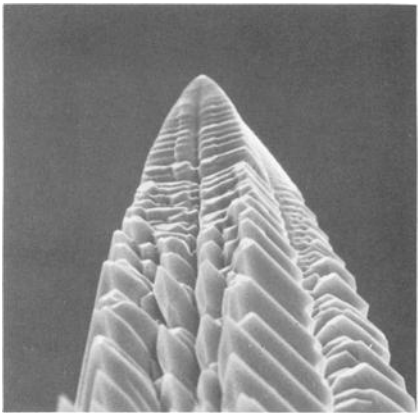

FIG. 23—*Surface of tungsten trioxide crystal showing growth on crystallographic planes* (×*1100*).

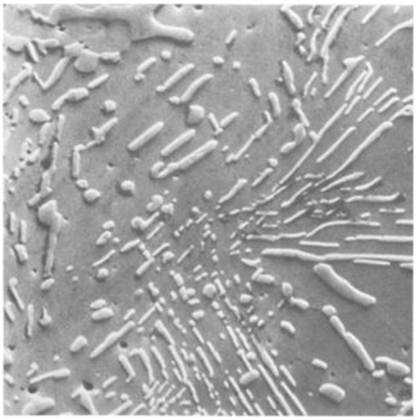

FIG. 24—*Microstructure of pearlite in steel* (×*1600*).

For very flat surfaces it is practical to use high accelerating voltages (such as 50 kV) to obtain the largest signal and best possible resolution and to tilt the specimen to about 30 deg to produce the optimum contrast.

Powders and Chips

Small particles are easily examined in the SEM, and again the easy change in magnification permits both surveys and close examination to be made. Mounting the particles is not always easy, however; sprinkling or dusting the powder onto double-sided sticky tape or a thin layer of glue on a specimen stub is commonly used, but sometimes the particles sink partially into the soft glue and cannot be seen in their entirety. Also, since the glues are generally nonconducting, it is usually necessary to coat the entire stub in an evaporator. Figure 26 shows peach pollen prepared in this way.

The first problem can be overcome by dispersing the particles in a fluid (water or alcohol) on a clean glass slide. As the fluid dries the particles adhere to the glass and produce a specimen quite suitable for examination after it has been cemented to a stub and coated. For powders that are electrically conducting, it is sometimes possible to avoid the need for coating the entire preparation by using glass slides previously coated with metal or by depositing the particles directly onto a copper or aluminum stub.

Soft Materials

Preparation procedures for fibers, polymers, or rubbers are usually identical to those for metals and other hard materials. For instance, the wool fiber in Fig. 27 was simply mounted in the silver paint and coated with metal. But for soft materials that contain volatile fluids, which would evaporate in the

FIG. 25—*Deeply etched cross section through zinc coating on sheet steel, showing crystalline structure of intermetallic compound.*

FIG. 26—*Peach pollen mounted with double-sided tape, showing tendency to sink into the adhesive.*

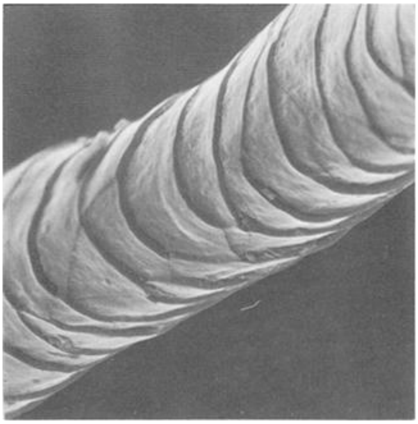

FIG. 27—*Wool fiber, being a natural hair, has growth scales that make it itchy* (×*650*).

vacuum of the SEM, techniques must be borrowed from the biological sciences. If the structure of the specimen is sufficiently rigid, the fluid can be removed by evaporation without concern; but, if the specimen collapses when the fluid is removed, other steps are necessary. The techniques of chemical fixation to strengthen the structure, freeze drying to remove the water without collapse, or replacement of the water with a hardenable resin are all useful in various situations.

Coating

For many of the types discussed above, the step of coating the specimen surface with a thin layer of metal was mentioned. This is conveniently done in a vacuum evaporator, using readily available metal chips or wire. Metal coatings of gold, 90 percent gold—10 percent palladium, or 60 percent gold—40 percent palladium are the most widely used. Other metals such as chromium, copper, silver, iron, and aluminum have been used slightly but are generally less satisfactory, either because they tend to evaporate nonuniformly or to develop a surface structure or because they are not as good emitters of secondary electrons as gold and palladium. The use of carbon by itself is generally unsatisfactory for the latter reason, although it is sometimes useful to apply a very thin (50 Å) layer of carbon followed by gold-palladium. This apparently improves the coating by promoting surface diffusion and adhesion (by matching coefficients of thermal expansion) and is especially useful for soft materials where uniform coatings are otherwise sometimes difficult to obtain.

Because the specimens examined in the SEM are often quite rough, they must be rotated and tilted through a wide range of angles in the evaporator to achieve a uniform coating. This is generally easier and more reliable than using multiple evaporation sources with either a fixed or rotating specimen, although these techniques have also been used. Shadowing from a low angle can sometimes be used to accentuate small ridges. This is especially useful for wear marks on metal surfaces.

The coating thickness must, of course, be thick enough to provide conductivity and thin enough that so the surface contours are not changed or any structure developed in the coating that can be confused with structure in the specimen. These criteria restrict the coating from 50 to about 1000 Å, and 100 to 500 Å is generally a desirable range. The thickness can be judged by the discoloration of the specimen or of a control surface, but this requires prior calibration and considerable operator skill. A better method is to use a known amount of material at the source calculated to produce the desired thickness of coating on the specimen.

Figure 28 is a nomograph used to simplify the calculation. The dashed lines show an example of its use. For a desired coating thickness of 200 Å and

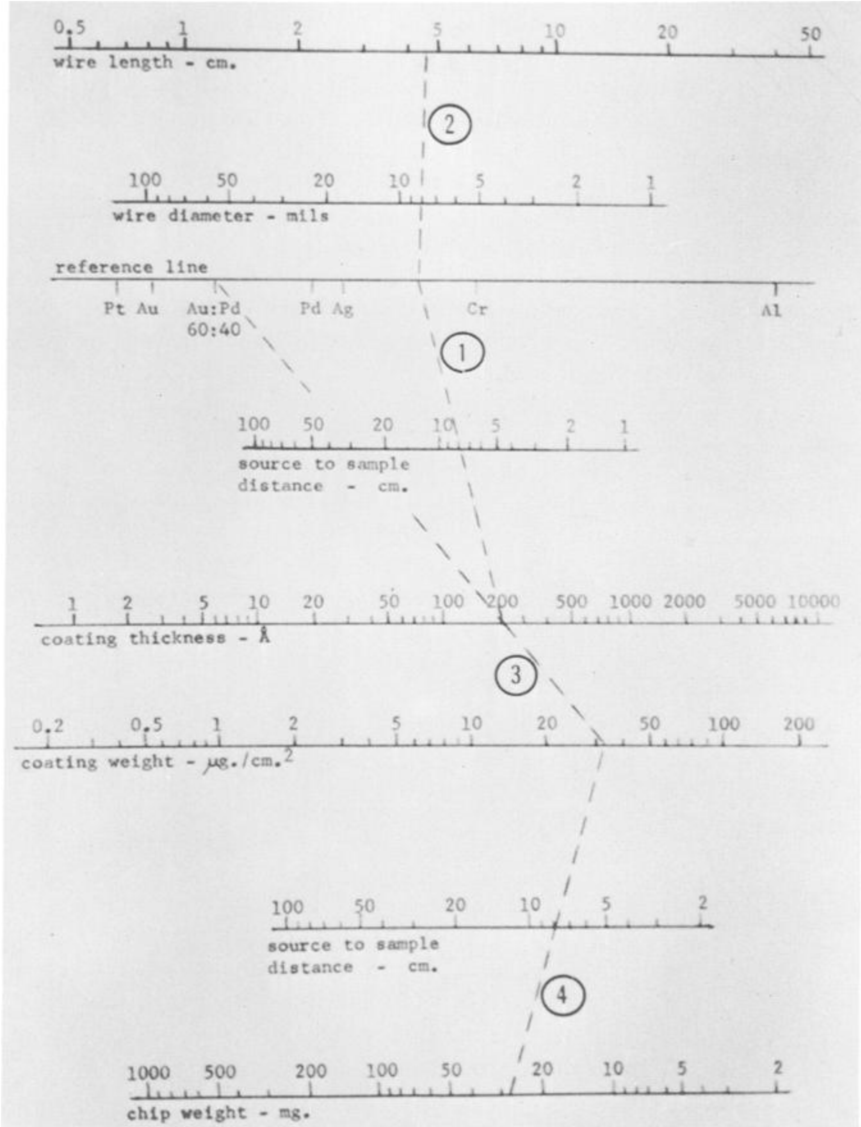

FIG. 28—*Nomograph for calculating coating weight and thickness.*

source-to-specimen distance in the evaporator of 8 cm we draw dashed line *1*, locating a point on the reference line. From this point we draw dashed line *2*, which shows that for a wire diameter of 8 mils we should use a 4.6-cm length of wire. No use is made of the alloy designations on the reference line.

Alternatively, if instead of using wire we are using chips, we must work with chip weight. We convert coating thickness to coating weight by drawing dashed line *3* from the point on the reference line corresponding to the alloy used— in this example 60Au-40Pd. This shows that a 200-Å coating of this alloy weighs 0.032 mg/cm^2. Dashed line *4* shows that for an 8-cm source-to-specimen distance we require a chip weight of 27 mg.

This nomograph is based strictly on geometrical considerations and overlooks any effect of surface diffusion of the coating or roughness of the specimen. It is wise to increase the amount of source material when coating a very rough surface to obtain the same desired coating thickness, since the rough surface will have more surface area than its plane projection.

There is some evidence that specimens should be examined as soon as possible after coating for the best results and that the quality of the results deteriorates gradually with time. The extent to which this depends on storage conditions is not known.

Interpreting the Image

Fractures

The rapidly growing use of the SEM for fracture examination takes advantage of the ease of specimen preparation in comparison to replica techniques for the TEM. In addition, it overcomes many of the limitations of the replica techniques: the difficulty of stripping the replica from rough surfaces and its tendency to break up at edges and ridges; the obscuring of part of the image by the supporting grid; the collapse of secondary cracks and general sag of elevations so that quantitative stereoscopy is impractical; the shift of position of extracted particles; the artifacts introduced in each step of making the replica; the impossibility of reaching multiply connected regions of the surface; and, finally, the impossibility of achieving a low-magnification image to permit survey work and location of features of interest.

Fortunately the information on fractography of various materials under a variety of conditions compiled using replica techniques is easily transferred and used for SEM fractography. The SEM images are easily interpretable and quite similar to TEM replica pictures [*12*]. The SEM has opened up, in addition, the possibility of examining many kinds of fracture surfaces previously not possible. Figure 29 shows a fracture of composite material that is not replicable because of its extreme roughness.

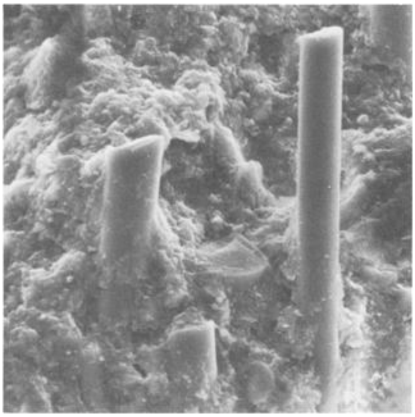

FIG. 29—*Fracture in glass-fiber-reinforced epoxy composite* (×*460*).

Considerable use of stereopairs should be made for any quantitative fractography to correct for the foreshortening of tilted surfaces. The technique of changing the raster pattern from a square to a trapezoid (*not* a rectangle, since one end of the tilted surface is farther from the lens) to compensate for foreshortening is not applicable to rough surfaces, because, even if the exact local tilt angle were known, the resulting distortion of protrusions and intrusions on the surface would greatly increase the difficulty of interpretation. Besides the usual stereopair technique of taking two photographs and examining them in a viewer, other techniques are available that make use of the TV display of the SEM. One records the two stereoimages on videotape and plays them simultaneously on the blue and red phosphors of a color TV. They can then be viewed directly through colored glasses [*13*].

Metallographic Specimens

The SEM image of a metallographically polished and etched specimen can be interpreted similarly to that obtained at lower resolution in a light microscope. The use of other display modes (such as X-ray) can give additional information. The appearance of the secondary electron image in the SEM is generally like that of oblique lighting in the light microscope because of the location of the detector at one side of the column. This is sometimes an aid in revealing fine structure, since it shows polishing or etching relief quite well.

Powders and Chips

Because the SEM image can be directly computer processed as a flying spot image, it is possible to use it for particle size measurements, counting, and other quantitative metallographic investigations. For polished specimens the same programs can be used as in light microscopy. However, powders introduce considerable additional complexity. Sophisticated pattern-recognition computer programs are required to recognize three-dimensional particles of any but the simplest shapes, even when stereopairs are used, and piles of particles in which some are partially hidden are nearly impossible to count. By preparing a well-dispersed sample of particles it is relatively easy to count and size them. It is sometimes advantageous to put the particles on a conducting surface and use the specimen current image which shows black silhouettes of the particles.

X-ray Data

For quantitative and semiquantitative analyses using wavelength-dispersive spectrometers, the extensive literature in the field of microprobe analysis can be used directly for SEM work [*14*]. The relatively new energy-dispersive spectrometers have been used to some extent for quantitative analysis and certainly will be more in the future because of their speed of data collection [*15*]. In the SEM their greatest contribution is the speed of obtaining qualitative analysis.

X-ray information can be presented in any of three ways with either type of spectrometer. The complete analysis of a simple point is obtained by positioning the beam using the secondary electron image as a reference and letting it remain in one place while a spectrum is obtained. For this work the speed of the energy-dispersive spectrometer is preferred, except for light element work where it is not suitable. Figure 30 shows an example. Another mode of

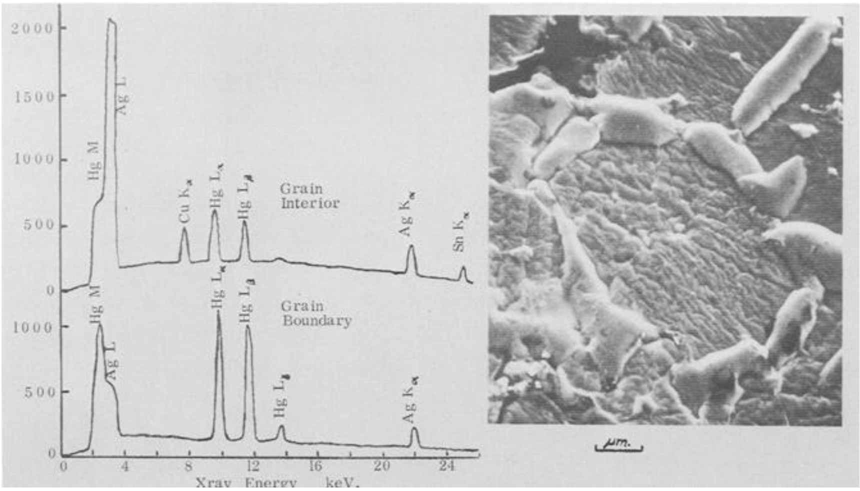

FIG. 30—*Point X-ray analyses of dental amalgam showing segregation of mercury to grain boundaries by application of pressure.*

operation is to set the spectrometer for a single element and measure its concentration along a line as the beam traverses the specimen. The wavelength-dispersive spectrometer's superior resolution is well suited for this. Finally, for qualitative work, the output of the spectrometer can be fed to the CRT display to produce for one element at a time an X-ray distribution image (Fig. 31). The superior resolution of the wavelength-dispersive spectrometer is balanced by the ease of setting a window with the energy-dispersive spectrometer, and both types work very well.

Transmission Scanning Microscopy

In most respects the transmission image in the SEM is identical to that in the TEM. The same types of contrast, including diffraction and phase contrast, are present, and both bright-field and dark-field examinations can be made. One exception is the use of contrast-stop, or strioscopic, dark-field images in which the direct beam is stopped and *all* of the diffracted beams are used to form the image. Very little work with this technique has been done with the TEM [*16*]. For amorphous structures this produces improved contrast, and for metal foils the interaction of the many beams can give useful information (for instance, about the strain field around a dislocation). Much more work is needed on the interpretation of these images.

Other Display Modes

One display mode that is used very little and widely misunderstood is deflection modulation (or y modulation). In this mode the signal is used not to control the brightness of the CRT but to deflect the beam vertically, producing a series of lines that blend to form an image. Unfortunately, the line scans are not surface contours of the specimen but merely the strength of the secondary electron signal, which is related in a very complicated and nonlinear way to surface slope (not elevation). The contrast in the image that is formed is caused by the decrease in brightness of the cathode-ray tube when the beam is being deflected vertically, so an approximation of the first derivative of the signal is obtained, but with unavoidable distortion.

It is preferable to produce an electronically differentiated signal and to display this by the normal intensity modulation display mode. The differentiated signal is useful for revealing fine detail in relatively flat surfaces or for enhancing the sharpness of edges and lines, as in psuedo-Kikuchi patterns. It does not, however, contain any more information than the normal image.

Process Stages

With the development of the rapid scanning television display, the SEM is capable of showing changes that occur in the specimen as it undergoes various processes [*17*]. To achieve this rapid display (30 frames per second)

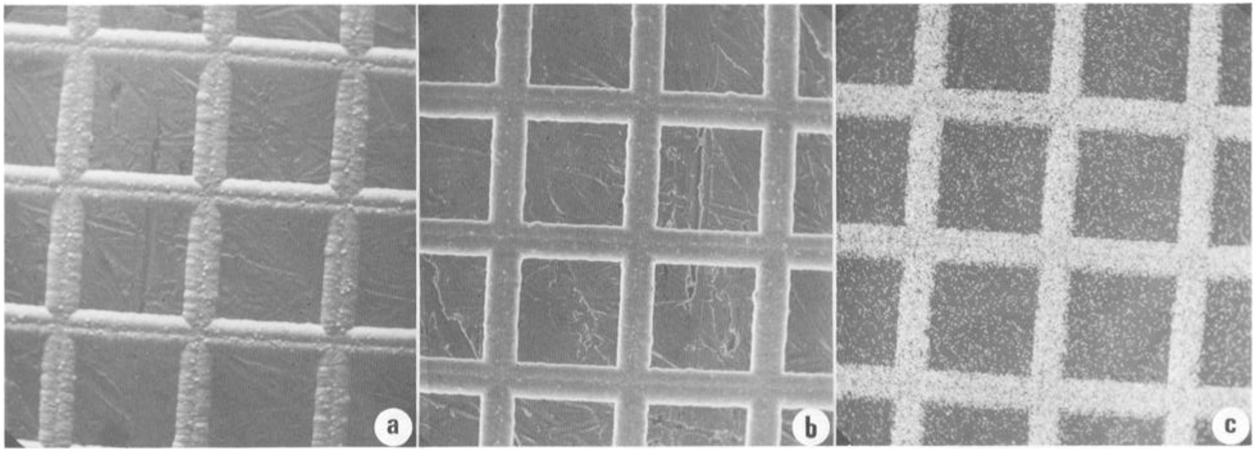

FIG. 31—*Nickel grid on a copper stub, showing nickel X-ray image in comparison to secondary and backscattered electron images:* (a) *backscattered electron image;* (b) *secondary electron image;* (c) *nickel X-ray image.*

it is necessary to use a secondary electron detector with a rapid response rate and a wide-band video amplifier, as well as specially modified scanning coils. Also, the beam current must be increased to obtain an adequate signal-to-noise ratio in the image, which increases the beam diameter and degrades the resolution somewhat so that the maximum useful magnification is about 10,000.

Using the TV display and a standard video tape recorder, shown schematically in Fig. 32, dynamic changes taking place in the specimen can be observed in real time, recorded, and played back in slow or stop action for careful examination. The process stages available for the SEM include ones that heat, cool, or strain the specimen, manipulators to work inside the vacuum chamber and gas reaction devices.

The heating and cooling stages facilitate the study of thermal expansion and contraction and phase transformations, including the study of molten metals. The temperature range available is from about liquid nitrogen temperature to 1100 C. This upper limit is not a design limit but is imposed by the thermal electrons emitted from the specimen; below 1100 C the thermal electrons have less energy than the secondary electrons and can be separated from the signal by a biased grid, while above 1100 C they have equal or greater energy and cannot.

Tensile stages that can apply loads up to 200 kg can be used to strain or fracture specimens of metal or fibers of plastics and textiles. Cracks can also be propagated cyclically to study fatigue. A manipulator can be used to scratch or cut materials and observe, for instance, the mechanics of chip formation. It is also useful for positioning a lead for voltage measurements in integrated circuits or for adjusting a mechanism while it is running. We have, for example, wound a watch (case removed) and observed the effect of dust particles and bearing eccentricity as the watch ran.

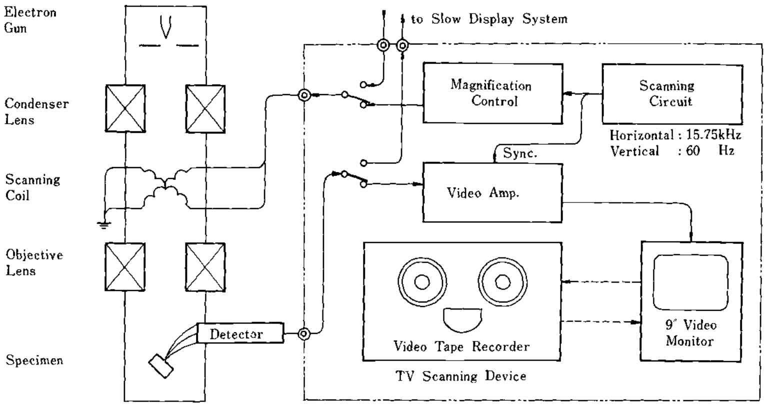

FIG. 32—*Schematic diagram of real-time TV scanning device.*

Gas reaction stages can be used to corrode specimens while observing the formation of the corrosion product (this can be combined, of course, with X-ray analysis of its composition). Similarly, ion guns can be used to bombard the specimen and erode its surface to uncover underlying structure.

All these process stages combine with the many types of information available in the SEM to make it an instrument of unparalleled versatility for the materials scientist.

References

[*1*] Oatley, C. W., Nixon, W. C. and Pease, R. F. W., *Advances in Electronics and Electron Physics*, AEERA, Vol. 21, Academic Press, N. Y., 1965, pp. 181–247.

[*2*] Kimoto, S. and Russ, J. C., *Materials Research and Standards*, MTRSA, Vol. 9, Jan. 1969, pp. 8–16.

[*3*] Everhart, T. E., Wells, O. C. and Oatley, C. W., *Journal of Electronics and Control*, JELCA, Vol. 7, 1959, pp. 97–111.

[*4*] *X-ray Emission Line Wavelengths and Two-Theta Tables, ASTM DS 37*, American Society Testing and Materials, 1965.

[*5*] Russ, J. C. and Kabaya, A., "Use of a Nondispersive X-ray Spectrometer on the Scanning Electron Microscope," Proceedings of the Second SEM Symposium, IITRI, Chicago, May 1969, pp. 57–64.

[*6*] Kimoto, S., Hashimoto, H. and Mase, K., "Voltage Contrast in Scanning Electron Microscopy," Fourth European Regional Conference on Electron Microscopy, Rome, Sept. 1968.

[*7*] Ritchie, M. H., Drew, C. M., Rose, J. H., Sulway, D. V. and Thornton, P. R., "An Experimental Technique to Investigate the Structure, Composition, and Electrical Properties of Chemically Deposited Lead Sulfide Detectors," Proceedings of the Second SEM Symposium, IITRI, Chicago, May 1969, pp. 415–424.

[*8*] Ogilvie, R. E., Schippirt, M. A., Moll, S. H. and Koffman, D. M., "Scanning Electron Mirror Microscopy," Proceedings of the Second SEM Symposium, IITRI, Chicago, May 1969, pp. 425–430.

[*9*] Crewe, A. V., "The Potentials of Scanning Microscopy," Proceedings of the Electron Microscope Society of America, Vol. 26, 1968, p. 352.

[*10*] Coates, D. G., "Psuedo-Kikuchi Orientation Analysis in the Scanning Electron Microscope," Proceedings of the Second SEM Symposium, IITRI, Chicago, May 1969, pp. 29–40.

[*11*] Boult, E. H. and Brabazon, E. J., *Journal of Scientific Instruments*, JSINA, Series 2, Vol. 1, 1968, pp. 565–566.

[*12*] Russ, J. C., "Modern Methods for Fracture Analysis," ASM Spring Lecture Series, General Motors Inst., Flint, Mich., March 1969.

[*13*] Eichen, E., Fitchmun, D. R. and Sefton, L. R., "Interpretation of Micrographs from a Scanning Electron Microscope," Proceedings of the Electron Microscope Society of America, Vol. 27, Aug. 1969, pp. 22–23.

[*14*] "Quantitative Electron Probe Microanalysis," Special Publication 298, National Bureau of Standards, K. F. J. Heinrich, Ed., Oct. 1968.

[*15*] Myklebust, R. L. and Heinrich, K. F. J., "Qualitative and Semiquantitative Analysis with Nondispersive X-ray Detectors," Proceedings of the Fourth National Conference on Electron Microprobe Analysis, Pasadena, Calif., 1969, p. 52.

[*16*] Dupouy, G. and Perrier, F., "Amelioration du Contraste en Microscopie Electronique," Sixth International Congress for Electron Microscopy, Kyoto, 1966, pp. 3–4.

[*17*] Kimoto, S., Sato, M. and Adachi, T., "The TV Scanning Device in a Scanning Electron Microscope and Its Application," Proceedings of the Second SEM Symposium, IITRI, Chicago, May 1969, pp. 65–72.

R. A. Rege,[1] *W. D. Forgeng, Jr.,*[1] *D. H. Stone,*[1]
and J. V. Alger[1]

Microcleanliness of Steel—A New Quantitative TV Rating Method

---

REFERENCE: Rege, R. A., Forgeng, W. D., Jr., Stone, D. H. and Alger, J. V., "**Microcleanliness of Steel—A New Quantitative TV Rating Method,**" *Applications of Modern Metallographic Techniques, ASTM STP 480,* American Society for Testing and Materials, 1970, pp. 249–272.

ABSTRACT: A general method for the rating of nonmetallic inclusions in steel by use of a quantitative television microscope (QTM) has been developed. The discussion of the method includes a special automatic specimen preparation procedure and a simplified statistical test to indicate the reliability and precision of the data. Information obtained with the QTM consists of area fraction of inclusions, number of inclusions, and distribution of inclusion lengths. These QTM parameters, or the values derived therefrom, have been used to express the overall inclusion rating for steel products and for comparison with standard rating methods. Steels have been ranked according to cleanliness by values derived from the QTM method similar to the ranking by values derived from inclusion rating methods described in ASTM Designation E 45. The QTM method has been shown to be versatile and to improve reproducibility by eliminating most of the variation due to human judgment.

KEY WORDS: inclusions, metallography, metallurgical analysis, ratings, steels, specifications, optical microscopes, television systems, evaluation, tests

At present, the standard methods of rating nonmetallics in steel, such as Methods A, B, and C of ASTM Recommended Practice for Determining the Inclusion Content of Steel (E 45 - 63), are intended to be applied to semifinished or other heavy products (large bars, billets, slabs). These methods generally involve an approximate measurement of inclusion lengths or comparison of the observed inclusion distribution with standard charts that represent a variation in the number and size of inclusions (from very few small inclusions to several such inclusions or to larger inclusions). Adaptation of these standard metallographic methods to finished products has been

---

[1] Senior research engineer, associate research consultant, research engineer, and section supervisor, respectively, Applied Research Laboratory, United States Steel Corp., Monroeville, Pa. 15146. Messrs. Forgeng and Alger are personal members ASTM.

attempted but usually without success, particularly for such light products as sheet, strip, and wire. Therefore, a strong need exists for a new method for determining the inclusion content of steel—one that is designed to fit the product, particularly the product in the final size at which it is to be used. In addition, a rating technique is needed that will make use of the many capabilities of the automatic instruments now becoming available for microstructural evaluation.

Present metallographic methods for inclusion rating are deficient in many other ways besides the product size limitation. The use of the optical microscope to obtain inclusion ratings necessitates considerable interpretation on the part of the observer. Consequently, the accuracy, reproducibility, and speed of the method are highly dependent on the observer's skill and experience. Furthermore, the type of information that is gathered for each standard rating technique differs sufficiently from that for each other technique to make comparison among ratings difficult. Finally, the standard rating magnification of 100 not only limits the standard techniques to the evaluation of heavy products but also makes it extremely difficult to compare steels intended for applications where ultraclean microstructures are required.

Automatic quantitative measurement systems are finding increasing acceptance in Europe for the assessment of inclusion content in steel [*1–3*].[2] Many European investigators are strongly convinced that comparative metallographic, inclusion rating methods should be discontinued in favor of quantitative instrumental methods. In the United States, however, much more knowledge and experience must be obtained in the use of such instrumental methods before they are accepted, even as supplements to comparative rating methods such as ASTM E 45.

The present investigation is based on the use of the quantitative television microscope (QTM) as an instrumental method of inclusion assessment. The authors show how this method can be used to supplement or replace the accepted metallographic comparative methods in which the optical microscope is used. This paper is concerned specifically with (1) a description of the QTM, its use and reliability, (2) a description of the special methods used to prepare metallographic specimens for QTM analysis, (3) statistics of sampling and analysis of data, (4) suggestions about the type of data to record, and (5) a comparison of the QTM and standard ratings to illustrate the use of QTM data in making quality comparisons.

Description of the QTM

The QTM system consists of a metallurgical optical microscope, a closed-circuit television system, and an image-analyzing circuit (Fig. 1). A low-power attachment of about 3 to 15 magnification (epidiascope) can replace

---

[2] Italic numbers in brackets refer to the list of references at the end of this paper.

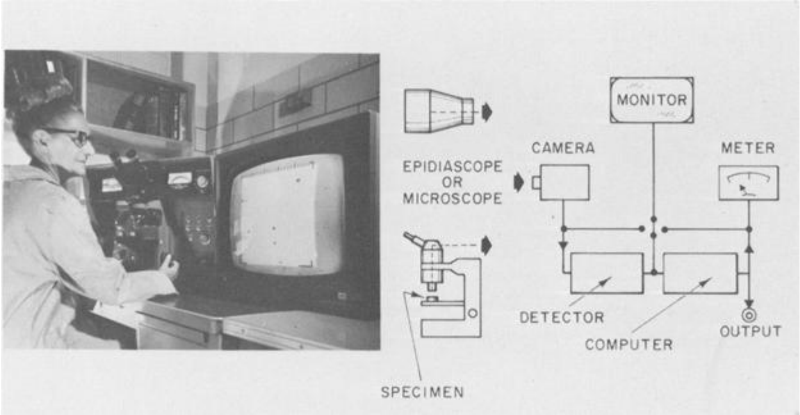

FIG. 1—*Quantitative television microscope.*

the microscope for the examination and measurement of features on charts, photographic prints, transparencies, or macrospecimens. The detector of the image-analyzing circuit discriminates and selects for measurement the desired features, such as inclusions, on the basis of a threshold intensity setting. The features selected may be either lighter or, for inclusions, darker than the general background. Detection and measurement are accomplished within a preset reference area (blank frame) on the monitor screen, which can be varied in size up to about 10 by 10 in. (25 by 25 cm). Signals from the features to be measured can be fed to the monitor for display, so that the operator can readily observe the objects being measured, and into the computer of the image-analyzing circuit. The computer is capable of determining the number, the total projected height, the area, or the size distribution of the features.

For a more complete description of the QTM and its capabilities for microstructural measurements other than inclusion content, the reader is referred to recent papers by Ratz [*4*] and Langhoff and Johnson [*5*].

Specimen Preparation for QTM Analysis

Experience at the U.S. Steel Applied Research Laboratory has shown that a single operator can rate about 30 specimens in an 8-h day when obtaining inclusion area, number, and selected length information on each field of 50 fields per specimen. Devices for automated movement of the microscope stage and for data printout are now available for the QTM, and these should greatly increase the number of specimens that can be rated in the same amount of time.

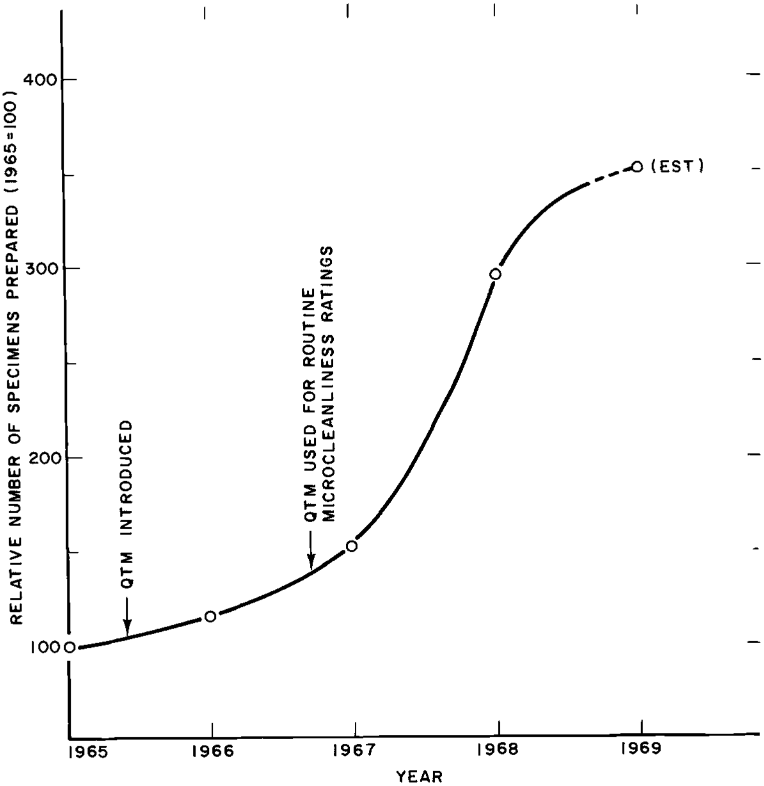

FIG. 2—*Effect of QTM on metallographic laboratory work load.*

The use of the QTM at our laboratory has increased metallographic laboratory output considerably, as evidenced by Fig. 2, which shows that the number of specimens prepared has nearly tripled since the QTM was first installed about three years ago. Obviously, to make full use of the ability of the QTM to rate these large numbers of specimens, some form of automatic specimen preparation is necessary.

The automatic grinding and polishing equipment used at the laboratory is commercially available. The technique developed by the laboratory to prepare specimens for QTM examination is summarized in Table 1. Specimens are surface ground before mounting. Specimens from slabs, billets, or plates are mounted individually in bakelite; several specimens from sheet, rod, or wire can be mounted in the same mounting. The parallel surfaces on the bakelite mount as it comes from the mounting press facilitate the automatic polishing step; the mounted specimens are therefore transferred directly to the automatic grinding apparatus without further hand grinding. The specimens are automatically ground, in successive stages with 240 to 600-grit

TABLE 1—*Specimen preparation for QTM inclusion assessment.*

Preparation Step	Remarks
1. Surface grind	Before mounting to facilitate automatic polishing, use about 120-grit finish.
2. Mount	Bakelite—1, 1¼, or 1½-in. mount; do not grind by hand after mounting.
3. Automatic grind	Start with 240-grit silicon carbide papers and repeat until all prior grinding marks are removed. Continue with 320, 400, and 600-grit papers, with 3 to 5 min per grind. Wash thoroughly with soap and water between grinds.
4. Automatic polish	
a) 3-μm diamond paste on microcloth.	Alcohol-glycol lubricant, alcohol cotton swab wash, alcohol rinse and dry.
b) 1-μm diamond paste on microcloth.	Alcohol-glycol lubricant, alcohol cotton swab wash, alcohol rinse and dry.
5. Touch-up polish	By hand on ¼-μm diamond paste if necessary; alcohol rinse and dry.

silicon carbide papers, in holders accommodating three, five, or six mounts, for 3 to 5 min in each stage. The best results are obtained when mounts containing steels with similar hardnesses are ground simultaneously. Each grinding step is repeated until all previous grinding marks are removed, and the specimens are given a thorough soap-and-water washing between papers, particularly after the final 600-grit paper. From the grinding papers the specimens are transferred in their holder to a microcloth polishing wheel charged with 3-μm diamond paste and wetted with an alcohol-glycol lubricant. Automatic polishing on the 3-μm diamond wheel is followed by careful cleaning with absolute methyl alcohol on a cotton swab and automatic polishing with 1-μm diamond on microcloth. During the 3 and 1-μm polishing it is imperative that no water be used. After 1-μm polishing the specimens are swabbed and rinsed with alcohol and dried. The specimens are examined under the microscope in the polisher holder, and if further polishing is necessary the specimens are returned to the appropriate stage in the polishing operation. If the specimens require no further polishing, they are removed from the holder and again thoroughly rinsed with methyl alcohol and dried.

Typical micrographs of the surface of specimens polished in accordance with this procedure are shown in Fig. 3. Note that the technique described has

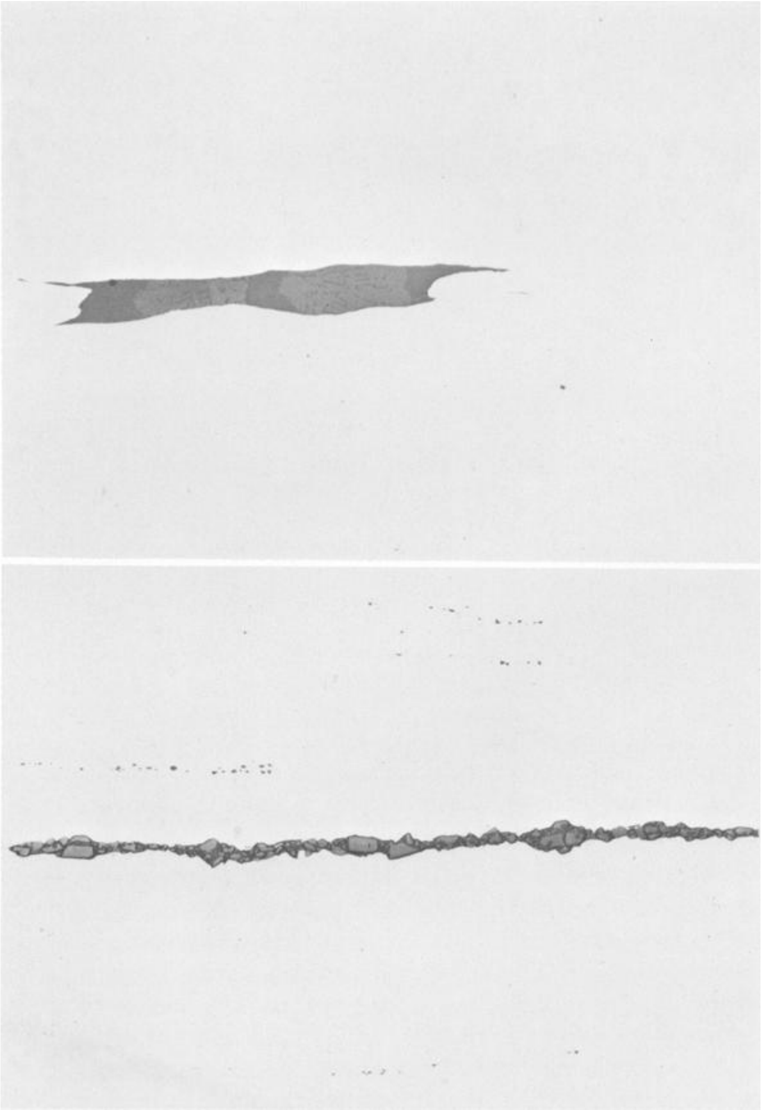

FIG. 3—*Inclusions in steel specimens polished in accordance with the procedure in Table 1* (×*100*)*:* (top) *multiphase silicate-type inclusions and* (bottom) *alumina inclusions.*

resulted in a specimen surface that lacks relief (a common polishing fault in specimens that are polished with aluminum oxide). Also note the excellent inclusion retention, which is difficult to attain by hand polishing.

Specimens should be stored in a desiccator until they can be examined. When storage for long periods of time is required, the specimens can be sprayed with clear acrylic lacquer, which can be removed at a later date by acetone, followed by an absolute methyl-alcohol rinse.

Selecting a Magnification to Suit the Product

For routine microcleanliness evaluation of products greater than ½ in. thick (1.3 cm), the ×5 objective on the microscope is normally selected, giving a final magnification on the monitor screen of 350. This magnification is chosen as the compromise between resolving power and area of coverage. At this magnification inclusions greater than 3 to 5 μm in width are detected and measured. This lower limit of detection compares favorably with the inclusion thickness of 4 to 9 μm depicted for all inclusion types in the thin series on the JK inclusion chart (ASTM E 45, Method A). With a blank frame of 25 by 25 cm, which is the size ordinarily used, the 350 magnification rates a specimen area of about 0.005 cm^2 per field. This area provides complete coverage of an average specimen without an excessive number of fields (several hundred) or, for a partial coverage of 25 to 100 fields, provides a reasonable total specimen area of about 0.1 to 0.5 cm^2. Furthermore, this field area is equal to the area of the field used (0.005 cm^2) in the standard JK inclusion chart, which facilitates comparison between QTM and JK ratings.

However, the 350 magnification may not be the one most suitable for all products. Very clean product, containing only fine inclusions, must be rated at a higher magnification to take advantage of the resolving power of the instrument, about 1 μm. Also, light-gage product containing typically very thin, elongated inclusions must be rated at a higher magnification. For example, in attempts to evaluate the cleanliness of 0.1-in. (0.25-cm)-thick sheet at the standard QTM magnification for heavy product (×350), the magnification was found to be too low to properly detect long, thin nonmetallics. Doubling the magnification helped but did not result in ratings sufficiently different from those obtained at the lower magnification. Increasing the magnification to 1300 did produce a significant difference in ratings, and therefore this magnification was selected for rating sheet product.

With an increase in magnification, however, the number of fields required to examine an area equivalent to that rated at a lower magnification increases by approximately the square of the ratio of the high to the low magnification. For a magnification increase from 350 to 1300, the number of fields would increase approximately by a factor of 14. Obviously, only a small portion of the specimen could then be scanned in rating times comparable to those used for lower magnification scanning.

To show the effectiveness of various rating configurations on a single sheet specimen rated at ×1300 by using a lower number of fields than the number used in rating the entire specimen, various rating configurations were tried, as shown in Fig. 4, and, in addition, the entire specimen was rated. In this

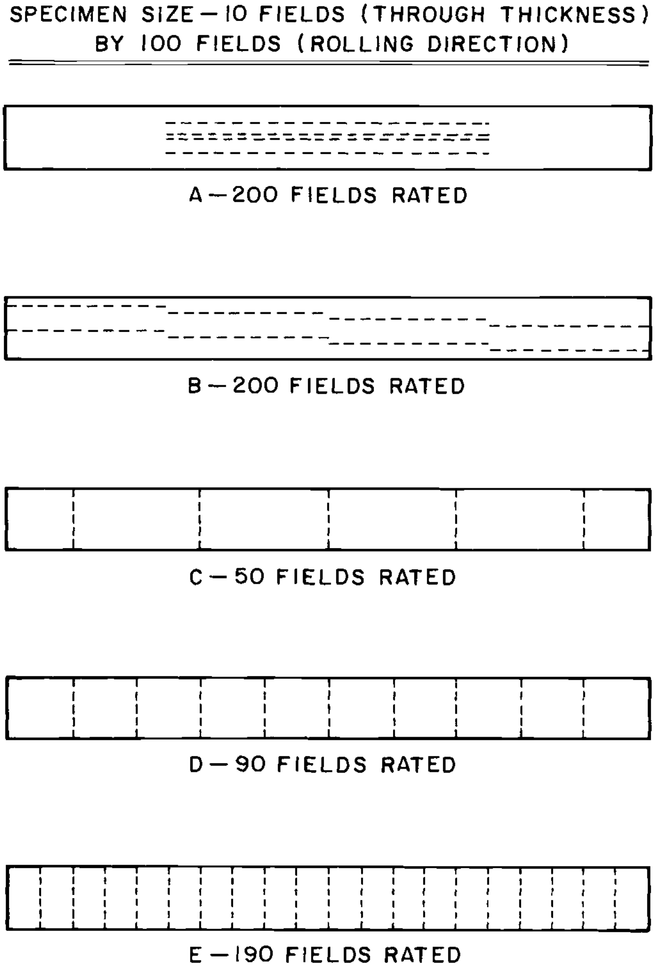

FIG. 4—*Schematic diagram of rows of adjacent fields rated on specimens.*

case an 0.1-in.-thick sheet specimen (Specimen A) was rated, and the results of ratings based on fewer fields were compared with the results of the entire specimen rating in which 1000 fields (10 fields thick by 100 fields long) covering the entire specimen were rated. The results of these ratings, Table 2, indicate that rating by Scheme C (Fig. 4) provides good correlation between the average inclusion area obtained by rating fewer fields and that obtained by rating 1000 fields, even though only 50 fields were rated in Scheme C. It is also significant that the rating direction of Scheme C (transverse to the rolling direction) is similar to the recommended direction of the magnetic lines of

TABLE 2—*QTM ratings at ×1300 on Specimens A and B.*

Rating Method	Incluson Area, % Average	Incluson Area, % Worst Fields	Length of Longest, μm	Number of Fields With Inclusion Area ≥ 0.5% per 100 Fields	Number of Fields Rated
		SPECIMEN A			
Entire specimen (10 × 100 fields)......	0.30	2.75	2500	16	1000
A Quarterthickness...	0.31	2.40	1300	18	100
Centerthickness....	0.40	2.00	2500	27	100
Average..........	0.36	...	...	22	200
B Top half..........	0.60	2.75	1800	45	100
Bottom half.......	0.13	0.44	200	0	100
Average..........	0.37	...	...	22	200
C....................	0.31	1.65	1300	18	50
D....................	0.30	1.90	2500	16	90
E....................	0.32	2.35	2500	16	190
		SPECIMEN B			
Entire specimen (10 × 100 fields)......	0.153	1.90	2200	8	1000
A Quarterthickness...	0.103	...	...	...	100
Centerthickness....	0.142	...	...	...	100
Average..........	0.122	...	...	...	200
B Top half..........	0.098	...	...	...	100
Bottom half.......	0.228	...	...	...	100
Average..........	0.163	...	...	...	200
C....................	0.148	0.94	1700	10	50
D....................	0.146	0.94	1700	10	90
E....................	0.153	1.90	2200	8	190

force for best detection of long nonmetallics by the magnetic particle test method (ASTM E 45). In addition, another specimen (Specimen B) with a different inclusion content was similarly rated, and the results, Table 2, show that the average inclusion area rating of Scheme C continues to correlate well with the entire specimen rating.

On the basis of the longest inclusion data in Table 2, it is evident that the Scheme E ratings correlate better with the entire specimen ratings than the Scheme C ratings, even though in rating each specimen the lengths of inclusions that extended beyond a field boundary were determined and recorded. However, Scheme E requires a rating time about 3½ times greater than that of Scheme C, and, if rating in terms other than the area percent is desired, the rating of 3½ specimens by Scheme C would furnish coverage of a greater length than would be covered by rating one specimen by Scheme E.

Analysis of Data

Accuracy of QTM Measurements

To determine the degree of precision inherent in the QTM, experiments were conducted to measure the amount of variation in controlled readings of area percentage. In the first experiment two artificial fields of rectangular inclusions with low (nominally 0.2 percent) and high (nominally 2 percent) area values were drawn within 3 by 3-in. (7.6 by 7.6-cm) areas on graph paper, and the areas were measured by using the low-power attachment to the QTM (epidiascope). Measurements were taken by an experienced operator five times on one day and one time the following day. For each reading the meter on the QTM was covered until the operator had judged that the inclusion area was properly filled. The results, Table 3, indicate that a standard deviation of about 10 percent can result from electronic variables and operator judgment in measuring a given area value.

TABLE 3—*Variations in the areal analysis of artificial inclusions by a single operator.*

		Inclusion Area, %	
Day	Time	Specimen 1	Specimen 2
1.......	9 a.m.	0.250	2.00
	11 a.m.	0.245	2.40
	12 noon	0.200	2.15
	2 p.m.	0.265	2.65
	5 pm..	0.270	2.20
2.......	9 a.m.	0.290	2.05
	Average	0.250	2.25
	Standard deviation	0.030	0.25

In the second experiment, to indicate differences between operators on the QTM, 20 separate fields on an actual specimen were rated at the same time, but independently, by two experienced operators. The differences in individual area readings, and particularly in the average inclusion-area values, Table 4, were very small. Therefore, it appears that whether one operator or more are conducting the tests, provided that the operators are well trained in the operation of the QTM, the major source of variation in QTM ratings of inclusions in steel is probably the variation in the distribution of the inclusions themselves.

TABLE 4—*Operator differences in QTM areal analysis.*

Field No.	Inclusion Area, %	
	Operator A	Operator B
1	0.16	0.15
2	0.38	0.41
3	0.26	0.22
4	0.39	0.39
5	0.16	0.13
6	0.68	0.60
7	0.42	0.36
8	0.40	0.36
9	0.64	0.61
10	0.50	0.42
11	0.32	0.30
12	0.54	0.42
13	0.16	0.12
14	0.37	0.39
15	0.28	0.22
16	0.40	0.26
17	0.04	0.03
18	0.18	0.13
19	0.04	0.02
20	0.27	0.21
Average	0.33	0.29

Determining the Number of Fields to Rate

Because of variation in the distribution of inclusions in steel, the manner in which the specimens are scanned must be carefully considered and a sufficient number of ratings of selected fields or random fields must be taken. Accordingly, a statistical method has been developed for determining the confidence intervals of data generated on the QTM, which enables the investigator to rapidly evaluate the data and to determine the minimum amount of data required to produce statistically significant results.

The developed procedure provides for rapidly determining when a desired confidence interval has been reached at which the accumulated data will have a certain probability of "surrounding" the true mean value for the constituent being measured [*6–8*]. At the same time, this method permits a statistically significant evaluation with the fewest possible observations and reduces the task of calculating the statistics necessary to construct the confidence intervals.

The developed method specifies the confidence interval or error as a function of the observed mean of the responsible variable. The method, in a way, fixes the length of a realistic confidence interval. The main objective of the developed method, however, is to collect the minimum amount of data so that the actual confidence interval is equal to or less than the specified confidence interval. Furthermore, this determination of whether the actual confidence interval is equal to or less than the specified confidence interval can be accomplished in a minimum time period. Because certain approximations to the theoretical probability distributions are made, the probability or confidence level attached to the confidence interval may not be exactly the specified probability but should be approximately the specified probability.

An example of the use of the statistical procedure and treatment of the data is shown in Table 5. The method requires that the experimenter first specify (set) the probability level and the length of the desired confidence interval before sampling of the steel specimen begins. The operator of the QTM then randomly selects five groups of five fields. From the information provided by the 25 fields, the operator determines whether the actual confidence interval is equal to or less than the specified confidence interval. If it is not, the operator randomly selects another group of five fields. This procedure continues until the actual confidence interval is less than or equal to the specified interval. When this occurs, sampling of the specimen stops, and the operator reports the arithmetic mean of all values of a response variable from all sampled fields. The operator then reports that the true mean has about a $1 - \alpha$ chance of being covered by the confidence interval specified by the experimenter. This interval is centered at the observed mean. All the parameters measured by the QTM can be statistically treated by the same methods.

TABLE 5—*Example of the use of the statistical procedure for treating inclusion data.*

1. Select the confidence $(1 - \alpha)$. For this case $\alpha = 0.05$ will be used.
2. Select the percentage (P) of the observed mean $(\bar{X})$ which will equal the length of the desired confidence interval $(L = P \times \bar{X})$. P will equal 0.20 since inclusion area is being determined in this example.
3. Select five sets $(K = 5)$ of five random fields $(n = 5)$. Determine the range of each group and the sum of the data.

Set	Data	Range	Sum
1	0.14, 0.20, 0.28, 0.11, 0.07	0.21	0.80
2	0.15, 0.23, 0.32, 0.09, 0.18	0.23	0.97
3	0.16, 0.17, 0.27, 0.10, 0.08	0.19	0.78
4	0.23, 0.22, 0.10, 0.19, 0.11	0.13	0.85
5	0.16, 0.23, 0.35, 0.07, 0.17	0.28	0.98
			4.38

(Continued)

TABLE 5—*Continued.*

4. Sum the ranges:

$$\Sigma R = 0.21 + 0.23 + 0.19 + 0.13 + 0.28 = 1.04$$

5. Multiply the sum of the data by 1.124 ($G_{K,n}/K_n$ shown below) and by P:

$$(4.38)\,(1.124)\,(0.20) = 0.98$$

Since the sum of ranges is greater than the product, five more random fields are taken

Set	Additional Data	Range	Sum
6	0.13, 0.15, 0.20, 0.11, 0.19	0.09	0.78

and the process is repeated from step 4:

$$\text{New } \Sigma R = 1.04 + 0.09 = 1.13$$

6. Repeat step 5 with new constants ($K = 6$, $n = 5$, $G_{K,n}/K_n = 1.243$):

$$\text{New sum} = 4.38 + 0.78 = 5.16$$

$$(5.16)\,(1.243)\,(0.20) = 1.28$$

7. Since the sum of the ranges is less than the product, stop testing, and determine the mean of the data and 0.20 of the mean:

$$\text{Mean} = \frac{\text{Total}}{\text{Number of Ratings}} = \frac{5.16}{30} = 0.17, \text{ Area} = 0.17 \pm 0.03$$

There is, therefore, at least 95 percent confidence that the true mean of the area of the specimen is within the above limits.

Values of Various Constants Used Above

						$\alpha = 0.05$ (95 % Confidence)		
K	n	Kn	$\sqrt{Kn}$	d_n[a]	$Kd_n\sqrt{Kn}$	$u_{(0.975,K,n)}$[b]	$G_{K,n}$[c]	$G_{K,n}/Kn$
1	5	5	2.236	2.326	5.20	2.63	1.98	0.396
2	5	10	3.162	2.326	14.71	2.25	6.54	0.654
3	5	15	3.873	2.326	27.03	2.15	12.57	0.838
4	5	20	4.472	2.326	41.61	2.10	19.81	0.990
5	5	25	5.00	2.326	58.15	2.07	28.09	1.124
6	5	30	5.477	2.326	76.44	2.05	37.29	1.243
7	5	35	5.916	2.326	96.32	2.04	47.22	1.349
8	5	40	6.325	2.326	117.70	2.03	57.98	1.450
9	5	45	6.708	2.326	140.43	2.02	69.52	1.545
10	5	50	7.071	2.326	164.47	2.01	81.83	1.637

[a] Ref *3*.

[b] Ref *2*.

[c] $G_{K,n} = \dfrac{Kd_n\sqrt{Kn}}{u_{(0.975,K,n)}}$.

Figure 5 shows a plot of the percent standard error versus the number of fields rated for a specimen in which the number of inclusions per field was determined. It can be seen in Fig. 5 that about 20 fields have to be rated to produce a standard error of 10 percent of the mean. A similar plot for the average inclusion area, Fig. 6, shows that 25 fields must be rated to produce a standard error of 20 percent of the mean. The error values for inclusion data must therefore be set large to be within the established confidence intervals. The error was chosen to be expressed as a percent of the mean when the inclusion count is being determined and 20 percent of the mean when the inclusion area is being determined.

Reporting the Results

One of the most important aspects of sample nonmetallic counts that can be evaluated by the QTM is the inclusion area of each field. We have found an increasing use at our laboratory for the average value of inclusion area. In addition, the frequency of fields equal to or greater than a particular inclusion area appears to be quite useful for expressing whether few very poor fields or several poor fields are included in the average.

With the increasing use of cleanliness ratings of steels based on inclusion area, comparison between QTM and conventional comparison rating methods

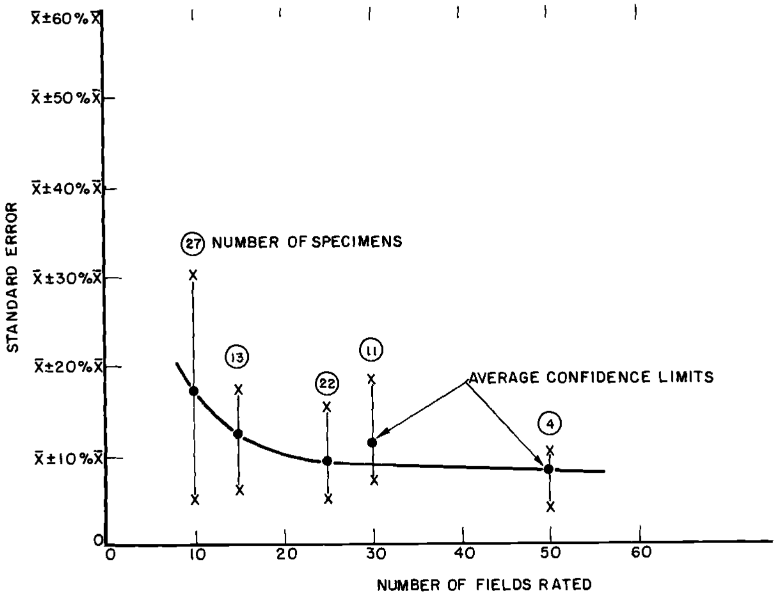

FIG. 5—*Effect of number of fields rated on the standard error in determining average number of inclusions per field in steel specimens.*

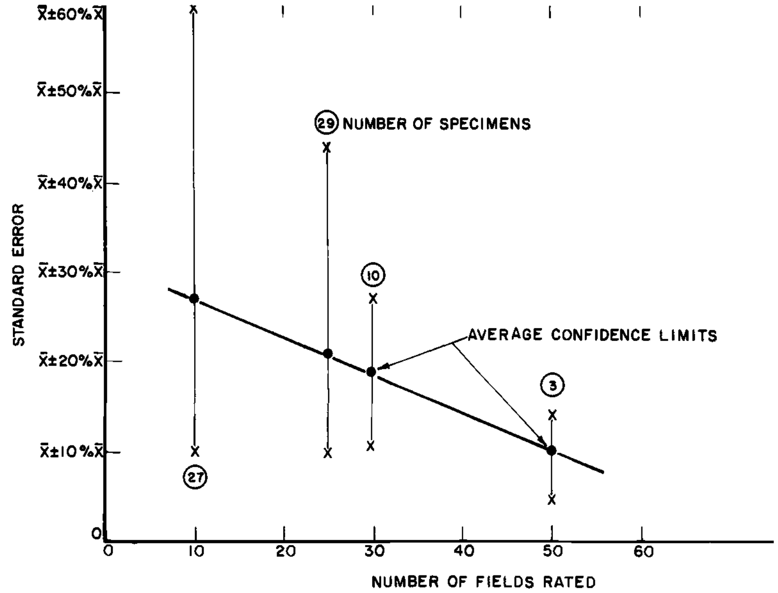

FIG. 6—*Effect of number of fields rated on the standard error in determining average inclusion area per field in steel specimens.*

has become desirable. For this comparison the JK inclusion charts (ASTM E 45, Plate I), which represent the most widely used inclusion comparison rating method, were rated by the QTM by direct measurement of area percentage at low power (×3.5). Because the JK chart depicts typical fields at ×100, the 3.5 magnification of the chart resulted in a total magnification of 350 on the television monitor screen. The area percentage occupied by the inclusions was determined in a reference area equal to that of the field area on the chart (the area within an 80-mm-diameter circle at ×100) so that the QTM reading gave the inclusion area percent for each field directly.

The charts measured at our laboratory were then sent to the Union Carbide Mining and Metals Division Laboratory, Niagara Falls, N. Y., where a second set of QTM inclusion area percent measurements was similarly made. In general, the results of the measurements by both laboratories were in good agreement, as shown in Table 6.

It should be remembered that the JK charts treat the individual types of inclusions (sulfides, alumina, silicates, and oxides) separately, whereas the QTM measures the total area of all inclusions visible in a field without regard to type. Therefore, direct comparisons between the JK area percentages determined in this study and inclusion areas measured by the QTM on real

TABLE 6—*QTM ratings of the JK inclusion charts (ASTM E 45, Plate I).*

	Area, %			Area %	
Inclusion Type and Severity	U.S. Steel	Union Carbide	Inclusion Type and Severity	U.S. Steel	Union Carbide
Sufides.... A_1 thin	0.14	0.16	Alumina.... B_1 thin	0.06	0.09
heavy	0.15	0.18	heavy	0.16	0.15
A_2 thin	0.42	0.56	B_2 thin	0.21	0.26
heavy	0.56	0.68	heavy	0.62	0.46
A_3 thin	1.15	1.10	B_3 thin	0.65	0.56
heavy	1.40	1.30	heavy	1.75	1.80
A_4 thin	2.65	2.70	B_4 thin	1.35	1.10
heavy	2.85	2.90	heavy	3.65	3.00
A_5 thin	4.10	3.40	B_5 thin	3.60	3.80
heavy	4.60	4.00	heavy	8.00	8.00
Silicates.... C_1 thin	0.14	0.17	Oxides.... D_1 thin	0.06	0.04
heavy	0.16	0.16	heavy	0.16	0.12
C_2 thin	0.36	0.35	D_2 thin	0.22	0.25
heavy	0.45	0.39	heavy	0.56	0.56
C_3 thin	0.65	0.67	D_3 thin	0.35	0.30
heavy	0.78	0.86	heavy	0.90	0.72
C_4 thin	1.05	0.70	D_4 thin	0.76	0.48
heavy	1.50	1.20	heavy	1.80	1.90
C_5 thin	1.85	1.85	D_5 thin	1.15	1.10
heavy	3.00	2.50	heavy	2.45	2.00

specimens should be used only for specimens that contain predominantly one type of inclusion.

An inclusion area of 0.5 percent was selected as a criterion to describe worst-field frequency, because this value equals or slightly exceeds the inclusion area read from the JK chart for B thin 2.5, B thick 1.5, C thin 2.5, and C thick 2.0—a series of maximum values for oxide (B-type) and silicate (C-type) inclusions selected from a specification for bearing-quality 52100 steel (ASTM Specifications for Carbon-Chromium Ball- and Roller-Bearing Steel (A 295 - 61)). In this instance the number of fields with inclusion area equal to or greater than 0.5 percent per 100 fields examined shows the frequency with which such a specification would be exceeded. When the number is zero, of course, the specification has not been significantly exceeded.

One other inclusion feature considered to be important is inclusion length. Some methods require that inclusion length over an arbitrarily chosen minimum size be recorded for each inclusion as the specimen is scanned. When this information was available several methods were tried to summarize the length data. Some methods require that the number of inclusions in various length categories be reported or that the average length of most of the inclusions or the length of the longest or combinations of each be shown. Obviously, it is desirable to use a reporting method that results in a single number to describe the length feature of inclusions in a specimen. At the Laboratory a unit length equal to 125 μm (0.005 in.) was chosen to conform to the ASTM E 45 Method B unit. Any inclusions with lengths less than 125 μm were ignored. The lengths of inclusions at least 125 μm in length were summed, and the number of 125-μm units per 100 fields rated was calculated from the data. This number is referred to as the QTM length factor. Of course, the number of inclusions per field can be recorded, and the inclusion area of the worst field can be selected from the original data and used if desired.

Comparison of QTM and Standard Ratings

Before proceeding with a comparison among the various rating systems, it should be understood that major errors occur in standard optical microscope rating methods that are of such magnitude that none of the ratings are fully satisfactory either in reproducibility or in accuracy [*9*]. Therefore, the comparisons discussed below between QTM ratings, which are said to be more reliable [*1*], and optical microscope ratings should not be considered as indicating the quantitative accuracy of correlations but, rather, as examples of how the QTM ratings can provide additional information or can describe quality trends that are similar or superior to those indicated by the standard rating techniques. Briefly, the ASTM standard rating methods develop the information presented below from a metallographic examination of the steel specimen.

ASTM E 45 Method A requires that only the worst fields of each inclusion type be recorded. In practice, however, some raters also record the number of fields in a specimen that exceed particular B- and C-type fields on the JK chart. To satisfy the requirements of Method B, the length of the longest inclusion (in 0.005-in. or 125-μm units), the number and average length of all inclusions equal to or greater than a unit length, and a worst-field background rating are recorded. Method C provides only information about the worst fields for each of two inclusion types—oxide and silicate stringers—and therefore has not been used in the present comparison.

Each of the ASTM rating methods provides specific information of a different nature, with the result that specific comparisons with the QTM ratings are very difficult. For example, a comparison of QTM inclusion area ratings with the thin and thick worst-field ratings for sulfide-, alumina-, silicate-, and globular oxide-type inclusions in accordance with Method A would be difficult, because special techniques are necessary for QTM ratings to discriminate among inclusion types. Fortunately, weighted counts or summations that do not discriminate among inclusion types have been used in the past to simplify standard ratings for comparative evaluations. An example of such a weighted count is shown in Appendix 1. Such a count (cleanliness index) is obtained from the additional information gathered while Method A ratings are determined. Likewise, a length factor can be determined from Method B ratings, as described in Appendix 2; the length factor is obtained from a summation of inclusion length units and thus provides a single number for comparison with the results of other rating methods. Note that the foregoing weighted count or summation emphasizes the number and length of inclusions equal to or greater than a selected minimum length.

Specimens of 16 production heats of various steel compositions were selected for rating. For each basic oxygen process (BOP) or open-hearth (OH) heat of steel rated, specimens from the middle and bottom portions of the middle ingot were forged into a 4 by 4 by 36-in. billet. Three standard (ASTM E 45) longitudinal ⅜ by ¾-in. (1 by 2-cm) microcleanliness specimens, centered at the quarterthickness and at the centerthickness, were prepared and rated from each 4 by 4-in. (10 by 10-cm) billet specimen (12 microcleanliness specimens per heat).

The specimens were rated at ×100 with the optical microscope by the standard rating Methods A and B, with slight modification, as described in the Appendix. In addition, the specimens were rated at 350 magnification by using the QTM to scan 100 fields on each specimen (four rows of 25 fields transverse to the rolling direction). For the BOP steels rated, Table 7 shows the QTM values for average inclusion area, the number of fields with inclusion area equal to or greater than 0.5 percent (per 100 fields), the QTM length factor, the Method A cleanliness index based on the frequency of worst fields of B- and C-type inclusions, and the Method B length factor. The corresponding values for the OH steels rated are shown in Table 8.

In general, higher cleanliness index numbers and Method B length factors were obtained for the bottom location of the ingot than for the middle portion. Although the QTM rating numbers based on inclusion area do not show this trend, the QTM length factor does (12 of the 16 bottom length factor ratings are higher than the middle ratings). Consequently, the inclusion area rating and the QTM length factor rating provide different information about the

TABLE 7—*Microcleanliness rating numbers for BOP steels.*

		QTM			ASTM E 45	
Steel	Ingot Test Location	Average Inclusion Area, %	Number of Fields With Inclusion Area $\geqslant 0.5$[a]	QTM Length Factor	Method A Cleanliness Index	Method B Length Factor
1008 or 1010 coarse grained	Middle	0.33	16	22	71	78
	Bottom	0.25	11	20	111	100
1021 coarse grained......	Middle	0.20	5	8	27	43
	Bottom	0.38	26	20	158	152
1021 coarse grained......	Middle	0.27	13	5	34	32
	Bottom	0.25	9	7	33	70
1021 coarse grained......	Middle	0.27	8	10	7	56
	Bottom	0.29	17	18	181	143
1021 fine grained	Middle	0.11	1	15	31	27
	Bottom	0.16	3	18	35	36
1021 fine grained	Middle	0.11	1	9	10	25
	Bottom	0.11	2	14	33	54
1021 fine grained	Middle	0.20	8	17	22	43
	Bottom	0.21	8	49	37	74
4140 fine grained	Middle	0.21	11	35	34	60
	Bottom	0.12	2	29	56	90
8620 fine grained	Middle	0.10	6	41	32	53
	Bottom	0.23	5	21	58	61
8620 fine grained	Middle	0.16	4	11	35	36
	Bottom	0.12	2	17	31	54

[a] Per 100 fields.

steel tested; that is, the QTM values based on inclusion area indicate that the volume of inclusion material does not vary considerably from the middle to the bottom of the ingot, whereas the weighted counts emphasize a difference in inclusion morphology between middle and bottom ingot locations. (The larger weighted counts at the bottom indicate that inclusions tend to be longer at the ingot bottom, although the frequency must be somewhat lower to maintain an equivalent average inclusion area.)

A comparison of the weighted counts from the standard ratings (cleanliness index numbers and Method B length factors) and average inclusion area ratings of the steels tested is shown in Fig. 7. As can be seen from the trend line through the data, the steels with high weighted counts also had generally higher inclusion area ratings. Thus the ingot locations with greatest or least

TABLE 8—*Microcleanliness rating numbers for OH steels.*

		QTM			ASTM E 45	
Steel	Ingot Test Location	Average Inclusion Area, %	Number of Fields With Inclusion Area ⩾ 0.5[a]	QTM Length Factor	Method A Cleanliness Index	Method B Length Factor
1021 coarse grained......	Middle	0.30	16	32	99	102
	Bottom	0.38	20	42	115	94
1048 modified..	Middle	0.24	9	20	23	58
	Bottom	0.20	6	22	26	61
4140 not vacuum carbon deoxidized...	Middle	0.25	11	12	56	71
	Bottom	0.27	12	7	64	83
4140 vacuum carbon deoxidized...	Middle	0.14	2	4	6	9
	Bottom	0.20	4	5	28	31
8620 not vacuum carbon deoxidized...	Middle	0.22	4	6	11	20
	Bottom	0.18	5	7	43	48
8620 vacuum carbon deoxidized...	Middle	0.19	7	4	4	24
	Bottom	0.16	2	8	10	36

[a] Per 100 fields.

inclusion content will be ranked as dirtiest or cleanest, respectively, by both the standard methods and the QTM method. As expected because of the poor reproducibility that has been reported [9] for standard (optical microscope) rating methods, the scatter of points around the trend line of the figure indicates a rather poor correlation between the counts and QTM inclusion area values. However, increasing use of the quantitative methods discussed should increase the confidence in using rating numbers to rank steels by actual nonmetallic content.

It should be pointed out that the heats of steel for which cleanliness data are shown in Tables 7 and 8 were not made to cleanliness specifications but were selected from regular production heats for comparison of OH and BOP melting methods. These tables show that the ranges of average inclusion area values were similar for both melting methods (0.10 to 0.38 for BOP steels and 0.14 to 0.38 for the OH steels), as were the ranges of values for the number of fields with inclusion area equal to or greater than 0.5 percent (1 to 26 for the

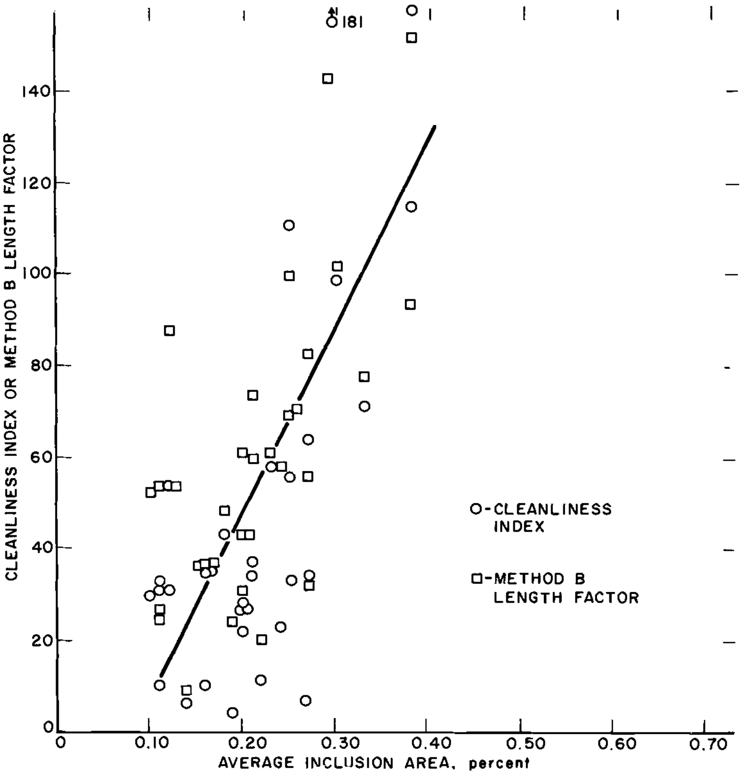

FIG. 7—*Comparison of cleanliness index numbers and Method B length factors with QTM values of average inclusion area.*

BOP steels and 2 to 28 for the OH steels) and for the QTM length factor (5 to 49 for the BOP steels and 4 to 42 for the OH steels).

Summary

The need for a method for the determination of the inclusion content of steel that is more versatile, accurate, and rapid than the presently used standard comparison methods has led to the development at the U. S. Steel Applied Research Laboratory of a general procedure for the rating of nonmetallics by the quantitative television microscope (QTM).

The use of a special automatic specimen preparation technique developed in conjunction with the QTM rating method provides the large number of metallographic specimens required by the QTM and also provides inclusion retention and freedom from relief that are superior to hand preparation methods.

A statistical analysis of QTM inclusion data, obtained by the newly developed method, has been conducted to indicate the reliability and precision of the data and to aid in selecting a rating scheme that is easily adapted to a variety of steel product shapes and sizes. The number of fields selected for rating, the pattern in which the fields are scanned on the specimen, and the magnification at which the ratings are made depend on the precision desired and on the type (size) of product being rated. Information obtained with the QTM consists of area fraction in inclusions, number of inclusions, and distribution of inclusion lengths. One or more of these QTM parameters, or the values derived therefrom, may be used to express an overall inclusion rating for a steel product.

The inclusion area percentage, particularly the area percentage distribution, correlated well with JK (ASTM E 45, Method A) chart ratings. However, it should be noted that direct comparisons of JK chart area percentage ratings and inclusion areas measured by the QTM on real specimens should be used only for those specimens that contain predominantly one type of inclusion unless special techniques are employed to discriminate among inclusion types on the QTM. Although the QTM parameters provided information that is comparable to weighted counts developed from ASTM E 45 inclusion rating methods, the correlation between QTM parameters and weighted counts was poor because of the lack of reproducibility of the latter ratings.

Because of the accuracy and reproducibility of the QTM method, and particularly because of its applicability to such a wide variety of steel products, the QTM method for inclusion assessment should find increasing use and may ultimately replace the present standard methods.

Acknowledgments

We wish to acknowledge the assistance of A. G. Lee, Sr., and G. M. Chalfant of the U. S. Steel Applied Research Laboratory for specimen preparation techniques and for obtaining the QTM data, respectively. The work of the Duquesne Plant Development Laboratory of National-Duquesne Works, U. S. Steel, where the standard cleanliness ratings were performed, and of M. J. Lalich of the Union Carbide Mining and Metals Division Laboratories, who helped obtain the QTM ratings of the JK charts, is also gratefully acknowledged.

APPENDIX 1

Cleanliness Index Based on ASTM E 45 Method A

The entire surface of the polished specimen (about ¼ in.^{2}) is examined at ×100. As each field is viewed it is compared with a chart—often referred to as the JK chart from the JK (Jernkonteret) method used in Sweden—that has frequency-severity gradations expressed as numbers from 1 to 5 and has notations of thin and heavy for four inclusion types (A sulfides, B alumina, C silicates, and D globular oxides). Theoretically the inclusion type and field number on the chart that are most like the field under observation are recorded for each field.

Usually, only the worst field of each inclusion type is reported for each specimen, and thus only the fields with the poorer ratings of each inclusion type are recorded as the specimen is being scanned. To obtain a worst-field rating for an entire heat, the worst-field ratings for individual specimens are totaled and an average is obtained for the entire heat of steel.

Some raters prefer the following nonstandard procedure based on the above standard rating method. Rate the specimen as above and, in addition, record the frequency of B and C fields that correspond to a particular specification and that correspond to increments of 0.5 above the specification. The cleanliness index (a weighted count) can then be calculated from these data by multiplying the field frequency thus recorded by a severity factor, as described below.

Record the number of fields that correspond to the Jernkonteret chart numbers below. Multiply the number of fields of each type below by the respective factors. Total the products for each specimen. The total of the products for the specimen is the cleanliness index.

B (Alumina Type)		C (Silicate Type)		
Thin	Thick	Thin	Thick	Factor
2.0	1.0	3.0	1.5	1
2.5	1.5	3.5	2.0	2
3.0	2.0	4.0	2.5	4
3.5	2.5	4.5	3.0	6
>3.5	>2.5	>4.5	>3.0	8

APPENDIX 2

Length Factor Based on ASTM E 45 Method B

The entire surface of the polished specimen (about ¼ in.^{2}) is examined at ×100. As each field is viewed it is compared with a chart for background inclusions (less than 0.005 in. long); the lengths of all inclusions 0.005 in. (125 μm) long or longer are recorded separately. Lengths of inclusions are recorded as the number of

0.005-in. units. The following data are reported for each specimen: the length of the longest inclusion in 0.005-in. units, the average length in 0.005-in units of all inclusions 0.005 in. long or longer (excluding the longest), and the background rating for the worst field (or for the average of several of the worst fields), given as a letter classification corresponding to ASTM E 45 Plates A, B, C, or D. The number of inclusions (excluding the longest) used to obtain the average length may also be reported (usually as a superscript to the average length).

A number called the Method B length factor has been calculated for comparison with the QTM length factor; this number represents the total number of length units per specimen (number of inclusions times the average length plus the length of longest inclusion in 0.005-in. units). This length factor can be calculated from the data when the superscript is given.

References

[*1*] Allmand, T. R. and Blank, J. R. in *Automatic Cleanness Assessment of Steel*, ISI Publication 112, Iron and Steel Institute, London, 1968, p. 47.

[*2*] Blank, J. R., *Microscope*, MICRA, Vol. 16, No. 2, 1968, p. 189.

[*3*] Roche, R., *Metaux Corrosion Industrie*, MTUXA, Feb. 1968, p. 49.

[*4*] Ratz, G. A., *Metal Progress*, MEPOA, Vol. 94, No. 2, Aug. 1968, p. 153.

[*5*] Langhoff, R. R. and Johnson, A. R. in *Fifty Years of Progress in Metallographic Techniques, ASTM STP 430*, American Society for Testing and Materials, 1968, p. 96.

[*6*] Dixon, W. J. and Massey, F. G., Jr., *Introduction to Statistical Analysis*, 2nd ed., McGraw-Hill, 1957.

[*7*] Lord, E., *Biometrika*, BIOKA, Vol. 32, 1947, p. 41.

[*8*] Patnaik, P. B., *Biometrika*, BIOKA, Vol. 37, 1950, p. 78.

[*9*] Blank, J. R. and Allmand, T. R. in ISI Publication 112, Iron and Steel Institute, London, 1968, pp. 1–13.